UNIVERSITY OF CALIFORNIA, SAN DIEGO

Physiological, ecological, and evolutionary studies of trace metal homeostasis in marine microbes

A dissertation submitted in partial satisfaction of the Requirements for the degree Doctor of Philosophy

in

Oceanography

by

Christopher Lee Dupont

Committee in charge:

Professor Katherine Barbeau, Co-Chair
Professor Brian Palenik, Co-Chair
Professor Bianca Brahamsha
Professor Philip Bourne
Professor Stanley Opella

2008

UMI Number: 3297530

UMI Microform 3297530

ProQuest Information and Learning Company
300 North Zeeb Road
P.O. Box 1346
Ann Arbor, MI 48106-1346

The Dissertation of Christopher Lee Dupont is approved, and it is acceptable in quality and form for publication on microfilm:

_____

_____

_____

_____
Co-Chair

_____
Co-Chair

University of California, San Diego

2008

TABLE OF CONTENTS

LIST OF FIGURES

LIST OF TABLES

ACKNOWLEDGEMENTS

My PhD. committee has been incredibly supportive and helpful, and I would also like to thank my MS committee of Professors Beth Ahner and Esther Angert. Members of the Palenik and Barbeau labs and the Scripps community have made my time in San Diego more enjoyable. For their encouragement and helpful discussions, I must thank R.J.P Williams, Ariel Anbar, F. M.M. Morel, F. Wolfe, S. Yang, R. Valois, A. Allen, and R. Goericke. My friends and occasional housemates Sebastian Sudek, Todd Franks, Drew Lucas, and John Grey III kept me sane and entertained. Finally, I want to thank my parents and Katherine Chang for not only tolerating me, but also supporting me through the best and worst.

François Morel and the Princeton Center for Environmental Bioinorganic Chemistry provided me with invaluable research funding, while the Department of Defense funded my National Defense Science and Engineering Graduate Research Fellowship. The National Science Foundations provided funding to Brian Palenik and Kathy Barbeau, and some of the work in this dissertation was supported by those grants.

Chapter 1, in full, is a reprint of the material as it appears in the Proceedings of the National Academy of Sciences, volume 103, pages 17822-17827. Song Yang, Brian Palenik, and Philip Bourne were co-authors. The dissertation author was the primary investigator and first author.

Chapter 2, in full, is a reprint of the material that has been accepted for publication without revision in Environmental Microbiology. K. Neupane, J. Shearer,

and B. Palenik were co-authers, while the dissertation author was the primary investigator and first author.

Chapter 3 is a reprint of material as it appears in Applied and Environmental Microbiology, volume 74, pages 23-31. K. Barbeau and B. Palenik were co-authors. The dissertation author was the primary investigator and first author.

Ian Paulsen, Bianca Brahamsha, Katherine Kang, and Aaron Johnson contributed significantly to the contents of chapter 4, which likely will be submitted for publication in the near future to a journal to be determined. The dissertation author was the primary investigator and first author.

Chapter 5 is a reprint of material to be submitted to Limnology and Oceanography. K. N. Buck, K. Barbeau, and Brian Palenik are co-authors. The dissertation author was the primary investigator and first author. The authors would like to thank Chief Scientists James Moffett, Fred Prahl, Brian Popp, and Mike Landry, as well as the crew of the *R/V* New Horizon and Knorr. Andrew L. King provided several Fe measurements.

VITA

2001	Bachelor of Science, Cornell University
2003	Master of Science, Cornell University
2008	Doctor of Philosophy, University of California, San Diego

ABSTRACT OF THE DISSERTATION

Physiological, ecological, and evolutionary studies of trace metal homeostasis in marine microbes

by

Christopher Lee Dupont

Doctor of Philosophy in Oceanography

University of California, San Diego, 2008

Professor Brian Palenik, Co-Chair
Professor Katherine Barbeau, Co-Chair

Trace metals are important for the catalytic function and proper folding of many proteins, and the complement of trace metals required by an organism depends upon the complement of metal-binding proteins, or metallo-enzymes required. As a result of oxygenic photosynthesis, trace metal bioavailability changed dramatically during the late Archaean and Early Proterozoic, theoretically influencing the biological selection of trace metals for usage. Here several linkages are made between modern physiology, ecology, and genetics and the environmental changes induced by the great oxygenation event. Across all of life, Prokaryotic proteomes are shown to contain more Fe, Mn, and Co-binding proteins, whereas Eukaryotic proteomes are comparatively rich in Zn-binding proteins, trends consistent with the hypothesized changes in trace metal bioavailabilty. The phylogenomic distribution of the gene

(*sodN*) coding for one oxygen-prompted enzymatic innovation, Ni-SOD, reveals a proliferation in marine microbles, particularly in the cyanobacteria, through horizontal gene transfer at the expense of a gene, *sodB*, that codes for an Fe-SOD. The exchange of a Ni-SOD for Fe-SOD may reduce Fe requirements, a valuable adaptation to the oxygen-induced drop in Fe availability. Consequently, some marine *Synechococcus* have an obligate requirement for Ni, and these strains control Ni uptake and assimilation through the feedback regulation of a Ni transporter likely acquired during the same transfer event begetting *sodN*. Possibly as a consequence of the usage of Ni-SOD, Ni appeared to limit cyanobacterial growth in the surface waters of the Gulf of California. Separately, off the coast of Peru where low Fe concentrations limit phytoplankton growth, a diatom-dominated community was unable to utilize added urea for growth unless Ni was added concurrently, a biochemical limitation related to the usage of a Ni-containing urease. Despite nanomolar Ni concentrations in Peru, biophysical modeling implies that the low Fe concentrations result in a saturation of the diatom cell surface with transporters, limiting the uptake of Ni and potentially other metals.

CHAPTER 1
Modern Proteomes Contain Putative Imprints of Ancient Shifts in Trace Metal Geochemistry

Abstract: Due to the rise in atmospheric oxygen 2.3 billion years ago (Gya) and the subsequent changes in oceanic redox state over the last 2.3-1 Gya, trace metal bioavailability in marine environments has changed dramatically. While theorized to have influenced the biological usage of metals leaving discernable genomic signals, a thorough and quanitative test of this hypothesis has been lacking. Using structural bioinformatics and whole genome sequences, the Fe, Zn, Mn, and Co-binding metallomes of 23 Archaea, 233 Bacteria, and 57 Eukarya were constructed. These metallomes reveal that the overall abundances of these metal-binding structures scale to proteome size as power laws with a unique set of slopes for each Superkingdom of Life. The differences in the power slopes describing the abundances of Fe, Mn, Zn, and Co-binding proteins in the proteomes of Prokayotes and Eukaryotes are similar to the theorized changes in the abundances of these metals following the oxygenation of oceanic deep waters. This suggests that Prokarya and Eukarya evolved in anoxic and oxic environments respectively, a hypothesis further supported by structures and functions of Fe-binding proteins in each Superkingdom. Also observed is a proliferation in the diversity of Zn-binding protein structures involved in protein-DNA and protein-protein interactions within Eukarya, an event unlikely to occur in either an anoxic or euxinic environment where Zn concentrations would be vanishingly low. We hypothesize that these conserved trends are proteomic imprints of changes in trace metal bioavailability in

the ancient ocean that highlight a major evolutionary shift in biological trace metal usage.

Introduction

The emergence of oxygenic photosynthesis is associated with major changes in global biogeochemistry and metabolism (100, 151). In particular, the rise in atmospheric oxygen around 2.3 Gyr ago (14, 63) potentially led to the oxygenation of the entire ocean (82), while an alternative theory proposes that the deep ocean became euxinic (anoxic and sulfidic) around 1.8 Gyr ago (8, 34), prior to an oxygenation of deep waters around 1 Gyr (33). Putting aside for now the when and where, these changes in the overall redox state of the ocean would dramatically influence trace metal chemistry and bioavailability, with an anoxic ocean being characterized by relatively high Fe, Mn, and Co but low Zn concentrations (162) (Fig. S1). A euxinic ocean would have comparatively lower concentrations of all of these metals, particularly Zn (162)(Fig. S1). The oxygenation of oceanic deep waters would have dramatically increased Zn concentrations, with concomitant yet less severe decreases in Fe, Mn, and Co levels (162)(Fig. 1.1). As postulated by Frausto da Silva and Williams (199), these drastic shifts in metal bioavailability theoretically influenced the selection of trace elements for biological usage leaving a record within the genomes and proteomes of extant organisms.

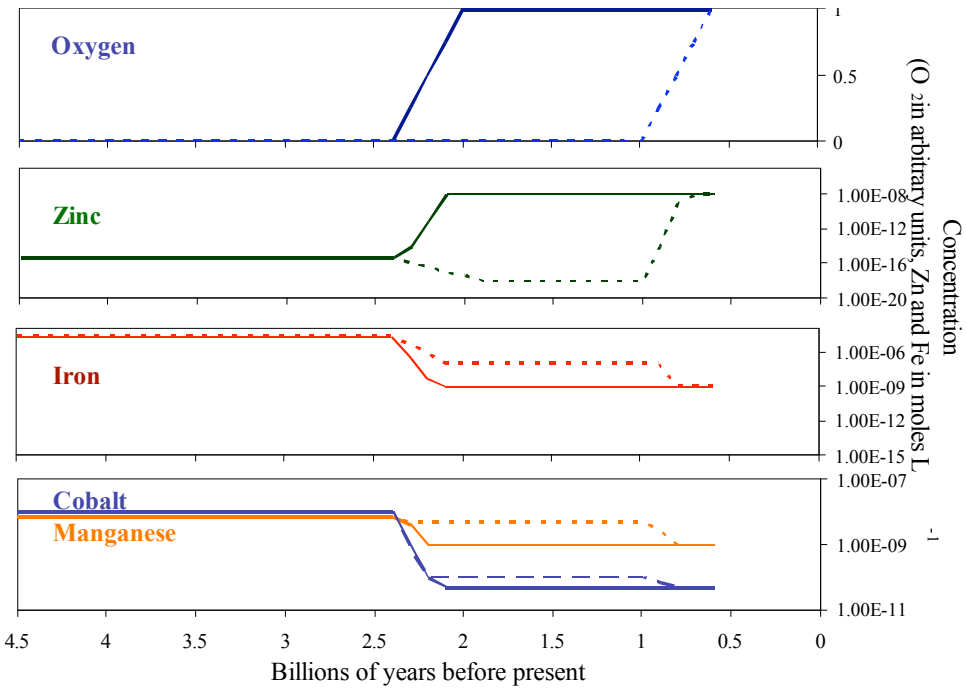

Figure 1.1: Oceanic Fe, Zn, Mn, and Co over geologic time. Plotted are the theoretical O_2, Fe, Zn, Mn, and Co concentrations in the deep ocean over the last 4.5 billion years, as modeled by Saito et al. (162). As it is debated whether the ocean became oxic shortly after the rise in atmospheric oxygent (2.3 Gya) or became euxinic (anoxic and sulfidic) until 1-0.6 Gya, both scenarios are shown (dotted lines, euxinic or Canfield ocean).

Protein structure has a remarkable level of redundancy, with a limited number of 3-dimensional folds describing all of life (38). Further, structure is retained over long evolutionary time scales even when most sequence homology is lost, and this provides an excellent tool for this study. Already, the identification of domains within protein structures and the systematic and hierarchical classification of these domains has been used to study evolution (99). Within these hierarchical classifications reside fold superfamilies (FSF) and fold families (FF); a FSF contains structures believed to be evolutionarily related despite a lack of clear sequence similarity, whereas a FF contains structures with evident structural, functional, and sequence similarities (a FSF is composed of one or more FF). The gain or loss of a FSF or FF by an organism constitutes an important evolutionary event, either reducing or expanding the repoitoire of functions available to that organism. Indeed, the presence or absence of FSFs in a proteome has been shown to discriminate species well enough to construct reasonable phylogenetic trees for all of life (205).

Here, we utilized structural bioinformatics to study the distribution of metal binding protein structures within the proteomes of Archaea, Bacteria, and Eukarya, which to our knowledge has not been done before. The results suggest that ancient changes in trace metal geochemistry do indeed leave imprints observable within the

genomes and proteomes of modern life and provide an important constraint on the evolution of Eukarya.

Results and Discussion

The Superfamily database (73, 74), derived from the Structural Classification of Proteins (SCOP) (129), provides an independent assessment of the presence and abundance of structural domains belonging to FSFs and FFs across a diverse set of species for which complete genome and translated proteome sequences are available. In order to extract the desired information from the Superfamily database we manually annotated SCOP version 1.69 according to metal binding (Appendix 1). Both the raw structural data from the Protein Data Bank (15) and the primary literature associated with each structure was used to identify covalently-bound metals. Protein domains that bind a metal-containing cofactor (e.g. Co-containing B_{12} and Fe-containing heme) were considered metal binding. Here, an *ambiguous* FSF is defined as one in which the structures comprising that FSF bind different metals, or contain a combination of both metal-binding and non-metal binding structures. Likewise, an *ambiguous* FF contains a mixture of metal and non-metal binding structures or structures binding different metals. Approximately half of the metal-binding FSFs and 10% of the metal-binding FFs are *ambiguous* (Table 1.1). Only *unambiguous* FFs were used for this study. When this hand curated literature annotation of the SCOP is combined with the unannotated Superfamily data, frequencies of Fe, Mn, Co, and Zn-binding

Table 1.1: The total numbers of of Fe, Zn, Mn, and Co binding FSFs and FFs in the SCOP database, along with the percent at both the FSF and FF level that is ambiguous. To be considered ambiguous, either the FFs or domains in a FSF, or the domains in a FF do not agree in terms of metal-binding. For example, the ferritin FSF is ambiguous as the daughter categories include both Fe (e.g. ferritins) and Mn-binding (e.g. Mn chelatase) FFs, but the FFs in the ferritin FSF are not ambiguous.

	Fold Superfamilies		Fold Families				
Metal	**Total**	**ambiguous**	**metal**	**Total**	**ambiguous**	**# counted**	**%coverage**
Fe	78	36	**Fe**	118	11	107	90.7
Zn	130	61	**Zn**	189	9	180	95.2
Mn	26	16	**Mn**	33	4	29	87.9
Co	12	8	**Co**	15	6	9	60.0

structural domains in the proteomes of 23 Archaea, 233 Bacteria, and 57 Eukaryote species are obtained, providing the first "metallome" based upon protein structure and the whole proteome of an organism. While metals such as Cu, Mo, and Ni are biologically relevant, given the limited number of FFs that bind these metals (< 0.3 % of the average proteome), we have excluded them from our analysis of the overarching trends that are the focus of this paper. These metals and the issue of ambiguous FFs and FSFs will be addressed in subsequent work.

Using the metallome data we observe that while the percentage of a proteome that binds a given metal differs between the Superkingdoms (Fig. 1.2), the abundances of metal-binding domains scale to proteome and genome size, therefore, stationary statistics like percentage are inappropriate for describing overall trends. Rather, the distributions of Fe, Zn, and Mn-binding domains within each Superkingdom conform to a power law ($y = bx^m$) (Fig. 1.3A, Table 1.2). Power law scaling to genome size has also been observed for functional categories of genes in Bacteria (98, 189), in contrast the scaling category here describes an aspect of teriary protein structure relatively independent of functional classification.

Based upon the theory proposed by van Nimwegen (189), the observed power law slopes describe evolutionarily constant ratios for the size of a category of proteins relative to the size of the entire proteome. A slope of 1 indicates that

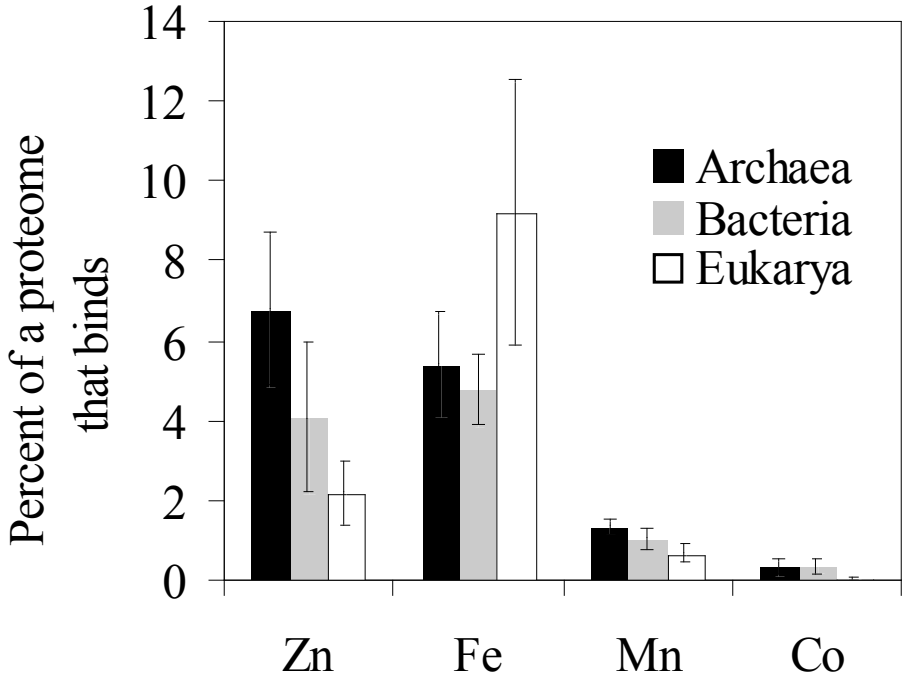

Figure 1.2: Percent of Archaeal, Bacterial, and Eukaryotic proteomes that are metal binding. Error bars denote 1 standard deviation. Note that these statistics are not adequate for fully describing the abundance of metal-binding domains within each Superkingdom (see main text).

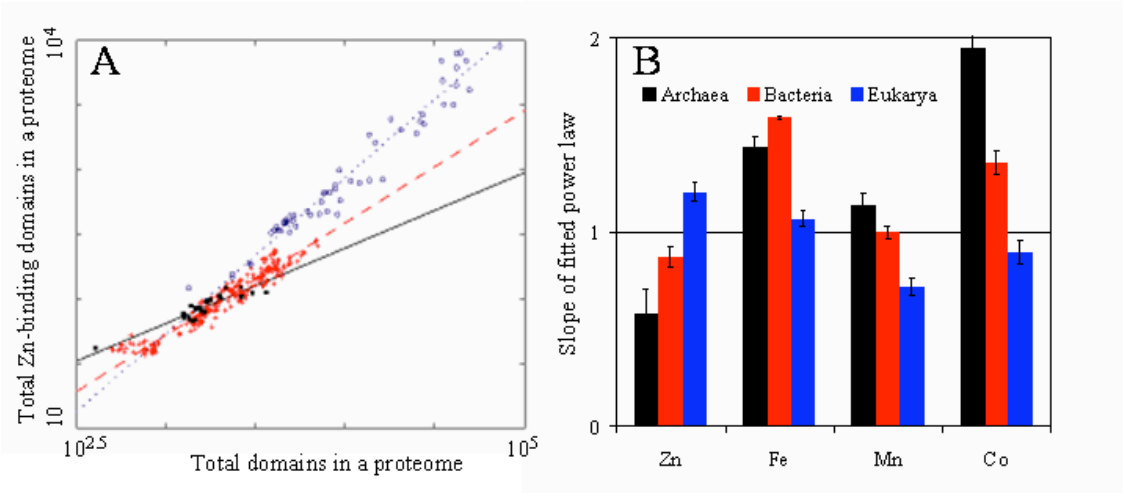

Figure 1.3: A) Log-log plot of the abundances of Zn-binding domains in Archaea (black □), Bacteria (red x) and Eukarya (blue o) compared to the total number of structural domains in a proteome. Each point represents the number of metal-binding domains and the total number of assigned protein domains in a discrete proteome. The total number of structural domains annotated in a proteome scales linearly to both genome size and gene number. Also shown are the fitted power laws (black solid - Archaea; red dashed - Bacteria; blue dotted – Eukaryotes). B) The power law slopes describing the abundances of Fe, Zn, Mn, and Co/B_{12} binding structural domains in the proteomes of Archaea (black), Bacteria (red), and Eukarya (blue). The error bars denote 1 standard deviation. The statistics for the quality of the power law fits are shown in Table 1. When the slopes of the curves are compared, they are significant as follows (A=Archaea, B=Bacteria, E=Eukaryote): **Zn**, all are significantly different at α =0.5 %. **Fe**, B vs A and B vs. E α = 0.1 %, A vs. E α = 5 %. **Mn**, A vs. E, B vs. E α= 0.5 %, A vs. B, not significantly different at α = 5%. **Co**, A vs E α = 1 %, B vs. E α = 5 %, A vs B not significantly different at α = 5%.

Table 1.2: Statistics on the quality of the power law fits. Both the F-values, which describe the fraction of the variance in the data explained by the fitted curves, and the r^2 values are shown.

	F values				r^2			
	Fe	**Zn**	**Mn**	**Co**	**Fe**	**Zn**	**Mn**	**Co**
Archaea	0.94	0.97	0.98	0.94	0.92	0.91	0.97	0.82
Bacteria	0.96	0.98	0.95	0.88	0.9	0.97	0.91	0.74
Eukarya	0.97	0.99	0.96	0.93	0.94	0.98	0.92	0.85

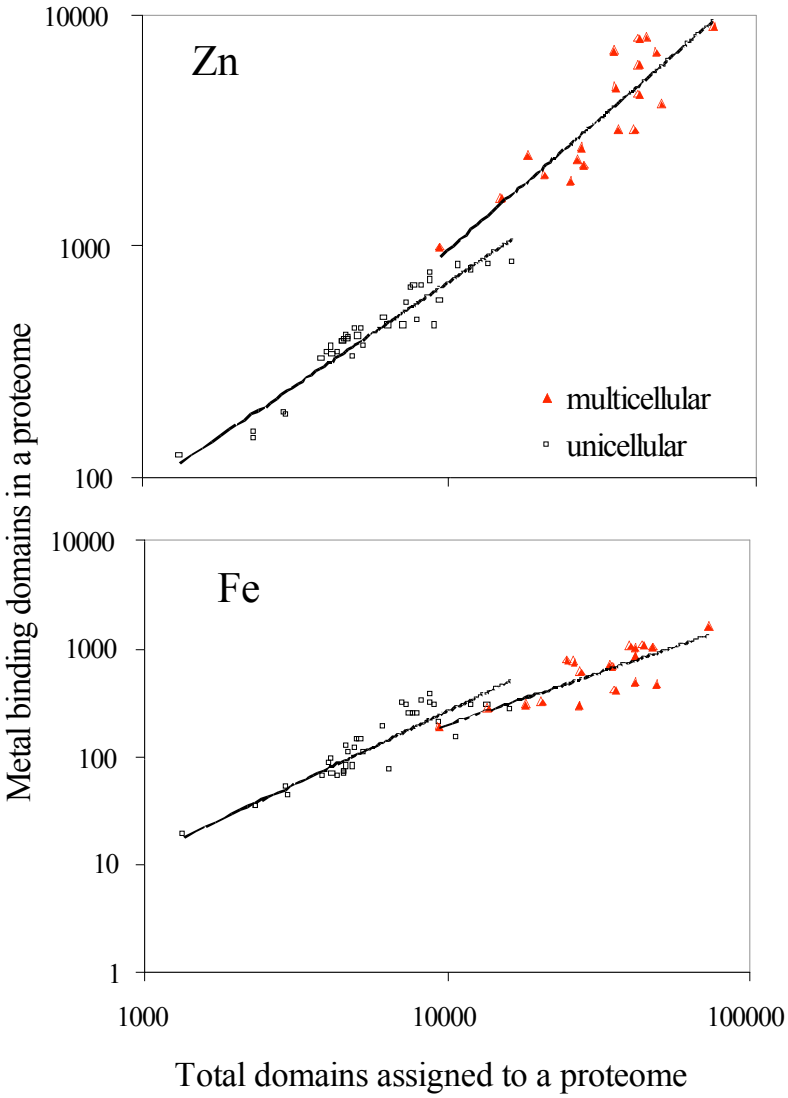

Figure 1.4: Log-Log plots of the abundance of Fe and Zn binding protein domains in Eukarya compared to total proteome size (in domains). The Eukarya were split according to cellular complexity, either being multi or unicellular. Shown are the fitted power laws for visualization.

the category is in equilibrium with proteome size, while slope greater than one indicates a preferential retainment of that catorgory during increases in proteome size (and visa versa for a slope <1). Being empirically derived from a set of modern proteomes that resulted from different evolutionary trajectories, these ratios appear to be independent of the mechanism of proteome evolution.

Put another way, any event that changes the size and content of a proteome adheres to a given stoichiometry defined by power laws. Given this conserved behavior, the differences between the Superkingdoms are compelling. The power law slopes for Fe, Mn, and Co/B_{12}-binding FFs within the proteomes of Bacteria and Archaea are greater than or equal to one, but less than one for Eukarya (Fig. 1.3B). This trend is reversed for the abundance of Zn-binding domains, with the Eukarya having a power law slope of greater than one and the Prokaryotic proteomes exhibiting slopes less than or equal to one (Fig. 1.3B). Notably, there appears to be an inflection point in the Eukarya between unicellular and multicellular organisms (Fig 1.4), but more complete proteomes are needed to robustly test this relationship.

The observed scaling is not due to a core set of abundant metal-binding proteins within a given Superkingdom– individual species have drawn broadly and diversely from the pool of available metalloproteins. That is, very few metal-binding domains are ubiquitous, or found within all the proteomes of a Superkingdom, yet many are present in at least one proteome (e.g. Fig. 1.5 for the

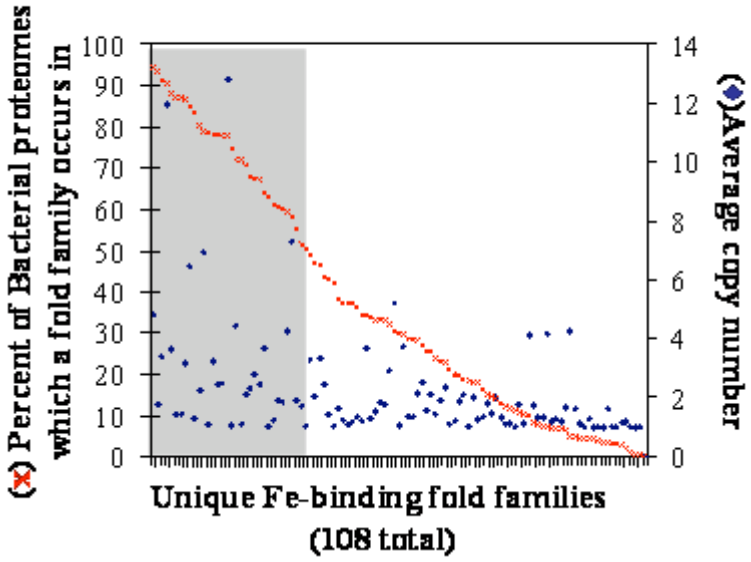

Figure 1.5: Diversity and abundance of Fe-binding fold families in Bacteria. For each Fe-binding fold family (tick marks on X-axis), the red x (left axis for scale) shows the percentage of proteomes that it occurs in, while the blue □ (right axis for scale) shows the average copy number in proteomes where it does occur. The shaded area highlights the number of fold families that occur in at least 50% of the Bacterial proteomes examined. Similar trends are observed for the other metals and Superkingdoms.
case of Fe in Bacteria). Additionally, structural domains found in all or

‘

most of the proteomes are not necessarily more abundant in those proteomes than structural domains found in only a few proteomes (Fig. 1.5). Essentially, different organisms have different metal-binding domains, a logical extension of the results of Yang et al. (205), yet the total abundances of Fe, Mn, Zn, or Co-binding domains within a proteome conform to fundamental constants defined by power laws. It appears that methodological limitations, including proteome coverage and sampling bias, do not contribute to the observed trends. According to Superfamily (74), on average, 55% of Archaeal and Bacterial proteomes, and 40% of Eukaryotic proteomes have fold families assigned. While this coverage may seem limiting, results from the Protein Structure Initiative suggest that approximately 90% of this unannotated space is comprised of variants of already discovered fold families (36), and that only 10% of the undiscovered fold families will actually be metal-binding (170). It appears that membrane proteins are similarly distributed, with the most abundant membrane folds being already described (135). Essentially, it seems unlikely that a new protein fold family will be discovered that is abundant enough to overly skew the observed results.

A further concern is that the observed results are biased by the available whole genomes. The Archaea sequenced are mostly thermophiles from anoxic environments (though this potentially provides a modern day glimpse into ancient bioinorganic chemistry), while the sequenced Eukarya are almost entirely aerobic. The dataset does include the Eukaryotic anaerobic amitochondritic parasite

Encephalitozoon cuniculi, which has metallomic features typical of aerobic Eukaryotes. In contrast, the analyzed Bacteria are from a broad array of environments and have a variety of oxygen tolerances, and therefore can be used to gain a preliminary understanding of the influence of modern environment and metabolism on metallomic content. Surprisingly, within the Bacterial Superkingdom, differences in oxygen tolerance do not seem to influence the proteomic abundance of metal binding domains (Fig. 1.6). Instead, Phylum or Classes roughly group together (Fig. 1.7), implying that the observed stoichiometries are vertically inherited. Future work will explore the causes of the non-size-dependent variance within the data (less than 10%, Table 1.2). Additionally, more genome and proteome sequences will allow for a continued updating of these results, with the proteomes of aerobic Archaea and anaerobic Eukaryotes providing key tests.

Accepting that the data are not limiting, the critical question remains as to the source of the Superkingdom level differences in the power law slopes. It seems reasonable to assume that the observed power law slopes are determined by selective pressure (188), and that trace metal bioavailability can produce such pressure (198). Hence, we hypothesize that the environmental bioavailability of trace elements during major periods of phylogenetic diversification shape the evolution of vertically inherited metal homeostasis systems that then continually influence the retention and loss of genetic material. The differences in the power

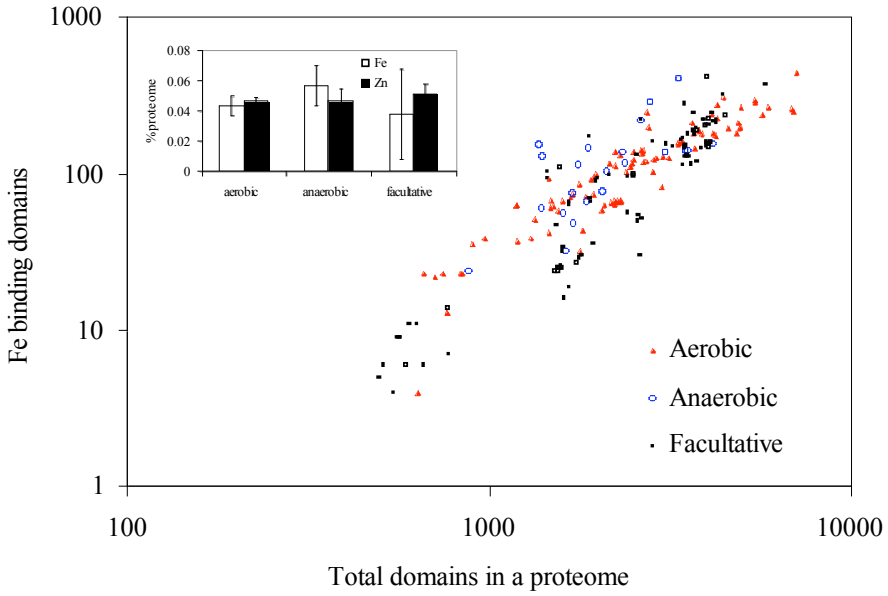

Figure 1.6: Log-Log plot of the abundance of Fe-binding domains versus total number of domains assigned to a give proteome in aerobic, anaerobic, and facultative Bacteria. The inset shows the average percentage of a proteome in each of the groupings of Bacteria that binds Fe. In general, the oxygen tolerance does not create any cohesive groupings within the scatter. Similar plots and trends are observed for Mn, Co, and Zn.

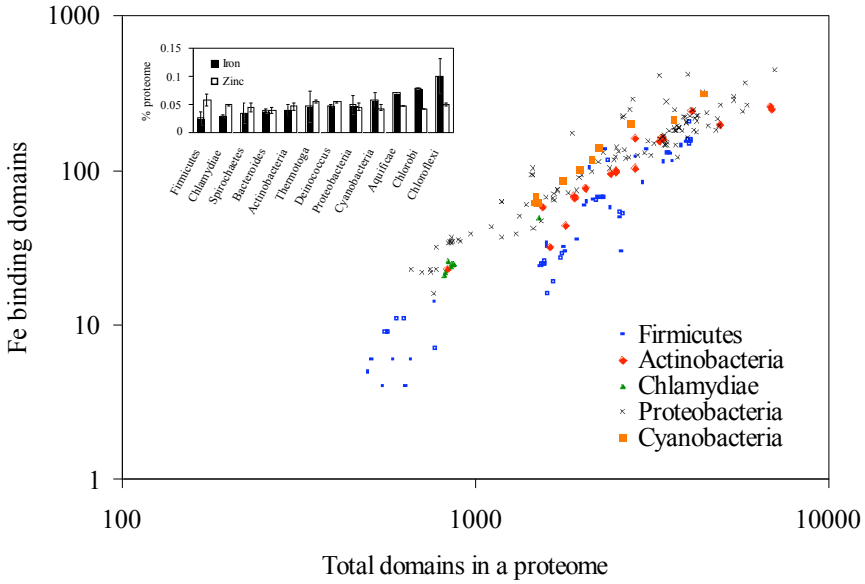

Figure 1.7: Log-Log plot of the abundance of Fe-binding domains versus total number of domains assigned to a give proteome in phylum level groupings of Bacteria. The inset shows the average percentage of a proteome in each of the groupings of Bacteria that binds Fe. Here, as opposed to Fig. 1.5, groupings are relatively apparent (note Firmicutes being offset downward). Similar plots and trends are observed for Mn, Co, and Zn. Some Phylum were not plotted due to the lack of numerous representative proteomes.

law scaling for metal-binding structures within Prokayotic and Eukaryotic proteomes are similar to the shifts in trace metal bioavailability caused by increasing oxygen, implying that Prokaryotic and Eukaryotic organisms diversified in anoxic and oxic environments, respectively. The proposed theory entails a closed feedback loop, whereby a biological phenomenon (cyanobacterial production of oxygen) incites a shift in trace metal geochemistry that in turn influences the evolution of bioinorganic chemistry. An alternative theory is that the observed differences between the Prokaryotes and Eukaryotes are due to an unknown but environmentally unrelated phenomenon. To address this possibility we further examined the functions and structures of Zn and Fe-binding proteins for environmentally consistent signals.

As stated, Eukaryotic and Prokaryotic proteomes show significant differences in the abundance of Zn-binding domains. These are wholly attributable to structures in the "small protein" structural class (Fig. 1.8A), typified by small Zn binding domains such as Zn fingers and RING domains involved in protein-DNA/RNA interactions and protein-protein interactions, respectively. Eukaryotic proteomes also encode for a greater structural diversity of "small protein class" fold familes that bind Zn (Fig. 1.8B), a noteworthy radiation in the diversity and usage of Zn within proteins, one which is predominantly structural. Most of the "small protein" class Zn-binding protein fold families are unique to Eukarya, though significant subset is shared with Archaea (Fig. 1.8B). As Zn concentrations would

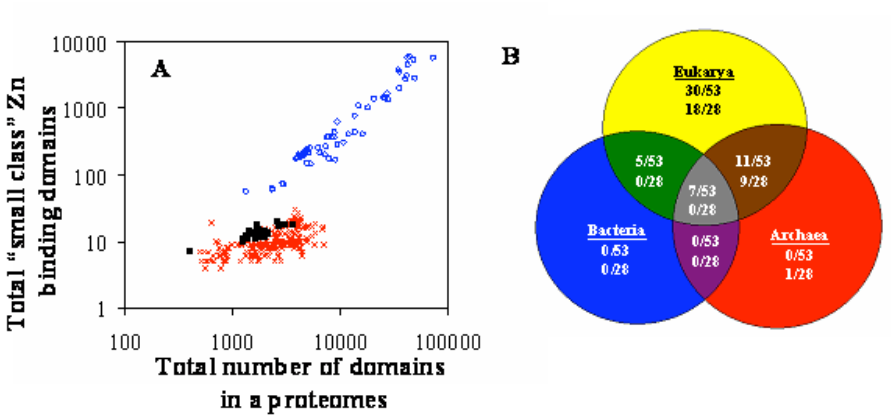

Figure 1.8: The abundance and diversity of "small protein" class Zn-binding structures. Panel A: Log-log plot of the abundance of Zn-binding domains belonging to the the "small protein" structural class in proteomes of Archaea, Bacteria, and Eukarya (symbols are the same as in Fig. 1.2). Panel B: The phylogenetic distribution of "small protein" class Zn binding fold families. There are 53 distinct "small protein" class Zn-binding fold families that occur in at least one proteome and the distribution of these is described by the top set of numbers in each set. The bottom numbers of each set detail distribution of fold familes that occur in at least 50% of the proteomes of a Superkingdom (28 "small protein" class Zn-binding fold families occur in at least 50% of the proteomes of at least one Superkingdom).

Table 1.3: The function and structure of abundant Fe-binding domains in each Superkingdom. The seven most abundant fold families in each Superkingdom are listed, along with the average percent of a proteome they comprise, the mode of Fe binding, and whether oxygen is directly involved in the catalyzed reactions. The final three columns show the overall percentage of Fe-S, heme, or amino-acid binding in the Fe-binding proteome for each Superkingdom.

					Overall percent of Fe bound by		
Superkingdom	**Fold Family**	**%**	**Fe-binding**	**O_2**	**Fe-S**	**heme**	**amino**
	Cytochrome P450	0.44 ± 0.48	heme	yes			
	Cytochrome c3-like	0.13 ± 0.3	heme	no			
	Cytochrome b5	0.12 ± 0.09	heme	no			
Eukarya	Purple acid phosphatase	0.11 + 0.08	amino	no	21 +9	47 + 19	32 + 12
	Penicillin synthase-like	0.07 + 0.1	amino	yes			
	Hypoxia-inducible factor	0.07 + 0.04	amino	yes			
	Di-heme elbow motif	0.06 ± 0.01	heme	no			
	4Fe-4S ferredoxins	1.80 + 0.7	Fe-S	no			
	MoCo biosynthesis proteins	1.60 + 0.3	Fe-S	no			
	Heme-binding PAS domain	1.10 ± 1.0	heme	no			
Archaea	HemN	0.80 ± 0.20	Fe-S	1	68 ± 12	13 ± 14	19 ± 6
	α helical ferrodoxin	0.60 ± 0.16	Fe-S	no			
	biotin synthase	0.55 ± 0.1	Fe-S	no			
	ROO N-terminal domain-like	0.5 + 0.1	amino	no			
	High potential iron protein	0.38 ± 0.25	Fe-S	no			
	Heme-binding PAS domain	0.3 ± 0.4	heme	1			
	MoCo biosynthesis proteins	0.21 ± 0.15	Fe-S	no			
Bacteria	HemN	0.2 +0.15	Fe-S	no	47 + 11	22 + 12	31 + 16
	4Fe-4S ferredoxins	0.2 + 0.2	Fe-S	no			
	cytochrome c	0.14 + 0.2	heme	no			
	α helical ferrodoxin	0.12 ± 0.09	Fe-S	no			

1. Some, but not all, PAS domains actually sense oxygen

be vanishingly low in an anoxic or euxinic environment (162, Fig. 1.1), it seems unlikely that such a diversification in the biological usage of Zn could a occur under such conditions.

The functions and structures of the prevalent Fe-binding domains in each Superkingdom also are consistent with the evolution of Eukarya in an oxic environment. Fe-binding FFs were characterized according to the mode of Fe binding (Fe-S, heme, or direct amino acid) and the abundances of these binding forms were quantified for each Superkingdom (Table 1.3). Archaeal and Bacterial metallomes have significantly more Fe-S proteins and fewer heme proteins than the Eukaryotic metallomes (Table 1.3). Both the observed Fe-S clusters and hemes function in e^- transfer reactions, but Fe-S clusters are oxygen sensitive and have more negative reduction potentials than heme-based Fe proteins such as cytochromes (105). The proteomes of aerobic Bacteria also contain fewer Fe-S clusters and more hemes than anaerobic Bacteria, suggesting that the actual repertoire of metalloproteins within the constrained totals may partially reflect physiological adaptions in addition to evolutionary history. Functionally, the most abundant Fe-binding domains in Archaea and Bacteria are involved in electron transfer, vitamin/cofactor biosynthesis, or dissolved gas sensing, with most of the catalyzed reactions excluding oxygen (Table 1.3). In contrast, the prevalent Eukaryotic Fe-binding domains catalyze a wide variety of mostly oxygen-dependent interactions, with the abundance of the hypoxia induction factor proteins

being particularly telling (Table 1.4). Note that some of the "non-O_2" domains do participate in O_2-dependent pathways, but that they do not actually contact oxygen. As structural protein domains can make diverse combinations (6), we feel that the direct interaction with O_2 is more pertinent to the issue at hand than a downstream or upstream interaction.

Evidence from the chemical fossil record and phylogenetic studies also corroborates the idea that the Prokaryotic and Eukaryotic Superkingdoms arose separately in anoxic and oxic environments, respectively. The Bacterial and Archaeal Superkingdoms certainly had undergone extensive diversification prior to the emergence of oxygenic photosynthesis (204). Eukaryotic-specific lipid biomarkers (which notably require oxygen to synthesize) have been found in rocks from 2.7 Gyr ago (23), while molecular clock studies date the early diversification events of Eukarya to the late Proterozoic (0.9-1.2 Gyr ago, 52). The deep ocean was potentially anoxic or euxinic during both of these periods (5), which has been used by some to argue that Eukarya evolved and diversified in anaerobic environments (180). This is contrary to the theory proposed by Anbar and Knoll that low Cu and Mo bioavailability in a euxinic ocean limited Eukaryotic diversification (5). Our results support the latter hypothesis that oxygen-induced changes in trace metal bioavailability occurred prior to the diversification of Eukarya and implicate Zn as another relevant metal. The fossil record indicates early evolutionary radiations of Eukarya likely occurred in shallow coastal

environments (88, 97), where a combination of high oxygen concentrations and a terrestrial supply of trace metals may have increased the bioavailability of Zn, Cu, and Mo. Note that while oxic microenvironments may have existed in the surface ocean since the advent of oxygenic photosynthesis, the supply of trace metals to these microenvironments would be unchanged until the oxygenation of deep waters, in contrast to coastal environments.

The idea that the rise in oxygen affected the usage of trace metals was originally proposed by Williams and Frausto da Silva, and a few studies have used sequence-based methods to study the co-evolution of biology and geochemistry. Morgan et al. (127) found that Eukarya have a higher diversity and abundance of Ca^{+2}-binding protein sequence families. Zerkle et al. (208) examined the distributions of open reading frames annotated as known metal binding proteins within the genomes of Prokarya, finding differences based upon metabolism and phylogeny. The analysis conducted here expands on these theories and efforts. Within a proteome, the abundances of metal binding domains conform to a stoichiometry defined by evolutionary constants despite the wide diversity of physiologies and environments of the analyzed organisms. Further, these constants exhibit Superkingdom-specific behaviour consistent with development within anoxic versus oxic environments. It must be noted that the observed proteomic stoichiometries likely do not define the physiological metal requirements of a specific organism. Single metalloproteins can constitute a large portion of an

organism's metal usage. However, whole proteomes are less susceptible to gene acquisition events or evolutionarily recent ecological or physiological adaptations, such as those observed in coastal and open ocean cyanobacteria (143). Hence, we feel that the whole-proteome patterns observed represent a broader and more durable view into the ancient environment of the Earth than physiological quotas.

Methods

Data Sources

The Structural Classification of Proteins (SCOP) (129) provides a heirarchacal classification of all protein domains published in the Protein Data Bank (PDB)(15). Version 1.69 has sorted 70,800 domains into 945 defined folds that are assigned to 1,539 superfamilies and that are further subdivided into 2,845 families. The Superfamily database (73, 74) was the source of all domain assignments. Release 1.69 covers 313 complete genomes (23 Archaea, 233 Bacteria, and 57 Eukaryota). The Superfamily database using a hybrid approach of a hidden Markov model searching protocol and subsequent pairwise comparisons (73) employs a probability cutoff of $E = 2 \times 10^{-2}$ for identifying likely members of a group; it also provides a confidence level (in the form of an E value) for every candidate identified. As was done in Yang et al. (205), a more stringent E value cutoff of 10^{-4} was employed for the domain assignments here.

Annotation of the SCOP per metal binding

Each fold superfamily (FSF) in the SCOP database was manually examined for structures containing a covalently-bound inorganic ion. This requires examining the fold families (FF), fold domains, and specific example structures within each FSF. For a FSF or FF to be considered metal-binding, only one of the representative structures has to contain a bound metal. If all of the representative structures in a FSF or FF bind the same metal, then the family is considered unambiguous, and only these FFs were used for this study.

Automated annotations of the SCOP in this fashion are inhibited by two factors: 1) Some structures are crystallized with non-native metals 2) Some PDB data files are less thorough in the description of binding mode and domain. The manual examination procedures were simplistic; the accompanying PDB file was examined for an inorganic ion and covalent binding of that ion. Some PDB files provide metal binding information (ie. heme, amino acid, specific binding residues), and whether the metal is native or simply part of the crystallization buffer. In the cases where this was not clear, the primary literature citation was examined. Attention was also paid to which structural domains actually bind the metal. For example, there are numerous distinct FSFs and FFs that contain domains of cytochrome c oxidase in the SCOP, and each entry states "*complexed with cdl, chd, cu, cua, dmu, hea, mg, na, pek, pgv, psc, tgl, unx, zn",* yet only a

select few are Cu, Fe, Mg, or Zn binding. The FFs that unambiguously bind Fe, Zn, Mn, or Co are shown in Appendix 1.

Data management and analysis

Matrices were constructed, with each row representing a distinct species and each column representing the abundances of a specific metal-binding FF in each species. For the power law distributions in Figure 1.2 the FFs in a given proteome that unambiguously bind a metal were summed and plotted against the total number of domains assigned to that proteome (the sum of all FF assignments for a proteome). For Table 1.4, the matrices were normalized by dividing the abundances of each FF within a species by the total number of structural domains assigned to that species' proteome. These internal percentages were then averaged over the entire Superkingdom.

Power law fits were determined in Matlab. The data was log transformed and the linear fit was found using a geometric mean least squares fitting technique. Groupings of points were compared using ANCOVA (aoctool function in Matlab). Slopes were compared using the multicompare function. Power law fit qualities (F-values, Table 1.3) were determined using the method of van Nimwegen (2006). Briefly, the data was log transformed. The distance from each point (defined by x_i, y_i) to the center of the scatter (D_c) is determined by D_c= square root ((x_i – mean of all x)^2 + (y_i- - mean of all y)^2). Then the distance of each point to the fitted line

(D_l) is determined by $D_l = \sqrt{((y_i - mx_i - b)^2 / (m^2 + 1))}$, where m and b equal the power law slope and intercept. Then the fraction of the variance explained by the data is given by $F = 1-(\Sigma (D_l)^2) / (\Sigma (D_c)^2)$.

Acknowledgements

Chapter 1, in full, is a reprint of the material as it appears in the Proceedings of the National Academy of Sciences, volume 103, pages 17822-17827. Song Yang, Brian Palenik, and Philip Bourne were co-authors. The dissertation author was the primary investigator and first author.

CHAPTER 2

Diversity, function, and evolution of genes coding for putative Ni-containing superoxide dismutases

Abstract: We examined the phylogenetic distribution, functionality, and evolution of the *sodN* gene family, which has been shown to code for a unique Ni-containing isoform of superoxide dismutase (Ni-SOD) in *Streptomyces*. Many of the putative *sodN* sequences retrieved from public domain genomic and metagenomic databases are quite divergent from structurally and functionally characterized Ni-SOD. Structural bioinformatics studies verified that the divergent members of the *sodN* protein family code for similar 3-D structures and identified evolutionarily conserved amino acid residues. Structural and biochemical studies of the N-terminus "Ni-hook" motif coded for by the putative *sodN* sequences confirmed both Ni (II) ligating and superoxide dismutase activity. Both environmental and organismal genomes expanded the previously noted phylogenetic distribution of *sodN*, and the sequences form 4 well-separated clusters, with multiple subclusters. The phylogenetic distribution of *sodN* suggests that the gene has been acquired via horizontal gene transfer by numerous organisms of diverse phylogenetic background, including both Eukaryotes and Prokaryotes. The presence of *sodN* correlates with the genomic absence of the gene coding for Fe-SOD, a structurally and evolutionarily distinct isoform of SOD. Given the low levels of Fe found in the marine environment from where many sequences were attained, we believe that the replacement of Fe-SOD with Ni-SOD may be an evolutionary adaptation to reduce iron requirements.

Introduction

The invention of oxygenic photosynthesis prompted an explosion of enzymatic and proteomic innovation (151). While O_2 provides a superior terminal electron acceptor for energy generation, the free radical superoxide (O_2^-) generated by electron transfer reactions is also very toxic. As such, superoxide dismutase (SOD), an enzyme that catalyzes the dismutation of superoxide into molecular oxygen and hydrogen peroxide, became an indispensable enzyme for aerobic organisms (69). SOD shuttles electrons to and from superoxide molecules to molecular protons and to date are metalloproteins with a redox-active metal. SOD isoforms are classified according to the redox metal in the active site, which includes Mn, Fe, Cu (with a structural Zn ion), and Ni. The first three isoforms, which form two sequence families, have been studied extensively, and much is known of their structure, phylogenetic distribution, and cellular localization (69, 121, 200).

Structurally, Ni-SOD folds as an up-down four α-helix bundle, with a Ni-binding catalytic site called a "Ni hook" at the N terminus. (12, 203) The N-terminus also includes a pro-sequence directly upstream of the Ni-binding site that must be cleaved by a signal peptidase-like protein for functionality (58, 93). Upon cleavage of the pro-sequence, the "Ni hook" motif (HCXXPCGCT according to Barondeau et al. 2003) binds Ni either as Ni (II) or Ni (III), allowing the enzyme to

be poised for the oxidation or reduction of superoxide radicals. Ni (II) is bound in a square planar fashion with two sulfur (both Cys side chains) and two nitrogen (N terminal amine, His-Cys amide) ligands, while Ni (III) is bound in a square pyramidal format with the aforementioned ligands and the imidazole side chain of His (12, 203).

Ni-containing SODs were originally isolated from the cytoplasm of *Streptomyces seoulensis* (206, 207), with recent data confirming a structure distinct from the other isoforms (12, 39, 203). The presence of putative *sodN* genes in the genomes of the ubiquitous marine cyanobacteria *Synechococcus* and *Prochlorococcus* (139) and the psychrophilic γ-Proteobacterium *Colwellia psychrerythraea* (120) has been noted, yet the environmental and phylogenetic scope of *sodN* is unknown.

Taking advantage of the wealth of public domain genomic data, including the Sargasso Sea metagenome (190), the phylogenetic distribution the *sodN* gene family was studied. The structural evolution of the proteins coded for by the putative *sodN* genes was studied using structural predictions and site specific evolutionary conservation. Functionality was verified using a recently developed maquette system (168), where polypetide sequences of the predicted N-terminus mimic the metal binding and functionality of the entire protein. Finally, we studied the phylogeny and possible evolution of the *sodN* family.

Results

Overview of the data set

Forty-three putative *sodN* sequences were found in the fully sequenced genomes of model organisms. Another forty-one sequences were obtained from the Sargasso Sea metagenome (190). Four additional sequences were obtained from the Sargasso Sea metagenome but were excluded for either lacking the metal-binding residues or being much shorter than the other sequences. One full sequence was obtained from the δ-1 endosymbiont assembly from the gutless worm metagenome (202). No sequences were found in the acid mine microbial consortium metagenome (187). While a host of good alignments to known *sodN* genes can be obtained from the recently deposited subset of the GOS dataset (158) and the depth dependent ALOHA-HOTS metagenomic sampling (47), most of these were only partial sequences and therefore inappropriate for the phylogenetic and structural bioinformatic analyses conducted here. The accession numbers for the *sodN* sequences used here, and where possible, *sodN* gene neighbors and the genomic presence of other isoforms of *sod* genes are listed in Table 2.1. Complete alignments of all *sodN* genes and just the genomically derived *sodN* genes were constructed and used for phylogenetic analyses.

Phylogeny of sodN

Phylogenetic trees constructed with the *sodN* sequences from model genomes revealed four well-supported clusters (clusters I-IV on Fig. 2.1). The cyanobacteria and actinomycetes formed two major clusters, with 3 and 2

Table 2.1: Information on sequences used in this study. n/a means not available.

Sequence Name	Accession number	Other SODs	Locus tag	Flank 1	Flank 2
Prochlorococcus marinus str. NATL1A	NC_008819.1	none	NATL1_17141	Ppiase (+)	peptidase (+)
Prochlorococcus marinus str. NATL2A	NC_007335.1	none	PMN2A_0861	Ppiase (+)	peptidase (+)
Prochlorococcus marinus str. MIT 9211	NZ_AALP01000001.1	none	P9211_02042	Ppiase (+)	peptidase (+)
Prochlorococcus marinus str. MIT 9515	NC_008817.1	none	P9515_14551	Ppiase (+)	peptidase (+)
Prochlorococcus marinus str. AS9601	NC_008816.1	none	A9601_14931	Ppiase (+)	peptidase (+)
Prochlorococcus marinus str. MIT 9303	NC_008820.1	none	P9303_19731	Ppiase (+)	peptidase (+)
Prochlorococcus marinus str. MIT 9301	NC_009091.1	none	P9301_14791	Ppiase (+)	peptidase (+)
Prochlorococcus marinus str. MIT 9312	NC_007577.1	none	PMT9312_1390	Ppiase (+)	peptidase (+)
Prochlorococcus marinus MED4 (CCMP1986)	NC_005072.1	none	PMM1294	Ppiase (+)	peptidase (+)
Prochlorococcus marinus MIT9313	BX548175	none	PMT0340	Ppiase (+)	peptidase (+)
Prochlorococcus marinus SS120 (CCMP1375)	AE017126	none	Pro1368	Ppiase (+)	peptidase (+)
Prochloron didemi	TIGR draft	none	n/a	n/a	n/a
Synechococcus sp. BL107	NZ_AATZ01000003.1	Cu	BL107_11116	Ppiase (+)	peptidase (+)
Synechococcus sp WH8102	BX548020	none	SYNW1626	Ppiase (+)	peptidase (+)
Synechococcus sp CC9605	NC_007516.1	Cu	Sync9605_0873	Ppiase (+)	peptidase (+)
Synechococcus sp CC9311	NC008319.1	Cu	SYNC0755	Ppiase (+)	peptidase (+)
Synechococcus sp CC9311	NC008319.1	Cu	SYNC2434	hypothetical	hypothetical
Synechococcus sp CC9902	NC_007513.1	Cu	Sync9902_1525	Ppiase (+)	peptidase (+)
Trichodesmium erythraeum IMS101	NC_008312.1	Mn	Tery_0891	hypothetical	peptidase (+)
Crocosphaera Watsonii	NZ AADV01000059	Mn	CwatDRAFT_2983	peptidase (+)	LytR (+)
Rhodopirellula baltica SH1	BX119912	Mn	RB12634	ACC	hypothetical
Desulfotalea psychrophila LSv54	NC 006138.1	Fe	DP2504	hypothetical	rpoD
Ostreococcus lucimarinus	CP000581.1	Mn, Cu	OSTLU_29162	Bol A	none
Polaribacter irgensii 23-P	AAOG01000003.1	none	PI23P_10892	Fur-like(-)	hypothetical (+)
Ostreococcus tauri	CR954201.2	Mn, Cu	Ot01g05280	BolA (+)	none
Marinomonas sp. MED121	NZ_AANE01000001.1	none	MED121_16039	hypothetical	Putative peptidase (+)
Colwellia psychrerythraea 34H	NC_003910.7	Fe	CPS_0444	hypothetical	putative peptidase (+)
Psychroflexus torquis ATCC 700755	NZ_AAPR01000012.1	none	P700755_03788	hypothetical	Putative peptidase (+)
Shewanella woodyi ATCC 51908	NZ_AAUO01000012.1	none	SwooDRAFT_1656	hypothetical	putative peptidase (+)
Marinomonas sp. MWYL1	NZ_AAVH01000005.1	none	Mmwyl1DRAFT_1406	hypothetical	putative peptidase (+)
Nocardioides sp. JS614	NC_008699.1	none	Noca_1725	Phage Integrase(-)	Peptidase (+)
Streptomyces avermitilis MA-4680	NP629400	Fe	SAV2988	Peptidase (-)	MarR
Janibacter sp. HTCC2649	NZ_AAMN01000001.1	none	JNB_07194	lipoprotein (-)	peptidase (+)
Micromonospora sp. ATCC 39149	DQ354151.1	Fe	n/a	n/a	n/a
Saccharopolyspora erythraea NRRL 2338	NC_009142.1	Fe	SACE_6419	Peptidase (-)	AraC (+)
Salinispora arenicola CNS205	NZ_AAWA01000013.1	none	SareDRAFT_3855	Peptidase (-)	Anti sigma factor
Salinispora tropica CNB-440	NC_009380.1	none	Strop_3697	Peptidase (-)	hypothetical (+)
Acidothermus cellulolyticus 11B	NC_008578.1	none	Acel_0566	Peptidase (-)	Anti sigma factor
Streptomyces coelicolor A3(2)	NC_003888.3	Fe	SCO5254	Peptidase (-)	hypothetical (-)
Streptomyces seoulensis	P80734	Fe	n/a	n/a	n/a
Frankia sp. EAN1pec	NZ_AAII01000047.1	Fe/Mn, Cu	Franean1DRAFT_3466	Peptidase (-)	acetyltransferase (+)
Mycobacterium vanbaalenii PYR-1	NC_008726.1	Cu	Mvan_5671	Peptidase (-)	hypothetical (+)
Mycobacterium gilvum PYR-GCK	NC_009338.1	Cu	Mflv_1135	Peptidase (-)	hypothetical (+)
O.algarvensis Delta1	AASZ01000981.1	Mn/Fe	gws2_d1_0038_1	Excisonase (-)	hypothetical (-)
SarSea26	AACY01468979	n/a	n/a	chaperonin	n/a
SarSea24	AACY01091612	n/a	n/a	chaperonin	corA
SarSea27	AACY01057452	n/a	n/a	chaperonin	corA
SarSea19	AACY01113625	n/a	n/a	chaperonin	corA
SarSea16	AACY01767480	n/a	n/a	chaperonin	n/a
SarSea22	AACY01000402	n/a	n/a	n/a	corA
SarSea21	AACY01140392	n/a	n/a	n/a	n/a
SarSea20	AACY01743194	n/a	n/a	n/a	n/a
SarSea25	AACY01035484	n/a	n/a	hypothetical	n/a
SarSea6	AACY01019940	n/a	n/a	signal peptidase	tRNA synthase
SarSea5	AACY01029649	n/a	n/a	signal peptidase	tRNA synthase
SarSea4	AACY01090912	n/a	n/a	signal peptidase	tRNA synthase
SarSea3	AACY01344846	n/a	n/a	n/a	tRNA synthase
SarSea1	AACY01228513	n/a	n/a	signal peptidase	n/a
SAR1Actinobacteria	AACY01074675	n/a	n/a	signal peptidase	tRNA synthase
SarSea2	AACY01569147	n/a	n/a	signal peptidase	n/a
SarSea7	AACY01521365	n/a	n/a	signal peptidase	n/a
SarSea14	AACY01650071	n/a	n/a	signal peptidase	n/a
SarSea9	AACY01731255	n/a	n/a	signal peptidase	n/a
SarSea11	AACY01130179	n/a	n/a	signal peptidase	n/a
SarSea12	AACY01659410	n/a	n/a	n/a	n/a
SarSea10	AACY01089094	n/a	n/a	Ppiase	signal peptidase
SarSea18	AACY01227969	n/a	n/a	n/a	signal peptidase
SarSea15	AACY01089661	n/a	n/a	n/a	signal peptidase
SarSea13	AACY01728750	n/a	n/a	Ppiase	n/a
SarSea8	AACY01029649	n/a	n/a	signal peptidase	n/a
SarSea17	AACY01047955	n/a	n/a	signal peptidase	n/a
SarSea48	AACY01105944	n/a	n/a	n/a	n/a
SarSea38	AACY01596105	n/a	n/a	n/a	n/a
SarSea45	AACY01463980	n/a	n/a	n/a	n/a
SarSea43	AACY01612123	n/a	n/a	n/a	n/a
SarSea44	AACY01091423	n/a	n/a	n/a	n/a
SarSea37	AACY01288536	n/a	n/a	n/a	n/a
SarSea39	AACY01382148	n/a	n/a	n/a	n/a
SarSea41	AACY01106273	n/a	n/a	hypothetical	n/a
SarSea49	AACY01111382	n/a	n/a	putative transporter	n/a
SarSea40	AACY01495770	n/a	n/a	n/a	n/a
SarSea42	AACY01478698	n/a	n/a	n/a	n/a
SarSea46	AACY01227944	n/a	n/a	hypothetical	n/a
SarSea47	AACY01094121	n/a	n/a	hypothetical	n/a

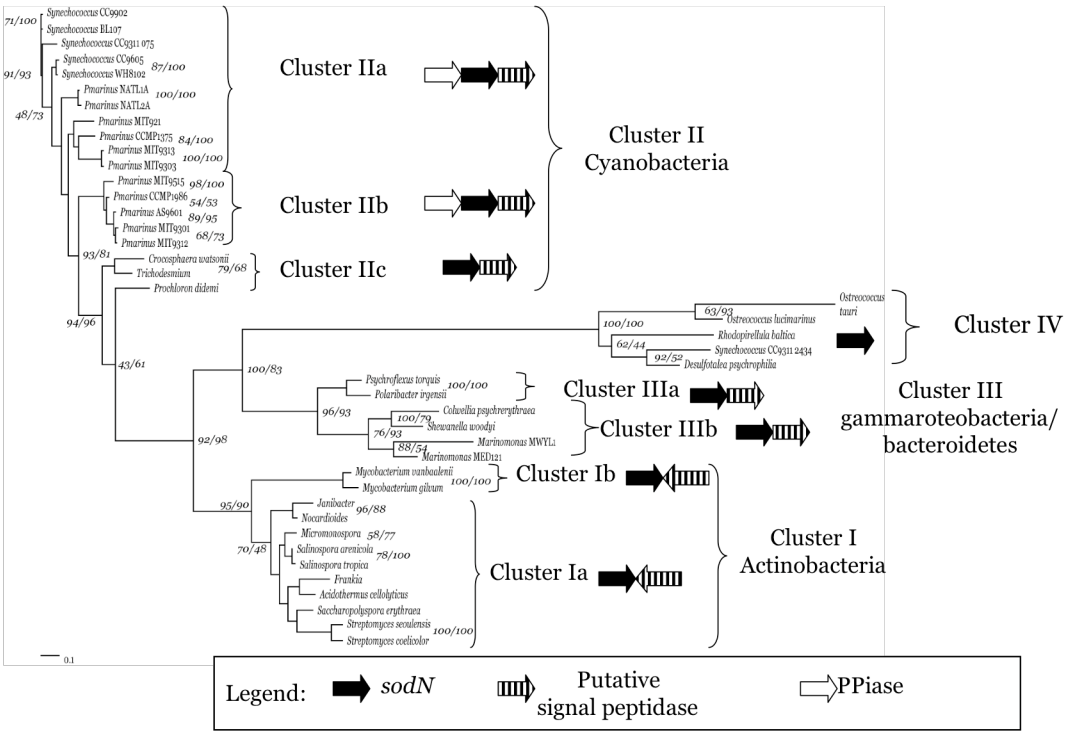

Figure 2.1: Phylogeny of *sodN* from model genomes. Shown is a neighbor-joining tree of protein sequences of *sodN* attained from sequenced genomes. Numbers at branch points indicate the bootstrap support from 100 interations of parsimony (left) and distance (right) analyses. Clusters are annotated and the conserved genomic neighborhoods are shown.

subclusters respectively (Fig. 2.1). The cyanobacteria *sodN* cluster was broken into three groups containing the low-light adapted *Prochlorococcus* and all marine *Synechococcus* (IIa, Fig. 2.1), the high-light adapted *Prochlorococcus* (IIb), and finally two diazotrophs and *Prochloron* (IIc). Cluster IIc was the most divergent, and given the branch lengths and phylogenetic distance between the representative diazotroph and *Prochloron* parent genomes, it seems likely to be subdivided with the future accumulation of more *sodN* sequences. The actinomycete sodN sequences branched into two subclusters, one containing two *sodN* sequences from *Mycobacterium* (Ib) and the other containing the remaining sequences (Ia, Fig. 2.1). A third cluster included two subclusters containing *sodN* sequences from gammaproteobacteria and bacteroidetes, respectively (IIIa and IIIb, Fig. 2.1). Within clusters I, II, and III, a putative signal peptidase was found adjacent to the *sodN* gene (Fig. 2.1). In clusters IIa and IIb, *sodN* genes were also neighbored by a peptidyl-proline isomerase with a putative Ni transporter (*sodT*) adjacent to the signal peptidase.

An additional, deep branching cluster on the genomic *sodN* tree contained sequences from phylogenetically distant bacteria, including planctomycetes, cyanobacteria, and deltaproteobacteria (IV, Fig. 2.1). Curiously, the *sodN* sequences from two species of the marine Eukaryote prasinophyte *Ostreococcus* formed a separate subcluster within cluster IV (Fig. 2.1). In addition to the incongruent phylogeny of the model organisms within this cluster, neighboring

genes were not conserved (Table 2.1), suggesting that horizontal gene transfer may be responsible for this grouping. Consistent with this, two *sodN* sequences were found in the genome of *Synechococcus* CC9311, one with a "cyanobacterial" phylogeny (CC9311_SYNC0754, Cluster IIa, Fig. 2.1) and gene neighborhood (Table S1), and another phylogenetically divergent gene (CC9311_SYNC2458, Cluster IV, Fig. 2.1) with an abnormal gene neighborhood found in a putative genomic "island" of recently acquired open reading frames with divergent %GC and GC-skew compared to the genome averages (142).

A consensus phylogeny of *sodN* protein sequences from both metagenomic and genomic sequences provided further insight into the phylogenetic distribution of *sodN* (Fig. 2.2). The *sodN* genes from the Sargasso Sea (SarSea#) metagenome fell into three categories: 1) Sequences within already defined phylogenetic clusters from model genomes, 2) Sequences forming new clusters with ascribable phylogeny, and 3) sequences with unassignable phylogeny. Within category 1, eleven SarSea sequences grouped closely with *sodN* sequences from marine *Prochlorococcus* and *Synechococcus* (IIa and IIb, Fig. 2.2), while another SarSea sequence clustered with the two *sodN* sequences from *Ostreococcus*. The SarSea sequences associated with the cyanobacterial cluster were contained within contigs containing genes with sequence similarity to the signal peptidases, peptidyl proline isomerases, and Ni transporters found in the genomes from model cyanobacteria (Fig. 2.2), suggesting that the genomically characterized *sodN*-utilizing marine

Figure 2.2: Phylogeny of all *sodN*. Shown is a neighbor-joining tree of protein sequences of *sodN* attained from both sequenced genomes and metagenomic datasets. Numbers at branch points indicate the bootstrap support from 100 interations of parsimony (left) and distance (right) analyses. Not all bootstrap values are shown for clarity, though major branch points are annotated. Stars indicate new clusters, for which the conserved genomic neighborhoods are shown.

cyanobacteria are indeed representative of the natural cyanobacteria populations. The similarity of various *Synechococcus, Prochlorococcus,* and *Ostreococcus* genomic sequences to sequences within the Sargasso Sea metagenome has been noted previously (140, 158, 190), and the results presented here are consistent with those findings.New clusters where phylogeny could be assigned (category 2) with reasonable confidence were observed twice. Seven SarSea sequences formed a new subcluster close to the Actinomycetes *sodN* sequences (Ic, Fig. 2.2). One of the *sodN* genes from cluster Ic was found in a large scaffold designated SAR1-Actinobacteria by Venter et al. (190), due to the presence of typical marker genes. The *sodN* genes from the genomic and the SarSea actinomycetes are clearly genetically distinct, as is the genomic architecture near *sodN* (Fig. 2.1 and 2.2), therefore we believe that this cluster likely represents *sodN* sequences from a group of marine actinomycetes for which an applicable reference genome is not yet available.

Another subcluster formed near the *sodN* sequences from gammaproteobacteria and bacteroidetes (IIIc, Fig. 2.2). One of the *sodN* genes in subcluster IIIc (SarSea19) was part of a large multi-gene contig that contained a putative gene for the ribosomal protein S16. Phylogenetic analysis of S16 sequences from the SarSea19 contig and numerous bacterial genomes places the unknown S16 sequence amidst gammaproteobacteria (not shown). Therefore, we propose that this cluster is composed of yet-unsequenced gammaproteobacteria.

The gene neighborhood of the cluster IIIc *sodN* genes was conserved and included a putative metal transporter unrelated to the cyanobacterial *sodT* and a chaperone protein (Table 2.1).

Several SarSea *sodN* genes were only loosely associated with cluster IV, which has an unassignable phylogenetic origin (cluster IV, Fig 2.1 and 2.2). The cluster IV *sodN*-containing SarSea contigs were often short enough to only contain one open reading frame, but those that did had different flanking genes (Table 2.1). The *sodN* sequence obtained from the Gutless worm deltaproteobacterial symbiont genome assembly also grouped within this cluster. We have already hypothesized that this cluster to be the result of relatively recent horizontal gene transfers, and the metagenomic data is consistent with this. The loose but poorly supported association of SarSea8 and SarSea17 with cluster IIc further supports the conclusion that this group cyanobacterial *sodN* may be more diverse than previously known.

Structure and function of putative sodN genes

The *sodN* gene codes for a protein that requires post-translational removal of several amino-acid residues from the N-terminus (93), therefore it was not surprising to find a signal peptidase co-localized with *sodN* in many of the analyzed sequences (Fig. 2.1, 2.2). However, the pro-sequence was quite variable in length and content and therefore difficult to align. This region was removed, starting each

sequence with the metal-binding sequence HCXXC. An alignment of all sequences is included in the supplementary material.

Some of the sequences are quite similar to the structurally characterized *Streptomyces sodN,* but others are less than 30% similar, precluding the assumption of structural similarity based on sequence similarity alone (155). The metal binding and catalytic site is conserved, but to further test the plausibility of our putative *sodN* sequences, a homology modeling and similarity search was performed using PHYRE, a fold recognition and prediction server based upon 3D-PSSM (92). Using representative sequences from each of the phylogenetic clusters of *sodN*, 3-D structures were predicted. For nearly all of the putative *sodN* sequences, the sequence and predicted secondary structures could be aligned to the *Streptomyces* Ni-SOD satisfactorily (Fig. 2.3). The general changes observed were extensions of the loop between α-helices 1 and 2 (Fig. 2.3). Another change observed is an extension to the C-terminus following the end of α-helix 4 (Fig S2), particularly in cluster III where a proline-rich, presumably disordered, C-terminal tail is observed (Fig 2.3). The sole structure that could not aligned with acceptable RMSD values was the *sodN* sequence from *Ostreococcus tauri*, which appears to lack α-helices 3 and 4 (Fig. 2.3). It is unclear what this means for functional SOD activity, as it does retain a "Ni hook" motif.

Using the alignment and phylogeny generated here we studied the evolutionary conservation of specific amino acid residues in the originally solved

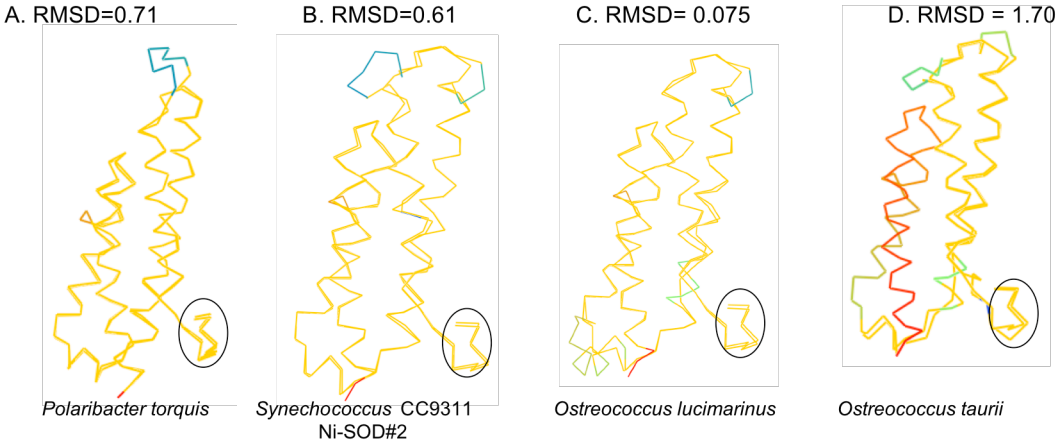

Figure 2.3: The structures of Ni-SOD proteins coded for by *sodN* genes of novel phylogeny were predicted and structurally aligned with the experimentally determined structure of Ni-SOD from *Streptomyces* (PDB id: 1t6u). Gold indicates a close alignment, blue and green indicate new loops or turns, red and orange indicate extensions or major deviations, and the overall root mean square deviation in angstroms between the two structures is noted. All of the predicted structures have minor changes in turn structures but close alignments in the Ni-binding functional site, which is circled. The Ni-SOD from the proteorhodopsin-containing *Polaribacter torquis* (A) has a unique glycine-rich C-terminus extension. A unique C-terminus extension is also observed in a Ni-SOD recently acquired by horizontal gene transfer is *Synechococcus* CC9311 (B), which has additional Ni-SOD similar to ones typically found in cyanobacteria. The Ni-SOD structure from the first *sodN* gene observed in a Eukaryote, *Ostreococcus lucimarinus,* aligns exceptionally well with the *Streptomyces* Ni-SOD (C) despite being only 13% identical at the amino-acid level. Curiously, the Ni-SOD from the closely related species of the same genus, *Ostreococcus tauri,* does not align well to the *Streptomyces* structure (D), suggesting a possible loss in function.

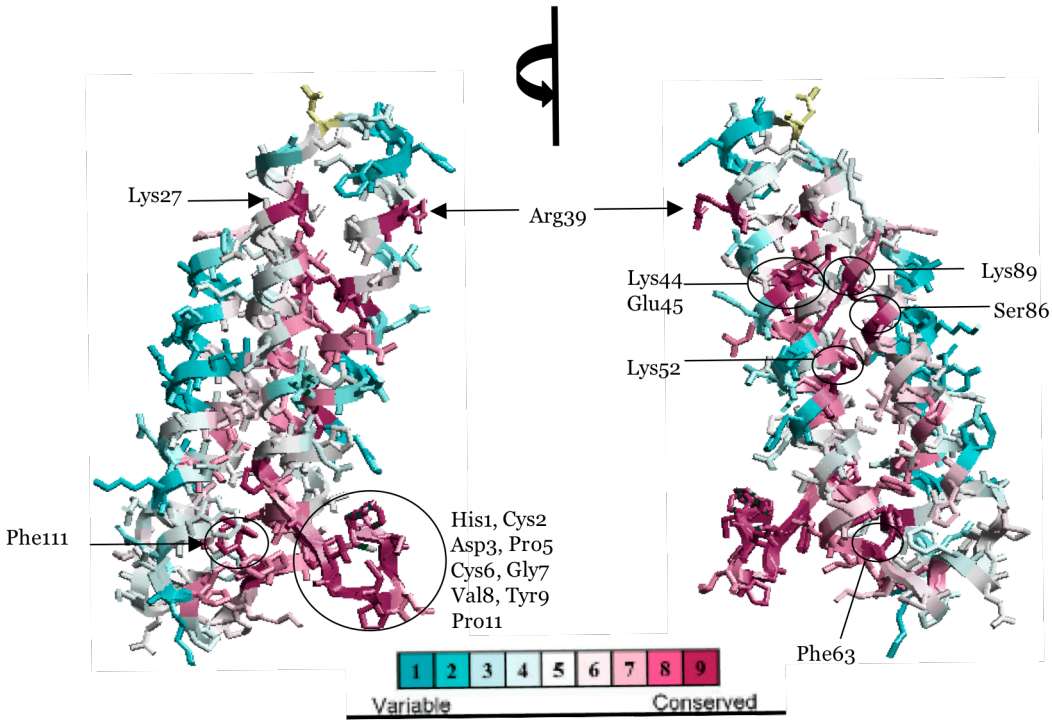

Figure 2.4: Evolutionary conservation specific residues of Ni-SOD. Using the alignment and phylogeny generated here, the conservation of the amino-acid residues in the *Streptomyces* Ni-SOD structure (pdb id: 1t6u) were calculated using CONSURF and then visualized on the 3D structure using RASTOP. The most conserved amino acid residues are annotated.

structure from *Streptomyces* using CONSURF (102). This information is displayed in Figure 2.4. Magenta colored residues are chemically conserved across the entire gene family while blue residues are variable. Yellow indicates residues where a conservation level could not be confidently assigned. Many of the residues in the "Ni-hook" motif were strongly conserved across the entire gene family (CONSURF score of 9, Fig. 2.4). However, several other residues also had CONSURF scores of 9, including Lys27, Arg39, Lys44, Glu45, Lys52, Phe63, Ser86, Lys89, Phe111. Of these, Arg39, Glu45, Lys52, Ser86, and Lys89 are important for the formation of the native hexamer structure, Phe63, Phe111, and Lys89 contribute to the tertiary folding, and Lys27 is involved in electrostatic guidance (12, 203). All three Lys residues (27, 64, and 115) believed to form a superoxide electrostatic guidance site are well conserved (CONSURF scores of 9, 7, and 8 respectively). Several residues not previously implicated in either tertiary or quaternary structure or electrostatic guidance with CONSURF scores of 8 include Ala18, Ser20, Val24, Arg47, Ala51, Asn79, Gly90, and Ile107. Most of the residues that were variable in the database assembled here are on the outside surface of protein, which faces away from the active site (Fig. 2.4).

Barondeau et al. (12) proposed that the N-terminus "Ni-hook" motif (HCXXPCGXY) provides a diagnostic for Ni-SODs. Recently, it was shown that the Ni (II)-metallated "Ni-hook" polypeptide mimics Ni-SOD function and structure (132, 168), providing a powerful tool to study the functionality of the

putative *sodN* genes found in our assembled database. The multiple sequence alignment was employed to screen for phylogenetic variations of the "Ni-hook" motif. Without exception, the Ni-ligating residues His-1, Cys-2, and Cys-6 are conserved, while phenylalanine replaces Tyr-9 in only one sequence found in Cluster IV. Many deviations from the *Streptomyces* "Ni hook" motif were phylogenetically consistent. Asp-3 in *Streptomyces* is replaced by glutamine in all of the putative *sodN* sequences found within cluster IV, except in the gutless worm endosymbiont where it is replaced by glutamate. Gly-7 is replaced by either alanine or lysine in all of the cluster IIIa and IIIc *sodN* sequences. Val-8 is replaced by isoleucine in several sequences within clusters III and IV. In the two *sodN* sequences from *Mycobacterium* (cluster Ib, Fig. 2.1), Pro-5 is replaced by either tyrosine or phenylalanine.

Several metalloprotein maquettes based on the Ni-binding hook (Ni binding form designated [Ni(SOD^{M1})]; where the peptide sequence SOD^{M1}: NH_2–HCDLPCGVYDPA-COOH is from the well characterized *Streptomyces* Ni-SOD) (168) were constructed and characterized to probe the influence that the observed changes to the non-ligating residues has on the structure and SOD activity of the resulting maquette (Table 2.2). The new maquettes have single amino-acid changes in the parent maquette SOD^{M1}; Asp3Gln indicates that the Asp-3 in the SOD^{M1} sequence is replaced by a glutamine and the Ni-binding form of this maquette would be [Ni(SOD^{M1}D(3)G)]. The SOD^{M1} derivatives Asp3Gln, Gly7Lys,

Table 2.2. Summary of the preparation of peptide maquettes and Ni (II) metallated maquettes. Shown are the names and amino acid sequences of the maquettes, as well as the calculated and ESI-MS determined mass to charge ratio (*m/z*) of the non-metallated and metallated maquettes.

		Non-metallated ESI-MS M- ***m/z***		**Ni (II) metallated ESI-MS M-** ***m/z***	
Maquette	**Sequence**	**calculated**	**found**	**calculated**	**found**
$SOD^{M1}D(3)A$	N_2H-HCALPCGVYDPA	1245.4	1245.5	1301.2	1301.6
$SOD^{M1}D(3)Q$	N_2H-HCQLPCGVYDPA	1302.5	1302.5	1358.2	1358.7
$SOD^{M1}P(5)G$	N_2H-HCDLGCGVYDPA	1249.4	1249.4	1305.8	1305.9
$SOD^{M1}G(7)A$	N_2H-HCDLPCAVYDPA	1303.5	1303.3	1359.2	1359.2
$SOD^{M1}G(7)K$	N_2H-HCDLPCKVYDPA	1360.6	1360.6	1416.3	1416.6
$SOD^{M1}Y(9)F$	N_2H-HCDLPCGVFDPA	1273.5	1273.4	1329.1	1329.5

Table 2.3: Summary of the [$Ni^{II}(SOD^{M1}X(n)Z)$] maquette studies. All of the maquette sequences are NH_2–HCDLPCGVYDPA-COOH except for the noted amino acid changes (His is residue 1). a) λ is in nm and ε is in units of M^{-1} cm^{-1}. Only the characteristic well defined peak at ~460 nm is reported (Figure 2.4). b) This feature is a shoulder and not a well defined peak.

Maquette	**Cluster**	**λ (ε)[a]**	**SOD activity**	**Mass (GPC)**	**Ni^{II} Coordination Environment**
[$Ni^{II}(SOD^{M1}D(3)Q)$]	IV	461 (310)	0.7(1) μM	1341 Da	2 Ni-N at 1.88 Å; 2 Ni-S at 2.17 Å
[$Ni^{II}(SOD^{M1}D(3)A)$]	n/a	469 (273)	1(1) μM	1362 Da	2 Ni-N at 1.87 Å; 2 Ni-S at 2.18 Å
[$Ni^{II}(SOD^{M1}P(5)G)$]	n/a	412 (284)[b]	n/a	2710 Da	3.5 Ni-N at 1.98 Å; 0.5 Ni-S at 2.28 Å
[$Ni^{II}(SOD^{M1}G(7)A)$]	IIIa/c	462 (299)	2(1) μM	1386 Da	2 Ni-N at 1.91 Å; 2 Ni-S at 2.17 Å
[$Ni^{II}(SOD^{M1}G(7)K)$]	IIIa/c	472 (277)	1(1) μM	1398 Da	2 Ni-N at 1.88 Å; 2 Ni-S at 2.18 Å
[$Ni^{II}(SOD^{M1}Y(9)F)$]	IV	458 (285)	1(1) μM	1312 Da	2 Ni-N at 1.92 Å; 2 Ni-S at 2.17 Å

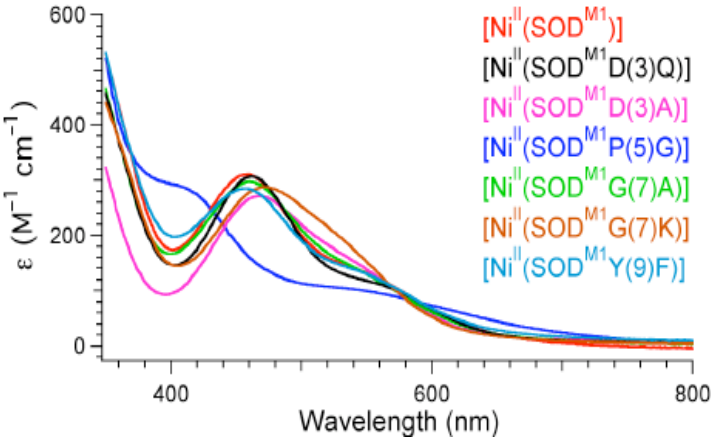

Figure 2.5: Ni (II) binding by Ni-SOD maquettes. Electron absorption spectroscopy of Ni binding is shown for each of the maquettes detailed in Table 2.2.

Gly7Ala, and Tyr9Phe were synthesized to examine the structure of the Ni-binding site and SOD activity of the non-functionally characterized *sodN* sequences comprising clusters III and IV. The extended alignment also provides putative targets in the identification of structurally important residues beyond those that bind Ni. For example, Pro5 is entirely conserved in the alignment except within *Mycobacterium*, yet the structural importance of this residue is unknown, therefore the SOD^{M1} derivative Pro5Gly was prepared. Similarly, the Asp3Ala derivative was constructed to examine the possible importance of charge of this residue, which is either acidic or basic in the entire alignment, by providing a neutral side chain.

Electronic absorption spectroscopy was used as an initial probe to determine the Ni^{II} coordination environments provided by the maquettes (Figure 2.5, Table 2.3). [$Ni(SOD^{M1})$] is characterized by ligand-field bands at 552, 458, and 337 nm (132, 168). The band at 458 nm is characteristic of the N_2S_2 coordination environment provided by [$Ni(SOD^{M1})$], and is therefore diagnostic of changes to the Ni^{II} coordination environment (65, 101, 167). We found that most of the maquettes investigated have ligand-field bands centered at ~458 nm indicating a similar N_2S_2 coordination environment. There were three notable exceptions to this: [$Ni(SOD^{M1}D(3)A)$], [$Ni(SOD^{M1}G(7)K)$], and [$Ni(SOD^{M1}P(5)G)$]. Both [$Ni(SOD^{M1}D(3)A)$] and [$Ni(SOD^{M1}G(7)K)$] displayed electronic absorption spectra reminiscent of the parent maquette [$Ni(SOD^{M1})$], but

the well defined bands at ~470 nm had red shifted into the low energy shoulders. This most likely results from an increase in the positive electrostatic charge about the Ni-center effected by the changes in these residues and not a change in the Ni^{II} ligand environment. In contrast, [Ni($SOD^{M1}P(5)G$)] displayed a well defined shoulder at ~422 nm and a very broad ill-defined shoulder in the lower energy region of the spectrum (Fig. 2.5). This strongly indicates that the Ni^{II} coordination environment in [Ni($SOD^{M1}P(5)G$)] is different than the other maquettes investigated for this study.

An extended X-ray absorption fine structure (EXAFS) analysis of the maquettes verified the above conclusions. All of the maquettes with the exception of [Ni($SOD^{M1}P(5)G$)] had two Ni-S interactions at ~2.17 Å and two Ni-N interactions at ~1.90 Å (Table 2.3). None of these nitrogen ligands were derived from the imidazole found on His1. In contrast [Ni($SOD^{M1}P(5)G$)] was best modeled by a mixed N/S ligand environment environment with less than one sulfur coordinated to each Ni-center on average. Furthermore, in order to adequately model the EXAFS region of [Ni($SOD^{M1}P(5)G$)] we had to include multiple scattering interactions due to the imidazole nitrogen from His1, indicating it is coordinated to Ni. This indicates that there is more than one species present in solutions of Ni^{II} and $SOD^{M1}P(5)G$.

Gel permeation chromatography indicated that all of the maquettes are monomeric in solution with the exception of [Ni($SOD^{M1}P(5)G$)]. We found that

the major constituent of solutions of [Ni(SOD^{M1}P(5)G)] was a species that utilizes two peptides to ligate one Ni^{II}-center (Table 2.3). This strongly indicates that the peptide SOD^{M1}P(5)G is ineffective at ligating Ni^{II} as a monomeric species, and provides the reason for the unusual mixed ligand environment (i.e. less than one sulfur per Ni^{II}) indicated by the EXAFS studies. The exact reasons for this will be the subject of a future communication focusing on the chemistry and electronic structure of these maquettes, but we speculate that the proline residue is helping to enforce the turn structure of the Ni-binding hook. Once Pro5 is deleted from the sequence the peptide cannot effectively wrap about the Ni^{II} ion and the dimeric metallopeptide is favored.

Superoxide dismutase activities were examined using a xanthine/xanthine oxidase assay (179). This is an indirect assay where xanthine oxidase produces superoxide upon xanthine oxidation, which in turn reduces the colorless compound nitro-bluetetrazolium to the blue colored compound formazan. The concentration of an SOD active compound needed to effect a 50% reduction in the rate of formazan production is the compound's IC_{50} value, therefore lower concentrations indicate a higher SOD activity. The parent maquette [Ni(SOD^{M1})] displays an IC_{50} = 0.2(1) μM (mean = 0.2, standard error = 1). We find that the maquettes investigated have IC_{50} values ranging between 0.7(1) to 2(1) μM (Table 2.3). For comparison Cu/Zn SOD displays an IC_{50} = 0.04 μM (179), while a dead catalyst can give IC_{50} values as low as 0.5 mM. Therefore all of the maquettes investigated

in this study by the xanthine/xanthine oxidase assay displayed SOD activities not significantly different from the parent maquette, which is representative of the well characterized Streptomyces Ni-SOD.

The maquettes studied here lack outer sphere interactions found in the native metalloproteins, and the results need to be treated with some caution. The strong conservation of residues interacting with the Ni-hook motif (Fig. 2.4) suggests that outer sphere differences will be minimal. It seems likely that most, if not all of the *sodN* sequences analyzed here code for a functional and properly folding Ni-containing superoxide dismutase. However, some sequence variations of the Ni-hook were not tested. It is not known if the two sequences from *Mycobacterium*, where phenylalanine or tyrosine replaces Pro-5, are functional. Also not tested was the replacement of Asp-3 with glutamate, which occurs in the *sodN* sequence from the gutless worm δ−1 endosymbiont, though the exchange of one non-ligating acidic amino acid for another seems unlikely to change the functionality of this protein.

Distribution and evolution of the sodN *gene family*

The *sodN* gene and protein family has a relatively limited phylogenetic distribution relative to other *sod* genes (results here and (25, 200)). Given the indespensible nature of SODs in a modern, O_2-rich world, the modern phylogenetic distribution of the three SOD protein families (Cu/Zn, Fe and Mn, and Ni) should

reflect that an aerobic or facultative organism must either inherit a SOD from their predecessor or acquire a replacement isoform via horizontal gene transfer. Additionally, the evolution of the physiological need for a SOD is predated, though only barely, by the evolution of oxygenic photosynthesis providing the history of this enzyme with a molecular and geologic baseline.

Multiple lines of evidence suggest that the *sodN* sequences found within cluster IV were acquired by their host genomes via horizontal gene transfer. In contrast to clusters I-III, the genomes containing cluster IV *sodNs* are from phylogenetically distant organisms, and the genomic neighborhoods within this cluster are not conserved. The observation of a putative cluster IV *sodN* gene from *Synechococcus* CC9311 with abnormal %GC and GC skew compared to the rest of the genome provides more direct evidence for horizontal gene transfer. The cluster formed by the two *sodN* sequences from *Ostreococcus* was likely the result of a horizontal transfer (and retention) prior to the diversification of the two strains, as the genes are found in a syntenic region of chromosome 1 (140). The lack of a close phylogenetic relationship between the *sodN* genes from modern cyanobacteria and *Ostreococcus* suggests that the original source of the *sodN* gene was not horizontal transfer from the plastid, but more likely, a Bacterium. The closely related green alga, *Chlamydomonas reinhardtii*, lacks a gene for Ni-SOD. Since all of the organisms in cluster IV contain genes for other isoforms of SOD(Table 2.1), the acquired *sodN* may bolster an already present SOD-based

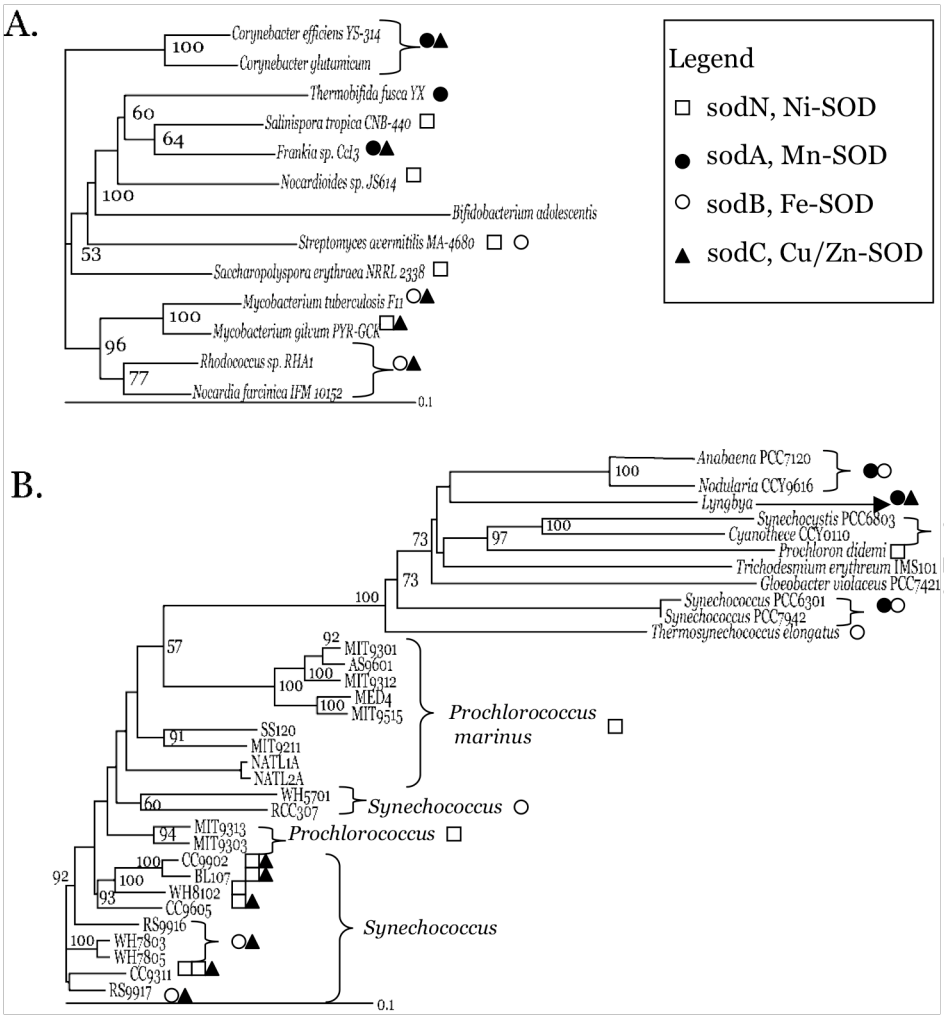

Figure 2.6: Phylogenetic distribution of *sod* genes in actinobacteria (A) and cyanobacteria (B). Neighbor-joining phylogenies were constructed using the full 16S nucleotide sequences of Actinobacteria and the full rpoC1 amino-acid sequences for cyanobacteria. Values at branch points are the bootstrap support (100 replicates) where greater than 50%. Noted at each leaf is the genomic complement of *sod* genes.

oxidative defense. While all of the clade IV sequences lack a cognate peptidase required for SOD activity in *Streptomyces* (93) and *Prochlorococcus* (58), other genomically coded peptidases may substitute.

The other clades of *sodN* amino acid sequences are phylogenetically consistent and often have conserved gene neighborhoods, implying vertical inheritance of this gene and its genomic context. However, to examine this further, we constructed phylogenies using typical marker genes of several actinobacteria (Fig. 2.6A) and cyanobacteria (Fig. 2.6B) and compared them with the genomically-encoded SOD complement. *sodN*-containing genomes appear in several separate branches of the actinomycete and cyanobacterial phylogenies, sometimes closely associated with a genome not containing *sodN* (Fig. 2.6). Further, almost all of the *sodN*-containing genomes sequenced to date do not contain a gene for a Fe-SOD (*sodB)*. For example, both *Mycobacterium* genomes contain a Cu/Zn-SOD, but *M. tuberculosis* contained a FeSOD while *M. gilvum* contained a NiSOD. In the cyanobacteria, marine clade *Synechococcus* WH7803, WH7805, RSS9917, and RSS9916 all contained a FeSOD, while the other marine clade *Synechococcus* contained a NiSOD. Similar trends were observed for the γ-proteobacteria and bacteroidetes.

There are two ways such a phenomenon could occur: 1) Ancestral lineages of the bacterial lineages in question contained all isoforms of SOD and selective loss occurred 2) Ancestral lineages contained one isoform of SOD,

acquired other isoforms via HGT, and subsequently lost the first. The lack of Ni-SOD within modern plants and many eukaryotic phytoplankton suggests that the first hypothesis is problematic, or else the Ni-SOD might have been acquired by cyanobacteria after the endosymbiotic event where a Eukarya assimilated much of the genome of an ancestral cyanobacteria (115). It is believed that the early cyanobacteria provided their Eukaryotic hosts with a Fe-SOD, as evidenced by the close phylogenetic relationship between the protein sequences of Fe-SODs from the chloroplast and freshwater cyanobacteria (25). Additionally, most gammaproteobacterial and bacteroidetes genomes deposited in NCBI to date contain *sodB*, as opposed to *sodN* (only 5 gammaproteobacterial and 2 bacteroidetes genomes contain *sodN*), which might suggest that the *sodB* gene was originally present. The *sodA*/*sodB* protein family are believed to be the original SOD family based upon the pervasive presence throughout the tree of life and in "primitive" organisms (95). Our data suggest that while ancestral lineages of some Bacteria originally contained a Mn or Fe SOD, select daughter lineages acquired a Ni-SOD during the 2.3+ billion years subsequent to the invention of oxygenic photosynthesis.

When lineages of actinobacteria, cyanobacteria, gammaproteobacteria, and bacteroidetes acquired *sodN*, the loss of *sodA*/*sodB* likely occurred; only one of the *sodN* containing genomes in these lineages contained *sodB* and only two contained the closely related Mn-containing *sodA* (Table 2.1). An examination of

the genomic regions where *sodN* and *sodB* are found in the genomes of *Synechococcus* WH8102 WH7803 revealed a strong level of sequence identity of several syntenic genes flanking the respective *sod* gene (Fig. S3). This suggests that *sodN-sodX-sodT* and *sodB* were directly exchanged, resulting in acquisition of one and loss of another. What could provide the selective pressure for such an event? All four isoforms of SOD have similar diffusion limited catalytic efficiency, and while it is possible that the different isoforms have different optimal temperatures this has not been investigated. Alternatively, the usage of different transition metals within the active site of SODs could be under a strong selective pressure. Over the 1+ billion years between the oxygenation of the atmosphere (2.3 Gigayears before present, Gya) and the ocean (1-0.6 Gya), the oceanic Fe concentrations likely fell four to five orders of magnitude (162), a change that greatly changed the proteomic utilization of trace elements by life (55, 198). During this time oceanic Ni concentrations are predicted to have remained stable (162). In the face of plummeting global Fe availability a savings on Fe requirements could possibly provide a strong ecological advantage to marine organisms. All of the hypothesized *sodN-sodB* exchanges occurred in organisms isolated from the marine environment, and *sodN* is not observed in any of the NCBI-deposited genomes of bacteria from other environments except within the actinomycetes. Further, putative *sodN* sequences could not be found in any of the non-marine metagenomes deposited in NCBI as of January 2008, despite the

presence of several soil metagenomes. As ecological Fe limitation is pervasive in the marine environment (46), the observed phylogenetic distribution is consistent with the hypothesis that environmental stress, in particular low Fe, promotes the resulting physiological benefits of replacing an Fe-SOD with a Ni-SOD.

While genomes from the actinobacteria lineage of *Streptomyces* contain both *sodN* and *sodB* (Fig. 5), they are convergently expressed, with the *sodB* gene being expressed only when the cell cannot acquire Ni (93). Further, biochemical assays suggest that many soil and clinical strains of *Streptomyces* have lost the Fe-SOD, while the Ni-SOD appears to be ubiquitous within this genus (103). The use of Ni-SOD to reduce Fe requirements may be an important factor in the pathogenesis of this genus, as the supply of Fe (35) or reduced SOD activity (10) can attenuate the virulence of pathogenic organisms within mammalian systems.

Given the proposed scenario of being able to reduce Fe requirements by swapping functionally equivalent SODs, a metallomic switch, one might expect the *sodN*-*sodB* exchange to be pervasive in the marine environment yet an opposing selective pressure is present. The obligate need for Ni-SOD results in an obligate requirement for Ni and its transport in marine cyanobacteria (53) and likely does the same in the other Bacteria containing only the *sodN* isoform, including the DMSP degrading *Marinomonas* MWYL1(184) and proteorhodopsin-containing *Polaribacter* and *Psychroflexus* (70, 72). A nutritional need for Ni might seem trivial given the difference in oceanic concentrations of Ni and Fe (3 nM vs 0.1-1

nM for Fe), yet Ni possesses slow ligand exchange kinetics that influence the metabolic cost of transport. For a marine bacteria to acquire the same amounts of Fe and Ni at the same extracellular concentrations, the ratio of Fe and Ni transporters required is 1:20 (85), a kinetics based phenomenon that would nearly negate the largest observed differences in the concentrations of these metals in seawater. Essentially, there is a physiological tradeoff related to metal transport and homeostasis; different SODs result in a need to acquire and handle either more Ni or more Fe for SOD activity. Such a tradeoff might correlate with environmental gradients or ecological niche that would be particularly important in the cyanobacteria, which already have elevated Fe requirements due to the Fe-rich photosynthetic apparatus. For example, *Synechococcus* WH7803, WH7805, RSS9916, RSS9917, WH5701, and RR307 might have a competitive advantage at high Fe concentrations relative to the Ni-SOD-containing strains of *Synechococcus*. The correlation of the relative amounts of cyanobacterial *sodB* and *sodN* genes within the Global Ocean Survey metagenomic sequencing with historical measurements of Fe in the metagenome locations (Fe was not part of the ancillary data collected during the Global Ocean Survey) will allow a more systematic testing of this exact hypothesis.

Finally, in order for Bacteria to be able to complete the metallomic switch from Fe-SOD to Ni-SOD, the relevant Ni uptake and chaperone proteins would have to be present. As many Bacteria utilize Ni/Fe hydrogenases, the mechanisms

for acquiring and handling Ni would have already been present and potentially facilitated the acquisition and usage of a Ni-SOD. The other possible metallomic switch, from Fe-SOD to Cu/Zn SOD, would have been ineffective for Prokaryotes during ocean oxygenation, as Bacteria were likely ill-equiped to utilize either Cu or Zn, having diversified in a high Fe, Mn, Co, and Ni but low Cu, Zn, and Cd environment (55, 162, 197), and the dearth of Cu, Zn, and Cd homeostasis mechanisms might have precluded the acquisition of such an enzyme. This does not appear to be the case in Eukarya, where Cu/Zn SODs (200), as well as a corresponding Cu-Zn SOD specific Cu-shuttling metallochaperone (44), are prevalent, which is consistent with the evolution of these organisms in an oxygen rich environment.

Experimental Procedures

Bioinformatic methods

Genome sequences and metagenomes were searched iteratively using Blastp (3) and the *sodN* sequences of *S. coelicolor* and *Synechococcus sp*. WH 8102. *sodN* sequences found in early searches were used as a seed for subsequent searches. Following the construction of an alignment and the verification of the Ni-binding HCXXXC motif, the most distant sequences were used for a subsequent search. Alignments were constructed using Clustal X (182) with manual intervention. Incomplete sequences or sequences lacking the Ni-binding amino-acid residues (HCXXXC) were removed and the remaining sequences realigned.

The *sodN* gene codes for a protein that requires post-translational removal of several amino-acid residues from the N-terminus (93). As this region was quite variable in length and content, each sequence was trimmed to start with the metal-binding sequence HCXXC. The aligned sequences (~100-110 a.a. long) were then bootstrapped and analyzed with Phylip using both maximum parsimony and protein distance algorithms (64). To generate the maximum parsimony trees, SEQBOOT, PROTPARS, and CONSENSE were used sequentially, while SEQBOOT, PROTDIST, NEIGHBOR, and CONSENSE were used for protein distance analysis. The amino-acid sequences of the genes flanking putative *sodN* genes were obtained from the corresponding contig or genome file. These compiled sequences were then blasted against the NCBI database. For structural prediction, the amino-acid sequence, minus the N-terminal signal peptide, was submitted to the PHYRE server (92). Predicted structures were visualized and structurally aligned to the *Streptomyces* Ni-SOD structure (1t6u) using iMol. The alignment and phylogeny were used to study the functional conservation of the amino-acid sequences using CONSURF (102), which was visualized using RASTOP.

Peptide Synthesis and Metallopeptide Preparation

The results of the peptide synthesis and metallopeptide preparation are presented in Table 2.2. All peptides were prepared by manual solid phase peptide synthesis utilizing standard Fmoc/tBu based protection strategies on Wang resin with HBTU/HOBt/DIEPA coupling methods. The peptides were cleaved from the

resin using a mixture of 95% TFA/2.5% ethanedithiol/2.5% triisopropyl silane and then filtered. The filtrate was then evaporated under vacuum forming a glassy film, which was washed several times with freshly distilled diethyl ether resulting in tan-colored crude peptides. All peptides were then subsequently purified by reverse phase HPLC on a Waters DeltPrep 60 equipped with a Waters Atlantis C-18 reverse phase column (5 μm; 50 × 100 mm). A gradient of 10 - 29% MeCN (0.1% TFA) in H_2O (0.1% TFA) over 15 min. was used with a flow rate of 40 mL min^{-1}. The fractions containing the desired product were then lyophilized yielding white powders. The purity of each peptide was assessed by analytical reverse phase HPLC (Atlantis C-18 reverse phase column 5 μm; 4.6 × 100 mm; gradient: 10 - 65% MeCN (0.1% TFA) in H_2O (0.1% TFA) over 45 min; flow rate 1 mL min^{-1}) and mass spectrometry on a Waters Micromass 20 ESI mass spectrometer (negative ion mode).

Metallopeptides ($[Ni^{II}(SOD^{M2}X(n)Z)]$, where X is the native residue in position n and Z is the new residue) were prepared by adding one equivalent of $NiCl_2$ to one equivalent of the apo-peptide in 50 mM N-ethylmorpholine (NEM) buffer (pH = 7.5). Peptide concentrations were quantified by the procedure of Ellman (60). Ni^{II} was added to solution as $NiCl_2$ in neutral water and the pH of the metallopeptide solution adjusted to 7.4. Gel permeation chromatography studies were performed on a Waters DeltPrep 60 equipped with a Protein-Pak™ GPC column (7.8 × 300 mm; 60 μm pore size) using an aqueous solution of $NaHCO_3$

(sat.) under a positive pressure of He flowing at 1 mL min^{-1}. Data were recorded at 350 nm where the free peptides do not significantly absorb. Calibration curves were made using a Waters polyethylene glycol standard kit.

Electronic absorption, SOD Activity, and X-ray Absorption Studies

All solutions were prepared from water that had an initial resistance of at least 18 MΩ. Electronic absorption measurements were carried out on either a Varian Cary 50. SOD activity assays were performed at pH 7.4 utilizing the modified xanthine/xanthine oxidase assay of Tabbi *et. al.* as previously described (179). For the X-ray absorption studies freshly prepared samples of $[Ni^{II}(SOD^{M1})X(n)Z]$ (~1.0 mM, pH 7.4, 50 mM NEM) were injected into an aluminum sample holder between windows made from Kapton tape (3M, Minneapolis, MN; cat. no. 1205) and quickly frozen in liquid nitrogen. Data were collected at the National Synchrotron Light Source, Brookhaven National Laboratories (Upton, NY) on beamline X3b. The samples were maintained at 20 K throughout data collection using a He Displex cryostat. All spectra are reported as fluorescence data and recorded on a Canberra 13-element solid-state Ge fluorescence detector. X-ray absorption data collection and analysis were performed as previously described (132, 169).

Acknowledgements

Chapter 2, in full, is a reprint of the material that has been accepted for publication without revision in Environmental Microbiology. K. Neupane, J. Shearer, and B.

Palenik were co-authers, while the dissertation author was the primary investigator and first author.

CHAPTER 3

Ni uptake and limitation in marine *Synechococcus* Strains

Abstract: Ni accumulation and utilization was studied in two strains of marine *Synechococcus* isolated from coastal (CC9311, clade I) and open ocean (WH8102, clade III) environments and for which complete genome sequences are available. Both strains have genes encoding for a Ni-containing urease, and when grown on urea without Ni become Ni-N colimited. The Ni requirements of these strains also depend upon the genomic complement of genes encoding for superoxide dismutase (SOD). WH8102, with a gene encoding for only a Ni-SOD, has a novel obligate requirement for Ni, regardless of N source. Reduced SOD activity in Ni-depleted cultures of WH8102 supports the link of this strain's Ni requirement to Ni-SOD. The genome of CC9311 contains a gene for a Cu/Zn-SOD in addition to a predicted pair of Ni-SODs, yet this strain cannot grow without Ni on NO_3^- and can only grow slowly on NH_4^+ without Ni implying that the Cu/Zn-SOD cannot completely replace Ni-SOD in marine cyanobacteria. CC9311 does have a greater tolerance to Ni starvation. Both strains increase their Ni uptake capabilities and actively bioconcentrate Ni in response to decreasing extracellular and intracellular Ni. The changes in Ni uptake rates were more pronounced in WH8102 than in CC9311, and for growth on urea or nitrate compared to growth on ammonia. These results, combined with an analysis of fully sequenced marine cyanobacterial genomes, suggest that the growth of many marine *Synechococcus* and all *Prochlorococcus* will be dependent upon Ni.

Introduction

In surface seawater, nickel is generally present in low nanomolar amounts (3-4 nM, 26) with elevated concentrations in coastal waters due to natural terrestrial and anthropogenic inputs (27, 57). Ni concentrations in the ocean exhibit a "nutrient-like" depth profile, being depleted in the euphotic zone and increasing with depth (27), indicating that biological uptake and remineralization processes control Ni geochemistry. While no marine phytoplankton has previously been shown to have an obligate requirement for Ni, the role of Ni in urea assimilation is well established, and historically been used to explain the "nutrient-like" depth profile of Ni in seawater (125). Urease, an amidohydrolase with Ni in the active site (83), catalyzes the dissociation of urea into ammonia and carbon dioxide. For numerous alga taxa, it has been shown that growth with urea as the sole nitrogen source will be nickel dependent (56, 137, 141), with nickel-deprived cultures becoming Ni-N colimited (149). These Ni-N colimited phytoplankton can subsequently grow with the addition of Ni, which presumably results in a functional urease, or with the addition of ammonia, which does not require Ni for assimilation (149). The presence and regulation of urease in *Synechococcus* has been characterized (40), though the Ni dependency of growth on urea has not been shown. Most marine cyanobacteria genomes sequenced to date contain an operon encoding for the multi-domain Ni-containing urease (Fig.1). The sole other previously characterized use for Ni among marine phytoplankton is in Ni/Fe hydrogenases found in some nitrogen-fixing cyanobacteria, though the Ni-

starvation induced deficiency of this enzyme may not affect growth or nitrogen fixation (45).

It has long been recognized that phytoplankton metal physiology varies between closely related species or strains from different oceanic regimes. For example, centric diatoms from open ocean environments tend to have lower Fe requirements than coastal species (22, 176), though increased copper requirements are a consequence (145, 146). The discovery of plastocyanin in *Thalassiosira oceanica* provided a mechanistic explanation for the increased Cu requirements in oceanic diatoms (145). By providing a complementary approach to physiological experiments, genomics may facilitate the elucidation of the molecular and genetic reasons for ecotypic differences in metal physiology. Of particular relevance, a comparison of the genomes of coastal (CC9311) and oceanic (WH8102) strains of marine *Synechococcus* from phylogenetically distinct clades recently revealed a number of proteomic differences in the number and type of metallo-enzymes, implying differences in metal physiology (142).

Available genome sequences of marine cyanobacteria suggest another physiological usage of Ni in addition to urease. Many marine cyanobacterial genomes sequenced to date contain a gene potentially encoding for a Ni-containing superoxide dismutase (*sodN*, Fig. 3.1). Superoxide dismutases, of which there are Fe, Mn, Ni, and Cu/Zn-containing isoforms, catalyze the breakdown of superoxide into hydrogen peroxide and molecular oxygen (69). As both photosynthesis and

respiration generate toxic superoxide radicals, SODs play a critical role in protecting photosynthetic organisms from self- and environmentally-induced oxidative stress (200). Previously only observed in the soil actinomycete *Streptomyces* (94), Ni-SOD is the only predicted isoform of SOD in *Synechococcus* WH8102 (139) and in all strains of *Prochlorococcus* sequenced to date (Fig. 3.1). One strain of *Synechococcus*, CC9311, also has a second gene encoding for a protein with low sequence similarity (35%) to biochemically characterized Ni-SOD (Fig. 3.1), with a conservation of the Ni-binding residues (metal-binding residues from ref. 12). The genomes of several strains of *Synechococcus,* including CC9311, also contain a gene with sequence similarity to a Cu/Zn SOD (*sodC*, Fig. 1), an isoform of SOD previously unobserved in cyanobacteria (142). A few other marine *Synechococcus* genomes contain a gene encoding for a Fe-SOD (*sodB*) in lieu of *sodN* (Fig. 3.1), implying an evolutionary exchange of these two isoforms. Euryhaline cyanobacteria from freshwater and brackish environments contain either a Fe-SOD (RCC307, Fig. 3.1) or both an Fe and Mn-SOD (PCC7002, 181). The genomes of the nitrogen-fixing cyanobacteria *Trichodesmium* and *Crocosphaera* contain genes encoding for Mn (*sodA*) and Ni isoforms of SOD (Fig. 3.1) as well as a Ni/Fe-hydrogenase (not shown).

Here, we hypothesize that some marine cyanobacteria (eg. WH8102) will have an obligate growth requirement for Ni due to the obligate usage of Ni-SOD,

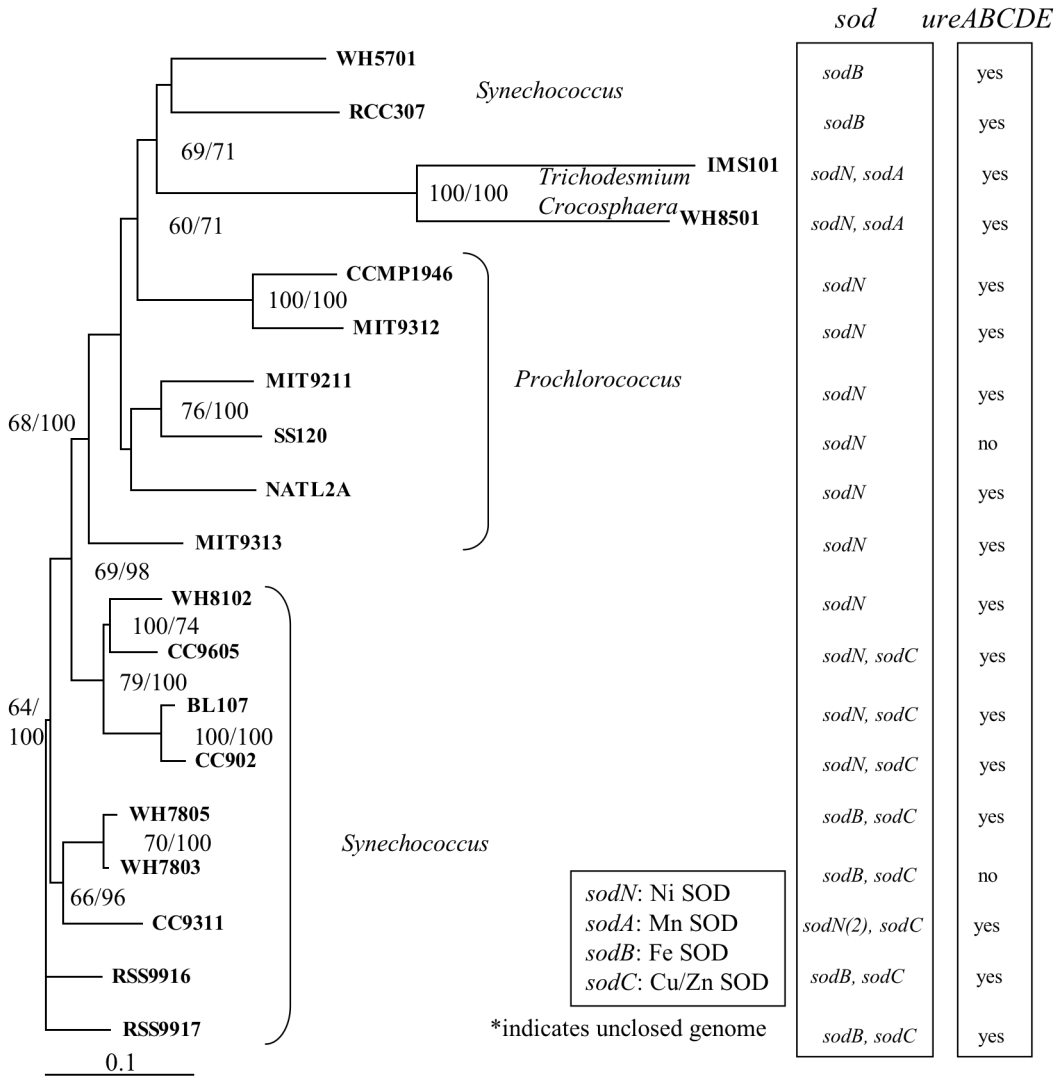

Figure 3.1: Phylogenomic mapping of genes coding for SODs and urease within the fully-sequenced genomes of marine cyanobacteria. The phylogenetic tree was drawn using the full-length amino-acid sequences of *rpoC2*. Numbers at branchpoints denote the bootstrap support for the topology (100 replicates), with left and right numbers corresponding to a protein parsimony and protein distance analyses, respectively.

one independent of nitrogen source used for growth. However, other strains (eg. CC9311) should not have this obligate requirement due to the ability to utilize a different isoform of SOD. The requirements of these organisms also should depend upon the nitrogen source provided; growth on urea should impose a greater need for nickel compared to growth on NH_4^+. Finally, the increased, and in the case of WH8102 likely constitutive, need for Ni will necessitate regulated Ni uptake and homeostasis. To test these hypotheses, we assayed the growth rates and cellular Ni concentrations of cultures of CC9311 and WH8102 over a range of free Ni^{+2} concentrations ($[Ni^{+2}]$). Superoxide dismutase activity was also determined for both Ni-replete and deplete cultures. Finally, the feedback regulation of Ni transport capabilities by extracellular and intracellular Ni was determined using radiotracer-based uptake experiments.

Methods

Bioinformatic analyses

Full genome sequences were searched using Blastp (3) and the *sodN, ureABCDE,* and *rpoC2* amino-acid sequences of WH8102 (139). The resulting amino acid sequences were aligned using ClustalX (182) with manual intervention. The alignment of the *sodN* sequences was used to screen the putative *sodN* genes for the "Ni-hook" motif, which is proposed to be characteristic of Ni-SOD (12). The aligned full length *rpoC2* sequences were bootstrapped and analyzed with

Phylip using both maximum parsimony and protein distance algorithms (64). To generate the maximum parsimony trees, SEQBOOT, PROTPARS, and CONSENSE were used sequentially, while SEQBOOT, PROTDIST, NEIGHBOR, and CONSENSE were used for protein distance analysis.

Media and culture manipulations

Synechococcus WH8102 and CC9311 were grown in synthetic ocean water minimally modified from the original recipe of Waterbury and Wiley (193)(SOW-Table 3.1). Several steps were taken in the media preparation and culturing process to prevent metal contamination. The media and added macronutrients were made trace metal free using column-based solid phase extraction with pre-cleaned Chelex-100 resin (pretreated according to 148) and microwave sterilized prior to the addition of filter sterilized trace metals, vitamins, and ethylenediaminetetraacetic acid (EDTA, Sigma Ultra Grade). All growth containers were rigorously cleaned as follows: 1) Soak in 1% citronox soap for at least one day followed by multiple rinses with 18.2 mΩ-water (milli-Q, Millipore) 2) Soak in 10% trace metal grade HCl (Fisher) for 2 days and 3) multiple rinses with milli-Q water. Containers were sterilized by microwaving while filled halfway with milli-Q water. Microwaving times varied according to volume, but a water temperature of 95^{o}C was attained, as determined by an infrared thermometer (Fisher). All additions were made with sterile pipet tips rinsed twice with 0.2 μm-

Table 3.1: Composition of SOW. All concentrations describe the final media.

Composition of SOW **Substance**	**Concentration (M)**
Artificial Seawater	
NaCl	4.2×10^{-1}
Na_2SO_4	2.88×10^{-2}
KCl	9.39×10^{-3}
$NaHCO_3$	3×10^{-3}
KBr	8.4×10^{-4}
H_3BO_3	4.85×10^{-4}
NaF	7.14×10^{-5}
$MgCl_2\ 6H_2O$	5.46×10^{-2}
$CaCl_2\ 2H_2O$	1.05×10^{-2}
$SrCl_2\ 6H_20$	6.38×10^{-5}
Nutrients (chelexed and filter sterilized)	
$NaHPO_4\ H_2O$ (3.5×10^{-2} stock)	7.7×10^{-5}
Nitrogen (1 M N atom stock) (urea, $NaNO3^-$, or $NH4^+$)	2×10^{-3}
Na_2CO_3	9.4×10^{-5}
Trace metal mix (made as 0.2μm filter sterilized 1000x stock)	
$ZnSO_4\ 7H_2O$	7.72×10^{-7}
$MnCl_2\ 4H_2O$	7.07×10^{-6}
$Co(Cl)_2\ 6H_2O$	8.59×10^{-8}
$Na_2MoO_4\ 2H_2O$	1.16×10^{-6}
$FeCl_3$	7.4×10^{-7}
Na_2SeO_3	5×10^{-8}
$CuCl_2$	5×10^{-8}
$NiCl_2$	varied
Citric acid hydrate	3×10^{-5}
Vitamin mix (made as 1000x stock)	
Vitamin B_{12}	1μg/L
Thiamine HCl	200 μg/L
d-biotin	1μg/L
Trace metal buffer (made as 0.2μm filter sterilized 200x stock)	
Ethylenediaminetetraacetic acid (Sigma ultra grade)	1.345×10^{-5}
NaOH (Sigma ultra grade)	4.2×10^{-5}

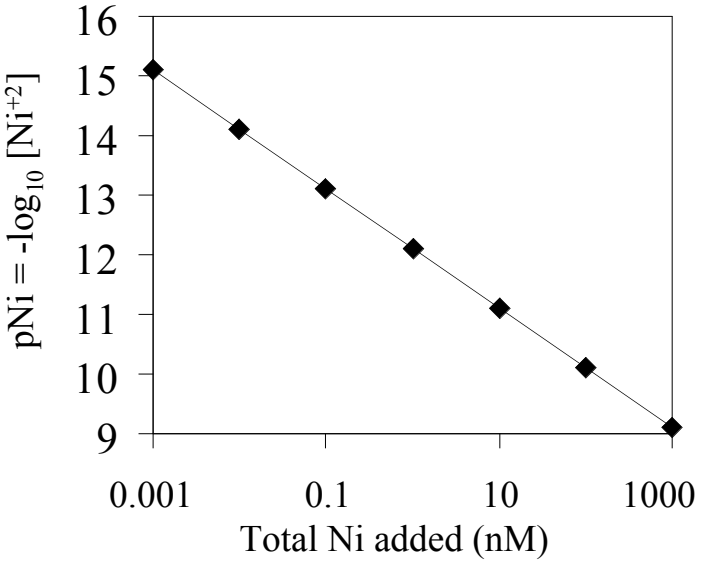

Figure 3.2: Ni speciation in SOW. The line shows the relationship between total and free nickel in SOW (recipe described in table 1). Most of the Ni is bound by EDTA, with a small percentage bound by citrate, and only minute amounts being in the bioavailable free ion (Ni^{+2} shown on y axis).

filtered HCl (10%) and milliQ water, and all manipulations were conducted in HEPA-filtered laminar flow benches. MINEQL (195) was used to determine the speciation of trace metals, and specifically Ni, in SOW (Fig. 3.2). Due to the constant presence of excess (13.45μM) EDTA, $[Ni^{+2}]$ is over 1000 times lower than the total Ni concentrations (Fig. 3.2) and will remain stable despite uptake by phytoplankton. For media containing 13.45 μM EDTA and 50 nM total Ni, $[Ni^{+2}]$ will only change from pNi 10.3 to pNi 10.6 with a pH change from 8.0 to 8.6. In order to vary $[Ni^{+2}]$, only the total Ni added was varied; this keeps all other micronutrient: EDTA ratios constant and also avoids potentially confounding effects different concentrations of EDTA may have on cyanobacteria.

Cultures were grown at 19°C (CC9311) or 24°C (WH8102) under continuous light (unless otherwise noted, 80 μM photons m^{-2} sec^{-1}). For the growth assays and Ni quota experiments, 25mL cultures were grown in capped 60mL glass tubes. Cultures for protein assays and short term uptake experiments were grown in 1L or 2.7L polycarbonate bottles with internal stir bars (100 rpm). The axenicity of the cultures was verified using agar plates supplemented with bactone and tryptone.

Determination of the specific growth rates and cellular Ni over a range of $[Ni^{+2}]$

Cultures (25 mL) were grown in semicontinuous fashion at fixed free ion concentrations of Ni. If transferred during mid-log phase of exponential growth, exponential growth is perpetuated, and due to the buffering by excess EDTA, $[Ni^{+2}]$

concentrations remain relatively constant and the cultures mimic trace metal "chemostats" (177). To further reduce batch effects, macronutrients are added in excess (Table 3.1). After growth equilibration (4-5 transfers of 1:200 dilution during mid-log phase growth, ~ 4 weeks), the cells were transferred (1:200 dilution) to media containing ^{63}Ni instead of "cold" Ni (^{63}Ni from Perkin Elmer diluted in Optima grade HCl, 0.1% in MilliQ). Following 10-12 doublings in the radioactive media, 10 mL of culture was gently filtered (Supor 0.2 μm 25mm), and the filter was rinsed sequentially with 5 mL of 8-hydroxyquinoline-5-sulfonic acid (sulfoxime, a Ni chelator, 1mM in SOW pH 8.0, Avocado Biochemicals) and SOW to remove surface bound ^{63}Ni (149) and placed in 15 mL of scintillation fluid (Ecolyte). Aliquots (150 μL) of the culture were also spiked into separate scintillation vials to determine the total ^{63}Ni (and therefore total Ni and [Ni^{+2}]) in each culture. The radioactivity of these samples was determined using standard scintillation counting with quench correction. Counts per minute were converted to DPM and compared to a dilution series (eg. standard curve) of the ^{63}Ni stock solution to convert to molar concentrations. Finally, glutaraldehyde (25%, Sigma) was added to 1mL aliquots of the cultures to a final concentration of 0.25 %. These samples were allowed to fix for 10 minutes and frozen at -70^{o}C until they were used for cell counts.

Culture phycoerythrin fluorescence was monitored as a proxy for culture biomass (Turner AU-10, excitation = 544 nM emission = 577 nM). The specific

growth rates of these cultures were determined using geometric mean linear regression of a plot of ln (culture fluorescence) versus time during mid-exponential phase. While the amount of phycoerythrin fluorescence per cell varies according to the Ni concentration in the media (not shown), the use of equilibrated semi-continuous cultures allows for reliable growth rate measurements once the fluorescence $cell^{-1}$ relationship stabilizes (114).

To determine the cell density of the cultures, the glutaraldehyde-fixed (0.25%, stored at -70°C) samples were thawed at room temperature. Following 20-fold dilution with SOW, samples were filtered onto 0.2 μm black polycarbonate filters (Millipore) using 11 μm nitex mesh filters (Millipore) as a support in glass chimney filter funnels (Fisher). Filters were mounted with immersion oil on glass slides and cells counts were conducted on an epifluorescence microscope. Fields were counted in triplicate for each slide, and if the counts for a given slide deviated by more than 10%, a new filter and slide were made.

Ni uptake kinetics

Growth equilibrated semicontinuous cultures of WH8102 were harvested during mid-log phase via centrifugation (9000g, 10 minutes) in acid-washed centrifuge tubes. The cells were washed twice by resuspension in chelexed and microwave sterilized SOW^- (no nutrients, EDTA, or trace metals) and centrifugation. The resulting cell pellet was resuspended with chelexed SOW^- and

aliquoted to acid-washed polycarbonate bottles (60mL). Half of these bottles were treated with 0.25% glutaraldehyde for 30 minutes (kill controls), at which point, the live-kill pairs received staggered additions of ^{63}Ni. For the time course study, 10 nM ^{63}Ni was added, and for the kinetic study, additions ranged from 100 pM to 100 nM. For the kinetics study, cell suspensions were filtered after 30 minutes. Cells were collected on 0.2 μm filters (25 mm, polyethersulfone, Supor) by gentle vacuum and rinsed sequentially with 5mL of sulfoxime (1 mM in SOW^-) and chelexed SOW. Samples were also taken to determine the total ^{63}Ni and cell density in the suspensions; these were handled as described above. Uptake is presented as live-kill (kills are typically 20-30% of the live).

Measurements of superoxide dismutase

Cultures (1-2L) of *Synechococcus* were grown under Ni-replete (50 nM Ni total) and Ni-deplete (no added nickel) conditions. Ni replete cultures were harvested during mid-log phase, while Ni-deplete cultures were harvested in late-log phase prior to the Ni-dependent cessation of exponential growth (initial decline in exponential growth). Cells were harvested by centrifugation (9000 rpm for 10 minutes in sterile acid-washed HDPE bottles), immediately frozen at -70^{o}C, and stored until extraction. For protein extraction, the cell pellet was resuspended in 2mL of sterile, cold buffer (0.1 M potassium phosphate, 0.1 mM EDTA, 0.1% triton-100, 1mM PMSF, pH=7.8) and passed twice through a french pressure cell

(20000 psi). Unbroken cells were removed from the resulting suspension by centrifugation (5000g for 5 minutes, twice). Superoxide dismutase activity was calculated using the ferricytochrome c reduction assay as described by Flohe and Otting (67). SOD activity was normalized to total protein concentrations determined using the BCA method (MicroBCA, Pierce).

Results

Essentiality of Ni to marine Synechococcus

To test if *Synechococcus* CC9311 and WH8102 require Ni, cultures were grown in SOW with and without Ni and either ammonium, urea, or nitrate as the added nitrogen source. As predicted, WH8102 cannot grow without Ni, though the nature of the resulting limitation is dependent upon the nitrogen source in the media. When grown on urea, WH8102 became Ni-N colimited after one transfer to Ni-free media, with either Ni or NH_4^+ additions restoring normal growth (Fig. 3.3A). After two to three transfers in Ni-free media, WH8102 was also unable to grow on NH_4^+ (Fig. 3.3B) or NO_3^- (Fig. 3.3B) without added Ni, and Ni additions restored growth (triangles on Fig. 3.3B and 3.3C). CC9311 also became Ni-N

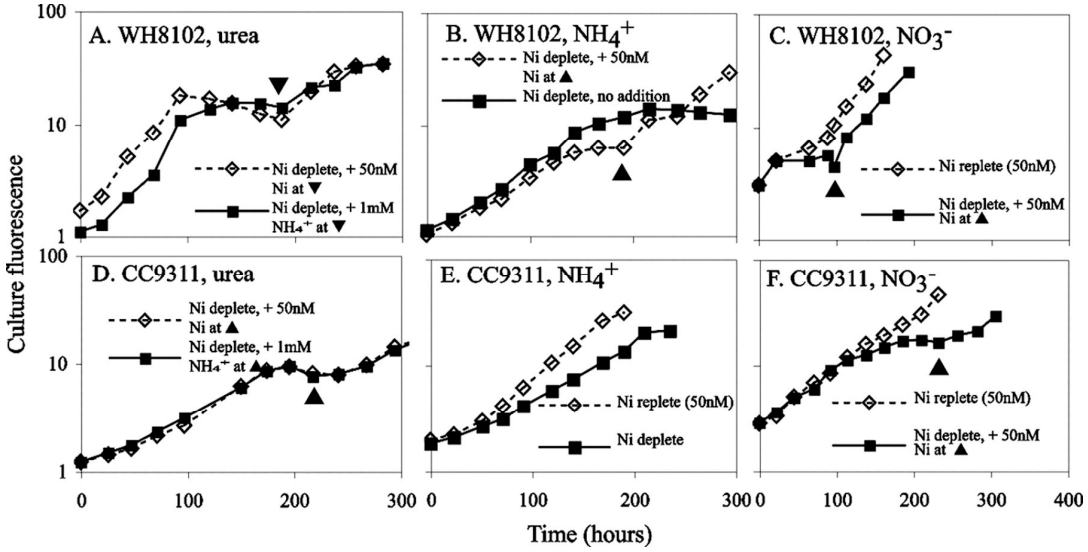

Figure 3.3: Ni limitation of marine *Synechococcus*. Representative growth curves are shown for A) WH8102 grown on urea without Ni and subsequently amended with Ni or NH_4^+ (triangles indicated addition to a limited culture), B) WH8102 grown on NH_4^+ without Ni and amended with Ni, C) WH8102 grown on NO_3^- without Ni and amended with Ni, D) CC9311 grown as in panel A, E) CC9311 grown on NH_4^+ with and without Ni, and F) CC9311 grown as in panel C.

Table 3.2: SOD activity in *Synechococcus*.

		SOD activity (units mg^{-1} protein)	
Strain		+Ni	-Ni
WH8102	urea	9.5 ± 1.0	0.7 ± 0.1
	NH_4^+	7.5 ± 0.7	1.7 ± 0.1
	NO_3^-	15.1 ± 1.5	1.3 ± 0.1
CC9311	urea	9.5 ± 0.9	3.6 ± 0.1
	NH_4^+	7.1 ± 1.4	13.6 ± 4
	NO_3^-	7.8 ± 0.4	8.6 ± 0.8

colimited when grown on urea without Ni (Fig. 3.3D), yet contrary to the original hypothesis, CC9311 was also not able to grow on NO_3^- without Ni (Fig. 3F) and could only grow on NH_4^+ at reduced rates compared to cultures provided with Ni (Fig. 3.3E).

Ni-limited cultures of WH8102 consistently exhibited greatly reduced SOD activity compared to Ni-replete cultures (Table 3.2), an intuitive consequence of Ni starvation for WH8102, which contains a gene only for the Ni-containing isoform of SOD. In contrast, Ni-limited cultures of CC9311 contained equal or greater SOD activity compared to Ni-replete cultures, except for growth on urea (Table 3.2). Ni additions restored maximal growth to Ni-limited CC9311 grown on NO_3^- or NH_4^+, therefore, either the Ni-limitation observed in CC9311 is attributable to an unknown Ni metalloenzyme, or the SOD activity observed in Ni-replete and Ni-limited cultures of CC9311 is not functionally equivalent.

To address the hypothesis that, when Ni starved, CC9311 is more susceptible to oxidative stress despite measurable SOD activity, cultures were grown with and without Ni and with NH_4^+ as a nitrogen source at several light intensities from 0.5 to 150 uE m^{-2} sec^{-1}. At 0.5 and 10 uE m^{-2} sec^{-1}, the Ni-deplete cultures grew only marginally slower or even faster than the Ni replete cultures (Fig. 3.4), but at 50 and 80 uE m^{-2} sec^{-1}, the Ni-deplete cultures grew significantly slower (Fig. 3.4). Even higher light levels (150 μEinsteins m^{-2} sec^{-1}) inhibited growth in Ni replete cultures, but were lethal to Ni-deplete cultures (Fig. 3.4). The

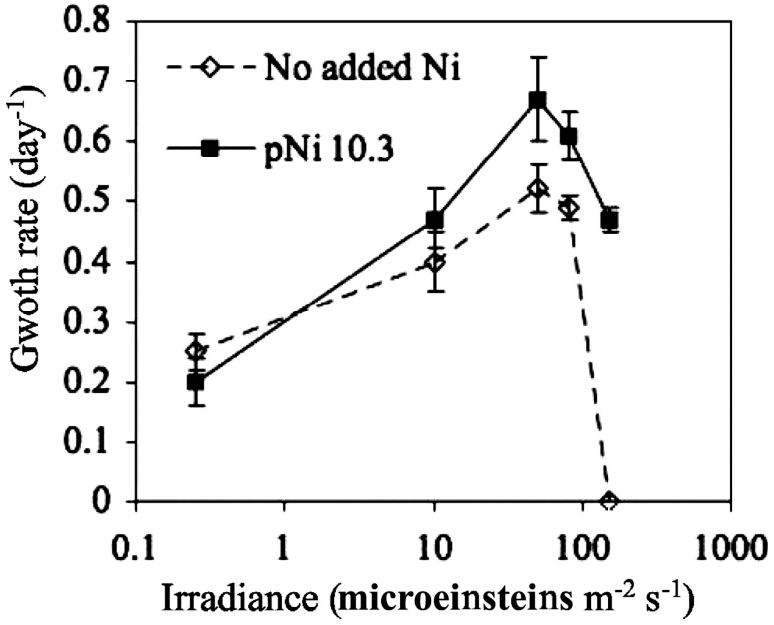

Figure 3.4: Growth rates of *Synechococcus* CC9311 over a range of irradiance intensities when supplied with NH_4^+ as a nitrogen source and either no Ni, or 50 nM total Ni. Error bars are for duplicate cultures.

Table 3.3: Maximum growth rates (μ) for each strain and nitrogen source, and the total concentration of Ni added for the experiments presented in Figures 5, 7, and 8. Concentrations vary between strains and nitrogen source because the results are the compilation of several experiments (all other conditions are identical between experiments).

Strain	N source	Max μ (day^{-1})	Ni added (nM)
WH8102	NH_4^+	0.8 ± 0.02	0.075, 0.3, 1, 1.75, 5, 7.5, 30, 100
	urea	1.20 ± 0.05	0.075, 0.8, 2, 3.5, 15, 50, 100
	NO_3^-	1.03 ± 0.01	0.075, 1, 2, 7.5, 15, 75, 100
CC9311	NH_4^+	0.7 ± 0.03	0.4, 2.5, 7.5, 20, 50, 200
	urea	0.88 ± 0.02	0.075, 0.4, 2, 5, 15, 35, 50, 250
	NO_3^-	0.49 ± 0.02	0.075, 0.4, 1.5, 2.5, 7.5, 20, 35, 250

decreased ability of CC9311 to tolerate high light when Ni starved leads us to believe that the SOD activity observed in Ni-deplete CC9311 extracts is not functionally equivalent to that observed in Ni-replete CC9311.

Growth rates of WH8102 and CC9311 over a range of [Ni^{+2}]

While the above studies are diagnostic for the absolute Ni requirements of *Synechococcus*, their environmental relevance is unclear given the observed nanomolar concentrations of Ni in seawater. However, most trace metals in seawater are bound by organic ligands that reduce the concentration of the bioavailable free and inorganic species of a metal (126). With this in mind, the specific growth rates (μ) were determined for *Synechococcus* supplied with a range of [Ni^{+2}] and either urea, nitrate, or ammonia as a nitrogen source. The total Ni concentrations for each experiment are summarized in Table 3.3, while the relationship between total Ni and free Ni concentrations in the SOW media is shown in Figure 3.2. The experiments tested a range of Ni concentrations that would roughly reflect the potential environmental range of [Ni^{+2}].

Normalizing the specific growth rates using the highest observed growth rates for each strain and nitrogen source (Table 3.3), the growth efficiency (% of maximal μ) over a range of [Ni^{+2}] was calculated (Figure 3.5). CC9311 was less affected by low [Ni^{+2}] than WH8102 for growth on urea and NO_3^- (Fig. 3.5A and 3.5C). Nitrogen source-specific differences in Ni requirements for growth were

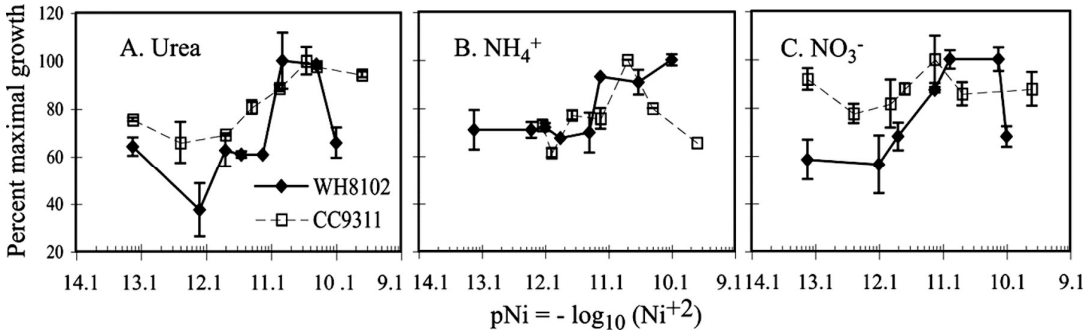

Figure 3.5: Growth efficiency over a range of $[Ni^{+2}]$ for *Synechococcus* grown on urea (A), NH_4^+ (B), and NO_3^- (C). Growth efficiency was calculated using the measured growth rates at a given $[Ni^{+2}]$ and the maximum growth rate observed for that strain and nitrogen source (Table 3.3). Error bars are the range for duplicate cultures.

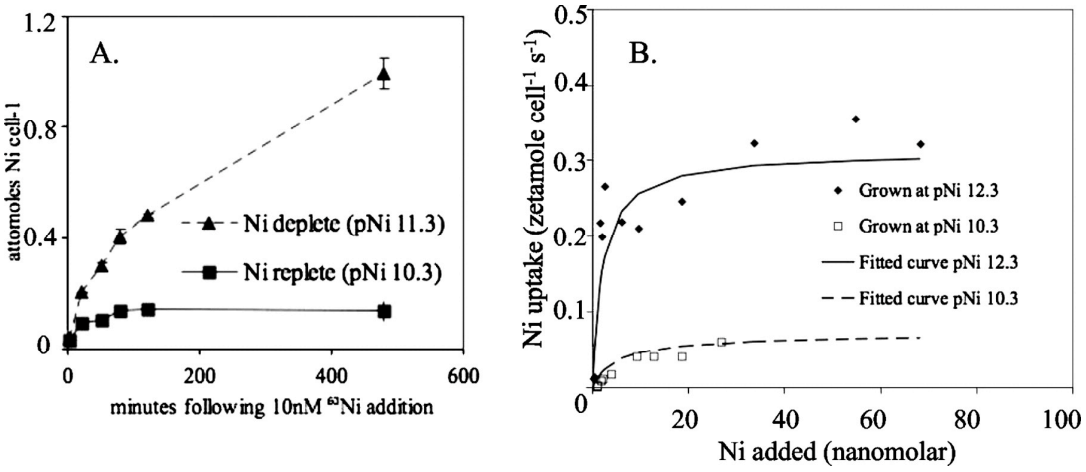

Figure 3.6: Regulated Ni uptake in WH8102. A. Time course of Ni uptake by cells grown at pNi 10.3 or pNi 11. Error bars are the range for duplicate kill-control-corrected cultures. B. Kinetics of Ni uptake. Symbols are the measured uptake rates for cells grown at either 0.5 nM (Ni deplete) or 50 nM (Ni replete) total Ni (pNi 12.3 and 10.3 respectively). The curves are the least squares regression fit of the hyperbolic Michelis-Menten relationship. The fitted ρ_{max} = 0.35 and 0.07 zetamoles (10^{-21}) Ni cell^{-1} day^{-1} for Ni starved and Ni replete cells, respectively. K_ρ = 2.5 and 3.5 nM for Ni starved and Ni replete cells, respectively.

also observed. For both strains, growth efficiency declined most severely with decreasing [Ni^{+2}] when urea was supplied as the nitrogen source, as was originally hypothesized (Fig. 5A). The growth efficiency of both strains was less affected by low [Ni^{+2}] when grown on NH_4^+ compared to urea (Fig. 3.5A and 3.5B). When growing on nitrate, the growth efficiency of the strains was affected by decreasing [Ni^{+2}] in different fashions (Fig. 3.5C). WH8102 growth rates declined with decreasing Ni at a lesser extent compared to urea grown cells (Fig. 3.5A and 3.5C). In contrast, CC9311 supplied with NO_3^- grew at near maximal rates over a broad range of [Ni^{+2}] (Fig. 3.5C). While not a focus of this study, reduced growth efficiency at higher Ni concentrations, presumably due to Ni toxicity, was also observed (Fig. 3.5).

Cellular Ni concentrations and Ni accumulation in WH8102 and CC9311

In order to determine directly if *Synechococcus* adjusts its uptake capabilities for Ni in response to Ni starvation, short term Ni uptake rates were determined for cultures grown at different [Ni^{+2}]. When supplied with a saturating pulse of Ni (10nM), *Synechococcus* rapidly takes up Ni for 30-60 minutes, with declining rates over time (Fig. 3.6A). Cultures grown at lower Ni concentrations took up Ni more rapidly than those grown at higher Ni (Fig. 3.6A). Ni uptake by WH8102 can be modeled well by traditional Michelis Menten kinetics ($\rho = \rho_{max}$ [Ni]/ (K_ρ + [Ni]), where ρ, ρ_{max}, and K_ρ are the uptake rate, the saturated uptake rate, and the half saturation constant, respectively). The uptake capacity (ρ_{max})

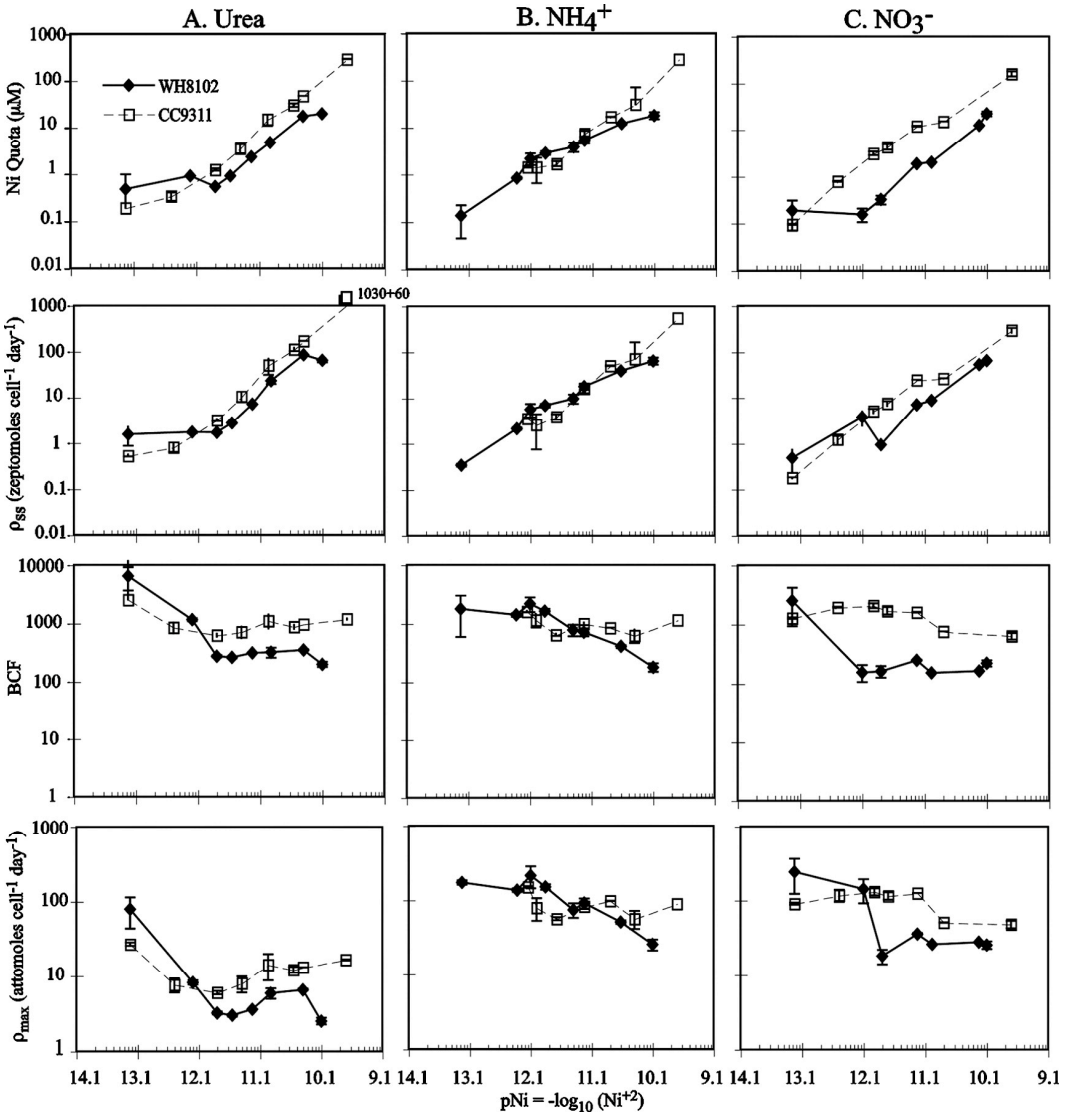

Figure 3.7: Cellular Ni quotas (Q_{Ni}), steady state Ni uptake rates (ρ_{ss}), bioconcentration factors, and maximum Ni uptake rates (ρ_{max}) for Synechococcus WH8102 and CC9311 grown on urea (A), NH_4^+ (B), and NO_3^- (C). Error bars are the range of duplicate cultures.

appears to be regulated to a greater extent than affinity (K_ρ) by Ni; cultures grown on NH_4^+ at 100-fold lower Ni concentrations exhibit a 5-fold increase in ρ_{max} with a less significant change in affinity (2.5 vs 3.5 nM, Fig. 3.6B). CC9311 also has a high affinity for Ni (~3nM), but the changes in ρ_{max} for similar conditions are decreased relative to WH8102 (2.5 fold vs. 5 fold, data not shown).

The cellular concentrations of Ni were determined for both strains during the growth experiments shown in Fig. 3.4 and used to provide insight to the regulation of Ni uptake rates and accumulation. For interpretation, the amount of Ni per cell was converted to intracellular molar concentrations (Ni quota, Q_{Ni}) by assuming a spherical cell with a radius of 1 μm (Fig. 3.7). While cellular size or carbon might actually change with decreasing Ni, this was not determined here. The Ni $cell^{-1}$ concentrations were also converted into steady state uptake rates ($\rho_{ss} = \mu Q$, where μ = specific growth rates (123)) and bioconcentration factors ($BCF = Q_{Ni} / Ni_T$, where Ni_T = total media Ni concentrations). Finally, ρ_{max} was calculated using ρ_{ss}, $[Ni^{+2}]$, K_ρ = 3 nM (from Fig. 3.6), and the Michelis Menten equation.

For growth on urea, both strains reduced their cellular Ni quotas with the reduction of $[Ni^{+2}]$ from ~pNi 10.7 to pNi 12 (Fig. 3.7A). Below pNi12, the urea-grown cells showed increased Ni uptake capacity (Fig. 3.7A), maintaining their Q_{Ni} above 300 nM through heightened uptake rates and bioconcentration factors (Fig. 3.7A). A similar trend was observed for the growth of WH8102 on nitrate (Fig. 3.7C). Elegantly, the observation of heightened Ni uptake rates at low $[Ni^{+2}]$

provides a mechanistic explanation for the sustained growth observed in Fig. 3.5A and 3.5C, and rules out Ni contamination as a potential explanation (all Ni added is ^{63}Ni). When grown on NH_4^+, Q_{Ni} and ρ_{ss} in CC9311 vary in a nearly linear fashion dependent upon the extracellular $[Ni^{+2}]$, with little change in ρ_{max} or BCF until $[Ni^{+2}]$ falls below pNi 12 where increase uptake rates are observed (Fig. 3.7B). WH8102 cells grown on NH_4^+ increased their BCF and ρ_{max} in a nearly linear fashion with decreasing $[Ni^{+2}]$ (Fig. 3.7B), thereby allowing Q_{Ni} to decrease only 2.2 orders of magnitude over a 3.5 order of magnitude change in extracellular $[Ni^{+2}]$. NO_3^- grown CC9311 exhibited only minor changes in ρ_{max} or BCF. Comparing the strains, CC9311 contained upwards of 2-fold more cellular Ni than WH8102 and exhibited higher uptake rates at comparable $[Ni^{+2}]$, except at the lower $[Ni^{+2}]$, where the trend was reversed.

Discussion

Ni requirements of marine cyanobacteria

For growth on urea, our genome-based predictions of the Ni requirements for CC9311 and WH8102 were correct, as both strains became Ni-N colimited when grown without Ni. Biochemically, the Ni-dependent deficiency of urease prevents the cell from acquiring nitrogen thereby halting growth. While reduced SOD activity was also observed for urea-fed Ni limited cultures (Table 3.2), the ability to at least initially recover growth with NH_4^+ additions (Fig. 3.3A) suggests

that the cell may be able to reallocate intracellular Ni from urease to Ni-SOD with the change in nitrogen source. Note that the recovery of growth with NH_4^+ additions only persists for a single transfer to NH_4^+ media with no added Ni, after which Ni becomes limiting. WH8102 cannot grow on NO_3^- or NH_4^- without Ni (Fig. 3.3B, C), a phenotype attributable to the deficiency in Ni-SOD activity (Table 3.2). While other marine phytoplankton have been shown to require Ni for growth on urea (131), this is the first marine phytoplankton shown to have an obligate growth requirement for Ni.

CC9311 also cannot grow well on NH_4^+ or at all on nitrate without added Ni, a phenotype contrary to our original hypothesis. While SOD activity was observed in protein extracts from Ni-depleted CC9311, it does not appear to be a completely functional replacement for Ni-SOD, as implied by the Ni dependent cessation of growth. The light dependency of the Ni-limitation observed for NH_4^+-grown CC9311 supports this hypothesis as superoxide production would be predicted to increase with increasing light. The non-Ni-dependent SOD activity did not facilitate growth on NO_3^- without Ni. The Ni-SOD may be specifically targeted to the cytoplasm, with a separate targeting for the Cu/Zn SOD. In *Synechococcus* PCC7942, the Fe and Mn SODs are localized to the cytoplasm and thylakoid membranes, respectively, with –FeSOD mutants being more susceptible to methyl viologen, which generates superoxide radicals in the cytoplasm (181). If Ni-SOD is localized to the cytoplasm, cells growing on NO_3^- without Ni would be

particularly susceptible to superoxide radicals created by the reduction of oxygen by nitrate reductase (11). It must be noted however, that the observed "non-Ni dependent SOD activity" does allow CC9311 to grow, albeit slowly, on NH_4^+ without Ni and may allow a relaxation of Ni requirements in CC9311 by protecting the cell from some oxidative stress.

The competition for intracellular Ni between urease and Ni-SOD may be an important determinant of Ni requirements and the resulting phenotype. The urease operon is upregulated for growth on NO_3^- relative to NH_4^+ (175), and NO_3^- or urea grown *Synechococcus* have higher urease activity than NH_4^+ grown cultures (40). High levels of urease, as well as the attendant Ni-binding metallochaperone *ureE* (130), may scavenge Ni away from Ni-SOD. Consistent with this, NO_3^- grown cultures are more susceptible to low Ni than NH_4^+ grown cells (Fig. 3.7).

The growth experiments conducted over a broad range of $[Ni^{+2}]$ show that WH8102 is affected by decreasing extracellular and intracellular Ni to a greater extent than CC9311. This is surprising given that WH8102 was isolated from an oligotrophic environment with lower Ni concentrations, but this result is also consistent with CC9311 being able to at least partially employ the non-Ni dependent SOD activity as a replacement for Ni-SOD. For example, when grown on urea, if CC9311 can partially scavenge superoxide radicals using a Cu/Zn-SOD, then more intracellular Ni can be allocated to urease, whereas WH8102 must devote more of the Q_{Ni} to Ni-SOD. The greater reduction in the growth rates with

decreasing [Ni^{+2}] observed for growth on urea compared to ammonia for both strains is also consistent with the dependence upon a pair of Ni metalloenzymes. The phylogenomic mapping in Fig. 1 shows that the *sodN* gene (Ni-SOD) does not co-occur within a genome containing *sodB* (Fe-SOD). The replacement of an Fe-SOD with a Ni-SOD would be a logical evolutionary adaptation allowing for the reduction of Fe requirements in an environment where Fe concentrations are low and can be limiting to cyanobacterial growth (113). Indeed, a strain utilizing the Fe-SOD (WH7803) is more susceptible to Fe-limitation than *Synechococcus* A2169 (79), and the use of a Ni-SOD by A2169 could be a ready explanation, though the phylogeny of this strain is not known.

We have shown that at least one strain of marine *Synechococcus* has an obligate growth requirement for Ni, something not previously observed in phytoplankton. Given the requirements of our two model marine cyanobacteria and the complements of Ni metalloenzymes found in cyanobacterial genomes (Fig. 3.1), we suspect that all marine *Prochlorococcus* also have obligate Ni requirements, while many strains of *Synechococcus*, *Trichodesmium,* and *Crocosphaera* are partially dependent upon Ni for growth. Fe-SOD containing strains of *Synechococcus* (WH5701, RCC107, WH7805) likely do not have a requirement for Ni except for growth on urea, and WH7803 might have no Ni requirement as it lacks both Ni-SOD and urease (Fig. 3.1). The strains containing

Fe-SOD instead of Ni-SOD probably have increased Fe requirements as a consequence.

Regulated Ni accumulation by Synechococcus

To date, Ni-specific transporters or regulatory proteins have not been molecularly characterized in marine phytoplankton. The physiological studies presented here attests to the presence of a regulated Ni uptake system in marine *Synechococcus*. Both strains actively accumulate Ni in a regulated fashion: both strains concentrated Ni out of the media 100-10000 times (Fig. 3.7C) and *Synechococcus* grown at lower [Ni^{+2}] have increased maximal uptake rates (Fig. 3.6). The increase in Ni uptake rates restored, or at least maintained, growth rates in both strains at low [Ni^{+2}] by maintaining Q_{Ni}. (Fig. 3.5, 3.7). The regulation of the Ni uptake capacity is different for each strain and nitrogen source. In general, much greater changes in ρ_{max} were observed in WH8102 compared to CC9311 (Fig. 3.7), indicating a more stringent regulation or possibly a greater transport potential. For both strains, the greatest changes in ρ_{max} were observed for growth on urea compared to growth on NO_3^- or NH_4^+ (Fig. 3.7D, 3.7B). The dependence of Ni uptake rates upon nitrogen sources has been observed in the marine diatom *Thalassiosira weissflogii* (149). The nitrogen source specific differences observed here suggest that the global nitrogen sensing regulator *ntcA* (175) may play a role in modulating Ni uptake.

Using the published cellular carbon and phosphorus quotas for *Synechococcus* WH8103 grown under nutrient replete conditions (16), we calculate ranges of Ni:C and Ni:P of 5.6×10^{-7}- 5.6×10^{-4} and 1.5×10^{-4}-1.5×10^{-1} moles moles^{-1}, respectively. The Ni:C ratios observed here bracket the highest Ni concentrations observed for diatoms growing on urea (Ni:C $= 1.7 \times 10^{-6}$ moles moles^{-1}) (149) and Ni:P ratios of 5×10^{-5} to 2×10^{-1} have been observed in *Cyanothece* sp., a marine nitrogen fixing cyanobacteria (66). Due to the sheer abundance of cyanobacteria in both coastal and open ocean ecosystems (144, 163), the Ni:C and Ni:P quotas for *Synechococcus* indicate that these organisms must contribute to the observed surface depletion in oceanic Ni concentrations. For example, a bloom of cyanobacteria assimilating 0.1 μM P (organic or inorganic) will also take up to 15 nM Ni, well in excess of the typical surface ocean concentration of 3 nM Ni. This would suggest that Ni is recycled within the euphotic zone prior to export to deep waters, or else surface seawater would be entirely depleted of Ni given the calculated nutrient drawdown.

Ni limitation in marine ecosystems?

Environmental relevance is a pertinent question for any culture-based study; to what extent are the results laboratory oddities or ecological realities? The strains used in this study have genomes that are well represented in metagenomic libraries of marine environments (158), therefore the question lies in the geochemistry of Ni. The few published measurements of total and chemically

labile Ni in natural marine systems using competitive ligand exchange adsorptive cathodic stripping voltammetry (CLE-ACSV) have suggested that 10-60% of the Ni in coastal and open ocean environments is bound by organic ligands (49, 160). Given these numbers and our measurements of growth rates at fixed [Ni^{+2}] (Fig. 3.5), environmental [Ni^{+2}] seems unlikely to limit cyanobacterial growth except on urea. However, the 2-3 nM nickel in surface seawater has been suggested to be non-bioavailable based on both ecological stoichiometry (109) and physicochemical speciation measurements (194). Ni also possesses extremely slow coordination kinetics, theoretically retarding the maximum possible biological uptake rates relative to other metals (86). Given the lack of a consensus on the bioavailability of Ni from chemical measurements, it is difficult to confidently argue for or against the possibility for Ni limitation in natural systems at this time.

Acknowledgements

Chapter 3 is a reprint of material as it appears in Applied and Environmental Microbiology, volume 74, pages 23-31. K. Barbeau and B. Palenik were co-authors. The dissertation author was the primary investigator and first author.

CHAPTER 4

Global transcriptional response to Ni deprivation and the identification of putative Ni transporters in marine *Synechococcus*

Abstract: An obligate nutrient requirement for Ni is a consequence of the evolutionary exchange of the gene for an Fe-SOD (*sodB)* with that for a Ni-SOD (*sodN),* a trade that has occurred within many marine cyanobacteria, including *Synechococcus sp*. Strain WH8102 (WH8102). In this strain, intracellular Ni concentrations are controlled; in response to Ni deprivation, WH8102 up-regulates the activity of an unknown high-affinity Ni tranporter and reduces growth rates to maintain a minimum intracellular Ni concentration. Full genome microarray analysis of gene expression suggests that Ni deprivation triggers a series of general stress responses that are consistent with the hypothesized biochemical deficiencies in Ni-metalloenzymes Ni-superoxide dismutase and urease activity. Regardless of the nitrogen source provided for growth, Ni-deprivation prompts WH8102 to reduce the expression of genes involved in the synthesis of chl a and heme, possibly decreasing light adsorption or electron transport rates. The concerted induction of seven genes coding for three terminal oxidases may compensate for the deficiency of Ni-SOD by reducing oxygen with electrons from plastoquinone and other donors. The terminal oxidases may also complete a water-water electron flow through the photosystems, scavenging the source of superoxide, free oxygen, while also generating ATP. Another series of general responses were dependent upon the nitrogen source provided for growth, being reversed for growth on urea relative to NH_4^+. The response of the ntcA regulon suggests that at least part of this reversal is due to contrasting balances of C and N. Given the role of the Ni

metalloezyme urease in both catabolic and anabolic nitrogen assimilation, it seems possible that these inbalances are due to the relative effects of Ni deprivation on cellular urease activity. A series of bioinformatics, transcriptional, and genetic studies suggest that *sodT*, a putative transmembrane protein acquired as part of the *sodB*-*sodN* exchange, is involved in Ni uptake. Given the lack of a clear Ni regulatory protein, we propose a post-translational mechanism of regulating sodT activity involving the binding of Ni to a histidine-rich intracellular loop in the encoded sodT protein.

Introduction

As the most abundant photoautotrophs on the planet, the marine cyanobacteria *Synechococcus* and *Procholorococcus* contribute greatly to the global carbon and nitrogen cycles. In addition to the classical macronutrients nitrogen, phosphorus, and carbon, marine cyanobacteria also require several micronutrients such as Fe and Co in appreciable enough quantities to affect their distribution and abundance in natural marine systems (113, 161). Recently, marine *Synechococcus* strains CC9311 and WH8102 were shown to require Ni for growth at maximal rates regardless of the nitrogen source provided for growth, a requirement unique among marine phytoplankton (53). Low level Ni additions were recently shown to prompt growth in select natural populations of *Synechococcus* (Chapter 5), implying that this Ni requirement has ecological consequences.

The biological requirements for Ni are dependent upon the usage of at least two enzymes. Marine *Synchococcus* require a Ni-metalloenzyme, urease, to use urea as a nitrogen source (40) and possibly for arginine catabolism (150). Without added Ni, *Synechococcus* cultures provided with urea as a nitrogen source will cease to grow, with growth being restored by either the addition of Ni, resulting in a functional urease, or NH_4^+, which does not require Ni for assimilation (53). Some *Synechococcus* and all *Prochlorococcus* strains have a gene (*sodN*) coding for a Ni-containing superoxide dismutase (Ni-SOD, 206) within their genomes (54, 139,

142). Ni-limited cultures of *Synechcoccus sp.* Strain WH8102 (WH8012) display reduced SOD activity, regardless of the nitrogen source used for growth, which is eventually lethal (53). Some strains, like CC9311, have a second SOD containing a Cu/Zn active site, and it appears that this facilitates growth without Ni, but only when supplied with NH_4^+ as a nitrogen source. Thus far, all marine *Synechococcus* sp. lacking a Ni-SOD (e.g. WH7803, WH7805) contain the gene for an Fe-containing SOD (*sodB*) in the corresponding genomic location of *sodN* in WH8102 (Fig. 4.1A, 54). This evolutionary exchange that likely results in a loss of an obligate Ni requirement, but increased Fe requirements as a consequence.

In cyanobacteria, nutrient deprivation often induces a stress response *specific* to the nutrient, but also a *general* stress response due to the perturbations in the intracellular balance of metabolites (165). In both CC9311 and WH8102, declining intracellular Ni concentrations induce an increase in the activity of a Ni-specific high affinity uptake system, maintaining intracellular Ni concentrations at 100-300 nM (53). In the simplest sense, this Ni *specific* stress response requires a transporter and a regulator.

In other Bacteria, Ni uptake has been shown to be catalyzed by one of three families of transporters, the Ni/Co permeases, the ABC-type NikABCDE transporter, and the ABC-type NikMNQO tranporters (153). In the genome of *Synechococcus* WH8102, two genes appear to code for proteins in the Ni/Co permease family. One, dubbed *sodT (59),* colocalizes in *Synechococcus* genomes

with *sodN* (Fig. 4.1A). *sodT* codes for a protein with a six transmembrane domain topology associated with the Ni/Co permease family (59). Between transmembrane helices three and four, an intracellular domain contains a high percentage of the Ni-binding amino acid histidine (Fig. 4.1B, C). The other Ni/Co permease has sequence similarity to the hydrogenease associated Ni-transporter *hupE* (*synw2127*), yet the presence of a predicted B12 riboswitch in the upstream promoter region of the gene led to the conclusion that the WH8102 *hupE* transports Co (153). In the Ni-Fe hydrogenase-containing cyanobacterium *Synechocystis* PCC6803, mutagenesis of *hupE* did not affect hydrogenase activity (81), further implying that *hupE* is not involved in Ni homeostasis. The WH8102 genome contains a putative transcriptional unit (*synw0708-0709*) coding for a transporter in the nickel/peptide/opine binding family, where *synw0709* codes for the putative periplasmic substrate-binding protein. While a homolog of *sodT* is found exclusively in *sodN*-containing *Synechococcus* and *Prochlorococcus* genomes, homologs of *hupE* and *synw0709* are also found in the *sodB*-containing *Synechococcus* genomes.

Ni uptake in many Bacteria is regulated at the transcriptional level by the protein NikR (51). In *Escherichia coli,* NikR is negative repressor of the ABC-type *nikABCDE* expression, thereby controlling Ni uptake activity (51). NikR also controls the expression of a Ni transporter in the Ni/Co permease family in *Helicobacter pylori* (62), indicating a certain evolutionary ability to exchange

regulator and transporter pairs. Another Ni regulatory protein, Nur, is a Fur family protein that represses Ni uptake in *Streptomyces* when intracellular Ni concentrations are sufficient for growth and Ni-SOD function (1). Homologues of both proteins are absent from the encoded proteomes of marine *Synechococcus* WH8102 and CC9311, implying a novel form of Ni transport regulation in these organisms.

Little is known about *general* stress responses to Ni deprivation, though an examination of the hypothetical biochemical consequences of Ni deprivation provides several hypotheses. *A priori*, Ni starvation should induce increased oxidative stress due to the reduced amounts of active Ni-SOD. The manifestation of this response can readily be compared to a wealth of relevant microarray studies in *Synechocystis* PCC 6803 (PCC 6803) on Fe starvation(171), UV and high light stress (84), and PSI/PSII-specific inhibitors(80). Ni deprivation could also reduce the amount of active urease in the cell, affecting anabolic (40) and catabolic (150) N assimilation and as a result, the balance between carbon and nitrogen assimilation. To study both the *specific* and *general* stress responses to Ni deprivation, semi-continuous cultures of *Synechococcus* were grown at two [Ni^{+2}] buffered to constant levels with excess EDTA, one sufficient for maximal growth (control) and another with Ni-limited growth rates (Ni deprived), with either NH_4^+ or urea provided as a nitrogen source. The global changes in gene expression

prompted by Ni deprivation were studied using full genome microarrays. In parallel, the inactivation of genes coding for putative Ni transporters was pursued.

Methods

Strains and culturing techniques

E. coli strains MC1061 (pRL528, pRK24) and DH5α (Table 4.1) were grown in Luria-Bertani medium. When appropriate, ampicillin (100 μg/ml), kanamycin (50 μg/ml), and chloramphenicol (10 μg/ml) were used for the selection and maintenance of plasmids in *E. coli*. *Synechococcus sp.* strains WH8102, CC9605, CC9902, and CC9311 (Table 4.1), were grown in SOW media made using the trace metal clean methods described in Dupont et al. (2008). Unless indicated, all cultures were grown at a constant light of 50 μmol photons m^{-2} sec^{-1} and a constant temperature of 19°C (CC9311) or 24°C (WH8102, CC9605, CC9902). In the presented experiments, variations were made in the nickel concentrations and the nitrogen source added for growth. $NiCl_2$ was added in final concentrations of 500 pM, 5 nM, or 50 nM to achieve Ni^{+2} concentrations of 0.5, 5, and 50 pM (195). Chelex-100 purified 1 M $NaNH_4$, 1M $NaNO_3$, or 1M urea was added to a final concentration of 2 mM-N for growth on the different N sources.

The cultures for the microarray experiments were grown in "semi-continuous" fashion, with constant Ni limited exponential growth being achieved and maintained through transfer. With macronutrients added in great excess and

bioavailable inorganic trace metal concentrations being buffered by ethylenediamine tetraacetic acid (EDTA), stable exponential growth rates and intracellular metal concentrations can be achieved, particularly if cultures are maintained at modest cell density (148, 178). When grown in this fashion, the cultures are essentially chemostats, where the limiting nutrient is the free metal concentration (178). Culture phycoerythryn fluorescence was monitored as a proxy for growth, and rates were determined by slope of the linear ln (phycoerythrin fluorescence) vs time relationship. Cultures were transferred during exponential growth to media with the same $[Ni^{+2}]$ until growth rates stabilized, at which time they were allowed to grow for 4-5 more generations prior to harvesting.

One additional experiment examined the response of Ni-limited *Synechococcus* WH8102 to the addition of Ni. Here, a 2 L culture of WH8102 was grown in a 4L polycarbonate carboy without any added Ni. Following the cessation of growth, increasing additions of $NiCl_2$ were made over the next 96 hours. 250 mL samples were removed cleanly at each time point by pouring in a HEPA-filtered laminar flow bench.

RNA isolation

Cultures were harvested by centrifugation (10,000 *g* for 10 minutes) in acid washed and autoclaved 250 mL bottles. Cells were lysed in Trizol (Invitrogen) by incubation at $60^{o}C$ for 1 hour, followed by RNA isolation according to the

manufactors instructions. DNA was removed and RNA further purified using a Qiagen RNeasy kit with DNase digest according to the manufacturers instruction.

Microarray hybridizations and analysis

In collaboration with Ian Paulsen (The Institute for Genomic Research and Macquarie University) complete genome microarray for WH8102 was constructed, consisting of a mixed population of PCR amplicons (2142 genes) and 70mer oligonucleotides (389 genes). Unique PCR amplicons representing each gene are 800 bp, or smaller if the gene size is smaller. Unique 70mer oligonucleotides were utilized for genes under 300 bp and for the two genes that we were unable to amplify by PCR. Six complete replicates of the 2526 member (2517 of these genes are annotated in NCBI) gene set are printed on aminosilane coated Corning ultraGAP glass slides and irreversibly bound by ultraviolet (UV) crosslinking. Each array slide also includes a variety of negative controls (50% DMSO /50% deionized water) and positive controls (including a total mix of WH8102 PCR amplicons, spiked *Arabidopsis* PCR amplicons and 70mer oligonucleotides.

Fluorescently labeled cDNA was generated from the purified RNA indirectly by synthesis in the presence of a nucleoside triphosphate analog containing a reactive aminoallyl group to which the fluorescent dye molecule is coupled. Control and treated samples are labeled with Cy3 and Cy5, respectively, pooled and hybridized to the same array. In addition, reverse labeling was

performed to reduce dye-specific biases in signal intensity. Slides were hybridized with labeled cDNA and then scanned and analyzed using TIGR's SPOTFINDER, MADAM and MIDAS software (ref). RNAs from five nitrate grown cultures and four ammonium grown cultures were used. Thirteen different hybridizations were carried out, of which six used different RNA pools and seven were replicates of these six experiments, either dye swapping experiments or direct replicates. Statistical analyses were carried out using the Significance Analysis of Microarrays (SAM) software package (185), with the hybridizations treated as independent experiments. SAM orders the genes by using a modified *t* statistic called relative difference based on the ratio of change in gene expression to standard deviation in the data for that gene. It declares a gene to be up- or down-regulated if the difference (*D*-value) between the observed relative difference and expected relative difference is above (*D*-value > 0) or below (*D*-value < 0) the global cutoff point, respectively (185). This procedure allows estimation of the median of false discovery rates, and a gene was considered down- or up-regulated by Ni deprivation if it displayed a negative or positive *D*-value beyond the selected 1% median false discovery rate.

RT-Q-PCR

Gene specific PCR primers (Table 4.2) were designed to amplify a 100-150 bp internal region of each gene of interest using Primer3. DNA-free RNA (100 ng)

was converted to cDNA by reverse-transcriptase PCR (SuperScript II Reverse Transcriptase, Invitrogen) with random hexamer primers (50 ng per reaction, IDT, Inc.) according to the manufacturer's instructions. Quantitative PCR was carried out with each gene specific primer pair at a concentration of 400 nM each with 2 μl of the cDNA synthesis reactions using the Brilliant SYBR green QPCR Master Mix kit and the Mx3000p real-time PCR thermocycler and fluorescence detection system (Stratagene). PCRs were carried out in 96-well plates in 25-μL volumes following the activation of the SureStart Taq DNA polymerase included in the kit at 95°C for 10 min. The cycling conditions were as follows: 95°C for 30 s, 60°C for 60 s, and 72°C for 60 s for 40 cycles, followed by a single cycle at 95°C for 30 s, 55°C for 30 s, and a ramp to 95°C at 0.2°C s-1 to determine the melting temperature of the amplified cDNA and to check for the absence of secondary products. Also analyzed for each primer pair was a standard curve of 0.001 to 1 ng genomic DNA from *Synechococcus*. All reactions were run in duplicate. Threshold fluorescences of unknown samples were converted to cDNA concentrations using the standard curves for each primer pair. Agarose gels (1.2%) and Q-PCR disassociation curves were examined to verify single amplicons for each primer pair. A suitable housekeeping gene is not known for WH8102, therefore changes were quantified as the ratio of expression between experimental (Ni deprived) and control (Ni sufficient) samples.

Genetic manipulations

Inactivations were performed and validated according to the methods presented in (21). Briefly, a *Synechococcus* gene-specific internal fragment (Table 4.2) was cloned into the EcoRI site of the suicide vector pMUT, which was introduced to the *E. coli* strain MC1061 (pRL528, pRK24, Table 4.1). The pMUT constructions were introduced to *Synechococcus* by conjugation with MC1061 (pRL528, pRK24) with subsequent selection of exconjugants on pour plated SN media (193) supplemented with at least 25 μg/mL filter sterilized kanamycin sulfate. Clonal isolates were inoculated into liquid SN supplemented with 25 μg/mL kanamycin and maintained in exponential growth until axenic, as determined by spotting on LB agar plates. The complete segregation of mutant chromosomes was verified using PCR as described in (117) with the verification primers from Table 4.2. In all experiments, to facilitate the isolation of Ni –uptake impaired exconjugants, SN-agar media was amended with 5 nM $NiCl_2$. In the experiments with Cu/Zn-SOD containing *Synechococcus* strains, SN-agar media was amended with 5 nM $CuCl_2$, and 0.5 mM NH_4^+ to mimic the conditions where Ni limited CC9311 can grow (Chapter 3).

Ni uptake rates

Ni uptake kinetics were determined as outlined in chapter 3. Briefly, cells were harvested by centrifugation (10,000 x*g* for 10 minutes) in acid washed

polycarbonate bottles, rinsed twice with SOW containing no added EDTA or trace metals, and resuspended in 10 mL SOW with no added EDTA or trace metals in 70 ml acid-washed polycarbonate bottles. To measure Ni uptake rates, ^{63}Ni was added to final concentrations of 0.1 to 20 nM. Follwing a 30 minute incubation at standard growth conditions, experiments were terminated by filtration onto 0.2 μm pore size filters (Supor, polyethersulfone). The filters were rinsed with 5mL of sulfoxime (a Ni chelator, 1 mM in SOW, Avocado Biochemicals) and 5 mL of SOW to remove surface bound ^{63}Ni prior to being added to 15 mL of scintillation fluid (Ecolyte). To determine the total added ^{63}Ni, small aliquots (150 μL) of unfiltered media were added to 15 mL of scintillation fluid. Radioactivity was assayed using standard scintillation counting with quench correction. Disintegrations per minute were converted to ^{63}Ni concentrations using a dilution curve to ^{63}Ni.

Results and Discussion

Overall physiological and transcriptional effects of Ni deprivation

Ni deprivation was examined in cultures of WH8102 growing on NH_4^+ (hereafter referred to as WH8102-NH_4^+), urea (WH8102-urea), or nitrate (WH8102-NO_3^-) as a nitrogen source. To induce Ni deprivation, cultures were maintained in exponential growth at constant [Ni^{+2}] of 0.5 and 50 pM until growth rates were stable (at least 20 doublings), at which point they were harvested. At the

lower [Ni^{+2}], growth rates were repressed 15-20% and Ni uptake rates increased 400-500% (Table 4.3). Using a maximum false positive rate of 1% as a selection criteria (see methods), 100-300 open reading frames were determined to be significantly up- or down-regulated in response to Ni deprivation in each experiment except for WH8102-NO_3^- (Table 4.3). The technical and biological replicates of this experiment were of poor relative quality, with average pairwise correlation coefficients over the 6 microarrays of less than 0.25 (compared to 0.45 and 0.53 for the WH8102-urea and WH8102-NH_4^+ experiments). This experiment is excluded from further discussion.

The nitrogen source for growth drastically affected the transcriptional response of WH8102 to Ni deprivation (Figure 4.2). Sixty-five genes were regulated in the same fashion in both WH8102-NH_4^+ and WH8102-urea experiments (Table 4.4), and these were denoted as *coordinately-expressed*. Another thirty-eight genes were *divergently expressed* in the two experiments, being induced in one and repressed in another (Table 4.5). Complete lists of up and down regulated genes in both experiments and the associated SAM scores and fold changes are available in appendix.

Ni deprivation induced changes in gene transcription

Repressed expression of genes involved in ATP synthesis and translation

Genes for three of the 10 genomically-coded subunits of ATP synthase were down-regulated in both experiments (Table 4.4), while several other subunits were down-regulated in the individual experiments. The genes coding for elongation factor EF-G and two tRNA synthases were down-regulated in both experiments (Table 4.4), while a further four and seven tRNA synthases were down-regulated in the WH8102-NH_4^+ and WH8102-urea experiments, respectively. Five and six genes coding for ribosomal subunits were down-regulated in the WH8102-NH_4^+ and WH8102-urea experiments, respectively, though none were shared. The down-regulation of genes involved in ATP generation and translation is consistent with the reduced growth rates observed in the Ni deprivation experiments (Table 4.3).

Chaperones and typical stress responses

Genes coding for numerous chaperones and protein degradation proteins, including two copies of *dnaJ*, *dnaK,* and several subunits of Clp protease, were up-regulated by Ni deprivation for cells growing on NH_4^+, but not by Ni deprivation for cells provided with urea. In sharp contrast, the expression of Clp protease was strongly repressed by Ni deprivation for cells growing on urea (Table 4.5). Transcription of a gene coding for a putative protein in the redox-regulated HSP33 family was repressed in both experiments (Table 4.4). HSP33 family proteins are post-translationally regulated by the presence of reactive oxygen species like hydrogen peroxide and the observed repression may prevent an overabundance of

activated HSP33 protein. While homologues of the peroxiredoxin and associated regulatory element involved in the oxidative stress response in PCC 6803 (89) are missing from the *Synechococcus* WH8102 genome, a gene coding for a protein with a putative CXXC thioredoxin domain was upregulated in both experiments (*synw1522,* Table 4.4).

Transcription and regulatory elements

Ni deprivation elicited changes in the expression of genes coding for putative transcriptional regulatory proteins, but with remarkable differences according to the provided N source. As an extreme example, two type II σ factors (*synw1509* and *synw2427*) and one response-regulator (*synw2289*) were divergently expressed in the two experiments, being repressed in one but induced in the others (Table 4.5). Overall, five of the nine response regulators and two of the five histidine kinases found in the WH8102 genome (139) were differentially regulated in one of the experiments, but never in the same fashion in both experiments.

Coordinated expression of regulatory genes in both experiments was observed for other less traditional regulatory elements. Genes coding for two putative methyltransferases (*synw0899*, *synw1072*) were down-regulated in both experiments (Table 4.4). A gene (*synw0328*) coding for a protein with a histidine-triad motif (InterPro id IPR001310), a conserved nucleic-acid binding protein

family with putative orthologues in all of marine cyanobacterial genomes was up-regulated in both experiments (Table 4.4) and may be a potential Ni-metalloregulatory protein.

Expression of the ntc regulon and carbon assimilation related genes

In cyanobacteria, the cAMP receptor protein NtcA controls the expression of genes involved in nitrogen assimilation though the binding to canonical palindromic promoter sequences (68). Recently, the subset of genes regulated in WH8102 by ntcA was examined using a combination of bioinformatic and microarray-based approaches (WH8102 ntcA regulon, 175). Putative ntcA promotor sequences are located upstream of 9 and 16 of the genes up- and down-regulated, respectively, in response to Ni deprivation for growth on NH_4^+. Of these, 5 of the 9 up-regulated genes are known to be positively regulated by NtcA, whereas three of the 16 down-regulated genes are known to be negatively regulated by ntcA. Only one down-regulated gene was shown to be positively regulated by ntcA in WH8102 for growth on nitrate relative to NH_4^+ (175).

A dramatically different response of the WH8102 ntcA regulon was prompted by Ni deprivation in cultures supplied with urea as a nitrogen source. Of the up-regulated genes, five have upstream ntcA binding sites and two (*synw2466* and *synw2496*) are negatively regulated by ntcA (175). Eleven down-regulated genes have putative ntcA binding sites and eight are positively regulated by ntcA,

including *ntcA* (*synw0275*) itself. Three genes of the ABC-type urea transporter (*synw2439-2441*) and one ferrodoxin (*synw1277*) were up-regulated in response to Ni deprivation if NH_4^+ was supplied as the nitrogen source, but down-regulated when urea was provided as a nitrogen source (Table 4.5).

Overall, these results suggest that Ni deprivation prompts a nitrogen-deprivation-like response from the WH8102 ntcA regulon for growth on NH_4^+, with an opposite effect for growth on urea. In cyanobacteria, it is generally agreed that NtcA monitors the intracellular concentrations of 2-OG, which reflects the balance between intracellular N and C assimilation (68).

In the simplest sense, the response of the ntcA regulon in response to Ni deprivation suggests an inbalance in carbon and nitrogen assimilation. Competition between urease and SOD for intracellular Ni may provide an explanation for different flows of N in the two experiments. For cells growing on NH_4^+, Ni deprivation results in inactive urease and a reduced catabolic flow of N relative to carbon catabolism and assimilation, which is Ni independent. When growing on urea, *Synechococcus* induces urease expression (40), and the increased amount of urease might compete better for Ni. As a result catabolic and anabolic NH_4^+ flow are maintained relative to carbon assimilation, resulting in a sufficiency of NH_4^+ relative to 2-OG. The competition for Ni with urease may explain why the lowest Ni-SOD activities are observed for Ni-deprived cells growing on urea in both WH8102 and CC9311 (53).

Carbon fixation and glycolysis

The expression of genes predicted to be part of an *in-silico* construction of the carbon fixation pathway in WH8102 (68) suggests that carbon assimilation is quite different in both experiments. In the WH8102-NH_4^+ experiment, numerous carbon fixation genes were down-regulated, including a putative carbonic anhydrase (*synw0897*), a structural carboxysome protein (*synw1715*), phosphoribulose kinase (*prk*, *synw0785*), *hemA (synw1117)*, *glyC (synw1118)*, *cbbE* (*synw1115*), *fabF* (*synw0142*). In constrast, only *fabF* and two genes (*synw1709-1710*) predicted to be part of a putative NADH-catalyzed carbon dioxide uptake mechanism (136) were down-regulated in the WH8102-urea experiment. Together, this suggests that carbon fixation may be repressed in the WH8102-NH_4^+ experiment relative to the WH8102-urea experiment, which is consistent with ntcA-implied imbalances between 2-OG and NH_4^+.

A gene for transaldolase (*synw1759*), which may be involved in regulating the flow of carbon through the pentose phosphate pathway, was down-regulated in WH8102-NH_4^+ and up-regulated in WH8102-urea. Genes coding for the subunits of Rubisco were not differentially regulated in either experiment. Two genes involved in glycolysis, including pyruvate dehydrogenase (*synw1620*) and pyruvate kinase (*synw1298*) were down-regulated in both experiments (Table 4.4), which may reduce the generation of superoxide radicals by this pathway.

Photosynthesis

Ni deprivation did not overly affect the expression of the genes for the photosynthetic reaction centers and associated proteins: 1) *psaC* (*synw0144*) and *psbP* (*synw0927*) were up-regulated in WH8102-NH_4^+, 2) *psaK* (*synw1290*) and *psbY* (*synw0898*) were down-regulated in WH8102-NH_4^+, 3) CP43 (*synw0676*), *synw0683*, *psbP*, and *psb27* (*synw1772*) were down-regulated in WH8102-urea. This modest response is a stark contrast to the transcriptional response of the cyanobacterium *Synechocystis* PCC 6803 (PCC 6803) to either Fe deficiency (171) or UV-B stress (84), where down-regulation of most of the genes coding for photosynthetic reaction centers was observed. In contrast, additions of inhibitors of electron transport that result in a over-reduction or over-oxidation of the plastoquinone pool had very little effect upon the expression of the photosynthetic proteins in PCC 6803 (80), a scenario similar to the one observed here.

Porphyrins and phycobilisomes

Regardless of the nitrogen source provided, Ni deprivation prompted *Synechococcus* WH8102 to down-regulate four of the eight genes coding for proteins involved in the synthesis of protoporphyrin IX, the precusor of chlorophyll and heme, from glutamate including *hemA, hemC, hemE,* and *hemL* (Fig. 4.3). Two of the remaining four genes were down-regulated in one of the experiments

(Fig. 4.3) and the two genes coding for proteins involved catalyzing the insertion of Mg or Fe into protopophyrin IX, Mg-chelatase and ferrochelatase were also repressed (Fig. 4.3). The implications of this concerted down-regulation are unknown, but it may reduce the amount of chl a and therefore light adsorption at the photosynthetic reaction centers. Alternatively, reduced heme synthesis may indicate a reduced amount of electron transport chaperones in the photosynthetic reaction pathway. Only a few proteins involved in the phycobilisomes were differentially expressed, suggesting that these light harvesting complexes are unaffected.

Non-traditional electron flow

In both the WH8102-NH_4^+ and WH8102-urea experiments, subunits for a pair of putative cytochrome c oxidases are up-regulated in response to Ni deprivation (Table 4.4). The freshwater *Synechococcus sp.* strain PCC 7002 has a pair of functionally characterized cytochrome c oxidases; one (ctaI) was shown to act as a sink for excess electrons and oxygen in the thylakoids (133, 134). The second, ctaII, appears to regulate the cellular response to oxidative stress from one of the cellular membranes (134). A phylogenetic analysis reveals that ctaDIEIFI from PCC7002 corresponds to *synw1861-1863* while PCC7002 ctaDIIEIIFII matches to *synw1528-1530*. These oxidases may be important in detoxifying superoxide anions in the absence of Ni-SOD, or reducing the generation of

superoxide. While the electron donor is unknown, the likely electron acceptor would be oxygen.

The expression of a gene coding for a putative oxidase (*synw0887*) is also induced by Ni deprivation in both experiments. This gene has been suggested to code for a plastoquinone terminal oxidase (PTOX), based upon the sequence similarity to the well characterized PTOX found in plant chloroplasts (119). While the exact functional role in cyanobacteria remains unknown, in plastids PTOX couples the oxidation of plastoquinol with the reduction of water (4). In plant mitochondria, the alternative oxidase greatly reduces the potential for the generation of reactive species, presumably though the scavenging of oxygen (116). PTOX may act as a "safety valve" preventing the overreduction of photosystem I electron acceptors in plastids (157). In cyanobacteria, PTOX may stabilize the redox state of the plastoquinone pool, which is important in the regulation of NADPH dehydrogenase (NADI) catalyzed cyclic electron flow around photosystem I in cyanobacteria (107).

The physiological trademarks of a water-water cycle have been observed in marine cyanobacteria and evoked as a mechanism to scavenge oxygen radicals (90, 91, 122), yet the machinery involved is not known. These Ni responsive oxidases, particularly the thylakoid located PTOX and *ctaI* may catalyze a water-water cyclic electron flow similar to the Mehler reaction (9), generating ATP while compensating for the reduced Ni-SOD activity.

Identification of genes involved in Ni uptake in WH8102

Transcriptional response of genes coding for putative Ni transporters

Ni uptake rates are greatly enhanced by the changes in extracellular Ni concentrations (Table 3), therefore it came as some surprise that none of the three putative Ni transporters, *hupE*, *sodT,* and *synw0709*, were up-regulated in response to Ni deprivation in any treatment. *synw0709* was down-regulated in the WH8102-NH_4^+ experiment providing evidence this gene is not involved in high affinity Ni uptake.

The up-regulated genes from both the WH8102-urea and WH8102-NH_4^+ Ni deprivation experiments were further examined to determine putative Ni transporters and Q-RT-PCR targets of interest beyond *hupE* and *sodT*. Of the genes up-regulated in both experiments, 13 code for proteins with putative transmembrane domains (Table 4.4). Seven of these are involved in membrane-based electron transport or redox activity and a further two proteins have only one transmembrane domain, making them unlikely candidates. One of the remaining genes (*synw1916)* codes for a one part of a multigene operon potentially involved in osmotic balance, and this gene was not examined further. The final up-regulated gene *(synw1526)* shared between both treatments appears to be part of a putative transcriptional unit (*synw1525-1531*) involved in membrane based electron transport. One gene, up-regulated in the WH8102-NH_4^+ experiment, codes for a

putative member of the sodium-bile cotransporter family and also has an upstream NtcA binding site (*synw0635*). As the substrate specificity of this transporter family is completely unknown in Bacteria, the expression of this gene was examined.

Two further experiments were designed to manipulate the biological Ni uptake rates while examining the expression of *sodT, hupE,* and *synw0635* using RT-Q-PCR. In the first experiment, cultures of WH8102 were grown on NH_4^+ at constant [Ni^{+2}] of 0.5, 5, and 50 pM. While Ni uptake rates increased nearly five-fold, *sodT* and *hupE* expression were relatively constant, whereas *synw0635* transcript abundance increased with decreasing Ni, albeit at a fraction of the changes in Ni uptake rates (Fig. 4.4). In a second experiment, WH8102 was grown on NH_4^+ without any added Ni to the media, resulting in a cessation of growth due to Ni limitation (Fig. 4.5A). At this point, the culture received a Ni addition of 5 nM, stimulating a return to exponential growth (Fig. 4.5A) and a decline in Ni uptake rates (Fig. 4.5B). Again, *synw0635* displayed a profile of transcription similar to the observed changes in Ni uptake, though the changes in expression were minor compared to those observed in Ni uptake (Fig. 4.5B). The transcription of *sodT and hupE* did not resemble the changes in Ni uptake rates.

Inactivation of putative Ni transporters

Inactivation of genes in *Synechococcus* WH8102 can be achieved via conjugation with *E. coli* (21), providing a valuable tool for functional identification. *synw0635* was chosen for inactivation based upon the consistent transcriptional response to Ni deprivation. While constitutively expressed, *sodT* was chosen for inactivation due to the lack of functional information, the possibility of post-translational regulation, and the genomic co-localization with *sodN*. The coupling of the *hupE (synw2127)* expression data with the results from previous studies (81, 153) provides strong evidence that this gene is involved in Co, rather than nickel uptake.

An exconjugant was isolated and verified to contain an interruption of *synw0635*, with a complete lack of wild-type copies. The Ni uptake rates of this exconjugant (*synw0635*$^-$) were measured following growth at [Ni^{+2}] of 0.5 and 50 pM. As *synw0635*$^-$ needs to be maintained on 25 μg/ml kanamycin, which may affect the Ni speciation in an unknown fashion, the non-motile exconjugant *swmA*$^-$ (20, 118), was used as a control. The strains displayed similar changes of Ni uptake kinetics in response to reduced Ni concentrations (Fig. 4.6), indicating that *synw0635*$^{--}$ is either not involved in Ni transport, or that there are redundant transporters.

The presence of an ntcA-binding site in the promotor region of *synw0635* and the up-regulation in response to Ni starvation for growth on NH_4^+ is consistent

with a positive regulation by ntcA, as observed in the microarray experiments. This would imply that the encoded protein is involved in nitrogen assimilation, possibly the transport of an organic nitrogen substrate.

Despite several attempts, exconjugants of *sodT* in WH8102 could not be obtained, with no colony formation on selective plates. Conjugations and pour platings were performed in parallel with constructions specific for *–swmA* and *sywn0635* that were successful, providing positive controls. Given the obligate Ni requirement for growth, the inactivation of a Ni transporter could be fatal to this strain. Alternatively, *sodT* may be required for *sodN* activity through a non-transport based mechanism.

Synechococcus sp. CC9311 can grow on NH_4^+ without Ni, presumably due to the usage of a Cu/Zn- containing SOD (53). *Synechococcus* CC9902 and CC9605 also have a Cu/Zn-SOD in addition to a Ni-SOD. Therefore, pMUT100 plasmids were constructed for conjugation-based inactivation of *sodT* in *Synechococcus* CC9311, CC9902, and CC9605 (Table 4.1). In the case of CC9902, no colonies were obtained. PCR-based analyses of genomic DNA from putative exconjugants of CC9311-pMCC9311sodT obtained on kanamycin-amended SN plates revealed the presence of the wild-type gene (*sync_0753*) and lacked the gene for kanamycin resistance, suggesting a low rate of spontaneous evolution of kanamycin resistance in this strain. A similar scenario occurred for CC9605; an increase in kanamycin concentrations to 50 μg/mL prevented the

growth of colonies of wild-type CC9605, but again colonies of exoconjugants were not obtained following conjugation with pMCC9605sodT.

A theoretical model of Ni uptake and homeostasis involving sodT

Despite the lack of robust functional characterization, several lines of evidence suggest that *sodT* is involved in Ni transport and homeostasis in *Synechococcus* WH8102. The encoded protein has strong similarity to functionally characterized Ni transporters (59), genomic co-localization with *sodN* is well conserved (Fig. 4.1), and inactivation appears to be lethal, at least in WH8102. While genomically co-localized with *sodN*, *sodT* is transcribed on the opposite strand and it is unlikely the insertional inactivation of *sodT* would affect the transcription of *sodN*. As transcription of *sodT* and Ni uptake protein activity are uncoupled (Figs. 4.4 and 4.5), the activity of the protein must be controlled at a post-transcriptional or post-translational level, if *sodT* does indeed code for the Ni transporter.

The post-transcriptional regulation of metal transporter genes has not been observed in Bacteria, though positive regulation of genes like *sodB* and ferritin by Fur is achieved indirectly through Fur-dependent repression of an anti-sense regulatory small RNA that acts post-transcriptionally to reduce translation of *sodB* and ferritin (104).

Ni uptake in WH8102 may be regulated post-translationally. The protein coded for by *sodT* contains an intracellular loop laden with histidine residues (Fig. 4.1C), which have strong Ni-binding imidizole side chains. Constitutively expressed in high amounts, SodT would presumably be present in the periplasmic membrane and with sufficient intracellular Ni concentrations, the His-rich loop would be complexed with Ni. With declining intracellular Ni concentrations, Ni would disassociate from the His-rich loop. Potentially, the structural changes associated with Ni diassociation would activate the transport activities of the enzyme. In this scenario, the genomic locale displayed in Fig. 4.1 contains all of the elements required for marine cyanobacteria to use a Ni-containing SOD: 1) *sodN*, coding for apo-Ni-SOD, 2) *ppIase* and *sodX*, protein chaperones required for post-translational modifications of the apo-Ni-SOD following Ni binding (58, 93), and 3) *sodT*, which we hypothesize both senses and transports Ni.

An implication of this model is the lack of inducible high-affinity Ni uptake in all of the *sodB*-containing strains of marine *Synechococcus,* including WH7803, WH7805, RSS9917, RSS9916, and WH5701. While these strains do not need Ni for SOD activity, all but WH7803 have the genes for a Ni-containing urease. As a low affinity Ni uptake may be present, these strains may be able to grow on urea if provided with high enough Ni concentrations. However, one would expect that strains like WH8102 with high affinity Ni uptake and lower Fe requirements would have a competitive advantage in oligotrophic conditions where urea features

prominently in community metabolism (191). Essentially, the exchange of *sodN-sodX-sodT* for *sodB* may have created a major physiological divide of ecological implications in the marine *Synechococcus*.

Future directions

In its current form, this chapter lacks any robust functional or physiological characterization of the proposed hypotheses. It does however suggest several exciting new paths of research. Here, I hope to detail in a succinct fashion three different experiments, the completion of any one should ease the future trials of publication immensely.

1. Re-swap the SODs: Prepare pMUT plasmids for WH8102 *sodT* and *sodN* identical to the ones described in Table 4.1, but also clone the *sodB* gene from WH7803 into the BamHI site. Through conjugation, introduce these vectors into the open reading frames coding for *sodN* and *sodT*, selecting for kanamycin resistance. Exconjugants of *sodN* should exhibit inducible Ni uptake, but have Fe-SOD activity, which can be distinguished from Ni-SOD activity through inhibitor studies. Exconjugant of *sodT* should lack Ni uptake, and likely have Fe-SOD activity.
2. Metabolite profiling: Examine the effects of Ni deprivation on the ratios of cellular metabolites. This will be particularly useful in understanding how

the differential expression of poorly understood enzymes like arginase and transaldolase influence cellular physiology.

3. Gene expression studies of *ctaI*, *ctaII*, and PTOX: Examine the expression of these genes in Ni starvation time course and steady state experiments (RNA already available), as well as in response to the addition of superoxide generating compounds such as norflurazon and methylviologen.

Table 4.1: Strains and Plasmids used in this study

Strain or Plasmid		Relevant characteristics	Source or reference
Strain			
Synechococcus sp. Strain	WH8102	Clade III, used for microarray studies	Palenik et al. 2003
	CC9311	Clade I, coastal isolate, chromatic adapting	Palenik et al. 2005
	CC9606	Clade II, abundant serotype in stratified California current	Toledo and Palenik 2003
	CC9902	Clade IV, coastal isolate	Palenik et al unpublished
E. coli	MC1061	Host for pRK24, pRL528; donor in pMUT conjugations	Elhai and Wolk 1988
	DH5α	Recipient in transformations	
Plasmids			
pMUT100		Kan^r, Tet^r; suicide vector	Brahamsha 1996
pRK24		Tc^r, Amp^r; conjugal plasmid, RK2 derivative	Brahamsha 1996
pRL528		Cm^r; helper plasmid, carries *mob*	Brahamsha 1996
pCR2.1-TOPO		Kan^r, Amp^r; PCR product cloning vector	Invitrogen
pMSYN0635		pMUT100 containing *synw0635* fragment of nt 267821 to 268051	This work
pMSYNWsodT		as above: *synw1628* fragment of nt 174584 to 174839	This work
pMSYNCsodT		as above: *sync0753* fragment of nt 703532 to 703832	This work
pM9902sodT		as above: SynCC9902_0871 fragment of nt 842654 to 842947	This work
pM9605sodT		as above: SynCC9605_1528 fragment of nt 14748101 to 1478370	This work

Table 4.2: Primer used in this study

Name	Sequence	Purpose
Qsynw1628for	TCTGGTCCATGTTGAGACGA	Q-PCR of synw1628
Qsynw1628rev	TGACTGTGCAGCTCAAGACC	Q-PCR of synw1628
Qsynw0635for	AGTGCACCATCAGCATTGAG	Q-PCR of synw0635
Qsynw0635rev	CACAGCTGAGATTGCTCCAG	Q-PCR of synw0635
Qsynw2127for	GACCAATCTTCTGGCTTCTCC	Q-PCR of synw2127
Qsynw2127rev	GGGCTGGAGATCAATAGCAA	Q-PCR of synw2127
Qsynw1709for	TGAAGATTGCAGACCGACAG	Q-PCR of synw0709
Qsynw1709rev	AGTTGCGAAAGGCTGAAAAG	Q-PCR of synw0709
Incsynw1628for	CAGCATCCTCACCGGTTT	Inactivation of synw1628
Incsynw1628ref	GGCACCCACCACCAGTAG	Inactivation of synw1628
Incsynw0635for	GTTGCTGCACCCTCCATT	Inactivation of synw0635
Incsynw0635rev	AGCAGCCCACAAGGATCA	Inactivation of synw0635
Incsync0753for	AGCCATGAAGTCAGGAATGG	Inactivation of sync0753
Incsync0753rev	CTGGTCTTGGATTGCTCCAT	Inactivation of sync0753
IncCC9902sodTfor	CCAGAAGATGACTCGCACCT	Inactivation of CC9902 *sodT*
IncCC9902sodTrev	CGATTGGCTTGAAAGACCTC	Inactivation of CC9902 *sodT*
IncCC9605sodTfor	GCAGAGCATCGTCATCTTCA	Inactivation of CC9605 *sodT*
IncCC9605sodTrev	GATCGAGAGAGCACCTGTCC	Inactivation of CC9605 *sodT*
Versynw0635for	GCGCCATGG ATGTCCCTCGAGCGATTCACC	Verification of synw0635 interruption
Versynw0635rev	GCGAGATCTAGGGATGTGAGCTGTTGAGGA	Verification of synw0635 interruption

Table 4.3: Growth, Ni uptake, and gene expression in the microarray experiments.

	pNi = 12.3		pNi = 10.3		Differential gene expression median FDR of 1%	
Strain and Nitrogen source	μ (day^{-1})	Ni uptake zmoles $cell^{-1}$ min^{-1}	μ (day^{-1})	Ni uptake zmoles $cell^{-1}$ min^{-1}	Upregulated	Downregulated
WH8102-NH_4	0.43 ± 0.03	3.5 ± 0.05	0.49 ± 0.03	0.7 + 0.05	166	272
WH8102-Urea	0.375 ± 0.25	4.0 ± 0.05	0.52 ± 0.3	1 + 0.05	210	207
WH8102-NO3	0.43 ± 0.02	3.8 ± 0.1	0.55 ± 0.05	0.8 + 0.04	4	21

Table 4.4: Genes coordinately expressed the Ni deprivation experiments. Shown are fold changes of the gene in question, where the fold change is $\log_2$ (experimental/control). The presence of a ntcA motif in the promotor region of each gene (175) and the number of predicted transmembrane domains is also noted. Putative transcriptional units (37) are shown in bold (reverese strand) or bold italics (forward strand).

Locus	Description	FC-NH4	FC-urea	ntcA	TM domains
SYNW0014	RNA-binding region RNP-1 (RNA recognition motif)	0.41	0.9	no	0
SYNW0247	His-rich cyanobacterial conserved hypothetical protein	0.47	0.8	no	0
SYNW0328	cyanobacterial HIT (Histidine triad) family protein	0.19	0.18	no	0
SYNW0477	Hypothetical	0.21	0.2	no	0
SYNW0732	IPR012903 family protein-unknown nif protein	0.36	0.29	no	0
SYNW0738	conserved hypothetical protein	0.25	0.37	no	3
SYNW0778	conserved hypothetical	0.49	0.3	no	0
SYNW0786	hypothetical	0.24	0.35	no	0
SYNW0848	IPR013830 family protein-esterase	0.35	0.2	no	0
SYNW0887	Plastoquinol terminal oxidase	0.63	1.48	no	1
SYNW0916	hypothetical	0.25	0.28	no	0
SYNW0951	hypothetical	0.43	0.36	no	0
SYNW0991	conserved hypothetical protein	0.16	0.18	no	0
SYNW1124	conserved hypothetical	0.51	0.28	no	1
SYNW1400	hypothetical	0.48	0.23	no	0
SYNW1522	IPR012336 family protein-Thioredoxin	0.38	0.55	no	0
SYNW1526	***conserved hypothetical protein***	0.21	0.66	no	4
SYNW1529	***ctaDII-cytochrome c oxidase subunit I***	0.40	0.41	no	12
SYNW1814	conserved hypothetical protein	0.39	0.31	no	0
SYNW1859	**CtaI associated protoheme IX farnesyltransferase**	1.35	0.87	no	7
SYNW1860	**CtaI associated conserved hypothetical protein**	0.74	0.52	no	8
SYNW1861	***ctaCI-cytochrome c oxidase subunit II***	0.85	1.22	no	3
SYNW1862	***ctaDI-cytochrome c oxidase subunit I***	0.82	1.23	no	12
SYNW1863	***CtaEI-possible cytochrome c oxidase subunit III***	0.37	0.26	no	4
SYNW1916	ABC transporter glycine betaine/proline family	0.15	0.17	no	6
SYNW2160	**conserved hypothetical protein**	0.42	0.28	no	1
SYNW2161	**putative 4'-phosphopantetheinyl transferase**	0.45	0.34	no	0
SYNW2252	conserved hypothetical protein	0.21	0.2	no	0
SYNW2355	IPR006620 family protein-Fe (II) hydroxylase	0.99	0.28	no	0
SYNW2385	conserved hypothetical protein	0.62	0.93	no	0
SYNW0127	lysyl-tRNA synthetase	-0.36	-0.21	no	0
SYNW0142	3-oxoacyl-[acyl-carrier-protein] synthaseII	-0.68	-0.45	no	0
SYNW0397	conserved hypothetical protein	-0.27	-0.13	no	0
SYNW0490	ATP synthase subunit γ	-0.85	-1.04	no	2
SYNW0492	putative ATP synthase B chain	-0.63	-0.88	no	1
SYNW0512	ATP synthase β subunit	-0.85	-1.08	no	0
SYNW0673	O-acetylserine (thiol)-lyase A/cysteine synthase	-0.70	-0.3	no	0
SYNW0684	similar to methyltransferase	-0.23	-0.14	no	0
SYNW0820	*chlH*-Protoporphyrin IX Magnesium chelatase subunit	-0.69	-0.4	no	0
SYNW0899	probable glucose inhibited division protein	-0.50	-0.28	no	0
SYNW1072	SAM binding motif: Generic methyl-transferase	-0.78	-0.25	no	0
SYNW1117	Possible glutamyl-tRNA reductase	-0.58	-0.44	no	0
SYNW1153	possible 33kD chaperonin heat shockprotein HSP33	-0.16	-0.18	no	1
SYNW1197	tldD-putative modulator of DNA gyrase	-0.47	-0.56	no	0
SYNW1298	***pyruvate kinase***	-0.63	-0.35	no	4
SYNW1299	***possible ABC transporter***	-0.28	-0.18	no	1
SYNW1300	***FtsH ATP-dependent protease homolog***	-0.76	-0.71	no	0
SYNW1475	t-RNA synthetase class Ib:Tryptophanyl-tRNA synthetase	-0.36	-0.25	no	0
SYNW1495	***uroD/hemE-Uroporphyrinogen decarboxylase***	-0.59	-0.8	no	0
SYNW1496	***conserved hypothetical protein***	-0.46	-0.24	no	0
SYNW1620	Pyruvate dehydrogenase E1 alpha subunit	-0.25	-0.23	no	0
SYNW1721	conserved hypothetical protein	-0.30	-0.25	no	0
SYNW1734	**putative GTP cyclohydrolase I**	-0.70	-0.44	no	0
SYNW1738	**conserved hypothetical protein**	-0.53	-0.28	no	0
SYNW1747	*hemH*-Ferrochelatase	-0.27	-0.29	no	0
SYNW1774	Putative carbohydrate kinase pfkB family	-0.36	-0.3	no	0
SYNW1779	conserved hypothetical protein	-0.62	-0.14	no	2
SYNW1785	*hemC*-Porphobilinogen deaminase	-0.23	-0.37	no	0
SYNW1809	***hemL-glutamate-1-semialdehyde 21-aminomutase***	-0.48	-0.54	no	0
SYNW1810	***hypothetical***	-0.63	-1.18	no	0
SYNW2041	MRP protein homolog	-0.35	-0.22	no	0
SYNW2137	elongation factor EF-G	-0.62	-0.96	no	0
SYNW2147	putative aminotransferase	-0.39	-0.35	no	0
SYNW2255	putative RNA-binding protein (RRM domain)	-0.67	-0.27	yes (unk)	0
SYNW2266	Putative sugar-phosphate nucleotidyltransferase	-0.76	-0.39	no	0

Table 4.5: Genes divergently expressed the Ni deprivation experiments. Shown are fold changes of the gene in question, where the fold change is $\log_2$ (experimental/control). The presence of a ntcA motif in the promotor region of each gene (175) and the number of predicted transmembrane domains is also noted. Putative transcriptional units (37) are shown in bold (reverese strand) or bold italics (forward strand).

Locus	Description	FC-NH4	FC-urea	ntcA	TM domains
SYNW0004	Glutamine amidotransferaseclass-II:Phosphoribosyl transferase	0.36	-0.17	no	0
SYNW0927	photosystem II oxygen-evolvingcomplex 23K protein-PsbP	0.21	-0.47	no	0
SYNW0938	endopeptidase Clp ATP-binding chain C	1.03	-0.88	no	0
SYNW1061	*hypothetical*	1.54	-0.80	no	0
SYNW1277	ferredoxin	0.56	-1.44	yes (+)	0
SYNW1503	endopeptidase Clp ATP-binding chain B	1.14	-1.97	no	2
SYNW1587	cell division protein FtsH3	0.57	-1.10	no	0
SYNW1832	homologous to C-terminus of pilT2 protein	0.69	-0.43	no	0
SYNW2000	Phycobilisome linker polypeptide	0.50	-0.56	no	0
SYNW2289	two-component response regulator	1.27	-1.13	no	0
SYNW2439	**ATP-binding subunit of ABC-type urea transport system**	0.39	-0.47	yes (+)	0
SYNW2440	**Membrane protein of ABC-type urea transport system**	0.32	-0.69	yes (+)	9
SYNW2441	**Membrane protein of ABC-type urea transport system**	0.34	-0.59	yes (+)	8
SYNW0022	General secretion pathway protein E	-0.4	0.30	no	0
SYNW0424	***Possible HMGL-like family protein***	-1.09	0.47	no	0
SYNW0425	***Putative CMP-KDO synthetase***	-1.15	0.22	no	0
SYNW0436	putative cyclase hisF	-1.44	0.40	yes (unk)	0
SYNW0453	***Possible glycosyltransferase***	-1.01	0.37	no	0
SYNW0454	***Possible glycosyltransferase***	-0.99	0.46	no	0
SYNW0734	hypothetical	-0.3	0.13	no	0
SYNW0955	**hypothetical**	-0.49	0.23	no	1
SYNW0956	**conserved hypothetical protein**	-0.33	0.36	no	0
SYNW0957	**conserved hypothetical protein**	-0.51	0.39	no	4
SYNW1509	Possible type II alternative RNA polymerase σ factor	-0.65	0.78	no	0
SYNW1517	conserved hypothetical protein	-0.66	0.39	no	0
SYNW1518	conserved hypothetical protein	-0.96	0.73	no	0
SYNW1759	transaldolase	-0.32	0.52	no	0
SYNW1815	ABC transporter phosphate binding protein	-0.33	0.30	no	0
SYNW1950	***hypothetical***	-1.00	2.01	no	0
SYNW1951	***conserved hypothetical***	-0.74	1.68	no	0
SYNW2427	Possible type II alternative RNA polymerase σ factor	-0.30	0.31	no	0
SYNW2479	**ABC type transporter- possibly Zn transport**	-0.81	0.49	no	7
SYNW2480	**ABC type transporter-possibly Zn transport**	-1.38	0.96	no	0
SYNW2481	**ABC-type transporter- putative Zn-binding protein**	-1.05	1.14	no	0

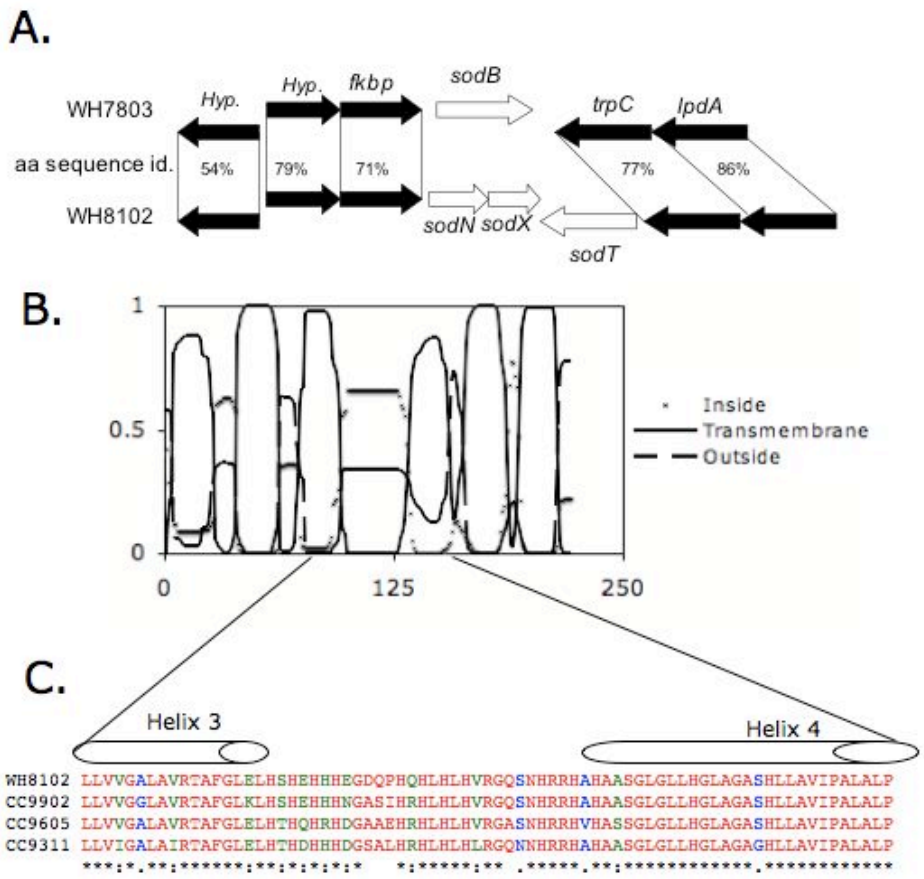

Figure 4.1: Genomic locale of *sodN* and *sodT*. A) A comparison of the genomic location where *sodB* and *sodN* are found in WH7803 and WH8102, respectively, as well as the nucleotide identity of flanking genes. B) The predicted locations of transmembrane domains in sodT. C) The sequence of the intracellular loop found between transmembrane helices 3 and 4 in WH8102.

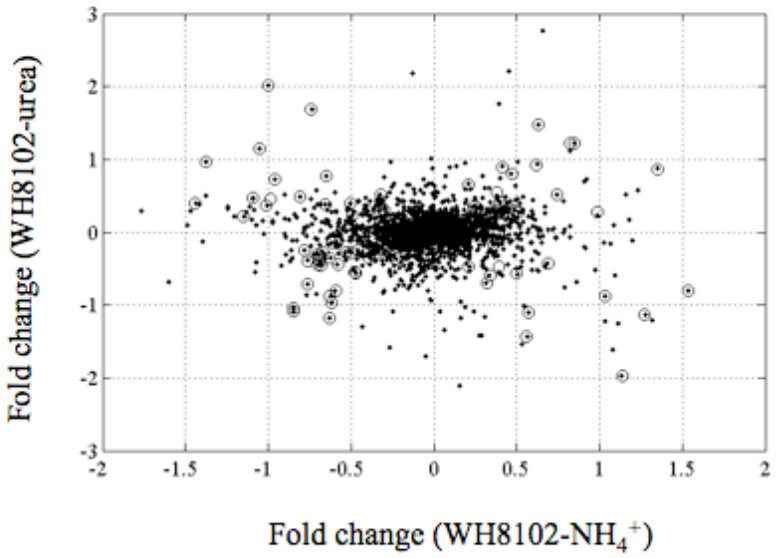

Figure 4.2: Comparison of the Ni-deprivation induced fold changes for growth on NH_4^+ (x-axis) and urea (y-axis). Genes determined to be differentially expressed in both experiments are circled.

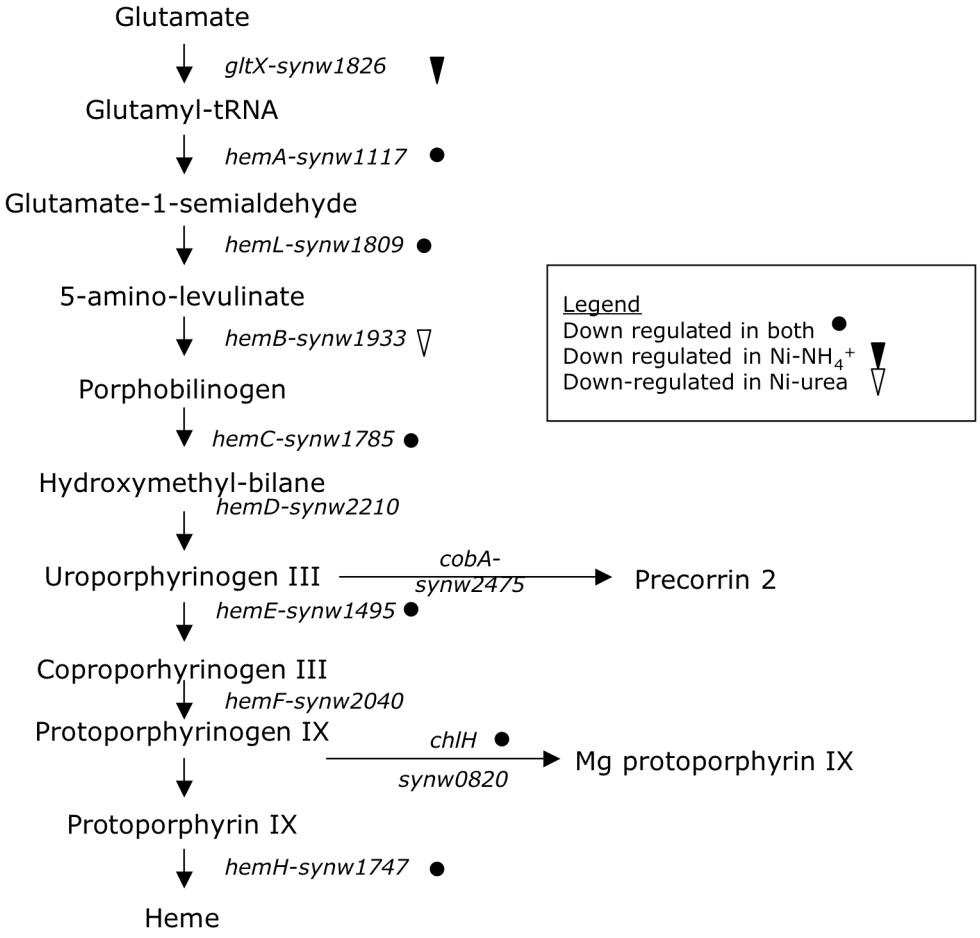

Figure 4.3: The average fold changes (log_2[experimental/control]) of the genes coding for A) *ctaI* B) *ctaII* and C) PTOX across a suite of microarray experiment examining a variety of stress responses, nutrient sources, and regulatory protein inactivations. The lower right panel provides the descriptions of the experimental and control conditions for each experiment. Unless otherwise noted, the microarray experiments were conduced with NO_3^- as an added nitrogen source.

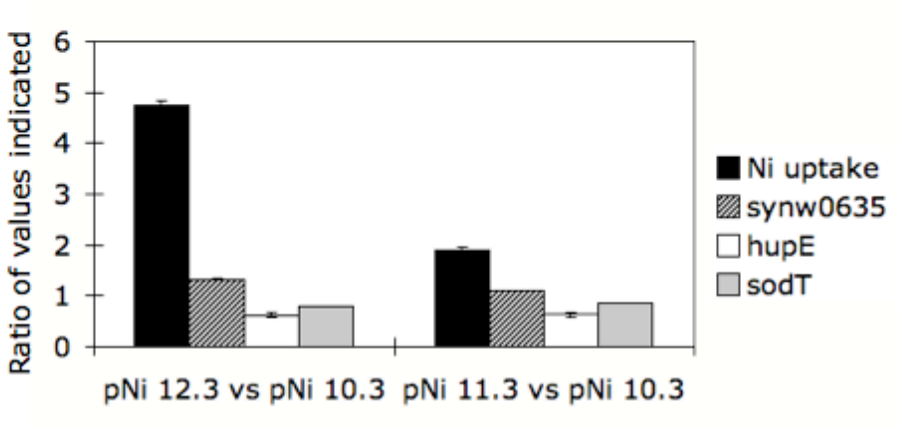

Figure 4.4: Ni uptake and putative Ni transporter expression at constant $[Ni^{+2}]$. Ni uptake rates and the expression of the indicated genes was determined for semi-continuous cultures grown at the indicated $[Ni^{+2}]$ where pNi = $-\log_{10}[Ni^{+2}]$. The values are shown as the ratios of the measured rates and gene transcript abundance for the indicated cultures.

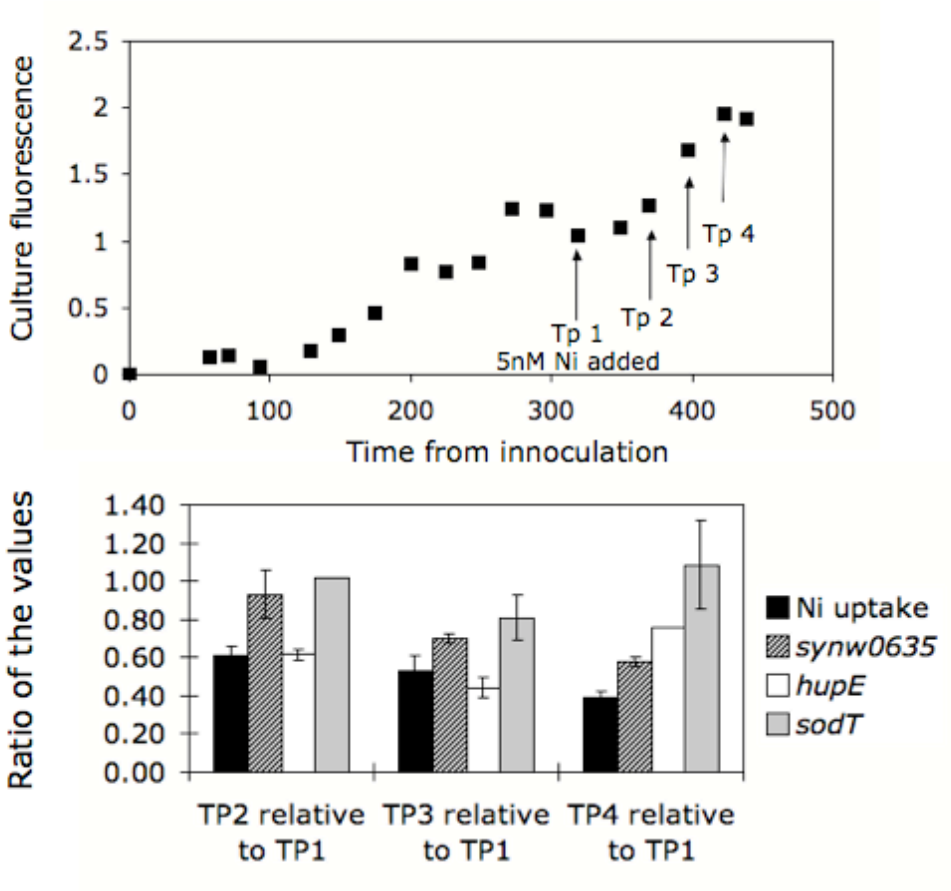

Figure 4.5: Time course of Ni limitation and putative Ni transporter expression. A) The top panel shows the culture fluorescence of a culture of WH8102 grown without added Ni until limitation (TP1). At this point, Ni was added, resulting in a return to exponential growth. B) Ni uptake rates and the expression of the indicated genes were determined at the indicated time points. Ratios of each time point with the initial Ni limited values are shown. Ranges are for duplicate cultures.

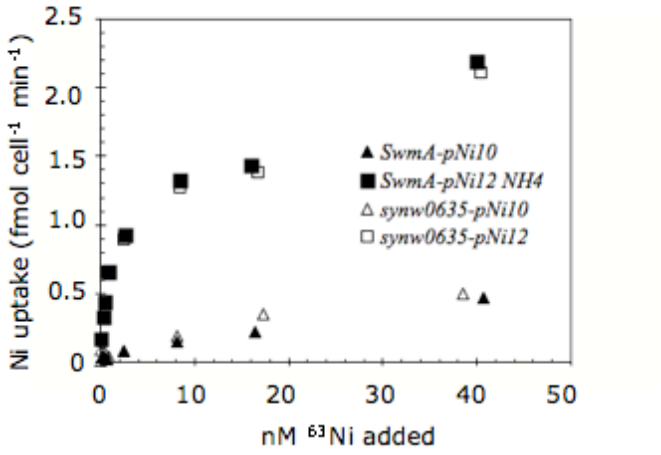

Figure 4.6: Ni uptake rates of Δ*synw0635* and *swmA* mutants of WH8102 grown at the Ni indicated (pNi = $-\log_{10}[Ni^{+2}]$).

CHAPTER 5
Contrasting scenarios of Ni utilization in phytoplankton assemblages from different biogeochemical regimes

Abstract

Monoculture studies have established the role of nickel (Ni) in the assimilation of urea in most marine phytoplankton and oxidative defense in marine cyanobacteria. Bottle-based fertilization experiments tested the effects of low-level additions of Ni, urea, or both Ni and urea on natural phytoplankton communities from surface waters several locations offshore of Peru and California, as well as in the monsoonal Gulf of California. Urea and Ni+urea additions always prompted phytoplankton growth and nutrient drawdown relative to control and Ni treatments, except in Peru. There, only concurrent Ni and urea additions resulted in increased phytoplankton pigments and nutrient drawdown, evidently due Ni-nitrogen colimitation of phytoplankton growth. Ni additions in isolation had little effect on phytoplankton communities, except in the Gulf of California where Ni resulted in greater concentrations of the pigments zeaxanthin, chl a, and divinyl chl a, as well as increased abundances of *Synechococcus* and picoeukaryotes. In parallel with the fertilization experiments, radiotracer-based uptake experiments were used to study the kinetics of biological Ni assimilation. The half saturation constants for Ni uptake in natural assemblages were similar to the low nanomolar values previously measured in *Synechococcus* cultures. The highest $V_{max}\ K_{\rho}^{-1}$ values, which reflect a competitive advantage in acquisition at low Ni concentrations, and the highest biomass normalized Ni uptake rates were observed in stratified nitrogen deplete communities, linking Ni and nitrogen biogeochemistry. Maximal Ni uptake rates

varied from 5 to 200 picomoles L^{-1} hr^{-1} and correlated with chl a levels. Relative to the Fe-replete California stations, biomass-normalized uptake rates were an order of magnitude lower in the Fe-deplete Peru stations. This empirical result and theoretical calculations suggest that saturation of the cell surface with Ni and Fe transporters may be the cause of the observed Ni-nitrogen colimitation in Peru.

Introduction

The dissolved concentrations of many of the nutrients required by marine phytoplankton are drawn down to a minimum in the surface ocean and increase with increasing depth. The underlying mechanisms behind these gradients are the assimilation of dissolved nutrients by photosynthetic prokaryotes and eukaryotes in the sunlit surface, and remineralization of sinking biomass by heterotrophic microbes at depth. The nutrient-like depth profile of dissolved Ni in seawater was noted in 1976, as was the strong correlation in dissolved Ni concentrations with the concentrations of the macronutrients H_4SiO_4 and PO_4^{-3} (166). At the time, no biological need for Ni in marine phytoplankton had been identified. Subsequently, trace metal chemists have observed nutrient-like depth profiles of Ni in almost all of the major oceans (18, 19, 26, 106, 108, 173).

Over the past 30 years, culture and genomic studies have identified two widespread biological requirements for Ni in marine phytoplankton. Most marine phytoplankton, including diatoms, cyanobacteria, coccolithophores, dinoflagellates, cryptophytes, chrysophytes, and prasinophytes, utilize the Ni-containing enzyme urease to hydrolyze urea to ammonium and carbon dioxide (40, 56, 138, 141, 149). Consequently, these phytoplankton require Ni to grow on urea, an ecologically important reduced nitrogen source that can support a significant fraction of oceanic primary production (191). Some phytoplankton of the green lineage, including *Chlamydomonas* and *Chlorella,* can cleave urea using the non-Ni containing

enzyme urea-amidolyase (76, 154), though these organisms are not prevalent in the marine environment.

The harmful oxygen species superoxide, generated circumstantially by electron transport chains in the presence of oxygen, is reduced and oxidized to molecular oxygen and hydrogen peroxide by superoxide dismutases (SOD, 69). The role of SOD in oxidative defense is such that a functional SOD is essential for growth in aerobic organisms. Ni-containing SOD, a recently discovered isoform of superoxide dismutase, is evolutionarily and structurally distinct from the Fe, Mn, and Cu containing isoforms of SOD (12, 203). The gene coding for the Ni-SOD, *sodN*, is found in the genomes of most marine cyanobacteria, including *Synechococcus, Prochlorococcus, Trichodesmium,* and *Crocosphaera,* the cosmopolitan picoeukaryote *Ostreococcus,* and a host of heterotrophic bacteria (54). *Synechococcus* strains with a Ni-SOD have an obligate need for Ni to maintain maximal growth rates irrespective of nitrogen source, with Ni deprivation causing a cessation of growth and reduced cellular superoxide dismutase activity (53). This physiological phenomenon, when coupled with comparative genomics, suggests that most marine *Synechococcus* and all *Prochlorococcus* have an obligate Ni requirement (53).

When a urease-utilizing phytoplankton utilizing urea as a nitrogen source is deprived of Ni, growth will cease due to Ni-nitrogen colimitation (53, 149). In this scenario, the addition of either Ni, which results in a functional urease, or NH_4^+,

which does not require Ni for assimilation, will restore growth. Further, reduced extracellular and intracellular Ni concentrations prompted increased maximal uptake rates, but this response was modulated by the nitrogen source for growth. The diatom *Thalasiosira weissflogii*, which requires Ni for urease, only accumulated Ni when growing on urea, otherwise eschewing the element (149). In contrast, *Synechococcus*, which require Ni for both urease and Ni-SOD, actively took up Ni when growing on NH_4^+, urea, or NO_3^-, with the highest uptake rates observed for growth on urea (53). These studies provide the mechanistic causes and links between biological activity and the deprivation of Ni in the surface ocean yet further imply that Ni cycling in the ocean depends upon phytoplankton community composition and nitrogen biogeochemistry. As an extreme example, nitrate-rich, diatom-dominated communities found in upwelled waters would be expected to have lower biomass-normalized Ni uptake rates compared to cyanobacteria communities growing on recycled nitrogen sources like urea and NH_4^+, a scenario common to stratified oligotrophic waters. To date, Ni uptake rates and kinetics have not been studied in oceanic communities.

On the basis of extended micronutrient: macronutrient stoichiometry from the equatorial Pacific, Mackey et al. (2002) concluded that the ~2.5 nmol L^{-1} of the Ni in surface seawater from this region is biologically refractive. This would suggest that Ni limitation may occur in nitrogen deplete communities growing on urea if dissolved Ni concentrations approach this refractory limit. The potential for

either Ni or Ni-urea colimitation in marine microbial assemblages has remained untested. Dissolved Ni concentrations in surface seawater are relatively high compared to those of Fe, Co, and Zn, metals shown to be limiting or colimiting to select marine phytoplankton communities (43, 46, 161). However, Ni has much slower ligand exchange kinetics, necessitating proportionately more membrane transporters and outer membrane space to attain equivalent metal uptake rates (86). Further, Ni may be bound by organic ligands reducing the bioavailable free ion chemical species of the metal, in concordance with the biologically refractory Ni suggested by Mackey et al. (2002). Ni speciation measurements in estuarine environments reveal the presence of remarkably strong Ni binding ligands (49), though no published measurements of Ni speciation are available for open ocean environments. To test the potential for Ni limitation or Ni-urea colimitation in a variety of surface ocean ecosystems bottle-based fertilization experiments were used. In parallel, community-scale Ni uptake kinetics were determined to gain insight to the potential interactions between community composition, nitrogen biogeochemistry, and Ni cycling.

Methods

Station locations and sampling

The work presented here was conducted on three separate cruises, and the dates and locations of the sampling are detailed in Table 5.1 and Figure 5.1. Water

columns were characterized less than an hour prior to trace-metal clean sampling using a SeaBird CTD equipped with fluorometer and oxygen sensors. For all incubation experiments, surface seawater was pumped using an acid-washed Teflon-lined diaphragm pump and Teflon tubing directly from a depth of 3 m into an acid-washed LDPE carboy within a laminar flow bench. Non-surface water samples were collected using Teflon-lined GO-FLO bottles deployed on poly line (LTER cruise) or mounted on a trace metal clean rosette deployed on Kevlar line (Peru cruise). GO-FLO bottles were pressurized using ultra high purity nitrogen gas to pump water directly into a laminar flow bench where subsampling occurred.

Fertilization experiments

Unfiltered surface seawater was dispensed to twelve 2.7 L bottles, which were treated in triplicate as follows: 1) No addition (controls) 2) 0.75 pmol L^{-1} Ni (500 μmol L^{-1} $NiCl_2$ in 0.1% v/v Ultrex grade HCl) 3) 2.5 μmol L urea (chelexed and filter-sterilized 1 mol L^{-1} stock made in Milli-Q) 4) both Ni and urea additions as described above. Bottles were sealed and placed in on-deck seawater-flow-through incubators screened to 10% ambient light. All sampling and manipulations of the bottles were conducted in a laminar flow bench using trace-metal clean methods. Bottles were rigorously cleaned prior to the experiment using sequential washes of 1% soap (2 days), 10% trace-metal grade HCl (2 days), and 1% trace metal grade HCl (2 days), with multiple rinses with Milli-Q water (18.2 MΩ, Millipore) following each step. Incubations were conducted as long as the

temperature of the on-deck incubators could be maintained at $\pm$ 2^{o}C of the starting temperature. NH_4^+ contamination in the urea stock was always less than 1%, as determined using the indophenol method.

Nutrient concentrations

Unfiltered seawater samples (40 mL) were dispensed into acid-washed 50 mL polyethylene tubes and frozen at -20 ^{o}C until analyses. Concentrations of ammonium, nitrate, nitrite, phosphorus, and silicate were determined at the Marine Analytical Facility of the University of California, Santa Barbara. Urea concentrations of unfiltered seawater were measured at the time of sampling using the diacetyl monoxime method (152).

Dissolved nickel and iron concentrations

Seawater was filtered through acid-washed polycarbonate pore filters (0.4 μm, Millipore) in Teflon filter holders and catch vessels (Savillex). Filtered water was dispensed to acid-washed LDPE bottles and acidified (pH ~1.8, Ultrex HCL). Bottles were double-bagged and stored for at least 1 year. Competing ligand exchange cathodic stripping voltammetry (CLE-CSV) was used to measure total dissolved Ni using the methods described in Saito et al. (160). Briefly, 10 mL aliquots of seawater were neutralized to pH = 8.0 using ammonia (1 mol L^{-1}, quartz distilled) and buffered with 200 μmol L^{-1} pH 8.0 EPPS (Sigma). The Ni chelator dimethyl glyoxime (DMG, Aldrich) was added to a final concentration of 100 μmol L^{-1} from a stock of 500 mmol L^{-1}. To reduce Ni contamination in the reagents,

DMG was recrystallized in 100 μmol L^{-1} EDTA and dissolved in Ultrex grade methanol and the EPPS was equilibrated with specially prepared Chelex-100 resin (148) prior to filter sterilization. Samples were analyzed on a BAS*i* hanging mercury drop electrode and Epsilon potentiostat (Bioanalytical Systems) run in linear sweep mode. Following a 2 minute purge with ultra high purity nitrogen gas and a 90 second deposition at -0.7 V, a high speed scan from -0.7 to -1.4 V was conducted at a speed of 10 V sec^{-1}. Nanomolar standard additions of Ni (Fisher AAS stock diluted to 340 nmol L^{-1} in 0.1% V/V Ultrex grade HCL) were made to determine the original Ni concentrations. The method was validated using the surface SAFe (17) and NASS5 standards; 1) SAFe reference value: 2.40 $\pm$ 0.03 nmol L^{-1} (M. Gordon, personal communication), measured value 2.43 $\pm$ 0.05 nmol L^{-1}; 2) NASS5 reference value: 4.31 $\pm$ 0.48 nmol L^{-1}, measured value 4.34 $\pm$ 0.24 nmol L^{-1}. The standard error associated with this method on this instrument is significantly improved over previously published measurements made using CLE-CSV (50, 160).

Acidified samples for total dissolved Fe were neutralized prior to analysis with 0.1 N quartz-distilled ammonium hydroxide (Q-NH_4OH). Total dissolved Fe concentrations were then measured using adsorptive cathodic stripping voltammetry (ACSV) with the added ligand salicylaldoxime and borate buffer on a BioAnalytical Systems (BASi) hanging mercury drop electrode with an Epsilon E2 potentiostat (30). Detection limits for this method are on the order of 0.01 nM, and

this method successfully participated in the international Sampling and Analysis of Fe (SAFe) intercalibration cruise.

Chlorophyll concentrations

Seawater was filtered onto 0.2 μm pore size filters (polyethersulfone, Supor) that were placed in 10 mL of 90% acetone and incubated in the dark at -20^{o}C for 12-24 hours. Chlorophyll concentrations of room temperature samples were determined using a fluorometer calibrated using commercial chlorophyll standards (Turner Instruments, 10-AU).

Phytoplankton pigment analyses

One liter of seawater was gently filtered onto a Whatman GF/F filter, which was placed in a cryogenic vial and stored in liquid nitrogen until analysis as described in Goericke and Montoya (71). For extraction of pigments, the filters were placed in 3 mL acetone, homogenized on ice with mortar and pestle, and allowed to incubate for 2 hr (4ºC, in the dark) following the addition of an internal standard (canthaxanthin in 50 μL of acetone). Prior to reverse-phase high performance liquid chromatography (RP-HPLC) analysis, the filter extracts were vortexed and centrifuged to remove cellular and filter debris. Samples (200 μL) of extract were manually injected onto a Waters HPLC system equipped with a Alltech Microsorp C-18 column and a UV-Vis detector (λ=440 nm). A ternary solvent system was employed for pigment separation and HPLC-grade solvents

(Fisher) were used to prepare eluents A, B and C: eluent A (MeOH:0.5 mol L^{-1} ammonium acetate, 80:20), eluent B (Methanol) and eluent C (acetone). The linear gradient used for pigment separation was (Time in minutes (%eluent A, %eluent B, %eluent C)): 0.0' (0, 100, 0), 5' (0, 85, 15), 10.0' (0, 70, 30), 14' (0, 20, 80), 16.0' (0, 20, 80), and 18.0' (100, 0, 0). The eluent flow rate was held constant at 1 mL min^{-1}. Eluting peaks were identified by comparing their retention times with those of pigment standards and algal extracts of known pigment composition. Pigments were quantified using external standard curves and the UV-Vis detector was calibrated spectrophotometrically using HPLC purified pigment standards. To convert pigment concentrations to taxon level contributions to total chl a, the ratios of the carotenoid pigments were optimized as described in Goericke and Montoya (1998).

Flow cytometry counts of picoplankton abundance

One milliliter samples of seawater were dispensed to sterile 1.5 mL cryogenic vials and allowed to fix for 10 minutes with glutaraldehyde added to a final concentration of 0.25% v/v from a stock of 25% (Sigma Chemicals) prior to immediate storage in liquid nitrogen. The samples were analyzed on a Becton Dickson FACSort flow cytometer using techniques described previously (42, 201). Green fluorescent beads (0.9 μm, Duke Scientific) were added to a final concentration of 25-30 beads μl^{-1} as an internal standard. The instrument settings were optimized to examine the abundance and fluorescence characteristics of

Synechococcus-like and chl a containing picoeukaryotic-like cells; the abundances of *Prochlorococcus*-like cells could not be confidently determined in some experiments and are not presented.

Ni uptake kinetics and rate measurements

In LTER experiments, seawater was dispensed to twenty-four acid-washed bottles (polycarbonate, 60 mL, Nalge Nunc), with eight bottles also being spiked with glutaraldehyde to a final concentration of 0.25% to serve as kill controls. Following 1 hour, eight concentrations of ^{63}Ni (Perkin Elmer, stored in 0.1% HCL-Milli Q water) from 0.1-20 nM were added to triplicate bottles every 10 minutes. Samples were incubated at constant temperature at the light level of water sampling using neutral density screening. Following 4-6 hours, samples were filtered in the order of ^{63}Ni addition, equalizing the incubation time for each addition. All samples were filtered onto 0.2 μm pore size filters (polyethersulfone, Supor). The GOCAL3 kinetics experiment was identical except except that 500 mL polycarbonate bottles were used and samples were split, with 100mL being filtered through a 0.2 μm filter and the remainder being passed through a 5.0 μm filter.

In the Ni uptake experiments conducted in the Peru upwelling, only a limited amount of ^{63}Ni was available, therefore kinetics experiments were not possible. To measure "tracer" Ni uptake rates, 1nM additions of ^{63}Ni were added to triplicate 70 mL bottles, one of which was pretreated with 0.25% v/v

glutaraldehyde as a kill control. Following 4-6 hours, the bottle contents were was passed through 0.2 μm polyethersulfone filters (Supor).

For all experiments, filters were sequentially rinsed with 10 mL of 10 mmol L^{-1} sulfoxime (a Ni chelator to remove surface bound Ni dissolved in 0.2 μm-filtered seawater, Avocado Biochemicals) and 10 mL of 0.2 μm-filtered seawater and subsequently placed in 10 mL of scintillation cocktail (Ecolyte). Samples were analyzed using standard scintillation counting with quench correction, and DPM were converted to molar concentrations using a dilution curve of ^{63}Ni. Concentrations were corrected for sample volume changes to calculate molar particulate ^{63}Ni per liter, and divided by the incubation time to obtain particulate Ni uptake rates for each bottle. Uptake rates are presented as (Mean (live samples) – kill treatment) $\pm$ SE (live treatments).

Modeling and interpretation of uptake results

All curves from uptake kinetics experiments were modeled using a least squares regression of the hyperbolic Michaelis-Menten equation ($\rho_{Nt} = [Ni] \times V_{max} \times (K_\rho + [Ni])^{-1}$, where ρ_{Ni} is the observed uptake rate at the added [Ni]) to the data using Matlab, with the parameters V_{max} and K_ρ being determined from the fitted relationship. Uptake rates measured using stable or radioactive isotopes depend upon an underlying assumption of isotope dilution in order to convert the measured uptake to *in-situ* uptake. Essentially, when the label isotope I′ is added to a solution containing the abundant isotope I, an assumption is that the resulting

concentration available for uptake to the particulate phase is I+I′ (i.e. isotope equilibration). The observed uptake of I′ (ρ′) is then proportional to the *in-situ* uptake rate ρ according to the equation $\rho = \rho' \times (I' \times (I'+I)^{-1})$, which seems quite appropriate for macronutrients. However, trace metals complexation by organic ligands is pervasive in surface seawater (125), potentially rendering the natural isotopes unavailable for isotope equilibration, particularly if the metal and ligand possess slow ligand exchange kinetics. To date, this possibility has not been investigated.

While the effects of isotope dilution cannot be observed with single addition experiments, the measurement of uptake rates for a range of I′ additions that bracket the natural concentrations of I should reveal the presence or absence of isotope dilution. The theoretical observed uptake rates of a compound by an organism with traditional Michaelis-Menten kinetics and either no isotope dilution or isotope dilution with I = 3 are shown in Figure 5.2A. The dilution of the added isotope reduces theoretical observed uptake rates at low substrate concentrations, resulting in a sigmoidal curve centered at the natural concentration I (Fig. 5.2A). Realistically, the differences in uptake rates are minor and unlikely to be observed. In contrast, a plot of the percent uptake of the added isotope ($\rho_{I'} = V_{max} \times (K_\rho + [I'])^{-1}$, Fig. 5.2b) relative to the added I′ displays the effects of isotope dilution clearly. Uptake rates were determined over a range of Ni concentrations in order to determine the community scale kinetics of Ni uptake, but also to examine the

extent of isotope equilibration between the added radiotracer ^{63}Ni and the "cold" Ni present in seawater. These experiments are analogous to the titrations performed in electrochemical speciation measurements, except that the competing ligands are the phytoplankton, or more specifically, the metal binding transport sites on the cells.

Results and Discussion

Station descriptions

Table 5.1 and Figure 5.1 provide the dates, locations, and a summary of the work conducted. Samples from the Gulf of California (GOCAL) were collected in the summer of 2005 from the nitrate-deplete surface waters of a strongly stratified water column in the Guaymas Basin (see 196). Stations Peru9, Peru12, and Peru26 were occupied during October 2005, with the former two located in a region where phytoplankton growth is limited by low levels of the micronutrient Fe (28). The California Current Ecosystem Long Term Ecological Research (LTER) cruise was in May 2006 and complete hydrographic data for each site is available at cce.lter.net. LTER1, a coastal site near Point Conception, was characterized by a recently upwelled, nitrate-rich water column. Near the outer edge of the North Pacific subtropical gyre, LTER2 and LTER 5 were in stratified environments with negligible surface NO_3^- and relatively deep (70-75m) subsurface chl maximum. LTER3 was in a shallow stratified nutrient rich coastal area, and LTER4 was in a

recently mixed, low nitrate "mesotrophic" water column with a subsurface chl max at 50m.

Fertilization experiments

The response of phytoplankton communities to the additions of 0.75 nmol L^{-1} Ni (+Ni), 2.5 μmol L^{-1} urea (+urea), or both (Ni+urea) was examined in order to test the hypothesis that Ni limitation or Ni-urea colimitation can occur in natural waters. Bottle-based fertilization experiments were conducted at GOCAL3, Peru12, LTER1, LTER2, and LTER5 (Fig. 5.1, Table 5.1) and the incubation length, initial macronutrient, Fe, and Ni concentrations are shown in Table 5.2. Two experiments (PERU12 and LTER1) began with relatively high chl a communities in recently upwelled waters with high nitrate concentrations but 10-fold difference in Fe concentrations (Table 5.2). The other 3 experiments were conducted with low chl a nitrogen-deplete phosphorus-replete surface waters overlying stratified water columns (Table 5.2). The urea additions substantially increased the total N at the beginning of each experiment. The total Ni concentrations were increased less than 25% by the Ni additions, minimizing the potentially toxic effects of Ni to phytoplankton grazers. The Gulf of California appears to be greatly enriched relative to the oceanic Pacific in Fe and Mn concentrations (87), possibly due to the dust and rain deposition from the summer thunderstorms sweeping off the Sonoran desert noted in sediment trap records (13,

183). The seemingly high Fe concentrations presented for the GOCAL3 experiment are consistent with this.

In each of the LTER fertilization experiments, the +urea and Ni+urea treatments resulted in significant increases in chl a, picoeukaryote and cyanobacteria abundance, as well as a decrease in nutrient concentrations, yet synergistic effects were not observed for the Ni+urea treatments (Table 5.2). The +Ni treatments did not prompt any noticeable biological effects relative to the controls (Table 5.2). The stimulation of phytoplankton growth with the addition of urea has been previously observed in the Southern California Bight (61), and the trace metal clean procedures used here verify that the bioavailable Ni concentrations are sufficient to support urea assimilation.

The GOCAL3 and Peru12 fertilization experiments provided a contrast to the LTER experiments, though in different fashions. In the GOCAL3 experiment, the +urea and Ni+urea treatments both stimulated increased chl a, picoplankton populations, and nutrient drawdown, as observed in the LTER experiments (Table 5.2). However, Ni additions also resulted in a modest, but significant (student's t-test, $p<0.05$) increase in chl a concentrations, a 3-fold increase in *Synechococcus* abundances, and minor (30%) yet significant increases in picoeukaryote abundance ($p<0.01$ students t-test, Table 5.2). Consistent with the flow cytometry counts, the ratios of the HPLC-determined phytoplankton pigments in the GOCAL3 fertilization experiment indicate that the phytoplankton community was

cyanobacteria-dominated, with high zeaxanthin (zeax) concentrations (Fig. 5.2A). 19'hexanoyloxy fucoxanthin (19'hex)-containing prymnesiophytes also contributed to the total chl a (data not shown). Following the 48 hour incubation following nutrient additions, there were increases in HPLC-measured chl a over the t = 0 sample in all treatments, with the +urea and Ni+urea treatments exhibiting the largest increases (Fig. 5.3A). The +urea and Ni+urea treatments were virtually indistinguishable from each other, but were significantly enriched compared to control bottles for all pigments. The +Ni treatment had minor increases in chl a and the cyanobacterial pigments zeax and divinyl chl a relative to the control bottles (Fig. 5.3A).

The added Ni may have inhibited grazers of cyanobacteria and picoeukaryotes in the GOCAL3 fertilization experiment, yet the Ni addition was modest and a similar effect was not observed in the other experiments. Alternatively, the cyanobacteria and picoeukaryotes may be Ni limited due to the usage of Ni-SOD. In this scenario, the addition of Ni restores Ni-SOD activity, improving oxidative defense and facilitating higher growth rates. While both cyanobacteria and picoeukaryotes require Ni to assimilate urea, the sole significant difference between the Ni+urea and +urea treatments was in PO_4^{-3} drawdown (Table 5.2), suggesting that Ni-urea colimitation did not occur, or at least was minor, in the GOCAL3 fertilization. The cyanobacterial community does appear to have been nitrogen limited, as greatly increased phycoerythrin fluorescence per

Synechococcus cell was observed in response to +urea and Ni+urea treatments (data not shown), which likely reflects a rapid synthesis of the phycobiliproteins (41). The urea additions may provide relief from nitrogen limitation, reducing both the associated oxidative stress and the biological need for Ni. *Synechococcus* were particularly responsive to urea additions in the LTER and GOCAL fertilizations (Table 5.2), which is consistent with the importance of this nitrogen source to the ecology of this organism (78).

In contrast to the other four fertilization experiments, urea additions had little effect relative to the controls in the Peru12 experiment; here only Ni+urea additions prompted a significant increase in chl a levels over the controls (Table 5.2). Dissoved PO_4^{-3} and H_4SiO_4 was drawn down to a greater extent in the Ni+urea treatment compared to the other treatments, which displayed greater urea drawdown relative to the +urea treatement (Table 5.2). HPLC-based pigment measurements revealed the Peru12 t=0 community was rich in the diatom pigment fucoxanthin (fucox), and pigment ratios suggested that the community was almost entirely composed of diatoms (data not shown), with only minor contributions by cyanobacteria and pelagophytes. Significant increases in fucoxanthin (fucox), 19'hex, chl $c_1 + c_2$, and chl a were observed in the Ni+urea treatment relative to the controls ($p<0.05$, students t-test, Fig. 5.3B). Of the less abundant pigments, 19'butanoyloxy fucoxanthin (19' but), diadinoxanthin (DD), alloxanthin (allox), diatoxanthin (diatox), zeaxanthin (zeax), and chl b also showed statistically

significant increases in the Ni+urea treatment relative to the other treatments ($p<0.05$, students t-test, Fig. 5.3B).

In terms of initial conditions, Peru12 and LTER1 both were N, P, and Si-replete, but vastly different in terms of Fe concentrations (Table 5.2). In Peru12, the low Fe concentrations may trigger a cascade of type III biochemically-dependent colimitations, where the assimilation of one substrate is dependent upon the presence of another substrate (159). Due to the role of Fe in NO_3^- and NO_2^- reduction, low ambient Fe can limit nitrate uptake resulting in Fe-nitrogen colimitation (147). The addition of the reduced nitrogen source, urea, should relieve the nitrogen limitation provided Ni is available. Increased nutrient drawdown and phytoplankton biomass were only observed in the Ni+urea additions, suggesting that the +urea treatments became Ni-Fe-nitrogen colimited (Table 5.2). Biochemically, the addition of Ni allows the hydrolysis of urea by the Ni metalloenzyme urease, providing a nitrogen source for growth and additionally relieving Fe requirements associated with the Fe metalloenzymes nitrate and nitrite reductase.

Ni uptake kinetics of marine microbial communities

Pilot experiments on a cruise to the Gulf of California were used to examine the temporal aspects of Ni uptake. Following a 10 nmol L^{-1} addition of ^{63}Ni to a natural surface phytoplankton community, particulate ^{63}Ni uptake in the kill control and live sample was equal and rapid for 1-2 minutes, followed by a plateau in the

kill control and a gradual increase in particulate Ni in the live sample. Uptake in the live control proceeded linearly for 6-8 hours, after which the rates decline. For a 1 nmol L^{-1} ^{63}Ni addition, uptake rates in the live samples proceeded linearly for 24-36 hours (data not shown).

Ni uptake kinetics was determined for two size fractions (0.2-5.0 μm and >5.0 μm) of a phytoplankton community in the surface of the Gulf of California (Fig. 1). The water column was strongly stratified, with an N-deplete P replete surface mixed layer, a subsurface chl maximum coincident with the nitracline, and high rates of N_2 fixation (196). The kill-corrected Ni uptake rates in the 0.2-5.0 μm and >5.0 μm size fractions were well modeled using Michaelis-Menten kinetics (fitted curves in Fig. 5.4A), with a K_ρ of 3 nmol L^{-1} for both size fractions (Table 5.3). At each ^{63}Ni addition, the 0.2-5 μm size fraction exhibited much greater Ni uptake rates relative to the > 5.0 μm size fraction (Fig. 5.4A and 5.4B). The % uptake rate declined with increasing ^{63}Ni additions, indicating a lack of isotope equilibration, except perhaps at the lowest ^{63}Ni additions (100 pmol L^{-1}, Fig. 5.4C). The decline in > 5.0 μm Ni uptake rates at the highest ^{63}Ni addition (20 nmol L^{-1}) is assumed to be the result of Ni toxicity or a negative feedback regulation of Ni uptake in this size fraction, which is a trademark of metal homeostasis.

Ni uptake kinetics were determined for communities collected from multiple depths in several different regimes of the California Current in the spring of 2006, but only for the >0.2 μm size fraction. The results of the uptake

experiments from three depths at the LTER3 station are shown in Figure 5.5, while complete information for all experiments is in Table 5.3. At LTER3, the uptake curves from all three depths conformed to Michaelis-Menten kinetics with increasing half saturation constants (Fig. 5.5, Table 5.3) and decreasing maximal uptake rates with increasing depth and decreasing chl a (Table 5.3, Fig. 5.5A). At each depth, the % uptake declines with increasing ^{63}Ni additions (Fig. 5.5B), indicating a lack of equilibration between the added ^{63}Ni and the ambient ~ 4 nmol L^{-1} Ni. Similar curves were obtained at all other stations, except at LTER1, where dilution was observed in waters collected from depths of 35 m and 60 m (Fig. 5.6). Moderate (10%) declines in Ni uptake rates at the highest ^{63}Ni additions (50 nmol L^{-1}) were observed with the LTER2 community from 5m (not shown).

The compiled kinetic parameters and attendant chl a and nutrient concentrations for all sites are shown in Table 5.3. Across all experiments, a correlation was observed between V_{max} and chl a (r^2=0.48). While other correlations were not observed across all samples, the depth dependent trends varied between oligotrophic and nutrient-rich sites. At LTER1 (Table 5.3) and LTER3 (Fig. 5.5), both V_{max} and K_ρ declined with chl a. In the stratified oligotrophic sites LTER2 and LTER5, maximum V_{max} values were observed at the subsurface chl max, while the highest affinity for Ni was observed in the surface waters (Table 5.3). Only two depths were analyzed at LTER4, but they displayed similar trends in V_{max} and K_ρ to that observed at LTER3. Healey (77) argued that

the ratio V_{max}:K_ρ, also known as the specific affinity (31), describes an organism's or community's competitive advantage for a nutrient at low concentrations, with higher values of V_{max}:K_ρ indicating an increased ability to acquire the nutrient at low concentrations. When V_{max} is normalized to chl a to account for community biomass, the highest V_{max}:K_ρ values were observed in the surface waters of the N-deplete GOCAL3, LTER2, and LTER5 (Table 5.3). This is consistent with the modulation of community Ni uptake rates with nitrogen nutrition, as has been observed in culture studies (53, 149).

Despite the importance of robust measurements or estimates of nutrient uptake kinetics in ecosystem modeling, there is a relative dearth of information on trace metals uptake kinetics or rates. The uptake rates of Cd and Fe have been measured in natural systems using single concentration additions of radioisotopes (48, 164), and Fe uptake kinetics were determined during a mesoscale Fe fertilization experiment (110). In the aforementioned studies, the authors present uptake rates corrected for the natural concentrations of the trace metal, with the tacit assumption that the added radioactive isotope chemically equilibrates with the non-radioactive isotopes and the metal-binding ligands within the system. In this study, dilution of the added ^{63}Ni was not observed, except at the actively upwelling LTER1 site (Fig. 5.6), rendering the extrapolation of the observed uptake rates to an estimation of an *in-situ* assimilation rate erroneous; rather, the observed uptake rates represent the affinity of the microbial community for Ni. Naturally, isotope

dilution or equilibration would be particularly important to consider prior to extrapolating metal and carbon uptake rates to estimated *in-situ* Metal:C ratios as has been done (48, 164, 174), with dilution resulting in overestimates of community metal:C ratios. This was actually observed in Fe uptake experiments conducted with two different Fe additions in Antartic phytoplankton communities (186). Conversely, in the sub-Antartic South Pacific, Mald0nado et al. (112) found that Fe uptake rates were constant over time, suggesting that the added radioactive Fe either equilibrates with the natural Fe ligands quite rapidly or not at all during those experiments.

Spatial and depth variance in Ni uptake rates

Depth profiles of Ni uptake rates were conducted at Peru9, Peru12, and Peru26 using 1 nmol L^{-1} "tracer" additions of ^{63}Ni (Table 5.4). Peru9 and Peru12 were part of a cross-shelf transect in Southern Peru, a region where the upwelled waters are deficient in Fe relative to the other macronutrients, leading to Fe limitation in the surface waters (28). Both sites were high in nitrate, with broad mixed layers coinciding with a chl a maxima overlying a suboxic zone (Table 5.4). Ni uptake rates were elevated in surface waters at both stations, with a decline in the oxycline. At station 9, uptake rates increased sharply below the oxycline to values similar to those observed in surface waters, despite no measurable chl a. At both stations a minor maximum in dissolved Ni was observed at the top of the suboxic zone (Table 5.4). A profile offshore of the broad continental shelf (Peru26,

Fig. 5.1) examined Ni uptake rates and Ni concentrations over the upper kilometer of the ocean (Table 5.4). Kill-control corrected Ni uptake rates of hundreds of femtomoles per hour were observed at several depths within the deep suboxic zone, suggesting that heterotrophic bacteria in the ocean's interior actively assimilate Ni. This is consistent with the observation of the Ni metalloenzymes in the genomes of bacteria found outside the euphotic zone. These include genes for Ni-containing urease and a Ni transporter in the genomes of both Bacterial and Archaeal NH_4^+ -oxidizers (75, 96).

The results of the Peru uptake rate measurements were pooled with the uptake rates for 1 nmol L^{-1} ^{63}Ni additions from the kinetics experiments. The tracer uptake rates correlated with chl a concentrations ($r^2 = 0.68$), but not with the concentrations of Ni or macronutrients (Table 5.4). The macronutrients PO_4^{-3}, NO_3^-, and SiO_4 were correlated with Ni concentrations over the entire dataset (r^2 = 0.81, 0.81, and 0.85, respectively). When normalized with chl a concentrations, Ni uptake rates were over an order of magnitude lower at the Peru upwelling sites compared to sites in the Gulf of California and California waters (Table 5.4). It seems unlikely that the difference was methodological, though the radiation laboratory used on the Peru cruise was about 2-3 ^oC colder than the ones used for the other cruises. Dilution of the added ^{63}Ni by the ambient Ni may have occurred during the Peru experiments, as data on Ni isotope dilution are not available for these locations. In spite of this, equilibration of the added 1 nmol L^{-1} ^{63}Ni with 3-5

nmol L^{-1} Ni would reduce the observed uptake rates three- to five-fold, an effect insufficient to explain the discrepancy. If the diatom-dominated communities in this region grow predominantly on nitrate, this could result in reduced Ni uptake rates (Price and Morel 1991). However, the f-ratio, the fraction of production supported by nitrate relative to recycled nitrogen sources like urea, may be repressed in Peru relative to some other eastern boundary currents (29). Further, the uptake of Ni by diatoms growing on NO_3^- has not been studied. Pervasive Fe limitation of phytoplankton communities in the Peru upwelling may also contribute to the regional differences in uptake rates, as discussed in the next section.

Modeling the uptake of Ni in HNLC and non-HNLC regions

Ni concentrations measured in the surface waters of Peru12 and GOCAL3 were 4-fold higher than the Ni additions, which would seem to be at odds with the observed biological response from the fertilization experiments. In previous reports of trace metal limitation or colimitation in oceanic ecosystems, the concentrations of the limiting nutrient were always drawn down to vanishingly low levels (43, 156, 161). The GOCAL3 community was dominated by *Synechococcus*-like cyanobacteria, and free [Ni^{+2}] less than 100 pM reduce the growth rates of *Synechococcus* (53). Therefore, a complexation of greater than 97% of the ambient Ni by organic ligands would result in growth limitation of *Synechococcus*. Chemical measurements of Ni speciation were not conducted, yet the biologically-tuned Ni uptake kinetics experiments from GOCAL3 reveal that most if not all of

the ambient 3.5 nmol L^{-1} Ni is not biologically available on time scales of less than 6 hours (Fig. 5.4). Therefore, it seems conceivable that the cyanobacteria-dominated community at GOCAL3 is simply limited by low free Ni concentrations. A similar argument could be applied for the Peru12 experiment, but the lack of an uptake kinetics experiment removes the empirical evidence available for GOCAL3.

An alternative explanation for the observed Ni and Ni-urea colimitation involves the kinetics of metal uptake and the available membrane space for transporters. Due to the low concentrations of bioactive metals in seawater, a paradoxically greater number of transporters are necessary to acquire the trace elements compared to the macronutrients C, N, and P, despite the disparity in cellular requirements (124). Trace metal uptake by phytoplankton in seawater is under kinetic control, therefore the number of surface transporters (L) required is directly related to the growth rate (μ) and cellular requirements for the substrate (Q) in question and inversely related to the ligand complex formation rate constant (K_f) and the labile concentrations of the metal ([M'] e.g. $[Ni^{+2}]$) (86). The available membrane area provides a biophysical limit on the maximum number of transporters (L_{max}), and trace metal limitation can theoretically occur through a saturation of the available membrane space with transporter proteins. Of the biologically-utilized trace elements, Ni and Fe have the slowest complex formation kinetics and are most likely to result in membrane saturation, though previously each metal was considered in isolation (124).

Using the relationships described above and simplified phytoplankton models representative of GOCAL3 and Peru12, the Ni concentrations resulting in a saturation of the surface of the cell with Ni transporters ($[Ni_{lim\text{-}MS}]$) were calculated. Two scenarios were tested (Table 5.5): 1) What [Ni'] results in a saturation of the available membrane space by Ni transporters and 2) What [Ni'] results in a saturation of available membrane space by Ni and Fe transporters assuming a constant [Fe']. The percent of the outer membrane available for transporters was varied from 2% to 50%, though 10% seems a plausible upper limit on the amount of space available for a single element transporter (31). The oceanic *Synechococcus sp.* WH8102 was chosen to represent the GOCAL3 community, with growth rates and Q_{Ni} being taken from Dupont et al. (2008). The Fe quotas for the cyanobacteria were calculated from the Fe associated with the cyanobacteria community in the FeCycle experiment, a *Synechococcus* dominated low nitrogen site (174). PERU12 was modeled using the oceanic diatom *T. oceanica*, with the Ni quotas from Price and Morel (1991, after scaling for the differences in cell size between *T. weissflogii* and *T. oceanica*) and the Fe quotas from Sunda and Huntsman (176). It was assumed that the measured total dissolved Fe concentrations (Table 2) represent bioavailable Fe, as has been suggested by culture studies and mesoscale Fe fertilization experiments (111, 156).

In Figure 5.7, the $[Ni^{+2}]$ that result in membrane saturation ($[Ni_{lim\text{-}MS}]$) are plotted against the fraction of the cell surface available for transporters. $[Ni^{+2}]$

lying below the plotted curves result in a Ni limitation caused by membrane saturation. Conversely, the lines also display the percent of the outer membrane (x-axis) required to grow at the specified [Ni^{+2}]. Considering just Ni requirements (case 1, Fig. 7A), the observed concentrations of Ni could only result in membrane saturation based limitation if Ni is bound by organic ligands (Fig. 5.7A). When the biological requirements for Fe transporters are taken into account (Fig. 5.7B), the portion of membrane space available for Ni transporters is decreased, resulting in significantly increased [$Ni_{lim\text{-}MS}$].

This modeling provides some explanation for the results from the fertilization experiments. Given even a conservative estimate of 100-300 pM [Ni^{+2}] from the kinetics experiment at GOCAL3 (Fig. 5.3), a potentially unreasonable amount (10-15%) of cell surface area is required for a cyanobacteria to grow at maximal rates (Fig. 5.7). However, due to the hyperbolic relationship of the trace metal concentrations and transporter abundance, an addition of 750 pM total Ni reduces the required membrane space to a near minimum (Fig. 5.7). In the theoretical Peru12 community, over 10% of the outer membrane space would be required to take up Ni for growth on urea (Fig. 5.7B), even in the absence of biological complexation. Again, an addition of 750 pM Ni would reduce this percentage greatly.

While the Ni limitation in Peru was artificially induced by the addition of urea to a community likely growing on nitrate, the result has implications for the

physiological state of the community. Diatoms have a complete urea cycle, which may be important in the intracellular recycling of nitrogen (2). Within this cycle, urease is required to recover NH_4^+ from arginase-produced urea, which theoretically is otherwise lost. Transporter ratios can be optimized to best satisfy moderately plastic cellular requirements in a given environmental condition (172). In the case of the Peru community, low Fe concentrations may force the diatoms to sacrifice urease activity to reduce Ni requirements and the attendant need for Ni transporters, providing an explanation for the low Ni uptake rates in Peru (Table 5.4). Consequently, intracellular nitrogen recyling would be affected.

Conclusions and future directions

Two distinct scenarios were observed where Ni affected the growth and biomass of natural phytoplankton communities. The observation of Ni limitation of a cyanobacteria-dominated community in the Gulf of California is consistent with studies demonstrating Ni limitation in *Synechococcus* monocultures and the estimates of bioavailable Ni from uptake kinetics experiments. While large abrupt inputs of urea to an oceanic environment are unlikely to occur, the Ni-urea colimitation observed in Peru nevertheless suggests that the phytoplankton in this region are denied the use of urea as a nitrogen source for growth. Naturally, further experiments in biogeochemically distinct regimes are required. Future incubation experiments should focus on the effects of Ni and urea additions on physiological parameters, particularly primary production, Ni and urea uptake rates, and active

fluorescence. The observed co-limitation, reduced Ni uptake rates, and theoretical models all imply that Fe limitation may have an ecologically relevant effect upon the acquisition of other nutrients beyond that described for nitrate and ammonium acquisition (7). Extended comparisons of the uptake kinetics of Ni and other metals between HNLC and non-HNLC regions are required to support this hypothesis. Measurements of community urease activity in different regimes would test that HNLC conditions result in a restructuring of urea and Ni metabolism. Additionally, biomass-normalized Ni uptake rates in HNLC waters should increase dramatically following the addition of Fe. Coupling the determination of Ni uptake kinetics and isotope dilution with more traditional chemical methods of Ni speciation measurements could be insightful to the biological relevance of the detection window of the chemical methods.

Acknowledgements

Chapter 5 is a reprint of material to be submitted to Limnology and Oceanography. K. N. Buck, K. Barbeau, and Brian Palenik are co-authors. The dissertation author was the primary investigator and first author. The authors would like to thank Chief Scientists James Moffett, Fred Prahl, Brian Popp, and Mike Landry, as well as the crew of the *R/V* New Horizon and Knorr. Andrew L. King provided several Fe measurements.

Table 5.1: Locations and dates of experimental work.

Station name	General Area	Date(s)	Latitude	Longitude	Type of Experiment
GOCAL3-1	Gulf of California	Aug. 6-7, 2005	27.0 N	111.45W	Growout
GOCAL3-2	Gulf of California	July 29, 2005	27.5 N	111.33W	Uptake (kinetics)
PERU9	Peru-nearshore	Oct. 20, 2005	15.63 S	75.13 W	Uptake (tracer)
PERU12	Peru-offshore	Oct. 22, 2005	16.28 S	75.61 W	Uptake (tracer), Growout
PERU26	Peru-offshore	Oct. 26, 2005	12.0 S	78.65 W	Uptake (tracer)
LTER06-1	California Current	May 11-15, 2006	34.30 N	120.8 W	Uptake (kinetics), Growout
LTER06-2	California-offshore	May 16-21, 2006	33.70 N	122.20 W	Uptake (kinetics), Growout
LTER06-3	California-nearshore	May 23, 2006	34.63 N	120.76 W	Uptake (kinetics)
LTER06-4	California Current	May 27-30, 2006	34.03 N	121.56 W	Uptake (kinetics)
LTER06-5	California-offshore	June 1-4, 2006	32.48 N	124.28 W	Uptake (kinetics), Growout

Table 5.2: Summary of Ni and urea fertilization experiments. Standard error is from 3 replicate bottles. Values that are statistically significant relative to the control treatment (t-test, $p < 0.05$) are indicated in bold italics.

		Incubation				
	Treatment	**GOCAL3**	**Peru12**	**LTER1**	**LTER2**	**LTER5**
Length (hr)		48	102	77	75	95
Ni (nmol L^{-1})	**t=0**	3.1 ± 0.07	4.19 ± 0.04	4.6 ± 0.5	3.47 ± 0.05	3.84 ± 0.18
Fe (nmol L^{-1})	**t=0**	3.67 ± 0.05	0.17 ± 0.03	1.96 ± 0.04	0.37 ± 0.02	0.13 ± 0.03
	t=0	0.15	1.19	2.6	0.045	0.087
	Control	0.14 ± 0.01	1.35 ± 0.18	16.6 ± 1.8	0.049 ± 0.01	0.078 ± 0.01
Chl a	**Ni**	***0.22 ± 0.03***	1.50 ± 0.07	19.2 ± 1.0	0.065 ± 0.01	0.076 ± 0.02
μg L^{-1}	**Urea**	***0.96 ± 0.01***	1.50 ± 0.17	***23.4 ± 2.0***	***0.32 ± 0.09***	***0.42 ± 0.06***
	Ni +urea	***0.99 ± 0.1***	***2.59 ± 0.00***	***20.9 ± 2.4***	***0.34 ± 0.07***	***0.38 ± 0.02***
	t=0	<0.1	<0.1	0.22 ± 0.01	<0.1	<0.1
	Control	<0.1	<0.1	<0.1	<0.1	<0.1
Urea	**Ni**	<0.1	<0.1	<0.1	<0.1	<0.1
μmol L^{-1}	**Urea**	<0.1	1 ± 0.3	<0.1	2 ± 0.2	<0.1
	Ni +urea	<0.1	<0.1	<0.1	1.9 ± 0.2	<0.1
	t=0	<0.1	10.75	8.6	<0.1	<0.1
	Control	<0.1	7.06 ± 0.36	0.11 ± 0.02	<0.1	<0.1
NO3+NO2	**Ni**	<0.1	6.13 ± 0.8	<0.1	<0.1	<0.1
μmol L^{-1}	**Urea**	<0.1	7.8 ± 0.25	<0.1	<0.1	<0.1
	Ni +urea	<0.1	6.8 ± 0.1	<0.1	<0.1	<0.1
	t=0	0.4	1.56	0.7	0.25	0.16
	Control	0.34 ±0.03	1.28 ± 0.02	0.13 ± 0.01	0.24 ± 0.1	0.15 ± 0
PO4	**Ni**	0.33 ± 0	1.25 ± 0.02	0.14 ± 0.01	0.17 ± 0.01	0.16 ± 0.01
μmol L^{-1}	**Urea**	0.29 ± 0.01	1.33 ± 0.08	0.15 ± 0	0.15 ± 0.02	0.13 ± 0
	Ni +urea	***0.25± 0***	***1.15 ± 0.02***	0.15 ± 0	0.15 ± 0.02	0.15 ± 0
	t=0	2.7	7.9	2.7	2.16	1.7
	Control	2.4 ± 0	3.4 ± 0.35	1.3 ± 0.1	1.5 ± 0.26	1.3 ± 0.15
SiO3	**Ni**	2.35 ± 0.05	2.63 ± 1.1	1.5 ± 0.2	1.6 ± 0.5	1.5 ± 0.2
μmol L^{-1}	**Urea**	2.25 ± 0.05	3.15 ± 0.5	1.4 ± 0.1	1.3 ± 0.15	0.9 ± 0.5
	Ni +urea	2.4 ± 0.1	***2.3 ± 0.5***	1.4 ± 0.2	1.4 ± 0.45	1.7 ± 0.1
	t=0	64	38	2.3	38	15.3
Synechococcus	**Control**	74 ± 28	25 ± 0	43.4 ± 4.9	20.6 ± 1.1	6.0 ± 0.6
10^3 cells ml^{-1}	**Ni**	***219 ± 61***	31 ± 12.1	45.6 ± 2.1	15.7 ± 4.0	6.7 ± 2.5
	Urea	***1416 ± 209***	15.6 ± 6.3	47.1 ± 4.5	***44.8 ± 2.2***	***28.4 ± 1.5***
	Ni +urea	***1727 ± 59***	31 ± 18	52.4 + 5.5	***46.3 ± 3.1***	***29.7 ± 1.9***
	t=0	2.1	102	2.9	13.5	6.8
Picoeukaryotes	**Control**	6.4 ± 0	46 ± 9.9	164.8 ± 10.2	12.2 ± 0.7	8.9 ± 1.3
10^3 cells ml^{-1}	**Ni**	***8.4 ± 0***	51.6 ± 10.4	161.1 ± 12.4	13.4 ± 1.8	10.8 ± 2.8
	Urea	***17.5 ± 4.0***	41.5 ± 8.3	***207 ± 18.3***	***44.7 ± 4.4***	***38.6 ± 3.6***
	Ni +urea	***20.6 ± 2.0***	50.3 ± 8.7	***200 ± 36.6***	***41.1 ± 4.5***	***35.8. ± 4.4***

Table 5.3: Summary of all uptake kinetics experiments.

		Ni uptake kinetics								
Station	**Depth**	**V_{max}**	**K_ρ**	**Affinity**	**Dissolved Ni**	**Chl a**	**NO_3**	**NH_4**	**SiO_3**	**PO_4**
	meters	***pmol L^{-1} hr^{-1}***	***nmol L^{-1}***	***V_{max} K_ρ^{-1}***	***nmol L^{-1}***	***µg L^{-1}***	***µmol L^{-1}***	***µmol L^{-1}***	***µmol L^{-1}***	***µmol L^{-1}***
GOCAL3-3	3	30	3	55.6	3.63±0.13	0.18	0	0	3	0.72
LTER1	3	129	34	0.8	4.6 ± 0.5	4.74	8.6	0.57	11.8	0.71
LTER1	35	110	39	2.2	5.07±0.17	1.27	9.4	1.09	12.9	0.78
LTER2	60	26	11	52.5	5.47±0.07	0.045	15.5	0.3	17.4	1.13
LTER2	5	28	11	254.5	3.45±0.09	0.01	0.06	0.48	2.16	0.2
LTER2	40	16	5	26.8	3.41±0.14	0.117	0.07	0.45	2.03	0.19
LTER2	75	132	26	10.4	3.51±0.12	0.49	1.75	0.61	3.85	0.36
LTER3	2	207	6	5.0	4.05±0.04	6.5	1.64	0.88	4.1	0.31
LTER3	12	39	8	1.3	4.3±0.14	3.75	5.37	0.93	11.81	0.58
LTER3	25	43	23	0.8	4.31±0.18	2.25	7.7	1.06	13.05	0.7
LTER4	10	6	1	6.7	3 ± 0.05	1.113	0.95	0.33	3.43	0.25
LTER4	50	31	7	5.5	3 ± 0.05	0.798	11.05	0.29	10.14	0.9
LTER5	5	25	10	20.7	3.84 ± 0.18	0.121	0.105	0.24	1.67	0.23
LTER5	50	49	9	9.9	3.81 ± 0.09	0.554	0.117	0.18	1.7	0.22
LTER5	78	103	15	12.4	4.14 ± 0.1	0.556	4.63	0.36	5.3	0.56

Table 5.4: Summary of all uptake rates determined using "tracer" 1 nmol L^{-1} ^{63}Ni additions

Station	Depth	Ni Uptake	Chl a	Ni uptake per ug chl a	Dissolved Ni	NO_3	NH_4	SiO_3	PO_4	Temperature	Oxygen
	meters	*pmol L^{-1} hr^{-1}*	*µg L^{-1}*	*pmol µg^{-1} hr^{-1}*	*nmol L^{-1}*	*µmol L^{-1}*	*µmol L^{-1}*	*µmol L^{-1}*	*µmol L^{-1}*	*(°C)*	*µmol L^{-1}*
GOCAL3-3	3	0.90	0.18	5.0	3.63±0.13	0	0	2	0.72	30.2	191
LTER1	3	13.30	4.74	2.8	4.6 ± 0.5	8.6	0.57	11.8	0.71	11.3	211
LTER1	35	2.80	1.27	2.2	5.07±0.17	9.4	1.09	12.9	0.78	11.2	205
LTER2	5	1.74	0.01	174.0	3.45±0.09	0.06	0.48	2.16	0.2	14.3	252
LTER2	40	1.10	0.12	9.4	3.41±0.14	0.07	0.45	2.03	0.19	14	253
LTER2	75	11.70	0.49	23.9	3.51±0.12	1.75	0.61	3.85	0.36	14	251
LTER3	2	40.20	6.50	6.2	4.05±0.04	1.64	0.88	4.1	0.31	14.1	310
LTER3	12	6.10	3.75	1.6	4.3±0.14	5.37	0.93	11.81	0.58	13.4	300
LTER3	25	4.80	2.25	2.1	4.31±0.18	7.7	1.06	13.05	0.7	12	213
LTER4	10	9.70	1.11	8.7	3 ± 0.05	0.95	0.33	3.43	0.25	14.7	248
LTER4	50	5.20	0.80	6.5	3 ± 0.05	11.05	0.29	10.14	0.9	10.9	170
LTER5	5	2.60	0.12	21.5	3.84 ± 0.18	0.105	0.24	1.67	0.23	16.2	240
LTER5	50	6.30	0.55	11.4	3.81 ± 0.09	0.117	0.18	1.7	0.22	15.3	252
LTER5	78	5.50	0.56	9.9	4.14 ± 0.1	4.63	0.36	5.3	0.56	12.6	232
Peru9	5	0.20	0.12	1.6	3.86±0.19	9.4	0	10.8	0.7	16.6	228
Peru9	20	0.40	0.36	1.1	4.37±0.21	10	0	7	0.7	16.3	225
Peru9	30	0.40	0.38	1.0	3.9±0.15	10.5	0	5.5	0.7	14.7	135
Peru9	40	0.13	0.19	0.7	4.12±0.18	12	0	18	1.2	14.3	40
Peru9	50	0.18	0.00	n/a	5.98 ± 0.18	14.9	0	26.4	1.6	13.5	1.8
Peru9	70	0.36	0.00	n/a	5.44±0.18	14.8	0	33	1.6	13.2	1.8
Peru12	10	0.30	0.87	0.3	4.19±0.14	10.9	0	10.4	0.7	15.5	204
Peru12	20	0.30	1.13	0.3	4.66±0.22	10	0	10	1	15.3	192
Peru12	30	0.27	0.72	0.4	4.51±0.23	10	0	10	1	15.3	184
Peru12	45	0.31	0.81	0.4	5.3±0.19	10	0	10	1	13.8	43
Peru12	65	0.12	0.13	1.0	4.77±0.29	9.1	0.9	12.6	1.1	13.2	1.9
Peru12	100	0.13	0.08	1.7	4.55±0.15	15.6	2	32.2	1.5	12.7	1.8
Peru26	8	0.51	n/a	n/a	3.89 ± 0.11	10.1	n/a	0.6	1.6	16.7	223
Peru26	70	0.44	n/a	n/a	4.55 ± 0.15	20.8	n/a	1.5	12.4	14.1	3
Peru26	200	0.11	n/a	n/a	5.79 ± 0.16	11.9	n/a	1.4	16.7	11.9	1.8
Peru26	300	n/a	n/a	n/a	6.39 ± 0.13	31.5	n/a	2.1	35.8	10.7	2
Peru26	400	0.00	n/a	n/a	7.09 ± 0.21	36.7	n/a	2.4	41.7	9.4	2
Peru26	500	n/a	n/a	n/a	7.15 ± 0.23	41.1	n/a	2.7	49.6	8.1	6
Peru26	600	0.29	n/a	n/a	7.72 ± 0.13	43.3	n/a	2.5	57.6	7	8
Peru26	1000	0.16	n/a	n/a	9.17 ± 0.17	42.4	n/a	2.5	90.1	4.6	42

Table 5.5: Equations and parameters for the modeling of cell surface saturation shown in Figure 5.7.

Case 1: [Ni'] resulting in saturation of 5-50% of the cell surface

$[Ni'] = \mu\ Q\ k_{fNi}^{-1}\ L_{sat}^{-1}$ where

$L_{sat} = \{0.05\text{-}0.5\}$ (cell r^2 x transporter r^{-2})

Case 2: [Ni'] resulting in saturation of 5-50% of the cell surface when accounting for required Fe transporters

$[Ni'] = \mu\ Q\ k_{fNi}^{-1}\ L_{sat}^{-1}$

$L_{sat} = \{0.05\text{-}0.5\}$ (cell r^2 x transporter r^{-2}) - L_{Fe}

$L_{fe} = \mu\ Q\ k_{fNi}^{-1}\ [Fe']^{-1}$

GOCAL 3 (cyanobacteria)	Peru 12 (diatoms)
$\mu = 1\ day^{-1}$	$\mu = 1.5\ day^{-1}$
$Q_{ni} = 10^{-20}$ mol cell^{-1}	$Q_{ni} = 2 \times 10^{-17}$ mol cell^{-1}
$Q_{fe} = 4 \times 10^{-19}$ mol cell^{-1}	$Q_{fe} = 2 \times 10^{-18}$ mol cell^{-1}
$K_{f\text{-}Ni} = 10^5$ L mol^{-1}sec^{-1}	$K_{f\text{-}Ni} = 10^5$ L mol^{-1}
$K_{fe} = 2 \times 10^6$ L mol^{-1}sec^{-1}	$K_{fe} = 2 \times 10^6$ L mol^{-1}sec^{-1}
Cell r = 0.5 μm	Cell r = 5.0 μm
Transporter r = 2.3 nm	Transporter r = 2.3 nm
[Fe'] = 170 pmol L^{-1}	[Fe'] = 1000 pmol L^{-1}

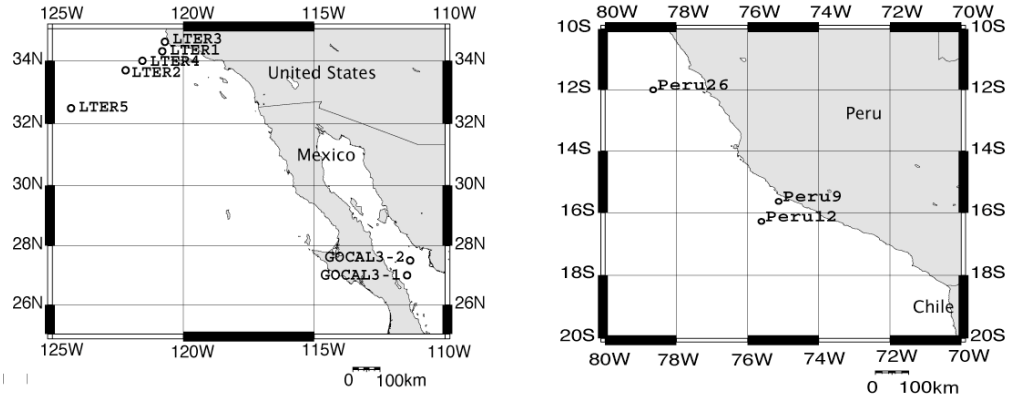

Figure 5.1: Locations and station designations of work detailed in table 1.

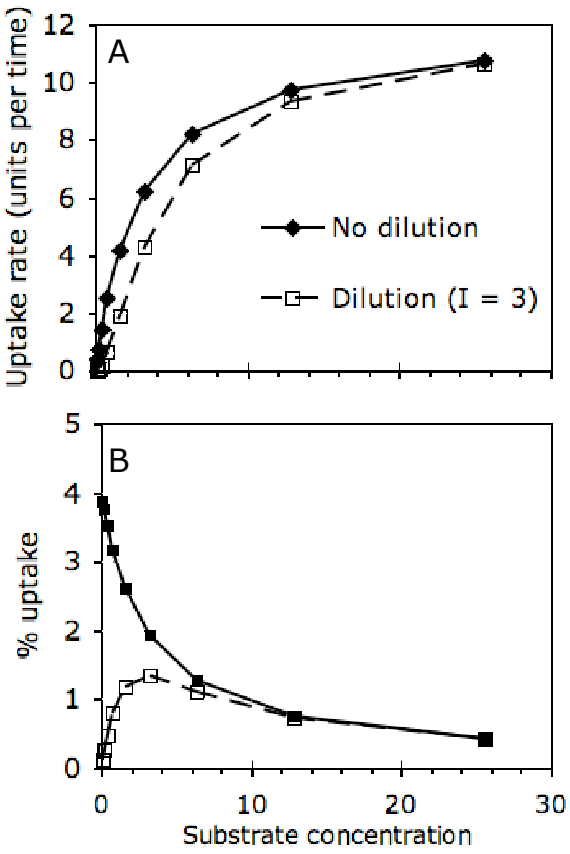

Figure 5.2: Effects of isotope dilution on nutrient uptake. Plotted are the theoretically observed uptake rates for organism with Michaelis-Menten kinetics where V_{max}= 12 and K_ρ = 3 where only the added isotope is present ("no dilution") or the added isotope equilibrates with 3 units of another isotope. The top plot shows the absolute uptake rates, while the bottom plot displays the % of the added isotope assimilated.

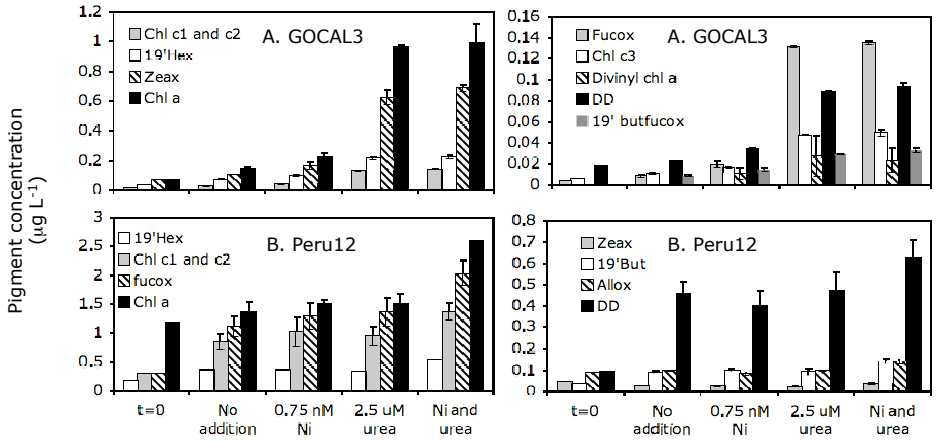

Figure 5.3: Effects of Ni and urea on phytoplankton communities. Shown are the most abundant phytoplankton pigments in the beginning and end of the bottle incubation experiments conducted at A) GOCAL 3-1 and B) Peru12. Error bars are the average of triplicate bottles.

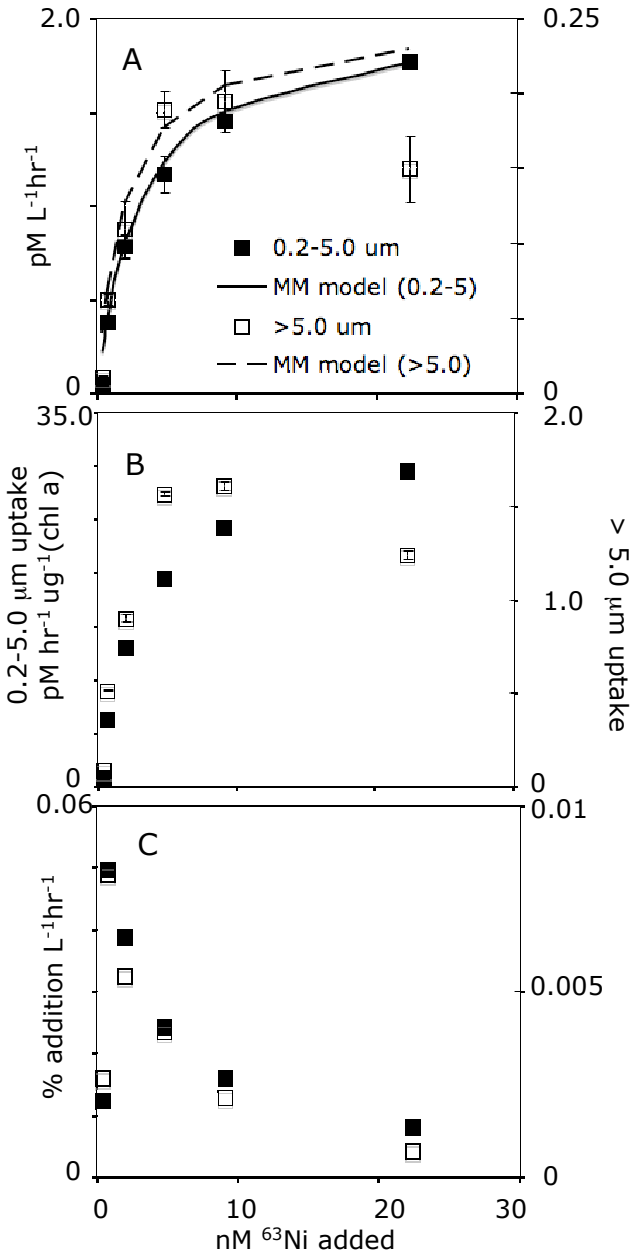

Figure 5.4: Ni uptake kinetics in the Gulf of California. A) Absolute Ni uptake rates observed for the 0.2-5.0 µm and >5.0 µm size fractions over a range of ^{63}Ni additions. Also shown are the fitted least squares regression models of the Michaelis-Menten equation. B) Chl a normalized Ni uptake rates for the same size fractions. C) % uptake of the added ^{63}Ni for the same size fractions. Error bars are the range of duplicate kill control corrected bottles.

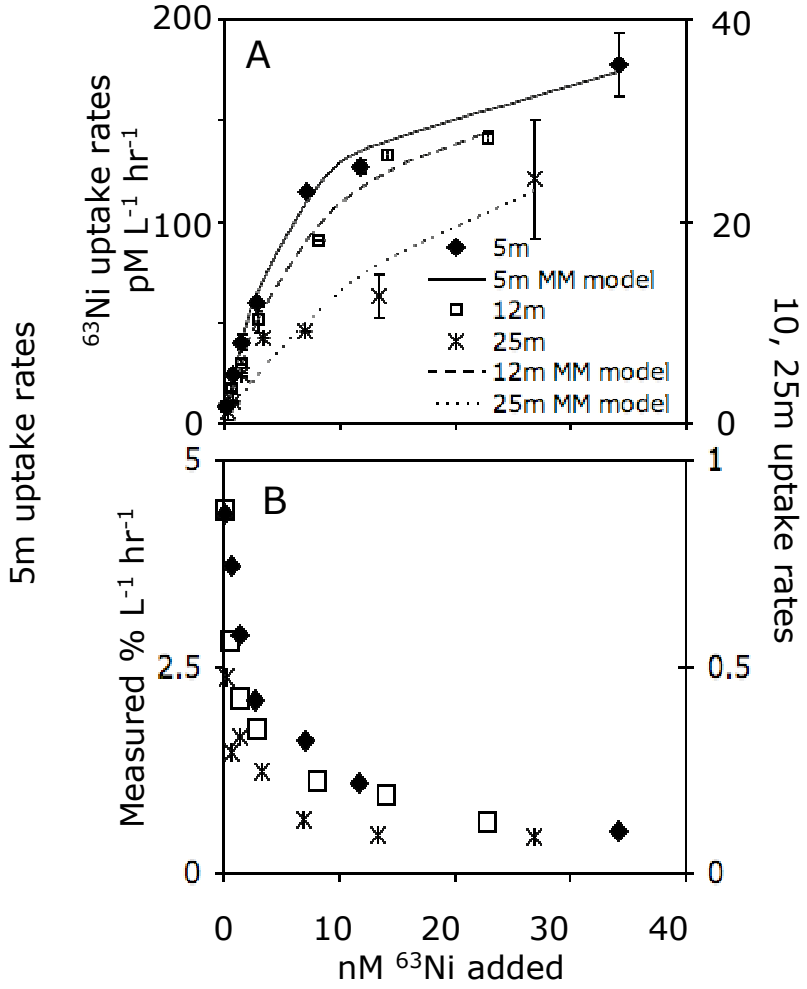

Figure 5.5: Ni uptake kinetics in coastal California. A) Absolute Ni uptake rates for a range of ^{63}Ni additions at water collected from 3, 12, and 25m at LTER3. Also shown are the fitted Michaelis-Menton curves. Error bars are the range of duplicate kill control corrected bottles. B) % uptake of the added ^{63}Ni for the same depths. Error bars here are not plotted for clarity, but are the standard error in percent displayed in plot A multiplied by the % uptake rate.

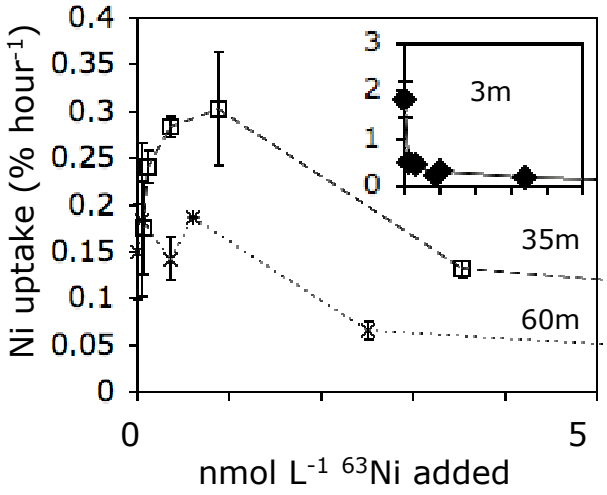

Figure 5.6: Isotope dilution of ^{63}Ni uptake in a coastal California upwelling plume. The % Ni uptake rates at 5m, 35m, and 60m water depth at the LTER1 station are shown. Error bars are the range of duplicate kill control-corrected bottles.

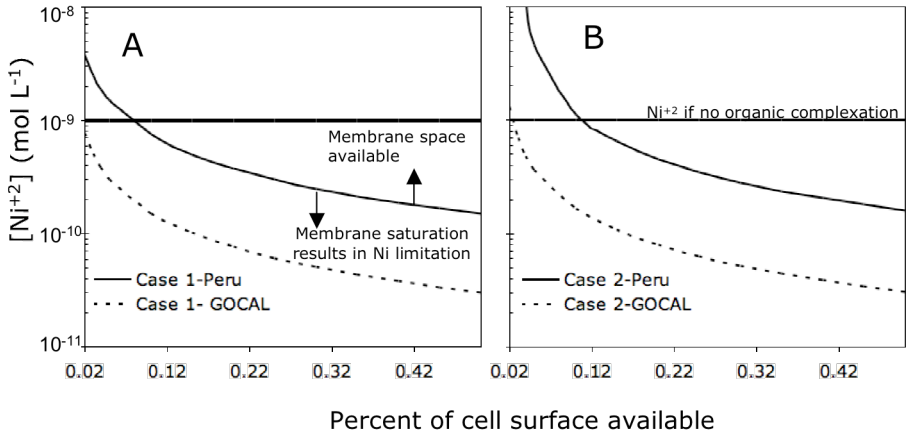

Figure 5.7: Membrane saturation by low Ni. The Ni concentrations (y-axis) resulting in a specific percent of the cell surface (x-axis) being occupied by Ni transporters are shown for model communities representative of the GOCAL3 and Peru12 experiments. Ni concentrations that lie below each curve will be growth limiting. In case 1, Ni is considered in isolation, while in case 2, a fraction of the cell surface is assumed to be occupied by Fe transporters. The models and associated are shown in Table 5.5. For reference, the horizontal line shows the Ni^{+2} concentrations are each location assuming no organic complexation.

CONCLUSIONS

In the previous chapters, a series of linkages between trace metal geochemistry, physiology, and ecology were demonstrated. A crucial theme to each of them is the biological ramifications of the environmental changes induced by a biological phenomenon, oxygenic photosynthesis. The infusion of highly oxidized and reactive oxygen gas into first the atmosphere and then the oceans spawned an enzymatic explosion (151) and potentially, in the second case, the birth of Eukarya. The resulting changes in trace metal concentrations are one of the most extreme changes life has experienced, theoretically having an indelible effect upon the biological selection of elements (199). Particularly important was the incredible drop in Fe concentrations, as it causes many of the phenomena described here.

In chapter one, phylogenetic divergences in proteomic complements of metal binding proteins were demonstrated unequivocally. While the observed trends are consistent with the hypothesized changes in oceanic metal chemistry, the link between the overlying power law differences, biological differentiation events, and geochemical change is still associative. Two complimentary approaches will be pursued to address these shortcomings. First, the proteomic complements of proteins that bind several other metals, including Cu, Mo, Ca, and Ni will be compiled in addition to the already existing data for Fe, Zn, Mn, and Co. This expanded data set will be used to explore the diversity within individual Superkingdoms. Using principal component analysis of the variations in metal-binding protein structure

abundance, phylogenetically consistent signals in the abundances of metal-binding domains will be identified at increasingly finer scales. This should provide insight to the upper limits of the plasticity a proteome has in terms of metal-binding capacity.

A second study will examine the appearance of metal-binding protein structures on a phylogenomic tree that details the evolution of protein architectures (192). Intrinsic to this tree are biological events or horizons, such as the appearance of the first Eukaryotic-specific protein structure. Most of the protein structures involved in central metabolism evolved quickly, prior to the appearance of any Superkingdom-specific protein structures (32), and very few metal-binding protein families emerged during this early period of biological life. Most metal binding folds actually evolved during Superkingdom diversification. Even more striking, the metal-binding protein structures that were present in the last common ancestor are mainly "promiscuous", that is they belong to fold superfamilies that, in their modern form, bind multiple different metals. Future work will attempt to couple the power law relationships that detail the evolutionary constants with the phylogenomic tree, which adds a relational constant, in order to speculate on the proteomic contents of the last common ancestor.

In chapter two, the evolution of a protein born out of the great oxidation was examined. Ni-containing superoxide dismutases appear to have proliferated in only select phylogenetic niches within Bacteria and Eukarya, with an overrepresentation in the marine environment. The acquisition of a Ni-SOD appears to have occurred at

the expense of an Fe-SOD, at least in cyanobacteria. Future comparative genomics should examine the other bacterial lineages for evidence of such an exchange similar to that shown for the marine *Synechococcus* WH7803 and WH8102. Given the current climate of genomic and metagenomic sequencing, the diversity of *sodN* genes is likely to explode, yet it will be curious to see if the phylogenetic distribution will continue to grow. With the Global Ocean Survey, a thorough comparison of the abundances of *sodB* and *sodN* from select phylogenies will certainly provide a better idea of the extent of the *sodB*-*sodN* exchange. Further functional work on the presence of Ni-SOD in Eukarya is paramount.

Chapters three and four describe the physiological ramifications of marine cyanobacteria acquiring a Ni-SOD. Given the importance of superoxide dismutase and the interstrain consistency in Ni requirements, it seems likely that the Ni requirement is extended to all Ni-SOD containing marine cyanobacteria. However, the Ni dependencies and uptake rates of Fe-SOD- and urease- containing strains (e.g. WH7805) should be examined. A lynchpin to understanding Ni homeostasis in *Synechococcus* lies in determining the function and role of *sodT*. It was hypothesized here that the *sodT* is a self-regulating Ni transporter; both genetic verification of a Ni transport phenotype and structural verification of Ni binding and conformational changes are needed.

The implication is that a single horizontal gene transfer event introduced both a new need for a metal and the entire system for intracellular homeostasis. The

selective advantages bestowed were consequential enough that most marine cyanobacteria contain *sodN*-*sodX*-*sodT*. Potentially, the system of Ni transport associated with hydrogenases in other cyanobacteria may have already been lost at the point, necessitating the need for a Ni transporter. The cyanobacteria already had a need for Ni in urease, but possibly not the system to acquire it. Gene clusters for urease also normally contain a gene for a Ni transporter, but this is lacking all cyanobacteria. Conversely, the acquisition of a Ni transporter might have allowed some marine cyanobacteria to better utilize urease.

While often simplistically viewed by oceanographers as an enzyme used for the anabolic assimilation of urea, urease certainly plays a critical role in the intracellular recycling of nitrogen (150). As a testament to that, the set of genes involved in nitrogen assimilation in WH8102 were particularly responsive to Ni deprivation even when urea was not provided as a nitrogen source. Metabolite profiling of Ni-deprived *Synechococcus* will be crucial to teasing out the role of urease in maintaining nitrogen flows. With reduced urease activity, cyanobacteria may be less able to recycle nitrogen efficiently, a critical attribute in the oligotrophic ocean. One selective advantage of the *sodB*-*sodN* exchange may be the acquisition of *sodT* and the attendant ability to tolerate long periods of low nitrogen supply through an efficient urease-facilitated catabolism.

Chapter five detailed a biological approach to studying Ni utilization and sufficiency in marine micriobial assemblages. Ni may be important in select

environments, and while unlikely to influence community biomass to a great extent, variations in Ni bioavailability may have broader biogeochemical impacts. For example, the ubiquitous and rapid release of organic nitrogen by marine phytoplankton (24) may be tied to Ni sufficiency of marine communities, which in turns affects urease activity. Future studies could benefit from another method of determining Ni bioavailability; while biologically relevant, the dilution effects phenomenon is only roughly quantitative. While chemical methods exist for determining Ni speciation (49, 160), they can only measure Ni-binding ligands many orders of magnitude stronger than the half saturation constant for Ni uptake in marine communities, and therefore are biologically irrelevant. On a side note, the "detection" windows of chemical speciation methods for Fe, Zn, and Cu are similar to the biological affinity for those metals and are likely insightful.

Given the current zeal in the oceanographic community for iron, the choice of studying Ni utilization may seem curious, but was deliberate. I believed that the limited number of biological usages for Ni (128) would facilitate hypotheses and modeling of homeostasis, at least relative to Fe or Zn, which are bound by hundreds of different protein folds (55). To some extent, this proved true, though the full genome microarray studies revealed that changes in Ni sufficiency have some very clear, but unexplained biochemical effects, such as the down-regulation of protoporphyrin synthesis. I also hoped to distance myself from the community studying iron, being generally claustrophobic in any large crowd, even academic

ones. The irony is that, as was made clear in numerous chapters, to study Ni in modern phytoplankton is to study the consequences of the low bioavailabilty of Fe in an oxygen-rich ocean.

APPENDIX

Fe binding Fold Families in the SCOP database

Scop ID	Description
a.1.1.1	Truncated hemoglobin
a.1.1.2	Globins
a.1.1.4	Nerve tissue mini-hemoglobin (neural globin)
a.1.2.1	Fumarate reductase/Succinate dehydogenase iron-sulfur protein, C-terminal domain
a.1.2.2	Dihydropyrimidine dehydrogenase, N-terminal domain
a.104.1.1	Cytochrome P450
a.110.1.1	Aldehyde ferredoxin oxidoreductase, C-terminal domains
a.118.1.15	Mo25 protein
a.119.1.1	Plant lipoxigenases
a.119.1.2	Animal lipoxigenases
a.132.1.1	Eukaryotic type heme oxygenase
a.132.1.2	Heme oxygenase HemO (PigA)
a.138.1.1	Cytochrome c3-like
a.138.1.2	Photosynthetic reaction centre (cytochrome subunit)
a.138.1.3	Di-heme elbow motif
a.24.3.1	Cytochrome b562
a.24.3.2	Cytochrome c'-like
a.24.4.1	Hemerythrin
a.25.1.1	Ferritin
a.25.1.2	Ribonucleotide reductase-like
a.3.1.1	monodomain cytochrome c
a.3.1.2	N-terminal (heme c) domain of cytochrome cd1-nitrite reductase
a.3.1.3	Cytochrome bc1 domain
a.3.1.4	Two-domain cytochrome c
a.3.1.5	Di-heme cytochrome c peroxidase
a.3.1.6	Quinoprotein alcohol dehydrogenase, C-terminal domain
a.3.1.7	Quinohemoprotein amine dehydrogenase A chain, domains 1 and 2
a.3.1.8	Di-heme cytochrome c SoxA
a.39.3.1	Cloroperoxidase
a.56.1.1	CO dehydrogenase ISP C-domain like
a.93.1.1	CCP-like
a.93.1.2	Myeloperoxidase-like
a.93.1.3	Catalase-peroxidase KatG
a.96.1.1	Endonuclease III
a.96.1.2	Mismatch glycosylase
b.1.13.1	Superoxide reductase-like
b.2.6.1	Cytochrome f, large domain
b.3.6.1	Aromatic compound dioxygenase
b.33.1.1	Rieske iron-sulfur protein (ISP)
b.33.1.2	Ring hydroxylating alpha subunit ISP domain
b.40.9.1	Heme chaperone CcmE
b.70.2.1	C-terminal (heme d1) domain of cytochrome cd1-nitrite reductase

b.82.1.12 Pirin

b.82.1.4 Homogentisate dioxygenase
b.82.2.1 Penicillin synthase-like
b.82.2.2 Clavaminate synthase
b.82.2.3 Gab protein (hypothetical protein YgaT)
b.82.2.4 Type II Proline 3-hydroxylase (proline oxidase)
b.82.2.5 TauD/TfdA-like
b.82.2.6 Hypoxia-inducible factor HIF ihhibitor (FIH1)
b.82.2.7 YhcH-like
b.82.2.8 gamma-Butyrobetaine hydroxylase
b.82.3.1 CO-sensing protein CooA, N-terminal domain
c.1.28.1 Biotin synthase
c.1.28.2 Oxygen-independent coproporphyrinogen III oxidase HemN
c.1.28.3 MoCo biosynthesis proteins
c.1.9.5 Cytosine deaminase catalytic domain
c.1.9.10 N-acetylglucosamine-6-phosphate deacetylase, NagA, catalytic domain
c.135.1.1 NIF3 (NGG1p interacting factor 3)-like
c.4.1.1 N-terminal domain of adrenodoxin reductase-like
c.47.1.11 Thioredoxin-like 2Fe-2S ferredoxin
c.56.1.1 Hydrogenase maturating endopeptidase HybD
c.66.1.39 Hypothetical protein TT0836
c.81.1.1 Formate dehydrogenase/DMSO reductase, domains 1-3
c.83.1.1 Aconitase iron-sulfur domain
c.92.1.1 Ferrochelatase
c.92.2.1 Periplasmic ferric siderophore binding protein FhuD
c.92.2.3 Nitrogenase iron-molybdenum protein
c.96.1.1 Fe-only hydrogenase
d.110.3.2 Heme-binding PAS domain
d.120.1.1 Cytochrome b5
d.129.3.3 Ring hydroxylating alpha subunit catalytic domain (Pfam 00848)
d.13.1.2 Hexose-1-phosphate uridylyltransferase
d.134.1.1 Sulfite reductase hemoprotein (SiRHP), domains 2 and 4
d.15.4.1 2Fe-2S ferredoxin-related
d.15.4.2 2Fe-2S ferredoxin domains from multidomain proteins
d.157.1.3 ROO N-terminal domain-like
d.159.1.1 Purple acid phosphatase
d.174.1.1 Nitric oxide (NO) synthase oxygenase domain
d.178.1.1 Aromatic aminoacid monoxygenases, catalytic and oligomerization domains
d.32.1.3 Extradiol dioxygenases
d.35.1.1 Heme-binding protein A (HasA)
d.58.1.1 Short-chain ferredoxins
d.58.1.2 7-Fe ferredoxin
d.58.1.3 Archaeal ferredoxins
d.58.1.4 Single 4Fe-4S cluster ferredoxin
d.58.1.5 Ferredoxin domains from multidomain proteins
e.18.1.1 Nickel-iron hydrogenase, large subunit

e.19.1.1	Nickel-iron hydrogenase, small subunit
e.26.1.1	Hybrid cluster protein (prismane protein)
e.26.1.2	Carbon monoxide dehydrogenase
e.26.1.3	Acetyl-CoA synthase
e.5.1.1	Heme-dependent catalases
f.21.1.1	Formate dehydrogenase N, cytochrome (gamma) subunit
f.21.1.2	Cytochrome b of cytochrome bc1 complex (Ubiquinol-cytochrome c reductase)
f.21.2.1	Fumarate reductase respiratory complex cytochrome b subunit, FrdC
f.21.2.2	Succinate dehydrogenase/Fumarate reductase transmembrane subunits (SdhC/FrdC and SdhD/FrdD)
f.21.3.1	Respiratory nitrate reductase 1 gamma chain
f.23.23.1	Cytochrome f subunit of the cytochrome b6f complex, transmembrane anchor
f.24.1.1	Cytochrome c oxidase subunit I-like
f.26.1.1	Bacterial photosystem II reaction centre, L and M subunits
g.35.1.1	HIPIP (high potential iron protein)
g.36.1.1	Ferredoxin thioredoxin reductase (FTR), catalytic beta chain
g.41.5.1	Rubredoxin
g.41.5.2	Desulforedoxin
c.7.1.3	Class III anaerobic ribonucleotide reductase NRDD subunit
d.278.1.1	H-NOX domain

Zn-binding Fold Families in the SCOP

Scop ID	**Description**
a.118.1.7	Leukotriene A4 hydrolase C-terminal domain
a.124.1.1	Phospholipase C
a.124.1.2	P1 nuclease
a.211.1.1	HD domain
a.137.4.1	Fe-only hydrogenase smaller subunit
a.29.7.1	Mob1/phocein
a.4.10.1	N-terminal Zn binding domain of HIV integrase
a.4.11.1	RNA polymerase subunit RPB10
a.60.2.2	NAD+-dependent DNA ligase, domain 3
b.1.8.1	Cu,Zn superoxide dismutase-like
b.2.5.2	p53 DNA-binding domain-like
b.35.1.2	Alcohol dehydrogenase-like, N-terminal domain
b.40.4.11	DNA replication initiator (cdc21/cdc54) N-terminal domain
b.40.4.7	Phage ssDNA-binding proteins
b.74.1.1	Carbonic anhydrase
b.82.1.3	Type I phosphomannose isomerase
b.88.1.1	RabGEF Mss4
c.1.10.3	5-aminolaevulinate dehydratase, ALAD (porphobilinogen synthase)
c.1.10.2	Class II FBP aldolase
c.1.15.1	Endonuclease IV
c.1.15.2	L-rhamnose isomerase
c.1.15.4	Hypothetical protein IolI
c.1.20.1	tRNA-guanine transglycosylase
c.1.26.1	Homocysteine S-methyltransferase

c.1.9.1	Adenosine deaminase (ADA)
c.1.9.11	D-aminoacylase, catalytic domain
c.1.9.13	Isoaspartyl dipeptidase, catalytic domain
c.1.9.3	Phosphotriesterase-like
c.1.9.4	Dihydroorotase
c.1.9.7	Renal dipeptidase
c.111.1.1	Molybdenum cofactor biosynthesis protein MoeB
c.111.1.2	Ubiquitin activating enzymes (UBA)
c.120.1.2	5' to 3' exonuclease catalytic domain
c.125.1.1	Creatininase
c.134.1.1	LmbE-like
c.23.5.3	Quinone reductase
c.26.1.1	Class I aminoacyl-tRNA synthetases (RS), catalytic domain
c.31.1.5	Sir2 family of transcriptional regulators
c.33.1.3	Isochorismatase-like hydrolases
c.42.1.2	Histone deacetylase, HDAC
c.52.1.15	Very short patch repair (VSR) endonuclease
c.53.2.1	beta-carbonic anhydrase, cab
c.56.5.1	Pancreatic carboxypeptidases
c.56.5.2	Carboxypeptidase T
c.56.5.3	Leucine aminopeptidase, C-terminal domain
c.56.5.4	Bacterial dinuclear zinc exopeptidases
c.56.5.5	Transferrin receptor ectodomain, protease-like domain
c.56.5.6	N-acetylmuramoyl-L-alanine amidase CwlV
c.6.2.1	alpha-mannosidase
c.6.3.1	PHP domain
c.6.3.2	RNase P subunit p30 (Pfam 01876)
c.74.1.1	AraD-like aldolase/epimerase
c.76.1.1	Alkaline phosphatase
c.76.1.4	Phosphonoacetate hydrolase
c.76.1.3	2,3-Bisphosphoglycerate-independent phosphoglycerate mutase, catalytic domain
c.8.8.1	Putative cyclase
c.82.1.2	L-histidinol dehydrogenase HisD
c.97.1.1	Cytidine deaminase
c.97.3.1	JAB1/MPN domain
c.99.1.1	Dipeptide transport protein
d.110.2.2	IclR ligand-binding domain-like (Pfam 01614)
d.113.1.4	NADH pyrophosphatase
d.115.1.2	3,4-dihydroxy-2-butanone 4-phosphate synthase, DHBP synthase, RibB
d.118.1.1	N-acetylmuramoyl-L-alanine amidase-like
d.129.7.1	TT1751-like
d.13.1.2	Hexose-1-phosphate uridylyltransferase
d.14.1.2	RNase P protein
d.144.1.5	MHCK/EF2 kinase
d.15.1.6	BM-002-like (UPF0185)
d.157.1.1	Zn metallo-beta-lactamase

d.157.1.2 Glyoxalase II (hydroxyacylglutathione hydrolase)

d.159.1.1 Purple acid phosphatase
d.159.1.2 5'-nucleotidase (syn. UDP-sugar hydrolase), N-terminal domain
d.159.1.3 Protein serine/threonine phosphatase
d.164.1.1 SMAD MH1 domain
d.17.6.1 Archaeosine tRNA-guanine transglycosylase, C2 domain
d.17.6.2 Hypothetical protein Ta1423, N-terminal domain
d.17.6.3 Nip7p homolog, N-terminal domain
d.184.1.2 Virulence effector SptP domain
d.193.1.1 Hsp33 domain
d.196.1.1 Outer capsid protein sigma 3
d.231.1.1 Receptor-binding domain of short tail fibre protein gp12
d.239.1.1 GCM domain
d.264.1.1 DNA primase
d.264.1.2 Bifunctional DNA primase/polymerase N-terminal domain
d.32.1.1 Glyoxalase I (lactoylglutathione lyase)
d.4.1.1 HNH-motif
d.4.1.2 Sm endonuclease
d.4.1.3 Intron-encoded homing endonucleases
d.4.1.5 Recombination endonuclease VII, N-terminal domain
d.4.1.6 Endonuclease I
d.4.1.7 Caspase-activated DNase, CAD (DffB, DFF40)
d.50.3.1 PI-Pfui intein middle domain
d.58.4.5 PG130-like
d.58.4.7 YciI-like
d.65.1.1 Muramoyl-pentapeptide carboxypeptidase
d.65.1.2 Hedgehog (development protein), N-terminal signaling domain
d.65.1.3 MepA-like
d.65.1.4 VanX-like (Pfam 01427)
d.66.1.2 Ribosomal protein S4
d.68.5.1 C-terminal domain of ProRS
d.79.5.1 2C-methyl-D-erythritol 2,4-cyclodiphosphate synthase IspF
d.92.1.1 Zinc protease
d.92.1.10 TNF-alpha converting enzyme, TACE, catalytic domain
d.92.1.11 Matrix metalloproteases, catalytic domain
d.92.1.12 Fungal zinc peptidase
d.92.1.13 Leukotriene A4 hydrolase catalytic domain
d.92.1.14 Anthrax toxin lethal factor, N- and C-terminal domains
d.92.1.15 Predicted metal-dependent hydrolase
d.92.1.2 Thermolysin-like
d.92.1.3 Leishmanolysin
d.92.1.4 Neutral endopeptidase (neprilysin)
d.92.1.5 Neurolysin-like
d.92.1.6 Serralysin-like metalloprotease, catalytic (N-terminal) domain
d.92.1.7 Clostridium neurotoxins, catalytic domain
d.92.1.8 Astacin

d.92.1.9 Hemorrhagin

d.96.1.2 6-pyruvoyl tetrahydropterin synthase
e.22.1.1 Dehydroquinate synthase, DHQS
e.22.1.2 Iron-containing alcohol dehydrogenase (Pfam 00465)
e.29.1.1 RNA-polymerase beta
e.29.1.2 RNA-polymerase beta-prime
f.13.1.2 Rhodopsin-like
f.4.4.2 Outer membrane adhesin/invasin OpcA
g.37.1.1 Classic zinc finger, C2H2
g.37.1.2 C2HC finger
g.37.1.3 Plant C2H2 finger (QALGGH zinc finger)
g.37.1.4 Spliceosomal protein U1C
g.38.1.1 Zn2/Cys6 DNA-binding domain
g.39.1.1 Erythroid transcription factor GATA-1
g.39.1.10 Transcription factor grauzone Cg33133-Pa, zinc finger associated domain
g.39.1.11 ClpX chaperone zinc binding domain
g.39.1.12 PARP-type zinc finger (Pfam 00645)
g.39.1.13 Prokaryotic DksA/TraR C4-type zinc finger (Pfam 01258)
g.39.1.2 Nuclear receptor
g.39.1.3 LIM domain
g.39.1.4 LASP-1
g.39.1.5 DNA repair factor XPA DNA- and RPA-binding domain, N-terminal subdomain
g.39.1.6 Ribosomal protein L24e
g.39.1.7 Ribosomal protein S14
g.39.1.8 C-terminal, Zn-finger domain of MutM-like DNA repair proteins
g.39.1.9 Hypothetical zinc finger protein YacG
g.41.1.1 Methionyl-tRNA synthetase (MetRS), Zn-domain
g.41.10.1 Zn-finger domain of Sec23/24
g.41.11.1 Znf265, first zinc-finger domain
g.41.12.1 NZF domain
g.41.13.1 Hypothetical protein Ta0289 C-terminal domain
g.41.2.1 Microbial and mitochondrial ADK, insert "zinc finger" domain
g.41.3.1 Transcriptional factor domain
g.41.3.2 DNA primase zinc finger
g.41.3.3 Prokaryotic DNA topoisomerase I, a C-terminal fragment
g.41.4.1 Casein kinase II beta subunit
g.41.7.1 Aspartate carbamoyltransferase, Regulatory-chain, C-terminal domain
g.41.8.1 Ribosomal protein L37ae
g.41.8.2 Ribosomal protein L37e
g.41.8.3 Ribosomal protein L44e
g.41.8.4 Ribosomal protein S27e
g.43.1.1 B-box zinc-binding domain
g.44.1.1 RING finger domain, C3HC4
g.46.1.1 Metallothionein
g.47.1.1 Zinc domain conserved in yeast copper-regulated transcription factors
g.48.1.1 Ada DNA repair protein, N-terminal domain (N-Ada 10)

g.49.1.1	Protein kinase cysteine-rich domain (cys2, phorbol-binding domain)
g.49.1.2	TFIIH p44 subunit cysteine-rich domain
g.49.1.3	C1-like domain (Pfam 07649; Pfam 03107)
g.50.1.1	FYVE, a phosphatidylinositol-3-phosphate binding domain
g.50.1.2	PHD domain
g.51.1.1	Zn-binding domains of ADDBP
g.52.1.1	Inhibitor of apoptosis (IAP) repeat
g.53.1.1	TAZ domain
g.54.1.1	DnaJ/Hsp40 cysteine-rich domain
g.59.1.1	Zinc-binding domain of translation initiation factor 2 beta
g.62.1.1	Cysteine-rich DNA binding domain, (DM domain)
g.66.1.1	CCCH zinc finger
g.67.1.1	Zinc finger domain of DNA polymerase-alpha
g.72.1.1	SBT domain
g.73.1.1	CCHHC domain
g.74.1.1	Sec-C motif
e.49.1.1	Recombination protein RecR
c.1.22.2	Cobalamin-independent methionine synthase (Pfam 01717)
a.211.1.2	PDEase
c.140.1.1	Hypothetical protein TT1679

Mn binding Fold Families in the SCOP

Scop ID	Description
a.2.11.1	Fe,Mn superoxide dismutase (SOD), N-terminal domain
a.39.3.1	Cloroperoxidase
b.82.1.10	Hypothetical protein TM1459
b.82.1.2	Germin/Seed storage 7S protein
b.82.1.9	Hypothetical protein TM1287
c.1.10.5	HMGL-like (Pfam 00682)
c.1.11.1	Enolase
c.1.11.2	D-glucarate dehydratase-like
c.1.15.2	L-rhamnose isomerase
c.107.1.1	Manganese-dependent inorganic pyrophosphatase (family II)
c.125.1.1	Creatininase
c.42.1.1	Arginase-like amidino hydrolases
c.68.1.10	N-acetylglucosaminyltransferase I
c.68.1.4	Galactosyltransferase LgtC
c.68.1.5	UDP-glucose pyrophosphorylase
c.68.1.7	1,3-glucuronyltransferase
c.68.1.9	alpha-1,3-galactosyltransferase-like
c.76.1.3	2,3-Bisphosphoglycerate-independent phosphoglycerate mutase, catalytic domain
c.77.1.2	Monomeric isocitrate dehydrogenase
c.91.1.1	PEP carboxykinase C-terminal domain
d.113.1.2	IPP isomerase-like
d.128.1.1	Glutamine synthetase catalytic domain
d.159.1.4	DNA double-strand break repair nuclease

d.218.1.7	Archaeal tRNA CCA-adding enzyme catalytic domain
d.218.1.3	Poly(A) polymerase, PAP, N-terminal domain
d.219.1.1	Protein serine/threonine phosphatase 2C, catalytic domain
d.44.1.1	Fe,Mn superoxide dismutase (SOD), C-terminal domain
d.60.1.1	Multidrug-binding domain of transcription activator BmrR
a.25.1.3	Manganese catalase (T-catalase)
a.211.1.1	HD domain

Co and B12 binding Fold Families in the SCOP

Scop ID	**Description**
c.1.19.1	Methylmalonyl-CoA mutase, N-terminal (CoA-binding) domain
c.1.19.2	Glutamate mutase, large subunit
c.1.19.3	Diol dehydratase, alpha subunit
c.23.6.1	Cobalamin (vitamin B12)-binding domain
c.43.1.1	CAT-like
c.51.3.1	Diol dehydratase, beta subunit
c.51.3.2	Glycerol dehydratase reactivase, beta subunit
c.92.1.2	Cobalt chelatase CbiK
f.22.1.1	ABC transporter involved in vitamin B12 uptake, BtuC

Down regulated by Ni deprivation for growth on ammonia

Locus Number	Description	**Sam Score**	**Fold Change**
SYNW0004	*Glutamine amidotransferaseclass-II:Phosphoribosyl transferase*	5.91	0.36
SYNW0014	RNA-binding region RNP-1 (RNA recognition motif)	4.05	0.41
SYNW0043	hypothetical protein	3.76	0.32
SYNW0068	conserved hypothetical protein	5.26	0.42
SYNW0109	conserved hypothetical protein	4.01	0.19
SYNW0129	conserved hypothetical protein	4.50	0.31
SYNW0144	photosystem I iron-sulfur center subunitVII (PsaC)	4.92	0.46
SYNW0156	putative phosphorylase	3.97	0.60
SYNW0171	Heme oxygenase	4.06	0.53
SYNW0187	putative polysialic acid capsule expression protein KpsF	5.36	0.43
SYNW0220	putative pleiotropic regulatory protein	6.03	0.59
SYNW0241	putative phosphorylase kinase	3.91	0.19
SYNW0244	tRNA-guanine transglycosylase	6.40	0.46
SYNW0245	Cobalamin-5-phosphate synthase-CobS	4.50	0.31
SYNW0247	conserved hypothetical protein	4.41	0.47
SYNW0255	conserved hypothetical protein	5.21	0.15
SYNW0261	CinA-like protein	6.12	0.54
SYNW0293	conserved hypothetical protein	8.23	0.59
SYNW0328	HIT (Histidine triad) family protein	4.15	0.19
SYNW0385	hypothetical	9.67	1.06
SYNW0386	hypothetical	5.46	1.03
SYNW0477	hypothetical	3.89	0.21
SYNW0506	putative aminopeptidase P	4.27	0.34
SYNW0531	conserved hypothetical protein	5.10	0.21
SYNW0543	conserved hypothetical protein	3.78	0.16
SYNW0572	hypothetical	4.96	0.46
SYNW0577	conserved hypothetical membrane protein	3.77	0.13
SYNW0594	hypothetical	4.58	0.12
SYNW0595	hypothetical protein	9.75	0.36
SYNW0597	translation initiation factor IF-2	6.34	0.74
SYNW0612	possible deoxyribonuclease similar to TatD	5.03	0.24
SYNW0627	DnaJ-like protein	4.94	0.39
SYNW0635	Sodium/bile acid cotransporter family	5.25	0.24
SYNW0636	putative DNA helicase	4.79	0.29
SYNW0722	conserved hypothetical protein	4.91	0.61
SYNW0732	conserved hypothetical	4.66	0.36
SYNW0738	conserved hypothetical protein	3.95	0.25
SYNW0766	conserved hypothetical protein	3.86	0.31
SYNW0767	possible ligand gated channel (GIC family)	6.60	0.52
SYNW0778	conserved hypothetical	5.27	0.49
SYNW0786	hypothetical	3.91	0.24
SYNW0815	conserved hypothetical protein	4.08	0.25

SYNW0832	conserved hypothetical protein	3.88	0.17
SYNW0848	hypothetical	6.20	0.35
SYNW0849	hypothetical	5.60	0.64
SYNW0856	conserved hypothetical protein	4.27	0.39
SYNW0857	putative glutathione S-transferase	7.04	0.29
SYNW0873	*hypothetical*	3.96	0.97
SYNW0887	Plastoquinol terminal oxidase (1)	6.01	0.63
SYNW0888	hypothetical	7.15	1.18
SYNW0889	conserved hypothetical protein	4.99	0.30
SYNW0911	conserved hypothetical protein	6.30	0.29
SYNW0916	hypothetical	5.52	0.25
SYNW0927	*photosystem II oxygen-evolvingcomplex 23K protein-PsbP*	3.98	0.21
SYNW0938	*endopeptidase Clp ATP-binding chain C*	8.17	1.03
SYNW0940	putative 2-hydroxy-6-oxohepta-24-dienoatehydrolase	7.29	0.63
SYNW0951	hypothetical	5.64	0.43
SYNW0966	Ribose-phosphate pyrophosphokinase	4.76	0.28
SYNW0991	conserved hypothetical protein	5.08	0.16
SYNW0992	conserved hypothetical protein	3.81	0.28
SYNW1026	*carbamoyl-phosphate synthase small chain*	4.25	0.21
SYNW1038	putative DNA primase	6.77	0.45
SYNW1043	putative UmuC protein	4.19	0.20
SYNW1053	Putative4-diphosphocytidyl-2C-methyl-D-erythritol kinase (CMK)	3.82	0.19
SYNW1060	conserved hypothetical protein	5.53	0.82
SYNW1061	*hypothetical*	10.59	1.54
SYNW1068	conserved hypothetical protein	4.65	0.30
SYNW1069	conserved hypothetical protein	7.81	0.64
SYNW1089	possible glycosyltransferase	6.24	0.34
SYNW1124	conserved hypothetical	5.75	0.51
SYNW1151	conserved hypothetical protein	3.81	0.27
SYNW1170	Putative phosphonate binding protein for ABC transporter	3.96	0.27
SYNW1205	conserved hypothetical protein	4.04	0.12
SYNW1265	probable methylthioadenosine phosphorylase	4.32	0.28
SYNW1269	Molecular chaperone DnaK-HSP70	5.48	0.33
SYNW1277	*ferredoxin*	4.56	0.56
SYNW1292	1-deoxy-D-xylulose 5-phosphate synthase	5.12	0.45
SYNW1297	conserved hypothetical protein	6.24	0.29
SYNW1310	3-dehydroquinate synthase	4.60	0.41
SYNW1333	conserved hypothetical	9.62	1.23
SYNW1338	conserved hypothetical protein	5.62	0.28
SYNW1357	conserved hypothetical protein	7.32	0.59
SYNW1364	RNA-binding protein	4.19	0.42
SYNW1400	hypothetical	6.60	0.48
SYNW1401	conserved hypothetical protein	4.12	0.12
SYNW1407	hypothetical	4.81	0.13
SYNW1409	hypothetical	3.94	0.33

SYNW1420	conserved hypothetical protein	4.80	0.17
SYNW1445	hypothetical	6.13	1.12
SYNW1446	hypothetical	8.18	1.32
SYNW1466	hypothetical	4.61	0.25
SYNW1484	lipase family protein	6.16	0.20
SYNW1503	*endopeptidase Clp ATP-binding chain B*	5.19	1.14
SYNW1504	conserved hypothetical protein	4.01	1.09
SYNW1511	*conserved hypothetical*	7.84	1.08
SYNW1522	conserved hypothetical protein	5.18	0.38
SYNW1526	conserved hypothetical protein	4.03	0.21
SYNW1529	ctaDII-cytochrome c oxidase subunit I (3)	4.37	0.40
SYNW1532	hypothetical	5.78	0.78
SYNW1544	ABC transporter ATP binding component	5.34	0.18
SYNW1558	hypothetical	4.21	0.32
SYNW1566	hypothetical	5.03	0.64
SYNW1587	*cell division protein FtsH3*	3.89	0.57
SYNW1592	Possible AraC-type regulatory protein	6.34	0.72
SYNW1608	putative circadian phase modifier CpmA-homolog	5.74	0.52
SYNW1621	Type II alternative RNA polymerase sigma factor s-70 family	5.35	0.26
SYNW1622	tRNA(5-methylaminomethyl-2-thiouridylate)-methyltransferase	7.06	0.38
SYNW1646	oxygen independent coproporphyrinogen III oxidase	7.17	0.28
SYNW1679	Sun protein (Fmu protein)	4.91	0.18
SYNW1684	GTP-binding protein LepA	4.17	0.57
SYNW1687	NifU-like protein	6.13	0.79
SYNW1688	conserved hypothetical protein	4.30	0.42
SYNW1697	conserved hypothetical protein	4.87	0.32
SYNW1705	conserved hypothetical protein	5.17	0.22
SYNW1766	conserved hypothetical protein	5.46	0.42
SYNW1814	conserved hypothetical protein	4.63	0.39
SYNW1818	conserved hypothetical protein	6.02	0.32
SYNW1821	conserved hypothetical protein	4.30	0.65
SYNW1831	homologous to N-terminus of PilT2 protein	4.45	0.13
SYNW1832	*homologous to C-terminus of pilT2 protein*	4.82	0.69
SYNW1857	putative multidrug efflux ABC transporter	4.33	0.36
SYNW1859	CtaI associated-putative protoheme IX farnesyltransferase	8.20	1.35
SYNW1860	CtaI associated conserved hypothetical protein (3)	5.55	0.74
SYNW1861	ctaCI-cytochrome c oxidase subunit II (3)	6.02	0.85
SYNW1862	ctaDI-cytochrome c oxidase subunit I (3)	4.44	0.82
SYNW1863	CtaEI-possible cytochrome c oxidase subunit III (3)	3.95	0.37
SYNW1893	hypothetical	5.67	0.91
SYNW1916	ABC transporter glycine betaine/prolinefamily	4.98	0.15
SYNW1963	putative sugar aldolase	4.84	0.22
SYNW2000	*Phycobilisome linker polypeptide*	5.26	0.40
SYNW2016	C-phycoerythrin class I alpha chain	4.19	0.79
SYNW2061	conserved hypothetical protein	5.90	0.91

SYNW2062	RecA bacterial DNA recombination protein	5.89	0.57
SYNW2119	putative RND family multidrug efflux transporter	4.03	0.45
SYNW2152	conserved hypothetical	5.92	0.42
SYNW2160	conserved hypothetical protein	4.72	0.42
SYNW2161	putative 4'-phosphopantetheinyl transferase	4.93	0.45
SYNW2177	conserved hypothetical protein	4.98	0.37
SYNW2188	possible Fe-S oxidoreductase	3.84	0.40
SYNW2221	putative HSP-DnaJ	5.44	0.28
SYNW2233	cyanobacterial conserved hypothetical protein	4.12	0.66
SYNW2252	conserved hypothetical protein	4.79	0.21
SYNW2263	NADH dehydrogenase I chain 4 (or M)	5.47	0.37
SYNW2289	*two-component response regulator*	8.28	1.27
SYNW2312	conserved hypothetical protein	4.80	1.08
SYNW2313	conserved hypothetical protein	5.32	1.20
SYNW2314	possible diacylglycerol kinase	4.73	0.38
SYNW2324	guanosine-3'5'-bis(diphosphate)3'-diphosphatase (ppGpp)ase	9.99	0.99
SYNW2355	conserved hypothetical protein	9.73	0.36
SYNW2362	SNF2 helicase homolog	6.24	0.53
SYNW2363	conserved hypothetical protein	5.92	0.63
SYNW2366	putative integral membrane protein	3.80	0.35
SYNW2382	glucose inhibited division protein A	5.25	0.30
SYNW2385	conserved hypothetical protein	4.09	0.62
SYNW2386	conserved hypothetical protein	6.08	1.16
SYNW2411	hypothetical	4.85	0.25
SYNW2422	arginase family protein	3.97	0.25
SYNW2428	Glutamine amidotransferase class-I:CTPsynthase	4.36	0.50
SYNW2439	*ATP-binding subunit of ABC-type urea transport system*	5.94	0.29
SYNW2440	*Membrane protein of ABC-type urea transport system*	7.02	0.32
SYNW2441	*ABC transporter for urea uptake*	4.61	0.34
SYNW2443	urease accessory protein G	3.84	0.12
SYNW2449	urease alpha subunit	4.78	0.36
SYNW2451	conserved hypothetical protein	5.82	0.19
SYNW2463	nitrate transporter-MFS family	5.40	0.21
SYNW2469	molybdenum cofactor biosynthesis protein-MoeA	5.53	0.25

Down regulated by Ni deprivation for growth on ammonia

Locus Number	Description	Sam **Score**	Fold **Change**
SYNW0006	conserved hypothetical protein	-5.61	-0.40
SYNW0022	*General secretion pathway protein E*	-3.64	-0.40
SYNW0028	UDP-N-acetylenolpyruvoylglucosamine reductase	-10.47	-0.42
SYNW0029	Probable UDP-N-acetylmuramate-alanineligase	-3.71	-0.41
SYNW0032	putative cyclophilin-type peptidyl-prolylcis-trans isomerase	-4.55	-0.17
SYNW0035	pdxA-putative pyridoxal phosphate biosynthetic protein	-4.73	-0.28
SYNW0060	putative glycosyltransferase	-4.14	-0.25
SYNW0064	ATP-dependent Clp protease proteolytic subunit	-4.65	-0.43

SYNW0083	putative deacetylase sulfotransferase	-5.37	-0.16
SYNW0085	swmA - cell surface protein required forswimming motility	-4.01	-1.39
SYNW0090	serine acetyltransferase	-5.93	-0.20
SYNW0099	Glutathione peroxidase	-4.45	-0.46
SYNW0103	hypothetical	-3.49	-0.35
SYNW0104	possible glycosyltransferase	-7.81	-0.79
SYNW0116	hypothetical	-5.86	-0.31
SYNW0119	putative adenosylhomocysteinase	-5.29	-0.43
SYNW0123	putative rod shape-determining protein	-3.92	-0.22
SYNW0126	two-component response regulator	-14.31	-1.49
SYNW0127	lysyl-tRNA synthetase	-4.70	-0.36
SYNW0142	3-oxoacyl-[acyl-carrier-protein] synthaseII	-6.95	-0.68
SYNW0160	conserved hypothetical protein	-3.66	-0.21
SYNW0173	putative multidrug efflux ABC transporter	-4.10	-0.15
SYNW0180	KDO 8-P synthase	-4.02	-0.29
SYNW0207	NADH dehydrogenase I chain 3 (or A)	-4.12	-0.39
SYNW0223	conserved hypothetical protein	-4.14	-0.14
SYNW0224	probable deoxyribodipyrimidine photolyase	-4.92	-0.35
SYNW0242	Glycosyl transferase WecB/TagA/CpsF family	-6.99	-0.30
SYNW0273	conserved hypothetical protein	-5.05	-0.26
SYNW0289	isoleucyl-tRNA synthetase	-3.97	-0.35
SYNW0314	phycobilisome rod-core linker polypeptidecpcG (L-RC 28.5)	-4.49	-0.90
SYNW0329	ABC transporter ATP binding protein	-4.54	-0.44
SYNW0336	ACC-acetyl-CoA carboxylase biotin carboxylase subunit	-6.66	-0.43
SYNW0338	putative methionine sulfoxide reductase family	-4.63	-0.10
SYNW0351	hypothetical	-11.02	-0.83
SYNW0374	putative urea binding protein	-3.97	-0.21
SYNW0392	putative sulfotransferase protein	-3.96	-0.74
SYNW0393	hypothetical	-3.67	-0.27
SYNW0394	putative N-acetylneuraminic acid synthetase	-7.69	-0.69
SYNW0395	conserved hypothetical protein	-3.52	-0.19
SYNW0397	conserved hypothetical protein	-3.53	-0.27
SYNW0405	Fumarate lyase:Adenylosuccinate lyase	-5.12	-0.35
SYNW0406	hypothetical	-6.55	-1.13
SYNW0419	conserved hypothetical protein	-4.18	-0.20
SYNW0424	*Possible HMGL-like family protein*	-10.48	-1.09
SYNW0425	*Putative CMP-KDO synthetase*	-5.45	-1.15
SYNW0426	haloacid dehalogenase-likehydrolase family protein	-7.51	-1.10
SYNW0427	possible multidrug efflux ABC transporter	-5.54	-0.97
SYNW0428	hypothetical	-7.41	-0.79
SYNW0429	hypothetical	-4.78	-1.47
SYNW0430	conserved hypothetical	-6.52	-0.97
SYNW0431	hypothetical	-5.19	-0.68

SYNW0432	Putative short-chain dehydrogenase family protein	-5.97	-0.83
SYNW0433	hypothetical	-6.06	-0.57
SYNW0434	conserved hypothetical protein	-4.36	-0.90
SYNW0435	putative glutamine amidotransferase	-15.80	-0.74
SYNW0436	*putative cyclase hisF*	-9.39	-1.44
SYNW0437	hypothetical	-5.37	-0.90
SYNW0438	xylanase chitin deacetylase	-5.30	-0.64
SYNW0439	conserved hypothetical protein	-5.63	-0.51
SYNW0440	hypothetical	-6.02	-0.66
SYNW0441	conserved hypothetical protein	-9.09	-1.42
SYNW0442	conserved hypothetical protein	-9.29	-0.78
SYNW0443	possible oxidoreductase GFO/Idh/MocAfamily protein	-4.25	-0.78
SYNW0450	putative sugar-phosphate nucleotide transferase	-4.88	-0.72
SYNW0451	putative O-acetyltransferase	-5.88	-1.08
SYNW0452	hypothetical	-9.88	-1.09
SYNW0453	*Possible glycosyltransferase*	-4.37	-1.01
SYNW0454	*Possible glycosyltransferase*	-4.04	-0.75
SYNW0455	Possible glycosyltransferase	-4.77	-0.50
SYNW0456	Possible glycosyltransferase	-7.38	-1.24
SYNW0457	hypothetical	-12.53	-1.25
SYNW0458	possible glycosyltransferase group I	-10.12	-0.95
SYNW0459	possible UDP-glucose 4-epimerase	-5.51	-0.88
SYNW0460	Putative glycosyltransferase family protein	-6.82	-0.64
SYNW0488	possible ATP synthase protein 1	-7.61	-0.92
SYNW0490	ATP synthase subunit c	-3.62	-0.85
SYNW0492	putative ATP synthase B chain	-4.04	-0.63
SYNW0512	ATP synthase b subunit	-3.51	-0.85
SYNW0516	hypothetical	-5.23	-0.68
SYNW0517	hypothetical	-10.30	-1.07
SYNW0533	putative D-3-phosphoglycerate dehydrogenase (PGDH)	-7.86	-0.46
SYNW0552	phosphoribosylglycinamide synthetase	-3.83	-0.11
SYNW0562	Leucine aminopeptidase	-4.46	-0.25
SYNW0564	conserved hypothetical protein	-5.81	-0.18
SYNW0590	possible succinate dehydrogenaseiron-sulfur protein	-3.98	-0.24
SYNW0622	conserved hypothetical protein	-7.49	-0.68
SYNW0623	conserved hypothetical protein	-5.10	-0.66
SYNW0624	possible 3Fe-4S ferredoxin	-4.09	-0.24
SYNW0642	hypothetical	-4.80	-0.57
SYNW0644	conserved hypothetical protein	-3.50	-0.45
SYNW0645	putative glycosyltransferase family protein	-5.65	-0.55
SYNW0669	putative long-chain-fatty-acid--CoA ligase	-4.05	-0.19
SYNW0673	O-acetylserine (thiol)-lyase A	-4.54	-0.70
SYNW0674	possible cystathionine gamma-synthase	-4.09	-0.32

SYNW0679	peptidyl-prolyl cis-transisomerase cyclophilin type	-8.50	-0.34
SYNW0684	similar to methyltransferase	-5.53	-0.23
SYNW0689	conserved hypothetical protein	-5.24	-0.26
SYNW0691	conserved hypothetical protein	-8.51	-0.84
SYNW0692	nicotinamide nucleotide transhydrogenase subunit a-1	-4.74	-0.31
SYNW0707	conserved hypothetical protein	-4.66	-0.20
SYNW0709	OppA-Peptide binding protein for ABC-type transporter	-6.66	-0.34
SYNW0718	putative beta-lactamase	-4.55	-0.49
SYNW0723	Glutamine amidotransferase class-I	-5.47	-0.58
SYNW0734	*hypothetical*	-5.10	-0.30
SYNW0745	hypothetical	-6.19	-0.46
SYNW0754	*conserved hypothetical*	-10.30	-0.70
SYNW0755	conserved hypothetical protein	-4.64	-0.46
SYNW0759	conserved hypothetical protein	-4.29	-0.63
SYNW0768	conserved hypothetical protein	-4.96	-0.15
SYNW0769	conserved hypothetical protein	-5.75	-0.35
SYNW0780	conserved hypothetical protein	-4.84	-0.42
SYNW0785	phosphoribulokinase	-5.35	-0.64
SYNW0807	two-component sensor histidine kinase	-3.68	-0.24
SYNW0816	UbiH-2-octaprenyl-6-methoxyphenol4-monoxygenase	-5.12	-0.31
SYNW0820	chlH-Protoporphyrin IX Magnesium chelatase subunit	-6.32	-0.69
SYNW0823	triosephosphate isomerase	-4.00	-0.29
SYNW0855	conserved hypothetical protein	-3.56	-0.20
SYNW0883	conserved hypothetical protein	-4.74	-0.51
SYNW0897	possible carbonic anhydrase	-4.56	-0.47
SYNW0898	psbY-possible photosystem II protein	-5.48	-1.08
SYNW0899	probable glucose inhibited division protein	-8.18	-0.50
SYNW0901	Carotenoid isomerase	-4.02	-0.34
SYNW0931	Glutathione S-transferase domain protein	-4.15	-0.26
SYNW0948	two-component sensor histidine kinase-phosphate	-4.72	-0.24
SYNW0955	*hypothetical*	-4.70	-0.49
SYNW0956	*conserved hypothetical protein*	-3.69	-0.33
SYNW0957	*conserved hypothetical protein*	-3.47	-0.51
SYNW0995	conserved hypothetical protein	-4.43	-0.51
SYNW1003	UDP-N-acetylglucosamine pyrophosphorylase	-4.46	-0.30
SYNW1011	polyprenyl synthetase; solanesyldiphosphate synthase	-6.02	-0.54
SYNW1018	ABC transporter-Phosphate binding protein	-3.65	-0.42
SYNW1027	conserved hypothetical protein	-9.06	-0.62
SYNW1035	ruvA-putative holliday junction DNA helicase	-3.97	-0.22
SYNW1072	SAM binding motif: Generic methyl-transferase	-5.11	-0.78
SYNW1074	phycobilisome core-allophycocyanin b-18 subunit	-6.19	-0.56
SYNW1107	hypothetical	-4.20	-0.35
SYNW1109	tyrosine binding protein	-5.63	-0.73
SYNW1110	conserved hypothetical protein	-5.94	-0.77
SYNW1115	Ribulose-5-phosphate 3-epimerase	-5.85	-0.86

SYNW1117	Possible glutamyl-tRNA reductase	-7.17	-0.58
SYNW1118	ADP-glucose pyrophosphorylase	-4.97	-0.76
SYNW1153	possible 33kD chaperonin heat shockprotein HSP33	-6.81	-0.16
SYNW1159	hypothetical	-6.42	-0.10
SYNW1175	carboxyl-terminal processing protease	-4.91	-0.61
SYNW1197	tldD-putative modulator of DNA gyrase	-5.54	-0.47
SYNW1202	putative acetazolamide resistance conferring protein	-4.66	-0.32
SYNW1213	thioredoxin peroxidase	-3.50	-0.68
SYNW1214	putative peptidase	-6.66	-0.74
SYNW1220	conserved hypothetical protein	-3.49	-0.18
SYNW1221	conserved hypothetical protein	-3.87	-0.29
SYNW1229	allophycocyanin alpha-B chain	-27.25	-1.03
SYNW1250	putative D-Ala-D-Ala carboxypeptidase 3 family (S13)	-5.31	-0.24
SYNW1251	conserved hypothetical protein	-3.50	-0.20
SYNW1252	conserved hypothetical protein	-3.70	-0.19
SYNW1257	conserved hypothetical protein	-3.61	-0.43
SYNW1258	conserved hypothetical protein	-5.23	-0.32
SYNW1273	TPR Domain containing protein	-8.51	-0.61
SYNW1279	50S ribosomal protein L28	-3.63	-0.89
SYNW1280	Alkyl hydroperoxide reductase/ Thiolspecific antioxidant	-4.26	-0.50
SYNW1290	possible photosystem I reaction centersubunit X (PsaK)	-4.24	-0.59
SYNW1296	conserved hypothetical protein	-3.77	-0.14
SYNW1298	pyruvate kinase	-6.31	-0.63
SYNW1299	possible ABC transporter	-5.48	-0.28
SYNW1300	FtsH ATP-dependent protease homolog	-6.39	-0.76
SYNW1302	conserved hypothetical protein	-11.27	-0.32
SYNW1350	hypothetical	-3.66	-0.39
SYNW1374	hypothetical	-3.58	-0.56
SYNW1402	conserved hypothetical protein	-3.69	-0.16
SYNW1450	conserved hypothetical protein	-4.09	-0.24
SYNW1452	predicted membrane protein of COG group 2259	-5.08	-0.59
SYNW1459	conserved hypothetical protein	-6.81	-0.34
SYNW1460	conserved hypothetical	-6.30	-0.54
SYNW1475	t-RNA synthetase class Ib:Tryptophanyl-tRNA synthetase	-4.57	-0.36
SYNW1476	possible endolysin	-4.01	-0.41
SYNW1494	14-alpha-glucan branching enzyme	-3.48	-0.27
SYNW1495	uroD-Uroporphyrinogen decarboxylase	-3.95	-0.59
SYNW1496	conserved hypothetical protein	-5.21	-0.46
SYNW1508	conserved hypothetical protein	-3.62	-0.31
SYNW1509	*Possible type II alternative RNA polymerase s factor*	-5.88	-0.65
SYNW1517	*conserved hypothetical protein*	-3.99	-0.66
SYNW1518	*conserved hypothetical protein*	-6.28	-0.96
SYNW1563	conserved hypothetical protein	-4.24	-0.48
SYNW1579	hypothetical	-5.02	-0.42

SYNW1620	Pyruvate dehydrogenase E1 alpha subunit	-3.81	-0.25
SYNW1644	ftsZ-cell division protein	-3.90	-0.21
SYNW1661	hypothetical protein	-4.08	-0.17
SYNW1678	putative penicillin binding protein	-3.64	-0.37
SYNW1696	possible fatty acid desaturase	-4.95	-0.72
SYNW1715	csoS3-carboxysome shell polypeptide	-4.64	-0.33
SYNW1721	conserved hypothetical protein	-4.67	-0.30
SYNW1734	putative GTP cyclohydrolase I	-3.89	-0.70
SYNW1735	putative short-chain dehydrogenase	-3.72	-0.32
SYNW1738	conserved hypothetical protein	-6.30	-0.53
SYNW1747	Ferrochelatase	-4.89	-0.27
SYNW1759	*transaldolase*	-3.54	-0.32
SYNW1765	Signal peptidase I	-4.59	-0.22
SYNW1767	putative arsenate reductase	-5.51	-0.56
SYNW1768	possible ferredoxin [2Fe-2S]	-4.66	-0.64
SYNW1773	Adenylosuccinate synthetase	-7.97	-0.35
SYNW1774	Putative carbohydrate kinase pfkB family	-3.78	-0.36
SYNW1779	conserved hypothetical protein	-5.45	-0.62
SYNW1785	Porphobilinogen deaminase	-6.10	-0.23
SYNW1797	idiA-ABC transporter Fe (III) binding protein	-8.89	-1.21
SYNW1798	putative iron ABC-type transporter	-8.38	-1.11
SYNW1800	conserved hypothetical protein	-3.85	-0.18
SYNW1807	exodeoxyribonuclease III	-4.45	-0.30
SYNW1809	glutamate-1-semialdehyde 21-aminomutase	-4.35	-0.48
SYNW1810	hypothetical	-7.64	-0.63
SYNW1812	conserved hypothetical protein	-5.05	-0.25
SYNW1815	*ABC transporter phosphate binding protein*	-3.63	-0.33
SYNW1826	glutamyl-tRNA synthetase	-5.58	-0.38
SYNW1845	conserved hypothetical protein	-6.23	-0.36
SYNW1853	hypothetical	-4.14	-0.35
SYNW1856	hypothetical	-4.03	-0.27
SYNW1889	conserved hypothetical protein	-4.59	-0.39
SYNW1892	conserved hypothetical protein	-4.33	-0.30
SYNW1928	GTP1/Obg family GTP-binding protein	-3.94	-0.16
SYNW1932	possible ring-cleaving dioxygenase	-8.82	-0.34
SYNW1942	conserved hypothetical protein	-4.47	-0.58
SYNW1950	*hypothetical*	-4.82	-1.00
SYNW1951	*conserved hypothetical*	-3.87	-0.74
SYNW1968	putative carboxyl-terminal processing protease	-3.47	-0.27
SYNW1993	conserved hypothetical protein	-3.98	-0.46
SYNW2003	CpeT homolog	-4.26	-0.58
SYNW2010	C-phycoerythrin class II g chainlinker polypeptide	-7.47	-0.59
SYNW2018	hypothetical	-4.84	-0.74
SYNW2019	conserved hypothetical protein	-3.58	-0.46
SYNW2025	putative phycocyanobilin lyase a and b fusion protein	-3.92	-0.51
SYNW2041	MRP protein homolog	-4.55	-0.35

SYNW2042	cell division protein	-3.75	-0.25
SYNW2089	30S ribosomal protein S11	-3.97	-0.90
SYNW2129	hypothetical	-6.15	-0.37
SYNW2137	elongation factor EF-G	-6.10	-0.62
SYNW2147	putative aminotransferase	-5.90	-0.39
SYNW2154	Phosphoglucomutase	-4.20	-0.43
SYNW2187	putative RND family-outer membrane efflux protein	-10.64	-0.85
SYNW2201	6-pyruvoyl-tetrahydropterin synthasehomolog	-7.92	-0.47
SYNW2204	conserved hypothetical protein	-3.50	-0.17
SYNW2205	putative glutathione S-transferase	-5.22	-0.44
SYNW2209	conserved hypothetical protein	-3.83	-0.26
SYNW2213	zeta-carotene desaturase	-5.93	-0.15
SYNW2223	possible porin	-7.53	-0.65
SYNW2224	possible porin	-6.55	-1.76
SYNW2255	putative RNA-binding protein (RRM domain)	-5.82	-0.67
SYNW2257	phytoene desaturase	-3.86	-0.47
SYNW2266	Putative sugar-phosphate nucleotidyltransferase	-6.43	-0.76
SYNW2275	citrate synthase	-5.03	-0.42
SYNW2295	hypothetical	-4.12	-0.36
SYNW2296	hypothetical	-6.17	-0.77
SYNW2340	50S ribosomal protein L7/L12	-6.61	-1.07
SYNW2341	50S ribosomal protein L10	-5.09	-0.87
SYNW2342	50S ribosomal protein L1	-4.70	-0.35
SYNW2357	putative thiamine biosynthesis oxidoreductase	-3.49	-0.25
SYNW2358	Nucleoside diphosphate kinase	-4.19	-0.49
SYNW2360	Alanyl-tRNA synthetase	-4.27	-0.15
SYNW2372	conserved hypothetical protein	-4.17	-0.33
SYNW2402	conserved hypothetical protein	-4.65	-0.27
SYNW2415	hypothetical	-10.56	-0.42
SYNW2423	hypothetical possible cyclicnucleotide-binding domain	-4.12	-0.20
SYNW2427	*Possible type II alternative RNA polymerase s factor*	-4.84	-0.30
SYNW2477	Ferredoxin--nitrite reductase	-8.66	-1.37
SYNW2479	*ABC type transporter- possibly Zn transport*	-8.67	-0.81
SYNW2480	*ABC type transporter-possibly Zn transport*	-13.13	-1.38
SYNW2481	*ABC-type transporter- putative Zn-binding protein*	-8.65	-1.05
SYNW2482	conserved hypothetical protein	-4.79	-0.72
SYNW2489	conserved hypothetical	-3.86	-0.35
SYNW2490	cyanate lyase	-3.86	-0.26
SYNW2495	putative polyphosphate kinase	-3.52	-0.25
SYNW2499	DAHP synthetase class I	-3.69	-0.44
SYNW2505	conserved hypothetical protein	-3.68	-0.48
SYNW2524	Protein kinase: ABC1 family	-5.73	-0.39
SYNW2525	conserved hypothetical protein	-4.30	-0.20

Up regulated by Ni deprivation for growth on urea

Locus Number	Description	**Sam Score**	**Fold Change**
SYNW0014	RNA-binding region RNP-1 (RNA recognition motif)	4.46	0.90
SYNW0021	homologous to N-terminus of pilT1 protein	3.26	0.15
SYNW0022	*General secretion pathway protein E*	4.78	0.30
SYNW0038	HNH endonuclease:HNH nuclease	4.36	0.23
SYNW0133	conserved hypothetical	3.48	0.11
SYNW0150	conserved hypothetical protein	3.24	0.89
SYNW0165	conserved hypothetical	6.34	0.18
SYNW0188	possible polyA polymerase	5.41	1.01
SYNW0196	putative alkaline phosphatase	4.17	0.32
SYNW0216	2-amino-4-hydroxy-6-hydroxymethyldihydropteridine pyrophosphokinase	3.09	0.66
SYNW0222	conserved hypothetical protein	3.73	0.59
SYNW0228	conserved hypothetical	5.86	0.42
SYNW0247	conserved hypothetical protein	8.18	0.80
SYNW0248	probable esterase	3.12	0.48
SYNW0294	conserved hypothetical protein	4.72	0.21
SYNW0307	hypothetical	3.87	0.44
SYNW0328	HIT (Histidine triad) family protein	3.34	0.18
SYNW0343	hypothetical	4.47	0.21
SYNW0344	conserved hypothetical protein	3.57	0.11
SYNW0362	hypothetical	3.03	0.62
SYNW0365	hypothetical	4.67	0.72
SYNW0375	conserved hypothetical protein	3.33	0.16
SYNW0380	conserved hypothetical protein	3.54	0.67
SYNW0381	hypothetical	5.23	2.76
SYNW0424	*Possible HMGL-like family protein*	3.38	0.47
SYNW0425	*Putative CMP-KDO synthetase*	3.36	0.22
SYNW0436	*putative cyclase hisF*	3.05	0.40
SYNW0453	*Possible glycosyltransferase*	3.15	0.37
SYNW0454	*Possible glycosyltransferase*	4.88	0.46
SYNW0467	conserved hypothetical protein	3.06	0.12
SYNW0472	putative c-type cytochrome biogenesisprotein CcdA	2.98	0.32
SYNW0477	hypothetical	3.75	0.20
SYNW0520	possible PyrR/uracil phosphoribosyltransferase	3.04	0.20
SYNW0529	conserved hypothetical protein	3.14	0.15
SYNW0549	KaiB: circadian oscillation regulator	4.00	0.25
SYNW0587	DNA binding protein HU	2.98	0.21
SYNW0602	hypothetical	3.66	0.11
SYNW0621	conserved hypothetical protein	3.91	0.29
SYNW0710	conserved hypothetical protein	3.88	0.20
SYNW0732	conserved hypothetical	7.69	0.29
SYNW0734	*hypothetical*	4.66	0.13
SYNW0738	conserved hypothetical protein	6.38	0.37

SYNW0740	bifunctional Methylenetetrahydrofolate dehydrogenase	3.23	0.13
SYNW0754	*conserved hypothetical*	6.26	0.38
SYNW0778	conserved hypothetical	3.05	0.30
SYNW0779	conserved hypothetical protein	3.76	0.55
SYNW0786	hypothetical	6.31	0.35
SYNW0787	putative type 4 prepilin peptidase	4.26	0.51
SYNW0795	hypothetical	3.05	0.45
SYNW0796	small mechanosensitive ion channel in the MscS family	5.44	0.31
SYNW0800	multidrug efflux transporter MFS family	3.21	0.20
SYNW0809	conserved hypothetical protein	3.11	0.15
SYNW0826	hypothetical	3.34	0.19
SYNW0848	hypothetical	5.75	0.20
SYNW0850	putative homoserine O-succinyltransferase	3.10	0.10
SYNW0861	hypothetical	4.67	0.19
SYNW0866	conserved hypothetical	4.29	0.14
SYNW0870	conserved hypothetical	3.59	0.19
SYNW0878	hypothetical	4.36	0.30
SYNW0879	hypothetical	4.80	0.40
SYNW0881	conserved hypothetical protein	3.87	0.38
SYNW0886	hypothetical	7.48	0.19
SYNW0887	Plastoquinone terminal oxidase	11.90	1.48
SYNW0916	hypothetical	3.04	0.18
SYNW0919	similar to mannose-6-phosphate isomerase WbpW	3.40	0.15
SYNW0943	similar to RlpA	2.98	0.43
SYNW0947	two-component response regulator: phosphate response	3.83	0.18
SYNW0951	hypothetical	3.79	0.36
SYNW0952	conserved hypothetical protein	3.71	0.77
SYNW0954	conserved hypothetical protein	4.60	0.38
SYNW0955	*hypothetical*	6.43	0.23
SYNW0956	*conserved hypothetical protein*	3.16	0.36
SYNW0957	*conserved hypothetical protein*	3.12	0.39
SYNW0977	conserved hypothetical protein	3.59	0.19
SYNW0985	conserved hypothetical	4.51	0.29
SYNW0991	conserved hypothetical protein	3.11	0.18
SYNW1015	putative bacterioferritin comigratory protein	3.42	0.31
SYNW1017	conserved hypothetical protein	3.46	0.31
SYNW1036	conserved hypothetical protein	4.62	0.24
SYNW1063	conserved hypothetical protein	3.12	0.14
SYNW1071	conserved hypothetical protein	6.78	0.45
SYNW1098	putative carboxypeptidase	3.67	0.13
SYNW1124	conserved hypothetical	3.94	0.28
SYNW1139	hypothetical	9.78	2.19
SYNW1162	hypothetical	3.00	0.33
SYNW1180	hypothetical	3.72	0.33
SYNW1184	hypothetical	3.64	0.17
SYNW1188	hypothetical	3.05	0.14

SYNW1208	conserved hypothetical protein	4.04	0.11
SYNW1211	cell division protein FtsH4	3.25	0.19
SYNW1212	conserved hypothetical protein	3.52	0.15
SYNW1219	conserved hypothetical	4.92	0.28
SYNW1281	Putative glucosyl-glycerol-phosphate synthase	3.51	0.55
SYNW1305	hypothetical	6.59	0.61
SYNW1306	conserved hypothetical protein	5.67	0.20
SYNW1327	hypothetical	3.20	0.14
SYNW1334	NUDIX family protein	3.17	0.16
SYNW1342	putative endonuclease	3.35	0.26
SYNW1345	conserved hypothetical protein	5.91	0.35
SYNW1352	hypothetical	9.27	2.21
SYNW1366	hypothetical	6.21	0.53
SYNW1380	possible DNA-binding response regulator	3.95	0.24
SYNW1382	conserved hypothetical	3.57	0.47
SYNW1389	hypothetical	3.72	0.10
SYNW1398	hypothetical	3.64	0.44
SYNW1400	hypothetical	5.00	0.23
SYNW1418	Putative Rieske [2Fe-2S] family protein	3.08	0.12
SYNW1437	conserved hypothetical protein	4.00	0.24
SYNW1453	conserved hypothetical protein	4.01	0.47
SYNW1454	conserved hypothetical protein	5.72	0.60
SYNW1461	conserved hypothetical	5.09	0.25
SYNW1462	possible transcriptional regulator	6.83	0.63
SYNW1463	hypothetical	7.67	0.97
SYNW1464	conserved hypothetical protein	5.19	0.74
SYNW1465	hypothetical	4.20	0.44
SYNW1505	histidine biosynthesis bifunctional protein: HisIE	4.05	0.24
SYNW1509	*Putative type II alternative RNA polymerase s factor*	7.48	0.78
SYNW1517	*conserved hypothetical protein*	3.83	0.39
SYNW1518	*conserved hypothetical protein*	4.54	0.73
SYNW1522	conserved hypothetical protein	9.67	0.50
SYNW1526	conserved hypothetical protein	15.54	0.66
SYNW1527	conserved hypothetical protein	4.79	0.48
SYNW1528	ctaII: possible cytochrome c oxidase subunit II	4.14	0.60
SYNW1529	ctaII: cytochrome c oxidase subunit I	3.52	0.41
SYNW1530	ctaII: possible cytochrome c oxidase subunit III	3.53	0.23
SYNW1534	conserved hypothetical protein	3.26	0.21
SYNW1546	hypothetical	3.40	0.12
SYNW1550	possible membrane protease complex subunit	3.62	0.30
SYNW1554	conserved hypothetical protein	4.46	0.17
SYNW1564	conserved hypothetical protein	4.57	0.33
SYNW1571	hypothetical	3.54	0.57
SYNW1575	hypothetical	3.86	0.11
SYNW1606	conserved hypothetical protein	7.51	0.42
SYNW1626	SodN: Ni-Superoxide dismutase	4.86	0.62

SYNW1632	conserved hypothetical protein	4.56	0.19
SYNW1655	hypothetical	3.09	0.12
SYNW1657	hypothetical	4.87	0.24
SYNW1664	conserved hypothetical protein	4.24	0.34
SYNW1670	truncated possible competence protein	3.25	0.11
SYNW1698	hypothetical	4.23	0.23
SYNW1699	hypothetical	3.15	0.15
SYNW1724	light-independent protochlorophyllide reductase ChlB	5.97	0.42
SYNW1732	conserved hypothetical protein	3.69	0.29
SYNW1736	acetyl-CoA carboxylase a subunit	3.13	0.16
SYNW1759	*transaldolase*	6.32	0.52
SYNW1770	conserved hypothetical protein	2.99	0.12
SYNW1783	Putative principal RNA polymerase s-factor	9.87	0.76
SYNW1793	conserved hypothetical protein	4.64	0.14
SYNW1814	conserved hypothetical protein	6.08	0.31
SYNW1815	*Phosphate binding component of ABC transporter*	5.17	0.30
SYNW1816	conserved hypothetical protein	6.71	0.45
SYNW1822	putative methionine aminopeptidase	4.69	0.43
SYNW1828	conserved hypothetical protein	3.00	0.11
SYNW1859	ctaI associated: putative protoheme IX farnesyltransferase	6.11	0.87
SYNW1860	ctaI associated: conserved hypothetical protein	3.83	0.52
SYNW1861	ctaI: possible cytochrome c oxidase subunit II	9.40	1.22
SYNW1862	ctaI: cytochrome c oxidase subunit I	10.51	1.12
SYNW1863	ctaI: possible cytochrome c oxidase subunit III	3.14	0.26
SYNW1880	conserved hypothetical protein	4.57	0.27
SYNW1904	hypothetical	3.12	0.17
SYNW1908	Possible Zn-dependent metalloprotease	3.81	0.16
SYNW1913	putative sarcosine-dimethylglycinemethyltransferase	3.70	0.17
SYNW1915	ABC transporter for glycinebetaine/proline	3.07	0.18
SYNW1916	ABC transporter for glycine betaine/proline	4.18	0.17
SYNW1926	conserved hypothetical protein	6.25	0.45
SYNW1927	conserved hypothetical protein	3.98	0.28
SYNW1950	*hypothetical*	11.78	2.01
SYNW1951	*conserved hypothetical*	20.72	1.68
SYNW1965	putative neutral invertase-like protein	7.77	0.53
SYNW2026	low molecular weight protein-tyrosine-phosphatase	3.36	0.18
SYNW2060	conserved hypothetical protein	3.18	0.30
SYNW2108	conserved hypothetical protein	4.57	0.16
SYNW2110	putative ABC transporter multidrug effluxfamily	3.46	0.13
SYNW2160	conserved hypothetical protein	5.66	0.28
SYNW2161	putative 4'-phosphopantetheinyl transferase	7.29	0.34
SYNW2176	possible serine protease	8.10	0.55
SYNW2199	hypothetical	4.42	0.22
SYNW2200	putative riboflavin-specific deaminase	3.12	0.20
SYNW2214	conserved hypothetical protein	3.58	0.23
SYNW2220	conserved hypothetical protein	3.31	0.15

SYNW2225	possible porin - likely pseudogene	3.52	0.26
SYNW2227	possible porin	5.56	0.77
SYNW2229	conserved hypothetical protein	2.99	0.23
SYNW2252	conserved hypothetical protein	3.67	0.22
SYNW2253	conserved hypothetical protein	4.54	0.22
SYNW2268	possible transcriptional regulator	3.85	0.43
SYNW2270	predicted inorganic polyphosphate /ATP-NAD+ kinase	3.05	0.11
SYNW2273	NADH dehydrogenase I chain I (or NdhI)	3.41	0.20
SYNW2345	putative preprotein translocase SecE subunit	3.91	0.26
SYNW2355	conserved hypothetical protein	3.95	0.28
SYNW2385	conserved hypothetical	4.81	0.93
SYNW2390	putative alkaline phosphatase/5'nucleotidase	3.59	0.67
SYNW2391	putative alkaline phosphatase	4.58	0.52
SYNW2399	conserved hypothetical protein	3.91	0.29
SYNW2401	Ferric uptake regulator family	3.20	0.16
SYNW2409	hemolysin-type calcium-binding protein; similar to HlyA	4.81	0.36
SYNW2413	hypothetical	5.78	0.09
SYNW2427	*Possible type II alternative RNA polymerasesigma factor*	3.00	0.31
SYNW2448	urease beta subunit	3.13	0.90
SYNW2450	hypothetical	4.39	1.77
SYNW2452	putative N-carbamoyl-L-amino-acid hydrolase	4.43	0.25
SYNW2466	hypothetical	5.62	0.87
SYNW2471	conserved hypothetical protein	4.46	0.66
SYNW2478	conserved hypothetical protein	4.53	0.63
SYNW2479	*ABC transporter component-Zn transport.*	3.50	0.49
SYNW2480	*ABC transporter ATP binding component-Zn*	6.10	0.96
SYNW2481	*ABC transport system: putative Zn-binding protein*	5.47	1.14
SYNW2496	Type II alternative RNA polymerase s-70 family	3.16	0.55
SYNW2518	hypothetical	3.13	0.34
SYNW2521	conserved hypothetical protein	3.29	0.23

Down regulated by Ni deprivation for growth on urea

Locus Number	Description	**Sam Score**	**Fold Change**
SYNW0004	*Glutamine amidotransferaseclass-II:Phosphoribosyl transferase*	-3.29	-0.17
SYNW0005	putative DNA topoisomerase chain A	-3.81	-0.18
SYNW0011	signal recognition particle docking protein FtsY	-4.17	-0.32
SYNW0024	DnaJ protein	-3.09	-1.41
SYNW0034	biotin carboxyl carrier protein of acetyl-CoA carboxylase	-3.02	-0.20
SYNW0056	conserved hypothetical protein	-3.96	-0.21
SYNW0066	aspartate-semialdehyde dehydrogenase	-3.46	-0.28
SYNW0074	putative Precorrin-8X methylmutase CobH	-4.61	-0.37
SYNW0087	conserved hypothetical protein	-3.28	-0.16
SYNW0096	conserved hypothetical	-5.76	-0.40
SYNW0110	hypothetical	-5.59	-0.38
SYNW0127	lysyl-tRNA synthetase	-4.42	-0.21

SYNW0141	transketolase	-3.10	-0.39
SYNW0142	3-oxoacyl-[acyl-carrier-protein] synthaseII	-3.46	-0.45
SYNW0159	conserved hypothetical protein	-3.22	-0.12
SYNW0166	Isocitrate dehydrogenase	-5.80	-0.33
SYNW0172	conserved hypothetical protein	-3.54	-0.58
SYNW0190	conserved hypothetical protein	-4.24	-0.19
SYNW0199	UDP-glucose dehydrogenase	-4.48	-0.27
SYNW0229	putative glycine betaine transporter BCCTfamily	-3.22	-0.21
SYNW0250	conserved hypothetical protein	-3.03	-0.32
SYNW0262	3-isopropylmalate dehydratase large chain	-6.36	-0.31
SYNW0265	conserved hypothetical protein	-3.92	-1.08
SYNW0270	conserved hypothetical protein	-4.21	-0.52
SYNW0272	conserved hypothetical protein	-5.00	-0.55
SYNW0275	ntcA-Global nitrogen regulatory protein	-3.72	-0.26
SYNW0288	conserved hypothetical protein	-5.24	-0.28
SYNW0319	ABC transporter membrane component	-3.48	-0.27
SYNW0325	conserved hypothetical protein	-4.63	-0.52
SYNW0330	possible high light inducible protein	-3.41	-0.49
SYNW0335	YGGT family	-3.29	-0.59
SYNW0355	hypothetical	-3.65	-0.24
SYNW0372	conserved hypothetical protein	-3.04	-0.23
SYNW0397	conserved hypothetical protein	-3.14	-0.13
SYNW0487	conserved hypothetical protein	-3.18	-0.16
SYNW0490	ATP synthase subunit c	-3.40	-1.04
SYNW0491	putative ATP synthase subunit B'	-3.62	-0.85
SYNW0492	putative ATP synthase B chain	-3.67	-0.88
SYNW0493	putative ATP synthase d chain	-5.56	-0.63
SYNW0494	ATP synthase subunit alpha	-9.16	-1.30
SYNW0495	ATP synthase subunit g	-5.09	-1.09
SYNW0498	conserved hypothetical protein	-5.83	-0.49
SYNW0500	conserved hypothetical protein	-4.99	-0.58
SYNW0512	ATP synthase beta subunit	-3.44	-1.08
SYNW0514	GroEL chaperonin	-5.50	-2.11
SYNW0526	conserved hypothetical protein	-2.98	-0.15
SYNW0545	conserved hypothetical	-4.41	-0.22
SYNW0556	UDP-3-0-acyl N-acetylglucosaminedeacetylase	-6.82	-0.63
SYNW0567	conserved hypothetical protein	-3.27	-0.26
SYNW0589	hypothetical	-3.65	-0.37
SYNW0614	RNA polymerase g subunit	-4.34	-0.37
SYNW0617	conserved hypothetical protein	-3.50	-0.28
SYNW0625	conserved hypothetical protein	-3.84	-0.22
SYNW0649	glucose-1-phosphate thymidylyltransferase	-4.14	-0.16
SYNW0653	PRECORRIN-2 C20-METHYLTRANSFERASE	-5.23	-0.55
SYNW0670	conserved hypothetical protein	-4.08	-1.42
SYNW0671	dihydrolipoamide acetyltransferase component (E2)	-5.51	-0.43
SYNW0673	O-acetylserine (thiol)-lyase A	-3.04	-0.30

SYNW0676	photosystem II chlorophyll-binding protein CP43	-2.98	-0.54
SYNW0683	chaperon-like protein for quinone binding in photosystem II	-4.19	-0.51
SYNW0684	similar to methyltransferase	-4.00	-0.14
SYNW0694	nicotinamide nucleotide transhydrogenase b subunit	-3.25	-0.34
SYNW0714	conserved hypothetical protein	-5.52	-0.72
SYNW0716	ChlI-Protoporphyrin IX Magnesium-chelatase	-3.73	-0.51
SYNW0724	Thioredoxin	-4.07	-0.46
SYNW0735	conserved hypothetical protein	-4.11	-0.28
SYNW0747	possible acylphosphatase	-4.25	-0.65
SYNW0757	hypothetical	-3.80	-0.52
SYNW0760	conserved hypothetical protein	-3.48	-0.20
SYNW0820	chlH-Protoporphyrin IX magnesium chelatase	-4.16	-0.40
SYNW0836	conserved hypothetical protein	-3.15	-0.16
SYNW0859	cell death suppressor protein Lls1 homolog	-3.13	-0.15
SYNW0869	hypothetical	-3.35	-0.44
SYNW0873	*hypothetical*	-4.84	-0.52
SYNW0899	probable glucose inhibited division protein	-5.78	-0.28
SYNW0904	two-component response regulator	-3.95	-0.41
SYNW0915	putative protein-tyrosine-phosphatase	-3.83	-0.36
SYNW0926	similar to membrane bound transcriptionalregulator	-5.04	-0.36
SYNW0927	*putative photosystem II oxygen-evolving complex 23K protein PsbP*	-9.08	-0.47
SYNW0930	conserved hypothetical protein	-5.19	-0.48
SYNW0933	biotin synthase	-5.13	-0.20
SYNW0936	diaminopimelate decarboxylase	-4.92	-0.73
SYNW0937	putative ribosomal-protein-alanine acetyltransferase	-5.70	-0.39
SYNW0938	*endopeptidase Clp ATP-binding chain C*	-5.27	-0.88
SYNW0939	putative glycerol dehydrogenase	-3.99	-0.68
SYNW0980	conserved hypothetical	-3.13	-0.44
SYNW0999	conserved hypothetical protein	-3.06	-0.17
SYNW1008	Possible nitrilase	-4.02	-0.18
SYNW1023	ABC transporter multidrug efflux family	-4.07	-0.27
SYNW1025	putative Anthranilate synthase component II	-3.33	-0.17
SYNW1026	carbamoyl-phosphate synthase small chain	-3.42	-0.22
SYNW1030	conserved hypothetical protein	-3.17	-0.38
SYNW1054	conserved hypothetical protein	-3.68	-0.34
SYNW1057	preprotein translocase subunit	-11.49	-0.30
SYNW1061	*hypothetical*	-8.79	-0.80
SYNW1072	Generic methyl-transferase	-4.09	-0.25
SYNW1073	Glutamine synthetase glutamate--ammonialigase	-11.08	-1.53
SYNW1075	serine:pyruvate/alanine:glyoxylateaminotransferase	-8.18	-0.61
SYNW1076	cytidine/deoxycytidylate deaminase familyprotein	-3.36	-0.51
SYNW1096	putative Glycyl-tRNA synthetase b subunit	-3.47	-0.18
SYNW1117	Possible glutamyl-tRNA reductase	-5.30	-0.44

SYNW1123	dihydroxyacid dehydratase	-6.65	-0.35
SYNW1152	conserved hypothetical protein	-3.35	-0.18
SYNW1153	possible 33kD chaperonin heat shockprotein HSP33	-3.27	-0.18
SYNW1196	possible modulator of DNA gyrase	-3.43	-0.37
SYNW1197	putative modulator of DNA gyrase; TldD	-6.69	-0.56
SYNW1225	30S ribosomal protein S18	-5.83	-0.48
SYNW1237	conserved hypothetical protein	-3.51	-0.20
SYNW1238	putative methionine synthase	-4.84	-0.32
SYNW1255	leucyl-tRNA synthetase	-3.14	-0.21
SYNW1262	N-acetyl-gamma-glutamyl-phosphate reductase	-3.87	-0.22
SYNW1276	histidyl-tRNA synthetase paralog	-3.06	-0.15
SYNW1277	*ferredoxin*	-5.28	-1.44
SYNW1278	heat shock protein HtpG	-3.88	-1.70
SYNW1291	conserved hypothetical protein	-3.14	-0.33
SYNW1298	pyruvate kinase	-4.63	-0.35
SYNW1299	possible ABC transporter	-4.29	-0.18
SYNW1300	FtsH ATP-dependent protease homolog	-5.52	-0.71
SYNW1328	conserved hypothetical protein	-3.11	-0.19
SYNW1332	hypothetical	-4.32	-0.22
SYNW1356	hypothetical	-3.43	-0.48
SYNW1471	conserved hypothetical protein	-4.06	-0.49
SYNW1474	conserved hypothetical protein	-4.66	-0.69
SYNW1475	t-RNA synthetase classIb:Tryptophanyl-tRNA synthetase	-5.29	-0.25
SYNW1478	threonyl-tRNA synthetase	-4.34	-0.25
SYNW1479	conserved hypothetical protein	-4.34	-0.59
SYNW1495	Uroporphyrinogen decarboxylase (URO-D)	-11.89	-0.80
SYNW1496	conserved hypothetical protein	-3.80	-0.24
SYNW1503	*endopeptidase Clp ATP-binding chain B*	-3.87	-1.97
SYNW1510	conserved hypothetical protein	-4.22	-1.01
SYNW1511	*conserved hypothetical*	-11.68	-1.62
SYNW1512	conserved hypothetical	-4.19	-0.64
SYNW1545	putative translation initiation inhibitor	-3.60	-0.52
SYNW1587	*cell division protein FtsH3*	-3.81	-1.10
SYNW1615	conserved hypothetical protein	-3.91	-1.17
SYNW1620	Pyruvate dehydrogenase E1 a subunit	-4.52	-0.23
SYNW1630	putative dihydrolipoamide dehydrogenase	-3.20	-0.33
SYNW1636	conserved hypothetical protein	-4.20	-0.32
SYNW1648	ATP-dependent Clp protease proteolytic subunit 4	-4.09	-0.72
SYNW1650	ketol-acid reductoisomerase	-3.73	-0.51
SYNW1676	conserved hypothetical protein	-6.01	-0.30
SYNW1677	chlorophyll synthase 33 kD subunit	-6.75	-0.65
SYNW1709	putative CO2 hydration protein ChpX	-5.22	-0.17
SYNW1710	NADH dehydrogenase I chain 4 (or M)	-4.00	-0.32
SYNW1721	conserved hypothetical protein	-3.48	-0.25

SYNW1726	Light dependent protochlorophyllideoxido-reductase	-5.85	-0.33
SYNW1734	putative GTP cyclohydrolase I	-3.29	-0.44
SYNW1738	conserved hypothetical protein	-5.09	-0.28
SYNW1746	acetolactate synthase	-5.82	-0.28
SYNW1747	Ferrochelatase	-3.53	-0.29
SYNW1769	inorganic pyrophosphatase	-3.88	-0.50
SYNW1772	possible photosystem II Psb27 protein	-4.88	-0.46
SYNW1774	Putative carbohydrate kinase pfkB family	-3.80	-0.30
SYNW1779	conserved hypothetical protein	-3.06	-0.14
SYNW1785	Porphobilinogen deaminase	-7.67	-0.37
SYNW1808	putative glycolate oxidase subunit GlcD	-3.02	-0.13
SYNW1809	glutamate-1-semialdehyde 21-aminomutase	-7.93	-0.54
SYNW1810	hypothetical	-3.01	-1.18
SYNW1819	conserved hypothetical protein	-5.74	-0.23
SYNW1832	*homologous to C-terminus of pilT2 protein*	-3.22	-0.43
SYNW1842	apocytochrome f	-3.49	-0.63
SYNW1846	putative exopolyphosphatase	-4.53	-0.21
SYNW1855	conserved hypothetical protein	-3.30	-0.62
SYNW1873	NADH dehydrogenase I chain 2 (or N)	-3.04	-0.40
SYNW1894	putative seryl-tRNA synthetase	-12.04	-0.51
SYNW1933	possible delta-aminolevulinic aciddehydratase	-4.44	-0.66
SYNW1940	hypothetical	-3.07	-0.92
SYNW1961	Formamidopyrimidine-DNA glycolase (FAPY-DNAglycolase)	-4.53	-0.51
SYNW1999	phycobilisome linker polypeptide	-3.65	-0.46
SYNW2000	*Phycobilisome linker polypeptide*	-3.71	-0.56
SYNW2006	hypothetical	-3.97	-0.36
SYNW2041	MRP protein homolog	-4.84	-0.22
SYNW2047	phosphoenolpyruvate carboxylase	-3.53	-0.21
SYNW2059	conserved hypothetical protein	-4.81	-0.43
SYNW2082	50S ribosomal protein L18	-3.60	-0.80
SYNW2127	putative hydrogenase accessory protein	-3.86	-0.53
SYNW2128	possible porin	-6.03	-1.18
SYNW2135	30S ribosomal protein S12	-3.94	-0.67
SYNW2136	30S ribosomal protein S7	-7.05	-0.78
SYNW2137	elongation factor EF-G	-6.34	-0.96
SYNW2143	conserved hypothetical protein	-4.55	-0.30
SYNW2147	putative aminotransferase	-5.16	-0.35
SYNW2190	conserved hypothetical protein	-5.80	-0.16
SYNW2255	putative RNA-binding protein (RRM domain)	-6.61	-0.27
SYNW2266	Putative sugar-phosphate nucleotidyltransferase	-4.98	-0.39
SYNW2280	Tryptophan synthase b chain	-3.87	-0.18
SYNW2288	probable pseudouridine synthase	-4.51	-1.23
SYNW2289	*two-component response regulator*	-4.86	-1.13
SYNW2300	hypothetical	-4.20	-0.31

SYNW2311	peptide chain release factor RF-2	-3.06	-0.34
SYNW2374	Glycine cleavage system P-protein	-4.93	-0.39
SYNW2378	50S ribosomal protein L9	-3.70	-0.27
SYNW2396	valyl-tRNA synthetase	-3.69	-0.25
SYNW2406	hypothetical	-6.96	-0.32
SYNW2417	conserved hypothetical protein	-3.00	-0.23
SYNW2426	Aspartyl-tRNA synthetase:GAD domain	-7.68	-0.21
SYNW2429	possible organic radical activating enzyme	-5.55	-0.33
SYNW2438	Putative ATP-binding subunit of urea ABCtransport system	-3.68	-0.33
SYNW2439	*Putative ATP-binding subunit of urea ABCtransport system*	-5.04	-0.47
SYNW2440	*Putative membrane protein of ABC transportsystem*	-3.62	-0.69
SYNW2441	*putative urea ABC transporter*	-3.05	-0.59
SYNW2487	putative cyanate ABC transporter	-5.26	-1.02
SYNW2500	aconitate hydratase B	-4.14	-0.19
SYNW2513	Argininosuccinate synthase	-7.12	-0.61
SYNW2519	GAR transformylase 2	-3.45	-0.19
SYNW2522	excinuclease ABC subunit A	-3.47	-0.23
SYNW2526	threonine synthase	-3.67	-0.22

REFERENCES

1. **Ahn, B.-E., J. Cha, E.-J. Lee, A.-R. Han, C. J. Thompson, and J.-H. Roe.** 2006. Nur, a nickel-responsive regulator of the Fur family regulates superoxide dismutases and nickel tranport in *Streptomyces coelicolor*. Molecular Microbiology **59:**1848-1858.

2. **Allen, A. E., A. Vardi, and C. Bowler.** 2006. An ecological and evolutionary context for integrated nitrogen metabolism and related signaling pathways in marine diatoms. Current Opinion in Plant Biology **9:**264-273.

3. **Altschul, S. F., W. Gish, W. Miller, E. W. Myers, and D. J. Lipman.** 1990. Basic local alignment search tool. Journal of Molecular Biology **215:**403-410.

4. **Aluru, M. R., and S. R. Rodermel.** 2004. Control of chloroplast redox by the IMMUTANS terminal oxidase. Physiologia Plantarum **120:**4-11.

5. **Anbar, A. D., and A. H. Knoll.** 2002. Proterozoic ocean chemistry and evolution: A bioinorganic bridge? Science **297:**1137-1142.

6. **Apic, G., J. Gough, and S. A. Teichmann.** 2001. Domain combinations in archaeal, eubacterial and eukaryotic proteomes. Journal of Molecular Biology **310:**311.

7. **Armstrong, R. A.** 1999. An optimization-based model of iron-light-ammonium colimitation of nitrate uptake and phytoplankton growth. Limnology and Oceanography **44:**1436-1446.

8. **Arnold, G. L., A. D. Anbar, J. Barling, and T. W. Lyons.** 2004. Molybdenum isotope evidence for widespread anoxia in mid-proterozoic oceans. Science **304:**87-90.

9. **Asada, K.** 2000. The water-water cycle as alternative photon and electron sinkgs. Philosophical Transactions: Biological Sciences **355:**1419-1431.

10. **Bakshi, C. S., M. Malik, K. Regan, J. A. Melendez, D. W. Metzger, V. M. Pavlov, and T. J. Sellati.** 2004. Superoxide dismutase B gene (sodB)-deficient mutants of *Francisella tularensis* demostrate hypersensitivity to oxidative stress and attenuated virulence. Journal of Bacteriology **188:**6443-6448.

11. **Barber, M. J., and C. J. Kay.** 1996. Superoxide production during reduction of molecular oxygen by assimilatory nitrate reductase. Archives of biochemistry and biophysics **326:**227-232.

12. **Barondeau, D. P., C. J. Kassman, C. K. Bruns, J. A. Tainer, and E. D. Getzoff.** 2004. Nickel superoxide dismutase structure and mechanism. Biochemistry **43:**8038-8047.

13. **Baumgartner, T. R., V. Ferreira-Bartrina, and P. Moreno-Hentz.** 1991. Varve formation in the central Gulf of California: A reconsideration of the origin of the dark laminae from the 20th century varve record., p. 617-635. *In* J. P. Dauphin and B. Simoneit (ed.), The gulf and penisular province of the Californias, vol. 47. American Association of Petroleum Geologists Memoir.

14. **Bekker, A., H. D. Holland, P. L. Wang, D. Rumble, H. J. Stein, J. L. Hannah, L. L. Coetzee, and N. J. Beukes.** 2004. Dating the rise of atmospheric oxygen. Nature **427:**117-120.

15. **Berman, H. M., J. Westbrook, Z. Feng, G. Gilliland, T. N. Bhat, H. Weissig, I. N. Shindyalov, and P. E. Bourne.** 2000. The Protein Data Bank. Nucleic Acids Research **28:**235-242.

16. **Bertilsson, S., O. Berglund, D. M. Karl, and S. W. Chisholm.** 2003. Elemental composition of marine *Prochlorococcus* and *Synechococcus*: Implications for the ecological stoichiometry of the sea. Limnology and oceanography **48:**1721-1731.

17. **Bowie, A. R., E. P. Achterberg, P. L. Croot, H. J. W. de Baar, P. Laan, J. W. Moffett, S. Ussher, and P. J. Worsfold.** 2006. A community-wide intercomparison exercise for the determination of dissolved iron in seawater. Marine Chemistry **98:**81-99.

18. **Bowie, A. R., D. J. Whitworth, E. P. Achterberg, R. F. C. Mantoura, and P. J. Worsfeld.** 2002. Biogeochemistry of Fe and other trace elements (Al, Co, Ni) in the upper Atlantic Ocean. Deep-Sea Research I **49:**605-636.

19. **Boyle, E. A., S. S. Huested, and S. P. Jones.** 1981. On the distribution of Cu, Ni, and Cd in the surface waters of the North Atlantic and North Pacific Ocean. Journal of Geophysical Research **86:**8048-8066.

20. **Brahamsha, B.** 1996. An abundant cell-surface polypeptide is required for swimming by the non-flagellated marine cyanobacterium *Synechococcus*. Proceedings of the National Academy of Sciences **93:**6504-6509.

21. **Brahamsha, B.** 1996. A genetic manipulation system for oceanic cyanobacteria of the genus *Synechococcus*. Appl. Environ. Microbiol. **62:**1747-1751.

22. **Brand, L. E.** 1991. Minimum iron requirements of marine phytoplankton and the implications for the biogeochemical control of new production. Limnology and oceanography **36:**1756-1771.

23. **Brocks, J. J., G. A. Logan, R. Buick, and R. E. Summons.** 1999. Archean molecular fossils and the early rise of Eukaryotes. Science **285:**1033-1036.

24. **Bronk, D. A., P. M. Glibert, and B. B. Ward.** 1994. Nitrogen uptake, dissolved organic nitrogen release and new production. Science **265:**1843-1846.

25. **Brown, J. R., and W. F. Doolittle.** 1997. *Archaea* and the Prokaryote-to-Eukaryote transition. Microbiology and Molecular Biology Reviews **61:**456-502.

26. **Bruland, K. W.** 1980. Oceanographic distributions of cadmium, zinc, nickel, and copper in the North Pacific. Earth and Planetary Science Letters **47:**176-198.

27. **Bruland, K. W., and R. P. Franks.** 1983. Mn, Ni, Cu, Zn and Cd in the Western North Atlantic, p. 395-414. *In* C. S. Wong, E. A. Boyle, K. W. Bruland, J. D. Burton, and E. D. Goldberg (ed.), Trace Metals in Seawater. Plenum Press, New York.

28. **Bruland, K. W., E. L. Rue, G. J. Smith, and G. R. DiTullio.** 2005. Iron, macronutrients and diatom blooms in the Peru upwelling regime: brown and blue waters of Peru. Marine Chemistry **93:**81-103.

29. **Brzezinski, M. A., D. R. Phillips, F. P. Chavez, G. E. Friederich, and R. C. Dugdale.** 1997. Silica production in the Monterey, California, upwelling system. Limnology and oceanography **42:**1694-1705.

30. **Buck, K. N., M. C. Lohan, C. J. M. Berger, and K. W. Bruland.** 2007. Dissolved iron speciation in two distinct river plumes and an estuary: Implications for riverine iron supply. Limnology and Oceanography **52:**843-855.

31. **Button, D. K.** 1998. Nutrient uptake by microorganisms according to kinetic parameters from theory as related to cryoarchitecture. Microbiology and Molecular Biology Reviews **62:**636-645.

32. **Caetano-Anolles, G., H. S. Kim, and J. E. Mittenthal.** 2007. The origin of modern metabolic networks inferred from phylogenomic analysis of protein architecture. Proceedings of the National Academy of Sciences **104:**9358-9363.

33. **Canfield, D. E.** 1998. A new model for Proterozoic ocean chemistry. Nature **396:**450-453.

34. **Canfield, D. E., and A. Teske.** 1996. Late Proterozoic rise in atmospheric oxygen concentrations inferred from phylogenetic and sulphur-isotope studies. Nature **382:**127-132.

35. **Cendrowski, S., W. MacArthur, and P. Hanna.** 2004. *Bacillus anthracis* requires siderophore biosynthesis for growth in macrophages and mouse virulence. Molecular Microbiology **51:**407-417.

36. **Chandonia, J., and S. E. Brenner.** 2006. The impact of structural genomics: Expectations and outcomes. Science **311:**347-351.

37. **Chen, X., Z. Su, P. Dam, B. Palenik, Y. Xu, and T. Jiang.** 2004. Operon prediction by comparative genomics: an application to the *Synechococcus* sp. WH8102 genome. Nucleic Acids Research **32:**2147-2157.

38. **Chothia, C.** 1992. Proteins-1000 families for the molecular biologist. Nature **357:**543-544.

39. **Choudhury, S. B., J.-W. Lee, G. Davidson, Y. Yim, K. Bose, M. L. Sharma, S. Kang, D. E. Cabelli, and M. J. Maroney.** 1999. Examination of the nickel site structure and reaction mechanism in Streptomyces seoulensis *superoxide dismutase*. Biochemistry **38:**3744-3752.

40. **Collier, J. L., B. Brahamsha, and B. Palenik.** 1999. The marine cyanobacterium *Synechococcus* sp WH 7805 requires urease (urea amidohydrolase, EC 3.5.1.5) to utilize urea as a nitrogen source: molecular-genetic and biochemical analysis of the enzyme. Microbiology **145:**447-459.

41. **Collier, J. L., and A. R. Grossman.** 1994. A small polypeptide triggers complete degradation of light-harvesting phycobiliproteins in nutrient-deprived cyanobacteria. EMBO Journal **13:**1039-1047.

42. **Collier, J. L., and B. Palenik.** 2003. Phycoerythrin-containing picoplankton in the Southern California Bight. Deep-Sea Research II **50:**2405-2422.

43. **Crawford, D. W., M. S. Lipsen, D. A. Purdie, M. C. Lohan, P. J. Statham, F. A. Whitney, J. N. Putland, W. K. Johnson, N. Sutherland, T. D. Peterson, P. J. Harrison, and C. S. Wong.** 2003. Influence of zinc and iron enrichments on phytoplankton growth in the northeastern subartic Pacific. Limnology & Oceanography **48:**1583-1600.

44. **Culotta, V. C., M. Yang, and T. V. O'Halloran.** 2006. Activation of superoxide dismutases: Putting the metal to the pedal. Biochimica y Biophysica Acta **1763:**747-758.

45. **Daday, A., A. H. Mackerras, and G. D. Smith.** 1985. The effect of nickel on hydrogen metabolism and nitrogen fixatino in the cyanobacterium *Anabaena cylindrica*. Journal of general microbiology **131:**231-238.

46. **de Baar, H. J. W., P. W. Boyd, K. H. Coale, M. R. Landry, A. Tsuda, P. Assmy, D. C. E. Bakker, Y. Bozec, R. T. Barber, M. A. Brzezinski, K. O. Buesseler, M. Boye, P. L. Croot, F. Gervais, M. Y. Gorbunov, P. J. Harrison, W. T. Hiscock, P. Laan, C. Lancelot, C. S. Law, M. Lavasseur, A. Marchetti, F. J. Millero, J. Nishioka, N. Yukihiro, V. O. T., U. Riebesell, M. J. A. Rijkenberg, H. Saito, S. Takeda, K. R. Timmermans, M. J. W. Veldhuis, A. M. Waite, and C.-S. Wong.** 2005. Synthesis of iron fertilization experiments: From the iron age to the age of enlightenment. Journal of Geophysical Research **110:**1-24.

47. **DeLong, E. F., C. M. Preston, T. Mincer, V. Rich, S. J. Hallam, N. Frigaard, A. Martinex, M. B. Sullivan, R. Edwards, B. R. Brito, S. W. Chisholm, and D. M. Karl.** 2006. Community genomics among stratified microbial assemblages in the ocean's interior. Science **311:**496-503.

48. **Dixon, J. L., P. J. Statham, C. E. Widdicombe, R. M. Jones, S. Barquero-Molina, B. Dickie, M. Nimmo, and C. M. Turley.** 2006. Cadmium uptake by marine micro-organisms in the English Channel and Celtic Seas. Aquatic microbial ecology **44:**31-43.

49. **Donat, J., K. Lao, and K. Bruland.** 1994. Speciation of dissolved copper and nickel in South San Francisco Bay: a multi-method approach. Analytica Chimica Acta **284:**547-571.

50. **Donat, J. R., and K. W. Bruland.** 1988. Direct determination of dissolved cobalt and nickel in seawater by differential pulse cathodic stripping voltammetry preceded by adsorptive collection of cyclohexane-1, 2-dione dioxime complexes. Analytical chemistry **60:**240-244.

51. **Dosanjh, N. S., and S. L. J. Michel.** 2006. Microbial nickel metalloregulation: NikRs for nickel ions. Current opinion in chemical biology **10:**123-130.

52. **Douzery, E. J. P., E. A. Snell, E. Bapteste, F. Delsuc, and H. Philippe.** 2004. The timing of eukaryotic evolution: Does a relaxed molecular clock reconcile proteins and fossils? PNAS **101:**15386-15391.

53. **Dupont, C. L., K. Barbeau, and B. Palenik.** 2008. Ni uptake and limitation in marine *Synechococcus* strains. Applied and environmental microbiology **74:**23-31.

54. **Dupont, C. L., K. P. Neupane, J. Shearer, and B. Palenik.** In press. Diversity, function, and evolution of genes coding for putative Ni-containing superoxide dismutases. Environmental Microbiology.

55. **Dupont, C. L., S. Yang, B. Palenik, and P. E. Bourne.** 2006. Modern proteomes contain putative imprints of ancient shifts in trace metal geochemistry. Proceedings of the National Academy of Sciences **103:**17822-17827.

56. **Dyhrman, S. T., and D. M. Anderson.** 2003. Urease activity in cultures and field populations of the toxic dinoflagellate *Alexandrium*. Limnology & Oceanography **48:**647-655.

57. **Eisler, R.** 1998. Nickel hazards to fish, wildlife, and invertebrates: A synoptic review. Biological sciences report 34. USGS.

58. **Eitinger, T.** 2004. In vivo production of active nickel superoxide dismutase from *Prochlorococcus marinus* MIT9313 is dependent on its cognate peptidase. Journal of Bacteriology **186:**7821-7825.

59. **Eitinger, T., J. Suhr, J. Moore, and J. A. C. Smith.** 2005. Secondary transporters for nickel and cobalt ions: themes and variations. BioMetals **18:**399-405.

60. **Ellman, G. L.** 1959. Tissue sulfhydryl groups. Archives of Biochemistry and Biophysics **82:**70-77.

61. **Eppley, R. W., A. F. Carlucci, O. Holm-Hansen, D. Kiefer, J. J. McCarthy, E. Venrick, and P. M. Williams.** 1971. Phytoplankton growth and composition in shipboard cultures supplied with nitrate, ammonium, or urea as the nitrogen source. Limnology and oceanography **16:**741-751.

62. **Ernst, F. D., E. J. Kuipers, A. Heijens, R. Sarwari, J. Stoof, C. W. Penn, J. G. Justers, and A. H. van Vliet.** 2005. The nickel-responsive regulator NikR controls activation and repression of gene transcription in *Helicobacter pylori*. Infection and Immunology **73:**7252-7258.

63. **Farquhar, J., H. Bao, and M. Thiemens.** 2000. Atmospheric Influence of Earth's Earliest Sulfur Cycle. Science **289:**756-758.

64. **Felsenstein, J.** 1989. PHYLIP - Phylogeny Inference Package (Version 3.2). Claudistics**:**164-166.

65. **Fielder, A. T., P. A. Bryngelson, M. J. Maroney, and T. C. Brunold.** 2005. Spectroscopic and computational studies of Ni superoxide dismutase: Electronic structure contributions to enzymatic function. Journal of the American Chemical Society **127:**5449-5462.

66. **Finkel, Z. V., A. Quigg, J. A. Raven, J. R. Reinfelder, O. E. Schofield, and P. G. Falkowski.** 2006. Irradiance and the elemental stoichiometry of marine phytoplankton. Limnology & Oceanography **51:**2690-2701.

67. **Flohe, L., and F. Otting.** 1984. Superoxide dismutase assays. Methods in Enzymology **105:**93-104.

68. **Flores, E., and A. Herrero.** 2005. Nitrogen assimilation and nitrogen control in cyanobacteria. Biochemical Society Transactions **33:**164-167.

69. **Fridovich, I.** 1997. Superoxide anion radical ($O_2^{\cdot-}$), superoxide dismutases, and related matters. The Journal of Biological Chemistry **272:**18515-18517.

70. **Giovannoni, S. J., L. Bibbs, J.-C. Cho, M. D. Stapels, R. Desiderio, K. L. Vergin, M. S. Rappe, S. Laney, L. J. Wilhelm, H. J. Tripp, E. J. Mathur, and D. F. Barofsky.** 2005. Proteorhodopsin in the ubiquitous marine bacterium SAR11. Nature **483:**82-85.

71. **Goericke, R., and J. P. Montoya.** 1998. Estimating the contribution of microalgal taxa to chlorophyll *a* in the field-variations of pigment ratios under nutrient- and light-limited growth. Marine Ecology Progress Series **169:**97-112.

72. **Gomez-Consarnau, L., J. M. Gonzalez, M. Coll-llado, P. Gourdon, T. Pascher, R. Neutze, C. Pedros-Alio, and J. Pinhassi.** 2007. Light stimulates the growth of proteorhodopsin-containing marine Flavobacteria. Nature **445:**210-213.

73. **Gough, J.** 2006. Genomic scale sub-family assignment of protein domains. Nucleic Acids Research **34:**3625-3633.

74. **Gough, J., K. Karplus, R. Hughey, and C. Chothia.** 2001. Assignment of homology to genome sequences using a library of hidden markov models that represent all proteins of known structure. Journal of Molecular Biology **313:**903-919.

75. **Hallam, S. J., T. Mincer, C. Schleper, C. M. Preston, K. Roberts, P. M. Richardson, and E. F. DeLong.** 2006. Pathways of carbon assimilation and ammonia oxidation suggested by environmental genomic analyses of marine *Crenarchaeota*. PloS Biology **4:**e95.

76. **Hausinger, R. P.** 2004. Metabolic versatility of prokaryotes for urea decomposition. Journal of Bacteriology **186:**2520-2522.

77. **Healey, F. P.** 1980. Slope of the Monod equation as an indicator of advantage in nutrient competition. Microbial Ecology **5:**281-286.

78. **Heil, C. A., M. Revilla, P. M. Glibert, and S. Murasko.** 2007. Nutrient quality drives differential phytoplankton community composition on the southwest Florida shelf. Limnology and Oceanography **52:**1067-1078.

79. **Henley, W. J., and Y. Yin.** 1998. Growth and photosynthesis of marine *Synechococcus* (Cyanophyceae) under iron stress. Journal of phycology **34:**94-103.

80. **Hihara, Y., K. Sonoike, M. Kanehisa, and M. Ikeuchi.** 2003. DNA microarray analysis of redox-responsive genes in the genome of the cyanobacterium *Synechocystis* sp. strain PCC 6803. Journal of Bacteriology **185:**1729-1725.

81. **Hoffmann, D., K. Gutekunst, M. Klissenbauer, R. Schulz-Freidrich, and J. Appel.** 2006. Mutagenesis of hydrogenase accessory genes of *Synechocystis* sp. PCC6803. FEBS Journal **273:**4516-4527.

82. **Holland, H. D.** 1984. The chemical evolution of the atmosphere and oceans. Princeton University Press, Princeton.

83. **Holm, L., and C. Sander.** 1997. An evolutionary treasure: Unification of a broad set of amidohydrolases related to urease. Proteins: Structure Function, and Genetics **28:**72-82.

84. **Huang, L., M. P. McCluskey, H. Ni, and R. A. LaRossa.** 2002. Global gene expression profiles of the cyanobacterium *Synechocystis* sp. Strain PCC 6803 in response to irradiation with UV-B and white light. Journal of Bacteriology **184:**6845-6858.

85. **Hudson, R. J. M., and F. M. M. Morel.** 1990. Iron transport in marine phytoplankton: Kinetics of cellular and medium coordination reactions. Limnology & Oceanography **35:**1002-1020.

86. **Hudson, R. J. M., and F. M. M. Morel.** 1993. Trace metal transport by marine microorganisms: Implications of metal coordination kinetics. Deep-Sea Research **40:**129-150.

87. **Huerta-Diaz, M. A., F. Leon-Chavira, M. L. Lares, A. Chee-Barragan, and A. Siqueiros-Valencia.** 2007. Iron, manganes and trace metal concentrations in seaweeds from the central west coast of the Gulf of California. Applied Geochemistry **22:**1380-1392.

88. **Javaux, E. J., A. H. Knoll, and M. R. Walter.** 2001. Morphological and ecological complexity in early eukaryotic ecosystems. Nature **412:**66-69.

89. **Kabayashi, M., T. Ishizuka, M. Katayama, M. Kanehisa, M. Bhattacharyya-Pakrasi, H. B. Pakrasi, and M. Ikeuchi.** 2004. Response to oxidative stress involves a novel peroxiredoxin gene in the unicellular cyanobacterium *Synechocystis sp.* PCC6803. Plant and Cell Physiology **45:**290-299.

90. **Kana, T. M.** 1993. Rapid oxygen cycling in *Trichodesmium thiebautii*. Limnology and Oceanography **38:**18-24.

91. **Kana, T. M.** 1992. Relationship between photosynthetic oxygen cycling and carbon assimilation in *Synechococcus* WH7803. Journal of Phycology **28:**304-308.

92. **Kelley, L. A., R. M. MacCullum, and M. J. Sternberg.** 2000. Enhanced genome annotation using structural profiles in the program 3D-PSSM. Journal of molecular biology **299:**499-520.

93. **Kim, E.-J., H.-J. Chung, B. Suh, Y. Chil Hah, and J.-H. Roe.** 1998. Transcriptional and post-translational regulation by nickel of *sodN* gene encoding nickel-containing superoxided dismutase from *Streptomyces coelicolor* Muller. Molecular Microbiology **27:**187-195.

94. **Kim, E.-J., H.-P. Kim, Y. C. Hah, and J.-H. Roe.** 1996. Differential expression of superoxide dismutases containing Ni and Fe/Zn in *Streptomyces coelicolor*. European Journal of Biochemistry **241:**178-185.

95. **Kirschvink, J. L., E. J. Gaidos, L. E. Bertani, N. J. Beukes, J. Gutzmer, L. N. Maepa, and R. E. Steinberger.** 2000. Paleoproterozoic snowball earth: extreme climatic and geochemical global change and its biological consequences. PNAS **97:**1400-1405.

96. **Klotz, M. G., D. J. Arp, P. S. G. Chain, A. F. El-Sheikh, L. J. Hauser, N. G. Hommes, F. W. Larimer, S. A. Malfatti, J. M. Norton, A. T. Poret-Peterson, L. M. Vergez, and B. B. Ward.** 2007. Complete genome sequence of the marine, chemolithoautotrophic, ammonia-oxidizing Bacterium *Nitrosococcus oceani* ATCC19707. Applied and environmental microbiology **72:**6299-6315.

97. **Knoll, A. H., E. J. Javaux, D. Hewitt, and P. Cohen.** 2006. Eukaryotic organisms in Proterozoic oceans. Philosophical Transactions of the Royal Society **361:**1023-1038.

98. **Konstantinidis, K. T., and J. M. Tiedje.** 2004. Trends between gene content and genomic size in prokaryotic species with larger genomes. Proceedings of the National Academy of Sciences **101:**3160-3165.

99. **Koonin, E. V., Y. I. Wolf, and G. P. Karev.** 2002. The structure of the protein universe and genome evolution. Nature **420:**218-223.

100. **Kopp, R. E., J. L. Kisrchvink, I. A. Hilburn, and C. Z. Nash.** 2005. The Paleoproterozoic snowball Earth: A climate disaster triggered by the evolution of oxygenic photosynthesis. Proc. Natl. Acad. Sci. USA **102:**11131-11136.

101. **Kruger, H.-J., G. Peng, and R. H. Holm.** 1991. Low-potential Nickel (III, II) complexes: New systems based on tetradentate amidate-thiolated ligands and the influence of ligand structure on potentials in relation to the nickel site in [NiFe]-hydrogenase. Inorganic Chemistry **30:**734-742.

102. **Landau, M., I. Mayrose, Y. Rosenberg, F. Glaser, E. Martz, T. Pupko, and N. Ben-Tal.** 2005. ConSurf 2005: the projection of evolutionary conservation scores of residues on protein structures. Nucleic Acids Research **33:**299-302.

103. **Leclere, V., P. Boiron, and R. Blondeau.** 1999. Diversity of superoxide-dismutases among clinical and soil isolates of *Streptomyces*. Current Microbiology **39:**365-368.

104. **Lee, J.-W., and J. D. Helmann.** 2007. Functional specialization within the Fur family of metalloregulators. BioMetals **20:**485-499.

105. **Lippard, S. J., and J. M. Berg.** 1994. Principles of bioinorganic chemistry. University Science Books, Mill Valley.

106. **Loscher, B. M.** 1999. Relationships among Ni, Cu, Zn, and major nutrients in the Southern Ocean. Marine Chemistry **67:**67-102.

107. **Ma, W., Y. Deng, and H. Mi.** 2008. Redox of plastoquinone pool regulates the expression and activity of NADPH dehydrogenase supercomplex in *Synechocystis* sp. strain 6803. Current Microbiology **56:**189-193.

108. **Mackey, D. J., J. E. O'Sullivan, R. J. Watson, and G. Dal Pont.** 2002. Trace metals in the Western Pacific: temporal and spatial variability in the concentrations of Cd, Cu, Mn, and Ni. Deep Sea Research I **49:**2241-2259.

109. **Mackey, D. J., J. E. O'Sullivan, R. J. Watson, and G. DalPont.** 2002. Trace metals in the western Pacific: temporal and spatial variability in the concentrations of Cd, Cu, Mn, and Ni. Deep-Sea Research I **49:**2241-2259.

110. **Maldonado, M. T., P. W. BOYD, J. LaRoche, R. Strzepek, A. Waite, A. R. Bowie, P. L. Croot, R. D. Frew, and N. M. Price.** 2001. Iron uptake and physiological response of phytoplankton during a mesoscale Southern Ocean iron enrichment. Limnology and oceanography **46:**1802-1808.

111. **Maldonado, M. T., and N. M. Price.** 2001. Reduction and transport of organically bound iron by *Thalassiosira oceanica* (Bacillariophyceae). Journal of Phycology **37:**298-309.

112. **Maldonado, M. T., R. F. Strzepek, S. Sander, and P. W. Boyd.** 2005. Acquisition of iron bound to strong organic complexes, with different Fe binding groups and photochemical reactivities, by plankton communities in Fe-limited subantartic waters. Global biogeochemical cycles **19:**GB4S23.

113. **Mann, E. L., and S. W. Chisholm.** 2000. Iron limits the cell division rate of *Prochlorococcus* in the eastern equatorial Pacific. Limnology and oceanography **45:**1067-1076.

114. **Marchetti, A., M. T. Maldonado, E. S. Lane, and P. J. Harrison.** 2006. Iron requirements of the pennate diatom *Pseudo-nitzschia*: Comparison of oceanic (high-nitrate, low chlorophyll waters) and coastal species. Limnology and oceanography **51:**2092-2101.

115. **Martin, W., T. Rujan, E. Richly, A. Hansen, S. Cornelsen, T. Lins, D. Leister, B. Stoebe, M. Hasegawa, and D. Penny.** 2002. Evolutionary analysis of *Arabidopsis*, cyanobacterial, and chloroplast genomes reveals plastid phylogeny and thousands of cyanobacterial genes in the nucleus. Proceedings of the National Academy of Sciences **99:**12246-12251.

116. **Maxwell, D. P., Y. Wang, and L. McIntosh.** 1999. The alternative oxidase lowers mitochondrial reactive oxygen production in plant cells. Proceedings of the National Academy of Sciences **96:**8271-8276.

117. **McCarren, J., and B. Brahamsha.** 2005. Transposon mutagenesis in a marine *Synechococcus* strain: Isolation of swimming motility mutants. Journal of Bacteriology **187:**4457-4462.

118. **McCarren, J., J. Heuser, R. Roth, N. Yamada, M. Martone, and B. Brahamsha.** 2005. Inactivation of *swmA* results in the loss of an outer cell layer in a swimming *Synechococcus* strain. Journal of Bacteriology **187:**224-230.

119. **McDonald, A. E., and G. C. Vanlerberghe.** 2006. Origins, evolutionary history, and taxonomic distribution of alternative oxidase and plastoquinol terminal oxidase. Comparative biochemistry and Physiology, Part D **1:**357-364.

120. **Methe, B. A., K. E. Nelson, J. W. Deming, B. Momen, E. Melamud, X. Zhang, J. Moult, R. Madupu, W. C. Nelson, R. J. Dodson, L. M. Brinkac, S. C. Daugherty, A. S. Durkin, R. T. DeBoy, J. F. Kolonay, S. A. Sullivan, L. Zhou, T. M. Davidsen, M. Wu, A. L. Huston, M. Lewis, B. Weaver, J. F. Weidman, H. Khouri, T. R. Utterback, T. V. Feldblyum, and C. M. Fraser.** 2005. The psychrophilic lifestyle as revealed by the genome sequence of *Colwellia psychrerythraea* 34H through genomic and proteomic analyses. Proc. Natl. Acad. Sci. USA **102:**10913-10918.

121. **Miller, A. F.** 2004. Superoxide dismutases: active sites that save, but a protein that kills. Current Opinion in Chemical Biology **8:**162-168.

122. **Milligan, A. J., I. Berman-Frank, Y. Gerchman, G. C. Dismukes, and P. G. Falkowski.** 2007. Light-dependent oxygen consumption in nitrogen-fixing cyanobacteria plays a key role in nitrogenase protection. Journal of Phycology **43:**845-852.

123. **Morel, F. M. M.** 1987. Kinetics of nutrient uptake and growth in phytoplankton. Journal of phycology **23:**137-150.

124. **Morel, F. M. M., R. J. M. Hudson, and N. M. Price.** 1991. Limitation of productivity by trace metals in the sea. Limnology & Oceanography **36:**1742-1755.

125. **Morel, F. M. M., A. J. Milligan, and M. A. Saito.** 2003. Marine bioinorganic chemistry: The role of trace metals in the oceanic cycles of major nutrients. *In* H. Elderfield, H. D. Holland, and K. K. Turekian (ed.), Treatise on Geochemistry: The oceans and marine geochemistry. Elsevier.

126. **Morel, F. M. M. M., and N. M. Price.** 2003. The biogeochemical cycles of trace metals in the oceans. Science **300:**944-947.

127. **Morgan, R. O., S. Martin-Almedina, J. M. Iglesias, M. I. Gonzalez-Florez, and M. P. Fernandez.** 2004. Evolutionary perspective on annexin calcium-binding domains. Biochimica et biophysica acta **1742:**133-140.

128. **Mulrooney, S. B., and R. P. Hausinger.** 2003. Nickel uptake and utilization by microorganisms. FEMS Microbiology Reviews **27:**239-261.

129. **Murzin, A. G., S. E. Brenner, T. Hubbard, and C. Chothia.** 1995. SCOP: a structural classification of proteins database for the investigation of sequences and structures. Journal of Molecular Biology **247:**536-540.

130. **Musiani, F., B. Zambelli, M. Stola, and S. Ciurli.** 2004. Nickel trafficking: insights into the fold and function of UreE, a urease metallochaperone. Journal of Inorganic Biochemistry **in press**.

131. **Muyssen, B. T. A., K. V. Brix, D. K. DeForest, and C. R. Janssen.** 2004. Nickel essentiality and homeostasis in aquatic organisms. Environmental reviews **12:**113-131.

132. **Neupane, K. P., and J. Shearer.** 2006. The influence of amine/amide versus bisamide coordination in nickel superoxide dismutase. Inorganic Chemistry **45:**10552-10556.

133. **Nomura, C. T., S. Persson, G. Shen, K. Inoue-Sakamoto, and D. A. Bryant.** 2006. Characterization of two cytochrome oxidase operons in the marine cyanobacterium *Synechococcus* sp. PCC 7002: Inactivation of *ctaDI* affects the PSI:PSII ratio. Photosynthesis Research **87**.

134. **Nomura, C. T., T. Sakamoto, and D. A. Bryant.** 2006. Roles for heme-copper oxidases in extreme high-light and oxidative stress response in the cyanobacterium *Synechococcus* sp. PCC7002. Archives of Microbiology **185:**471-479.

135. **Oberai, A., Y. Ihm, S. Kim, and J. U. Bowie.** 2006. A limited universe of membrane protein families and folds. Protein Science **15:**1723-1734.

136. **Ogawa, T., and H. Mi.** 2007. Cyanobacterial NADPH dehydrogenase complexes. Photosynthesis Research **93:**69-77.

137. **Oliveira, L., and N. J. Antia.** 1986. Nickel ion requirements for autotrophic growth of several marine microalgae with urea serving as nitrogen source. Canadian Journal of Aquatic and Fisheries Science **43:**2427-2433.

138. **Oliveria, L., and N. J. Antia.** 1986. Nickel ion requirements for autotrophic growth of several marine microalgae with urea serving as nitrogen source. Canadian journal of Fisheries and Aquatic sciences **43:**2427-2433.

139. **Palenik, B., B. Brahamsha, F. W. Larimer, M. Land, L. Hauser, P. Chain, J. Lamerdin, W. Regala, E. A. Allen, J. McCarren, I. Paulsen, A. Dufresne, F. Partensky, E. A. Webb, and J. B. Waterbury.** 2003. The genome of a motile marine *Synechococcus*. Nature **424:**1037-1042.

140. **Palenik, B., J. Grimwood, A. Aerts, P. Rouze, A. Salamov, N. Putnam, C. Dupont, R. Jorgensen, E. Derelle, S. Rombauts, K. Zhou, R. Otillar, S. S. Merchant, S. Podell, T. Gaasterland, C. Napoli, K. Gendler, A. Manuell, V. Tai, O. Vallon, G. Piganeau, S. Jancek, M. Heijde, K. Jabbari, C. Bowler, M. Lohr, S. Robbens, G. Werner, I. Dubchak, G. J. Pazour, Q. Ren, I. Paulsen, C. Delwiche, J. Schmutz, D. Rokhsar, Y. Van de Peer, H. Moreau, and I. V. Grigoriev.** 2007. The tiny eukaryote *Ostreococcus* provides genomic insights into the paradox of plankton speciation. PNAS **104:**7705-7710.

141. **Palenik, B., and S. Henson.** 1997. The use of amides and other organic nitrogen sources by the coccolithorphorid Emiliania huxleyi. Limnology & Oceanography **42:**1544-1551.

142. **Palenik, B., Q. Ren, C. L. Dupont, G. S. Myers, J. F. Heidelberg, J. H. Badger, R. Madupu, W. C. Nelson, L. M. Brinkac, R. J. Dodson, A. S. Durkin, S. C. Daugherty, S. A. Sullivan, H. Khouri, Y. Mohamoud, R. Halpin, and I. T. Paulsen.** 2006. Genome sequence of *Synechococcus* CC9311: Insights in adaptation to the coastal environment. Proceedings of the National Academy of Sciences **103:**13555-13559.

143. **Palenik, B., Q. Ren, C. L. Dupont, G. S. Myers, J. F. Heidelberg, J. H. Badger, R. Madupu, W. C. Nelson, L. M. Brinkac, R. J. Dodson, A. S. Durkin, S. C. Daugherty, S. A. Sullivan, H. Khouri, Y. Mohamoud, R. Halpin, and I. T. Paulsen.** 2006. Genome sequence of Synechococcus CC9311: Insights into adaptation to a coastal environment. PNAS **103:**13555-13559.

144. **Partensky, F., W. R. Hess, and D. Vaulot.** 1999. *Prochlorococcus*, a marine photosynthetic prokaryote of global significance. Microbiology and Molecular Biology Reviews **63:**106-127.

145. **Peers, G. S., and N. M. Price.** 2006. Copper-containing plastocyanin used for electron transport by an oceanic diatom. Nature **441:**341-344.

146. **Peers, G. S., S.-A. Quesnel, and N. M. Price.** 2005. Copper requirements for iron acquisition and growth of coastal and oceanic diatoms. Limnology and oceanography **50:**1149-1158.

147. **Price, N. M., L. F. Anderson, and F. M. M. Morel.** 1991. Iron and nitrogen nutrition of equatorial Pacific plankton. Deep Sea Research I **38:**1361-1378.

148. **Price, N. M., G. I. Harrison, J. G. Hering, R. J. Hudson, P. M. V. Nirel, B. Palenik, and F. M. M. Morel.** 1988/1989. Preparation and chemistry of the artificial algal culture medium Aquil. Biological Oceanography **6:**443-461.

149. **Price, N. M., and F. M. M. Morel.** 1991. Colimitation of phytoplankton growth by nickel and nitrogen. Limnol. Oceanogr. **36:**1071-1077.

150. **Quintero, M. J., A. M. Muro-Pastor, A. Herrero, and E. Flores.** 2000. Arginine catabolism in the cyanobacterium *Synechocystis* sp. strain PCC6803 involves the urea cycle and arginase pathway. Journal of Bacteriology **182:**1008-1015.

151. **Raymond, J., and D. Segre.** 2006. The effect of oxygen on biochemical networks and the evolution of complex life. Science **311:**1764-1767.

152. **Revilla, M., J. Alexander, and P. M. Glibert.** 2005. Urea analysis in coastal waters: comparison of enzymatic and direct methods. Limnology and oceanography: Methods **3:**290-299.

153. **Rodionov, D. A., P. Hebbeln, M. S. Gelfand, and T. Eitinger.** 2006. Comparative and functional genomic analysis of prokaryotic nickel and cobalt uptake transporters: Evidence for a novel group of ATP-binding cassette transporters. Journal of Bacteriology **188:**317-327.

154. **Roon, R. J., and B. Levenberg.** 1968. An adenosine triphosphate-dependent, avidin-sensitive enzymatic cleavage of urea in yeast and green algae. The Journal of Biological Chemistry **243:**5213-5215.

155. **Rost, B.** 1999. Twilight zone of protein sequence alignments. Protein Engineering **12:**85-94.

156. **Rue, E. L., and K. W. Bruland.** 1995. Complexation of iron(III) by natural organic ligands in the Central North Pacific as determined by a new competitive ligand equilibration/adsorptive cathodic stripping voltammetric method. Marine Chemistry **50:**117-138.

157. **Rumeau, D., G. Peltier, and L. Cournac.** 2007. Chlororespiration and cyclic electron flow around PSI during photosynthesis and plant stress response. Plant, Cell and Environment **30:**1041-1051.

158. **Rusch, D. B., A. L. Halpern, G. Sutton, K. B. Heidelberg, S. Williamson, S. Yooseph, D. Wu, J. A. Eisen, J. M. Hoffman, K. Remington, K. Beeson, B. Tran, H. Smith, H. Baden-Tillson, C. Stewart, J. Thorpe, J. Freeman, C. Andrews-Pfannkoch, J. E. Venter, K. Li, S. Kravitz, J. F. Heidelberg, T. Utterbeck, Y. Rogers, L. I. Falcon, V. Souza, G. Bonilla-Rosso, L. E. Eguiarte, D. M. Karl, S. Sathyendranath, T. Platt, E. Bermingham, V. Gallardo, G. Tamayo-Castillo, M. R. Ferrari, R. L. Strausberg, K. Nealson, R. Friedman, M. Frazier, and J. Venter.** 2007. The *Sorcerer II* global ocean sampling expedition: Northwest Atlantic through Eastern Tropical Pacific. PloS Biology **5:**398-431.

159. **Saito, M. A., T. J. Goepfert, and J. T. Ritt.** 2008. Some thoughts on the concept of colimitation: three definitions and the importance of bioavailability. Limnology and oceanography **53:**276-290.

160. **Saito, M. A., J. W. Moffett, and G. R. DiTullio.** 2004. Cobalt and nickel in the Peru upwelling region: A major flux of labile cobalt utilized as a micronutrient. Global Biogeochem. Cycles **18:**4030-4044.

161. **Saito, M. A., G. Rocap, and J. W. Moffett.** 2005. Production of cobalt binding ligands in a *Synechococcus* feature at the Costa Rica upwelling dome. Limnology & Oceanography **50:**279-290.

162. **Saito, M. A., D. M. Sigman, and F. M. M. Morel.** 2003. The bioinorganic chemistry of the ancient ocean: the co-evolution of cyanobacterial metal requirements and biogeochemical cycles at the Archean-Proterozoic boundary? Inorganica Chemica Acta **356:**308-3-18.

163. **Scalan, D. J.** 2003. Physiological diversity and niche adaptation in marine *Synechococcus*. Advances in microbial physiology **47:**1-64.

164. **Schmidt, M. A., and D. A. Hutchins.** 1999. Size-fractionated biological iron and carbon uptake along a coastal to offshore transect in the NE Pacific. Deep Sea Research II **46:**2487-2503.

165. **Schwartz, R., and K. Forchhammer.** 2005. Acclimation of unicellular cyanobacteria to macronutrient deficiency: emergence of a complex network of cellular responses. Microbiology **151:**2503-2514.

166. **Sclater, F. R., E. A. Boyle, and J. M. Edmond.** 1976. On the marine geochemistry of nickel. Earth and Planetary Science Letters **31:**119-128.

167. **Shearer, J., and A. Dehestani.** In review. Probing variable amine/amide ligation in $Ni^{II}N_2S_2$ complexes using sulfur K-edge and nickel L-edge X-ray absorption spectroscopies: Implications for the active site of nickel superoxide dismutase. Inorganic Chemistry.

168. **Shearer, J., and L. M. Long.** 2006. A nickel superoxide dismutase maquette that reproduces the spectroscopic and functional properties of the metalloenzyme. Inorganic Chemistry **45:**1358-2360.

169. **Shearer, J., and P. Soh.** 2007. The copper (II) adduct of the unstructured region of the amyloidogenic fragment derived from the human prion protein is redox-active at physiological pH. Inorganic Chemistry **46:**710-719.

170. **Shi, W., C. Zhan, A. Ignatov, B. A. Manjasetty, N. Marinkovic, M. Sullivan, R. Huang, and M. R. Chance.** 2005. Metalloproteomics: High-throughput structural and functional annotation of proteins in structural genomics. Structure **13:**1473-1486.

171. **Singh, A. K., L. M. McIntyre, and L. A. Sherman.** 2003. Microarray analysis of the genome-wide response to iron deficiency and iron reconstitution in the cyanobacterium *Synechocystis sp.* PCC 6803. Plant Physiology **132:**1825-1839.

172. **Smith, W. L., and Y. Yamanaka.** 2007. Optimization-based model of multinutrient uptake kinetics. Limnology and Oceanography **52:**1545-1558.

173. **Spivack, A. J., S. S. Huested, and E. A. Boyle.** 1983. Copper, nickel, and cadmium in the surface waters of the Mediterranean. *In* C. S. Wong, E. A. Boyle, K. W. Bruland, J. D. Burton, and E. D. Goldberg (ed.), Trace metals in sea water. Plenum Press, New York.

174. **Strzepek, R. F., M. T. Maldonado, J. L. Higgins, J. Hall, K. Sofi, S. W. Wilheim, and P. W. Boyd.** 2005. Spinning the "ferrous wheel": The importance of the microbial community in an iron budget during the FeCycle experiment. Global biogeochemical cycles **19:**GB4S26.

175. **Su, Z., F. Mao, P. Dam, H. Wu, V. Olman, I. T. Paulsen, B. Palenik, and Y. Xu.** 2006. Computational inference and experimental validation of the nitrogen assimilation regulatory network in cyanobacterium *Synechococcus* WH8102. Nucleic Acids Research **34:**1050-1065.

176. **Sunda, W. G., and S. A. Huntsman.** 1995. Iron uptake and growth limitation in oceanic and coastal phytoplankton. Marine Chemistry **50:**189-206.

177. **Sunda, W. G., N. M. Price, and F. M. M. Morel.** 2005. Trace metal ion buffers and their use in culture studies. *In* R. A. Andersen (ed.), Algal Culturing Techniques. Elsevier, London.

178. **Sunda, W. G., N. M. Price, and F. M. M. Morel.** 2005. Trace metal ion buffers and their use in culture studies, p. 35-64. *In* R. A. Anderson (ed.), Algal Culturing Techniques. Elsevier, Oxford.

179. **Tabbi, G., W. L. Driessen, J. Reedijk, R. P. Bonomo, N. Veldman, and A. L. Spek.** 1997. High superoxide dismutase activity of a novel, intramolecularly imidazolato-bridged asymmetric dicopper (II) species. Design, synthesis, structure, and magnetism of copper (II) complexes with a mixed pyrazole-imidazole donor set. Inorganic Chemistry **36:**1168-1175.

180. **Theissen, U., M. Hoffmeister, M. Grieshaber, and W. Martin.** 2003. Single eubacterial origin of Eukaryotic sulfide:quinone oxidoreductase, a mitochondrial enzyme conserved from the early evolution of Eukaryotes during anoxic and sulfidic times. Molecular biology and evolution **20:**1564-1574.

181. **Thomas, D. J., T. J. Avenson, J. B. Thomas, and S. K. Herbert.** 1998. A cyanobacterium lacking iron superoxide dismutase is sensitized to oxidation stress induced with methyl viologen but is not sensitized to oxidative stress induced with norflurazon. Plant Physiology **116:**1593-1602.

182. **Thompson, J. D., T. J. Gibson, F. Plewniak, F. Jeanmougin, and D. G. Higgins.** 1997. The ClustalX windows interface: flexible strategies for multiple sequence alignment aided by quality analysis tools. Nucleic Acids Research **25:**4876-4882.

183. **Thunell, R. C.** 1998. Seasonal and annual variability in particle fluxes in the Gulf of California: A response to climate forcing. Deep Sea Research II **45:**2059-2083.

184. **Todd, J. D., R. Roger, Y. G. Li, M. Wexler, P. L. Bond, L. Sun, A. R. J. Curson, G. Malin, M. Steinke, and A. W. B. Johnston.** 2007. Structural and regulatory genes required to make the gas dimethyl sulfide in bacteria. Science **315:**666-669.

185. **Tusher, V. G., R. Tibshirani, and G. Chu.** 2001. Significance analysis of microarrays applied to the ionizing radiation response. Proceedings of the National Academy of Sciences **98:**5116-5121.

186. **Twining, B. S., S. B. Baines, N. S. Fisher, and M. R. Landry.** 2004. Cellular iron contents of plankton during the Southern Ocean Iron Experiment (SOFeX). Deep Sea Research I **51:**1827-1850.

187. **Tyson, G. W., J. Chapman, P. Hugenholtz, E. E. Allen, R. J. Tam, P. M. Richardson, V. V. Solovyev, E. M. Rubin, D. S. Rokhsar, and J. F. Banfield.** 2004. Community structure and metabolism through reconstruction of microbial genomes from the environment. Nature **428:**37-43.

188. **van Nimwegen, E.** 2003. Scaling lawa in the functional content of genomes. Trends in Genetics **19:**479-484.

189. **van Nimwegen, E.** 2006. Scaling laws in the functional content of genomes: Fundamental constants of evolution. *In* E. V. Koonin, Y. I. Wolf, and G. P. Karev (ed.), Power laws, scale-free networks, and genome biology. Eurekah.

190. **Venter, J. C., K. Remington, J. F. Heidelberg, A. L. Halpern, D. Rusch, J. A. Eisen, D. Wu, I. Paulsen, K. E. Nelson, W. Nelson, D. E. Fouts, S. Levy, A. H. Knap, M. W. Lomas, K. Nealson, O. White, J. Peterson, J. Hoffman, R. Parsons, H. Baden-Tillson, C. Pfannkoch, Y.-H. Rogers, and H. O. Smith.** 2004. Environmental genome shotgun sequencing of the Sargasso Sea. Science **304:**66-74.

191. **Wafar, M. V. M., P. Lecorre, and S. Lhelguen.** 1995. F-ratios calculated with and without urea uptake in nitrogen uptake by phytoplankton. Deep Sea Research I **42:**1669-1674.

192. **Wang, M., L. S. Yafremava, D. Caetano-Anolles, J. E. Mittenthal, and G. Caetano-Anolles.** 2007. Reductive evolution of architectural repertoires in proeomes and birth of the tripartite world. Genome Research **17:**1572-1585.

193. **Waterbury, J. B., and J. M. Willey.** 1988. Isolation and growth of marine planktonic cyanobacteria. Methods in Enzymology **167**.

194. **Wen, L.-S., K.-T. Jiann, and P. H. Santschi.** 2006. Physiochemical speciation of bioactive trace metals (Cd, Cu, Fe, Ni) in the oligotrophic South China Sea. Marine Chemistry **101:**104-129.

195. **Westall, J. C., J. L. Zachary, and F. M. M. Morel.** 1976. MINEQL: A Computer Program for the Calculation of Chemical Equilibrium Composition of Aqueous Systems. Tech. Note 18. R. M. Parsons Lab., Mass. Inst. Technol.

196. **White, A. E., F. G. Prahl, R. M. Letelier, and B. N. Popp.** 2007. Summer surface waters in the Gulf of California: Prime habitat for biological N_2 fixation. Global biogeochemical cycles **21:**GB2017.

197. **Williams, R. J. P.** 1997. The natural selection of the chemical elements. Cellular and Molecular Life Sciences **53:**816-829.

198. **Williams, R. J. P., and J. Da Silva.** 2003. Evolution was chemically constrained. Journal of Theoretical Biology **220:**323-343.

199. **Williams, R. J. P., and J. J. R. Frausto da Silva.** 2006. The chemistry of evolution: The development of our ecosystem. Elsevier, Amsterdam.

200. **Wolfe-Simon, F., D. Grzebyk, C. J. Schofield, and P. G. Falkowski.** 2005. The role and evolution of superoxide dismutases in algae. Journal of Phycology **41:**453-465.

201. **Worden, A. Z., J. K. Nolan, and B. Palenik.** 2004. Assessing the dynamics and ecology of marine picophytoplankton: The importance of the eukaryotic component. Limnology & Oceanography **49:**168-179.

202. **Woyke, T., H. Teeling, N. N. Ivanova, M. Huntemann, M. Richter, F. O. Gloeckner, D. Boggelli, I. J. Anderson, K. W. Barry, H. J. Shapiro, E. Szeto, N. C. Kyrpides, M. Mussman, R. Amann, C. Bergin, C. Ruehland, E. M. Rubin, and N. Dubilier.** 2006. Symbiosis insights through metagenomic analysis of a microbial consortium. Nature **443:**950-955.

203. **Wuerges, J., J.-W. Lee, Y.-I. Yim, H.-S. Yim, S.-O. Kang, and K. D. Carugo.** 2004. Crystal stucture of nickel-containing superoxide dismutase reveals another type of active site. Proc. Natl. Acad. Sci. USA **101:**8569-8574.

204. **Xiong, J., W. M. Fischer, K. Inoue, M. Nakamura, and C. E. Bauer.** 2000. Molecular evidence for the early evolution of photosynthesis. Science **289:**1724-1730.

205. **Yang, S., R. F. Doolittle, and P. E. Bourne.** 2005. Phylogeny determined by protein domain content. Proc. Natl. Acad. Sci. USA **102:**373-378.

206. **Youn, H.-D., E.-J. Kim, J.-H. Roe, E. C. Hah, and S.-O. Kang.** 1996. A novel nickel-containing superoxide dismutase from *Streptomyces sp.* Journal of Biochemistry **318:**889-896.

207. **Youn, H.-D., H. Youn, J.-W. Lee, Y. Yim, J. Kug Lee, Y. Chil Hah, and S. Kang.** 1996. Unique isoenzymes of superoxide dismutase in *Streptomyces griseus*. Archives of Biochemistry and Biophysics **334:**341-348.

208. **Zerkle, A. L., C. H. House, and S. L. Brantley.** 2005. Biogeochemical signatures through time as inferred from whole microbial genomes. American Journal of Science **305:**467-502.